

Doctoral Theses at NTNU 2005:20

Bente Jeanette Foss

Synthesis and Physical Properties of Hydrophilic Carotenoid Derivatives

NTNU
Norwegian University of
Science and Technology
Doctoral thesis
for the degree of doctor scientiarum
Faculty of Natural Science and Technology
Department of Chemistry

Doktoravhandling ved NTNU (trykt utg.)

2005 Nr 20
GUNNERUS
T 14034

10.02.2005

Universitetsbiblioteket i Trondheim

 NTNU

Bente Jeanette Foss

Synthesis and Physical
Properties of Hydrophilic
Carotenoid Derivatives

Trondheim, January 2005

Doctoral thesis for the degree of doctor scientiarum

Norwegian University of Science and Technology
Faculty of Natural Science and Technology
Department of Chemistry



Acknowledgements

Most of the work presented in this thesis was carried out at the Department of Chemistry, Norwegian University of Science and Technology (NTNU) during the period of March 2000 to October 2004. During these years I was lucky to also get the opportunity to teach Chromatography at Sør-Trøndelag University College, and present fun chemistry and physics experiments in the children science TV-program “Newton”.

I am grateful to my supervisor Prof. Vassilia Partali for guiding me through the work and always encouraging me in every way. Dr. Hans-Richard Sliwka is also gratefully acknowledged for guidance, proof reading, and continuous inspiration.

Many thanks to Prof. Florinel G. Banica and Dr. Ana Ion for sharing their knowledge of electrochemical investigations of SAMs and for teaching me the experiments. Prof. Jostein Krane is thanked for the important shimming of the NMR instruments and for being an inspiration in learning NMR techniques and usage.

Thanks to all the co-authors for their collaboration and for making this work such a diverse and interesting endeavor. Dr. Stine Nalum Næss and Profs. Thor-Bernt Melø, K. Razi Naqvi, and Arnljot Egsæter (Department of Physics, NTNU) are thanked for dynamic light scattering and flash photolysis experiments. Thanks to Prof. Miklos Simonyi and Drs. Ferenc Zsila and Zsolt Bikadi (Department of Bioorganic Chemistry, Chemical Research Center, Budapest) for hosting me during my “CD-study”. Thanks also to Dr. Sam Lockwood (Hawaii Biotech, Inc.) for the EPR experiments.

Thanks to the exchange students Yu Qiang (China) and Cyril Blondel (France) who worked on some of the synthesis. Thanks to Dr. Eirik Sundby and Profs. Thorleif Anthonsen, Lise Kvittingen, and Rudolf Schmid for valuable discussions.

Thanks to my friends Drs. Ingrid Sletvold and Elisabeth Egholm Jacobsen for the help in using “FrameMaker” and giving me valuable comments on the thesis. A warm thank to Geoff for correcting my misspellings and being a great support. Thanks also to my other friends at the Department (Bjart Frode, Karina, Christian, Anders, Jon Erik, Trond, Sondre, Jørgen, Camilla, Silje, Einar, Janne, Jarle, and Freddy). You all made these years a very positive experience for me.

Finally, I want to thank my family for always supporting me.

Aloha.



Acknowledgements

Contents

Acknowledgements	I
Contents	III
Summary.....	VII
Articles	XIII
Abbreviations & Symbols	XV
Preface	XVII
1 Introduction.....	1
1.1 Carotenoids	1
1.2 Functions of carotenoids	4
1.2.1 In nature	4
1.2.2 In human	4
1.2.3 In medicine	6
1.2.4 In industry	7
1.2.5 Antioxidant action of carotenoids	7
1.2.6 Antioxidant interactions	9
1.2.7 Carotenoids in cell membranes	11
1.3 Absorption, metabolism, and transport of carotenoids	12
1.4 Industrial synthesis of carotenoids	15
1.5 Water-dispersible/soluble carotenoids	16
1.5.1 Naturally water-dispersible/soluble carotenoids	16
1.5.2 Water-dispersible/soluble carotenoids by inclusion and additives	19
1.5.3 Water-dispersible/soluble carotenoid derivatives by synthesis	22
1.6 Multifunctional carotenoid derivatives	27
1.7 Phospholipids	30
1.7.1 Functions of phospholipids	31
1.7.2 The role of phospholipids in the absorption of carotenoids	32
1.7.3 The role of unsaturated fatty acids in phospholipids	32
1.8 Aggregates and self-assembly monolayers (SAMs)	34
1.8.1 Self-assemblies in water	34
1.8.2 Self-assemblies on surfaces	36
2 Synthesis of hydrophilic, water-dispersible carotenoid derivatives.....	39
2.1 Synthesis of carotenoid lysophosphocholine <i>R-43a</i> and <i>43a/43b/43c</i> (<i>paper nr. 1, 2, and 9</i>)	39

2.2 Synthesis of phosphocholine esters from β -apo-8'-carotenoic acid (56) and 4-oxo- β -apo-8'-carotenoic acid (57)	42
2.3 Synthesis of potassium salts of β -apo-8'-carotenoic ethyl ester (62) and 4-oxo- β -apo-8'-carotenoic ethyl ester (63)	43
2.4 Synthesis of carotenoid-selena-phosphocholine 66	44
2.5 Structural elucidation by 1D and 2D NMR	46
2.5.1 Structural elucidation of the carotenoid monoglycerides 22a/22b	46
2.5.2 Structural elucidation of the carotenoid lysophosphocholines R-43a and 43a/43b/43b and their 2-bromoethyl derivatives (paper 2) ...	47
2.5.3 Structural elucidation of selena-carotenoid-phosphocholine 66	52
2.6 Water-solubility, water-dispersibility.....	53
2.7 Experimental	55
2.7.1 Synthesis of the phosphocholine esters of β -apo-8'-carotenoid acid (56) and 4-oxo- β -apo-8'-carotenoic acid (57)	55
2.7.2 Synthesis of potassium salts of β -apo-8'-carotenoic ethyl ester (62) and 4-oxo- β -apo-8'-carotenoic ethyl ester (63)	56
2.7.3 Synthesis of the carotenoid-selena-phosphocholine 66	57
3 Determination of surface properties	59
3.1 The Wilhelmy Plate Method	59
3.2 The Pendant Drop Method	60
3.3 Graphical determination of cmc	61
3.4 Calculation of thermodynamic data	62
3.5 Surface properties of water-dispersible/soluble carotenoids (paper 3, 4, and 5)	64
3.5.1 Sample preparation and recording	70
4 Aggregation behavior	71
4.1 UV-VIS spectroscopy of water-dispersible/soluble carotenoids (paper 3, 4, and 5)	71
4.2 Dynamic light scattering	75
4.3 Aggregate properties of water-dispersible/soluble carotenoids (paper 3, 4, and 5)	79
5 Biological activity	81
5.1 General	81
5.2 Direct superoxide anion ($O_2^{\bullet-}$) scavenging of carotenoid lysophosphocholine 43a/43b/43c evaluated by EPR spectroscopy (paper 6)	81
6 Laser flash photolysis of radicals and triplet states of carotenoids	85
6.1 General	85
6.2 The antioxidant properties of water-dispersible/soluble carotenoids (paper 7)	86

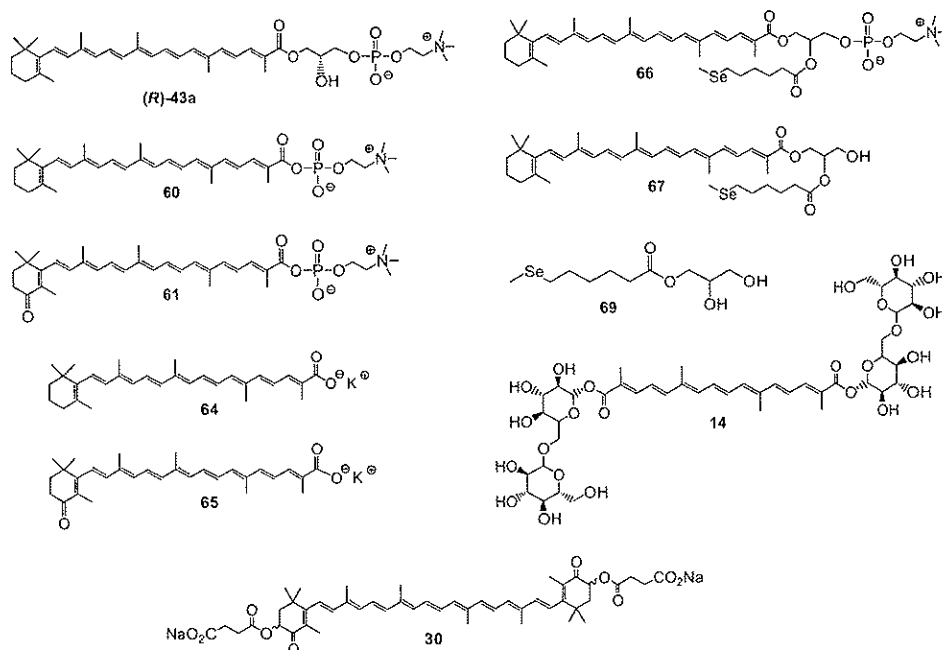
6.3 Aggregation vs. formation of ^3CAR and $\text{CAR}^{\bullet+}$ (<i>paper 7</i>)	88
7 SAM formation investigated by electrochemical methods	89
7.1 General	89
7.2 Electrochemical techniques	89
7.2.1 Cyclic voltammetry (CV)	89
7.2.2 Electrochemical impedance spectroscopy (EIS)	90
7.2.3 Electrochemical quartz crystal microbalance (EQCM)	91
7.2.4 Electrochemical studies on carotenoids	92
7.3 Investigation of the SAM formation of selena-glyceride 69 on a gold surface (<i>paper 8</i>)	92
7.4 SAM formation of carotenoid derivatives with selena-glyceride 69 as an anchor (<i>paper 8</i>)	97
8 Optical activity	101
8.1 Optical activity of monomeric carotenoids	101
8.2 Supramolecular induced exciton chirality of carotenoids	102
8.3 Optical activity of carotenoid lysophosphocholine R-43a (<i>paper 9</i>)	102
References.....	105
Appendices.....	119

Contents

Summary

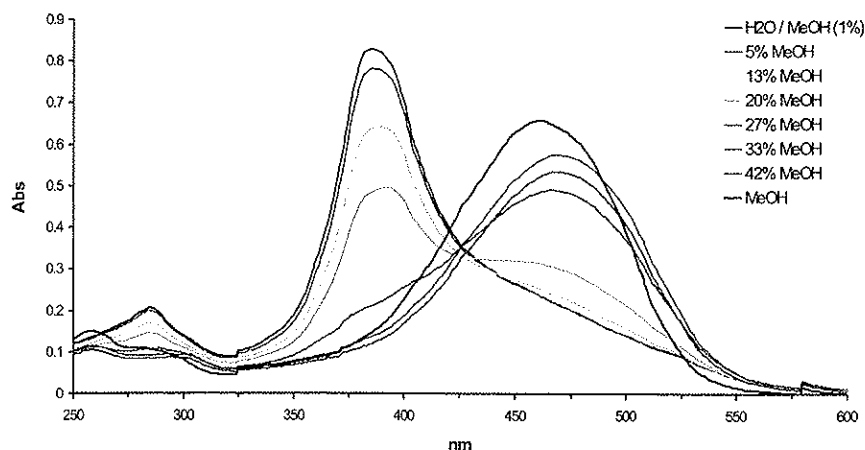
The main goal of this project was to synthesize new water-dispersible carotenoid derivatives, and to investigate their physical and biological properties in water. Additionally, the aim was to synthesize multifunctional seleno-carotenoid derivatives for the study of complex, self-assembled carotenoid monolayers on gold.

The water-dispersible carotenoid derivatives synthesized in this work were carotenoid lysophosphocholine **R-43a** and **43a/43b/43c** (mixture composed of regioisomers), the phosphocholine esters **60** and **61**, the carotenoid potassium salts **64** and **65**, and the carotenoid-selena-phosphocholine **66**. Additionally, the seleno-glyceride **69** and carotenoid-selena-glyceride **67** were synthesized for the study of SAM formation. All the compounds were obtained in yields ranging from 33 to 88 %. Included in some of the succeeding physical studies were the naturally occurring, water-soluble crocin (**14**) and the water-dispersible CardaxTM (**30**).



The new water-dispersible carotenoid derivatives dissolve either in pure water (**43a/43b/43c**, **R-43a**, **64**, **65**, **66**) or in 1% methanol/water (**60**, **61**). The water solubility varies from 1,5 mg up to 60 mg/ml, or higher.

UV-VIS spectroscopy revealed that most of the water-dispersible carotenoids show hypsochromic λ_{max} shifts (10-75 nm) upon addition of water, which may be a result of H-aggregate formation. Small shoulders observed around 500-520 nm (for crocin (**14**) at 480 nm) are thought to arise from J-aggregates. The aggregates are disrupted into monomers when organic solvents such as methanol, are added to the solutions.



UV-VIS of carotenoid phosphocholine ester **61** in water/methanol (99/1%, v/v) vs. dropwise addition of methanol

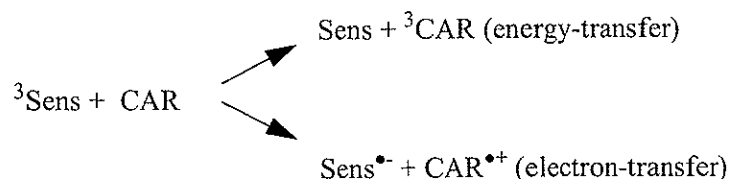
Surface tension was measured and thermodynamic data calculated for carotenoid lysophosphocholine **43a/43b/43c**, CardaxTM (**30**), crocin (**14**), and the carotenoid potassium salts C30:9-K **64** and C30:9-cantha-K **65**. The data revealed that these new surfactants all reach their critical micellar concentration (cmc) at relatively high concentrations, while lowering the surface tension markedly. Further, it was found that carotenoid lysophosphocholine **43a/43b/43c** is the most surface-active of the carotenoid surfactants investigated so far, which was shown by its large surface concentration ($\Gamma = 4.5 \cdot 10^{-6} \text{ mol/m}^2$), and an absorption micellar energy ratio (AMER) close to unity. These findings indicate dense monolayer formation, enhanced micelle concentration, and good cleansing and wetting properties.

From dynamic light scattering measurements of the carotenoid lysophosphocholine **R-43a** and **43a/43b/43c**, CardaxTM (**30**), and crocin (**14**) in water, the hydrodynamic radius (R_h) of their aggregates could be determined. The number-weighted distribution of **R-43a** and **43a/43b/43c** indicate a dominance of nanometer-sized aggregates of 6 and 8 nm, respectively, in addition to some larger ones (30-500 nm and 40-600 nm, respectively). CardaxTM (**30**) displayed a fast formation of aggregates of 1.2-1.3 μm size in both water and 0.15 M NaCl, while

in 0.5 M and 2.0 M NaCl a slow association of the aggregates to larger ones was observed. The glycosylester crocin (**14**) forms the smallest aggregates (1.6 nm) of the carotenoids investigated. At concentration (C) < cmc, only monomers are present for this compound, while carotenoid lysophosphocholines **R-43a** and **43a/43b/43c**, and CardaxTM (**30**) form aggregates at $C \ll$ cmc.

The biological activity of carotenoid lysophosphocholine **43a/43b/43c** was investigated by spin trap-DEMPO EPR spectroscopy, and was shown to be a potent aqueous phase direct scavenger of superoxide anion ($O_2^{\bullet -}$) produced from isolated human neutrophils. Over 90% of the superoxide anion was scavenged using a 10mM solution in water, or using a 3mM solution in ethanol/water.

The antioxidant properties of carotenoid lysophosphocholine **43a/43b/43c**, CardaxTM (**30**), and crocin (**14**) were investigated by laser flash photolysis using 1-nitronaphthalene as the sensitizer. The collision between 1-nitronaphthalene in the triplet state (3Sens) and the carotenoids either lead to energy- or electron-transfer, and the ratio of the reactions change with solvent polarity. In MeCN (less polar), energy- transfer was favored, while in aqueous solution (most polar), electron-transfer was dominant.

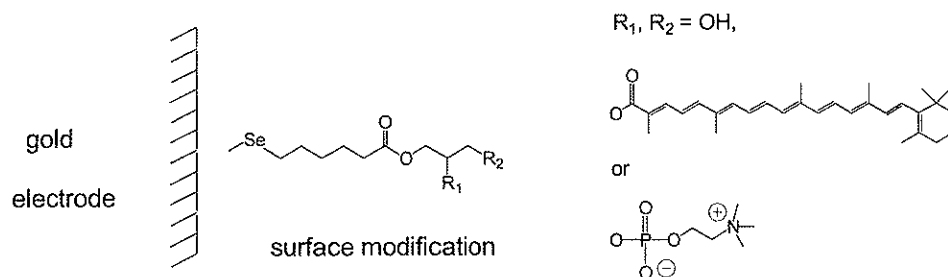


3Sens can initiate singlet oxygen (1O_2) production, hence, these reactions indirectly quench the formation of 1O_2 and may be direct evidence of antioxidant properties of **43a/43b/43c**, **30**, and **14**. It was also concluded that carotenoid lysophosphocholine **43a/43b/43c** and CardaxTM (**30**) both exhibit supramolecular self-protecting properties in water due to their aggregate formation where the sensitive polyene chain is placed into the interior of the aggregate.

The optical activity of enantiomeric **R-43a** was investigated by CD spectroscopy. It was found that **R-43a** is optical inactive in the monomer form (in methanol). On the other hand, when dissolved in water, a chiral aggregation is induced. CD spectra in water indicated no defined H- or J-aggregate formation. Based on molecular mechanics calculations, an enantiomeric oligomer composed of approximately eight monomers as the basic unit of the aggregates was proposed. This oligomer explains the spectroscopic properties of **R-43a**.

The self-assembled monolayer (SAM) formation of seleno-glyceride **69** was investigated by electrochemical methods (including cyclic voltammetry and

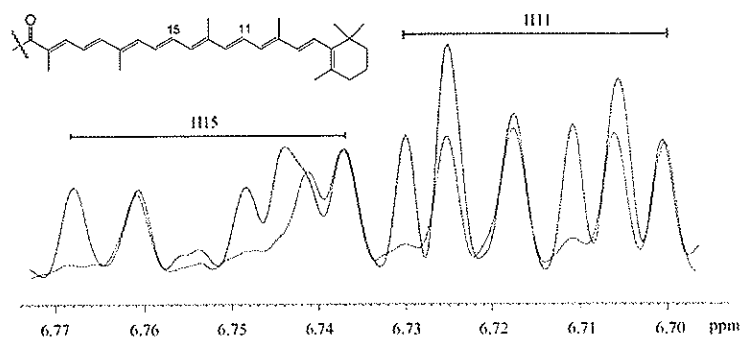
impedance spectroscopy). Seleno-glyceride **69** binds irreversibly to gold by the Se functionality, and the adsorption process is believed to take place via a cleavage of the Se-CH₃ bond. The monolayer formed is stable in the anodic region up to about 1.0 V, wherein gold oxide formation is initiated. The adsorbed compound also undergoes a cathodic process leading to the removal of the surface layer. The SAM formed by **69** is compact, with the coverage degree close to unity for an adsorption time of 30 to 80 min. The layer displays minute defects (pinholes) with a radius of ca 1 - 3 μm, separated by 6 - 50 μm intervals (depending on the adsorption time).



The free OH groups in seleno-glyceride **69** or its 2-acyl isomer can be used to prepare carotenoid-containing SAMs on gold. This was shown by the chemisorption of carotenoid-seleno-glyceride **67** and carotenoid-seleno-phosphocholine **66** on gold. Both compounds (**67** and **66**) adsorb to the surface via the selenium functionality. The anodic oxidation of the carotenoid moiety develops at a less positive potential for the highly hydrophilic carotenoid-seleno-phosphocholine **66** compared to carotenoid-seleno-glyceride **67**, indicating that the anodic process is facilitated by the presence of water molecules close to the reaction site. Carotenoid-seleno-phosphocholine **66** forms a less compact monolayer than carotenoid-seleno-glyceride **67**, which is believed to result from steric hindrance from the choline moiety. In conclusion, these investigations have been shown that SAM-carotenoid electron-transfer reactions can be studied in aqueous solutions.

1D and 2D NMR techniques were utilized for the structural elucidation of carotenoid lysophosphocholines **43a**, **43b** and **43c** as a mixture, as well as their synthetic precursors. The ratio of the individual carotenoid lysophosphocholines **43a**, **43b**, and **43c** was found to be 49:43:8, respectively. A 1D ¹H NMR subtraction spectrum of the mixture and the pure isomer [(**43a/43b**) - **R-43a**] showed that the ¹H shifts of the carotenoyl chain for the individual regioisomers differ. An example of the deviation of **R-43a** compared to **43b** is seen for the

chemical shifts of H11 and H15 (the concentration of **43c** was too low to give significant signals in the polyene chain region).



H15 and H11 signals for the isomeric mixture **43a/43b** (blue) and *R*-**43a** (red).

Similar differences of the polyene chemical shifts for the two individual regioisomers **43a/43b** and their 2-bromoethyl isomeric precursors were displayed by ^{13}C DEPT 135. Therefore, it was concluded that the characteristic polyenic ^1H and ^{13}C chemical shifts may be used to distinguish between positional isomers of (lyso)phosphocholines and their 2-bromoethyl derivatives.

Summary

Articles

1. B. J. Foss, S. N. Næss, H.-R. Sliwka and V. Partali. "Stable and highly water-dispersible, highly unsaturated carotenoid phospholipids – surface properties and aggregate size", *Angew. Chem. Int. Ed.* **2003**; *42*: 5237-5240.
2. B. J. Foss and J. Krane. "Structural elucidation by 1D and 2D NMR of three isomers of a carotenoid lysophosphocholine and its synthetic precursors". *Magn. Reson. Chem.* **2004**; *42*: 373-380.
3. B. J. Foss, H.-R. Sliwka, V. Partali, S. N. Næss, A. Elgsæter, T.-B. Melø. and K. R. Naqvi. "Hydrophilic carotenoids: surface properties and aggregation behavior of a highly unsaturated carotenoid lysophospholipid", *Chem. Phys. Lipids* **2004**, *accepted*.
4. B. J. Foss, H.-R. Sliwka, V. Partali, S. N. Næss, A. Elgsæter, T.-B. Melø, K. R. Naqvi, S. O'Malley and S. F. Lockwood. "Hydrophilic carotenoids: surface properties and aqueous aggregation of a rigid, long-chain, highly unsaturated dianionic bolaamphiphile with a carotenoid spacer", *Chem. Phys. Lipids* **2004**, *submitted*.
5. S. N. Næss, A. Elgsæter, B. J. Foss, H.-R. Sliwka, V. Partali, T.-B. Melø and K. R. Naqvi. "Hydrophilic carotenoids: Surface properties and aggregation of crocin, a natural, rigid, long chain, highly unsaturated biosurfactant", *to be published*.
6. B. J. Foss, H.-R. Sliwka, V. Partali, A. J. Cardounel and S. F. Lockwood. "Direct superoxide anion scavenging by a highly water dispersible carotenoid phospholipid evaluated by electron paramagnetic resonance (EPR) spectroscopy". *Bioorg. Med. Chem. Lett.* **2004**; *14*: 2807-2812.
7. T.-B. Melø, K. R. Naqvi, B. J. Foss, S. F. Lockwood, V. Partali and H.-R. Sliwka. "Carotenoids as electron donors and triplet energy acceptors in polar solvents: A flash photolysis investigation of crocin and water-soluble carotenoids using 1-nitronaphtalene as a sensitizer", *in preparation*.
8. B. J. Foss, A. Ion, V. Partali, H.-R. Sliwka and F. G. Banica. "O¹-[6-(Methylselanyl)hexonoyl] glycerol as an anchor for self-assembly of biological compounds at the gold surface", *Collect. Czech. Chem. Commun.*

2004; 69: 1971-1996.

9. B. J. Foss, H.-R. Sliwka, V. Partali, C. Köpsel, B. Mayer, H.-D. Martin, F. Zsila, Z. Bikádi and M. Simonyi. "Optically active oligomer units in aggregates of a highly unsaturated, optically inactive carotenoid phospholipid", *Chemistry - European Journal* 2004, submitted.

Reprints of Article 1, 2, 6, and 8, and manuscripts of Article 3, 4, 5, 7, and 9 are given as appendices to this thesis.

Abbreviations & Symbols

Abbreviations

TLC	thin layer chromatography
BHT	butylated hydroxytoluene
DCC	1,3-dicyclohexylcarbodiimide
CDI	1,1'-carbonyldiimidazole
DBU	1,8-diazabicyclo[5.4.0]undec-7-ene
GPC	<i>sn</i> -glycero-3-phosphocholine
DPPH	1,1-diphenyl-2-picrylhydrazyl
KOH	potassium hydroxide
MeCN	acetonitrile
EtOH	ethanol
UV	ultra violet
VIS	visible light
NMR	nuclear magnetic resonance
COSY	correlation spectroscopy (NMR technique)
DEPT	distortionless enhancement polarization transfer (NMR technique)
1D	one-dimensional
2D	two-dimensional
MS	mass spectroscopy
ESI	electro spray ionization
SDS	sodium dodecyl sulfate
AMER	absorption micellar energy ratio
DLS	dynamic light scattering
EPR	electron paramagnetic resonance
DEPMPO	5-(diethoxyphosphoryl)-5-methyl-1-pyrroline N-oxide
LFP	laser flash photolysis
CV	cyclic voltammetry
SAM	self-assembled monolayer
SCE	saturated calomel electrode
EIS	electrochemical impedance spectroscopy
EQCM	electrochemical quartz crystal microbalance
XPS	X-ray photoelectron spectroscopy
STM	scanning-tunneling microscopy
CD	circular dichroism
CE	cotton effect

Symbols

R_h	hydrodynamic radius
γ	surface tension
cmc	critical micellar concentration
Π	surface pressure/change in surface tension
Γ	surface concentration
a_m	area per molecule
ΔG_m^0	standard free energy of micellation
ΔG_{ad}^0	standard free energy of adsorption
k_m	equilibrium constant (micellation)
k_{ad}	equilibrium constant (adsorption)
E	potential
i	current
mV	millivolt(s)
μA	microampere(s)
t	time
min	minute(s)
Δf	frequency shift
θ	coverage degree
r_a	radius of pinholes
r_d	half-distance between pinholes
p	optical purity

Preface

This thesis contains eight chapters. Chapter 1 gives a general introduction to the chemistry of carotenoids and phospholipids, water-soluble carotenoid formulations, and self-assemblies of carotenoids, while the results are presented and discussed in Chapters 2 through 8.

Chapter 2 describes the synthesis of new carotenoid derivatives and the structural elucidation of carotenoid lysophosphocholine **R-43a** and its regioisomeric mixture **43a/43b/43c**. This work was performed by the author at the Department of Chemistry (NTNU). Most of the results are published in *paper nr. 1, 2, and 9*.

Chapter 3 and 4 discuss the surface properties and aggregation behavior of novel water-dispersible carotenoids, of which most of the work is published in *paper 3, 4, and 5*. The UV-VIS spectroscopy studies were performed by the author at the Department of Chemistry (NTNU). Surface tensions were measured by the author at SINTEF Materialer og Kjemi, Trondheim, with the advice from Dr. Anne Dyrli. The Pendant Drop method was studied at the Department of Chemistry, University of Oslo under the guidance of Prof. Finn Knut Hansen. The Dynamic Light Scattering measurements were performed in close collaboration with Dr. Stine Nalum Næss, Department of Physics (NTNU).

Chapter 5 discusses the biological activity of carotenoid lysophosphocholine **43a/43b/43c**, which was studied by Dr. Samuel F. Lockwood (Hawaii Biotech, Inc., Aiea) and Arturo J. Cardounel and Jay L. Zweier, Davis Heart & Lung Research Institute, Columbus, Ohio, USA (*paper nr 6*).

In Chapter 6 the energy- and electron-transfer reactions of carotenoid lysophosphocholine **43a/43b/43c**, CardaxTM (**30**), and crocin (**14**) are described (*paper nr. 7*). This work was accomplished by Profs. Thor-Bernt Melø and Kalbe Razi Naqvi at the Department of Physics (NTNU).

Chapter 7 summarizes the self-assembling monolayer (SAM) formation of seleno-glyceride **69**, carotenoid-selena-glyceride **67**, and carotenoid-selena-phospholipid **66** (*paper nr. 8*). The experimental work was completed by the author at the Department of Chemistry (NTNU) supervised by Prof. Florinel G. Banica and Dr. Ana Ion. The presented part of this work is published (*paper nr. 8*). Two more manuscripts are in preparation dealing with more extensive SAM formation studies of compounds **66** and **67** (not included in this thesis).

In Chapter 8, the optical activity of the *sn*-1-isomer of carotenoid lysophosphocholine **R-43a** is discussed (*paper nr. 9*). The CD measurements were performed at the Department of Molecular Pharmacology, Chemical Research

Center, Budapest, Hungary, by Dr. Ferenc Zsila and the author. The molecular mechanics and force field (CVFF) computation, and the absorption and CD spectra were calculated by Prof. Hans-Dieter Martin and Drs. Christian Köpsel and Bernhard Mayer, Institut Für Chemie, Heinrich-Heine-Universität, Düsseldorf, Germany.

The methods used in this work (*e.g.* surface tension, dynamic light scattering (DLS), cyclic voltammetry (CV), and circular dichroism (CD)) are described in many textbooks, but it was found appropriate to precede the chapters with a short explanation of each technique.

The work presented in this thesis is published in four articles and five manuscripts, of which two are submitted. All articles and manuscripts are given as appendices.

The results of related topics are discussed and summarized together. The experimental conditions are described in the papers. The experimental details for results that are not yet published are given in the thesis.

1 Introduction

1.1 Carotenoids

Carotenoids are red, orange, and yellow conjugated polyene pigments produced by bacteria, algae, and plants. The annual bioproduction of carotenoids is estimated to be 100 million tons. Carotenoids are the major endogenous pigments in flowers, fruits, and vegetables, and exogenous pigments in insects, birds, and fish. Carotenoids are also present in green vegetables, but their colors are masked by chlorophyll.^{1, 2}

The basic structure of carotenoids is a C_{40} conjugated polyene chain, built up of eight C_5 -isoprene units (1), as shown in Figure 1.1 for lycopene (2).

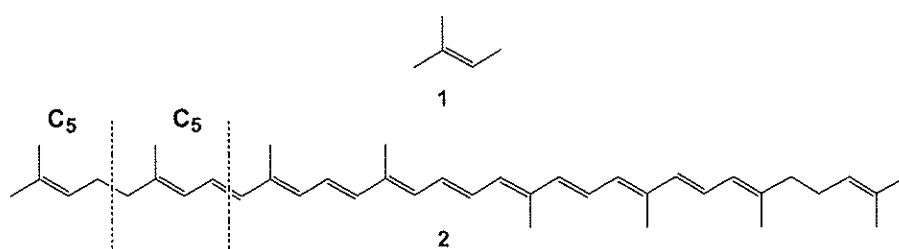


Figure 1.1 The basic C_5 -isoprene unit (1) and lycopene (2).

The chain can contain allenic or acetylenic moieties, as shown for fucoxanthin (3) and alloxanthin (4) respectively (Figure 1.2).

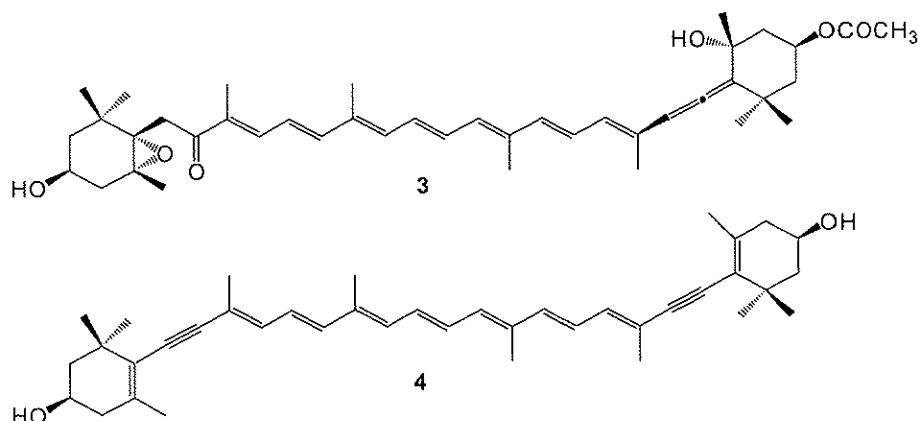


Figure 1.2 Fucoxanthin (3) and alloxanthin (4).

The ends of the polyene chain can be connected to cyclohexene rings as in (*R,R*)-zeaxanthin (**5**), aryl rings as in renieratene (**6**), or 5-membered rings as in capsorubin (**7**), as seen in Figure 1.3.

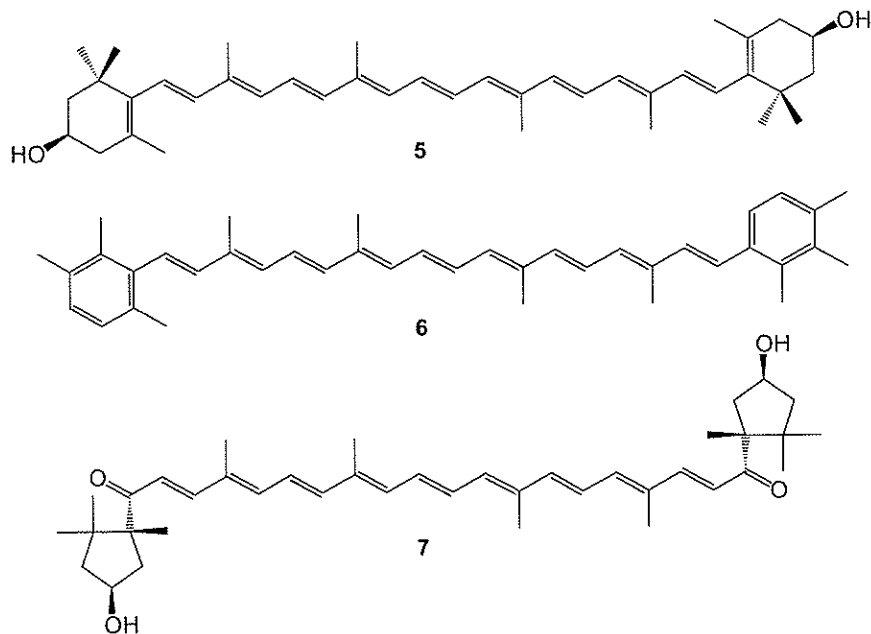


Figure 1.3 (*R,R*)-zeaxanthin (**5**), renieratene (**6**), and capsorubin (**7**).

Further, carotenoids may also contain 3 and 5-membered epoxides, as in fucoxanthin (**3**) (Figure 1.2) and luteoxanthin (**8**) (Figure 1.4).

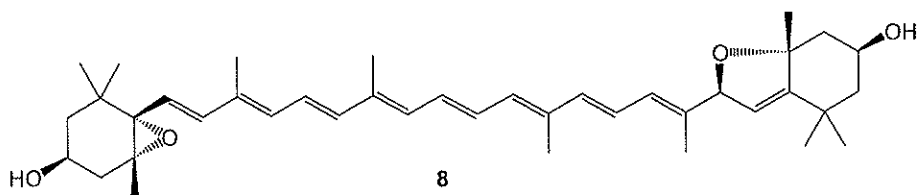


Figure 1.4 Luteoxanthin (**8**).

Carotenoids with longer and shorter polyene chains are known (e.g. trisanhydrobacterioruberin (**9**) and β -apo-8'-carotenal (**10**))³, Figure 1.5.

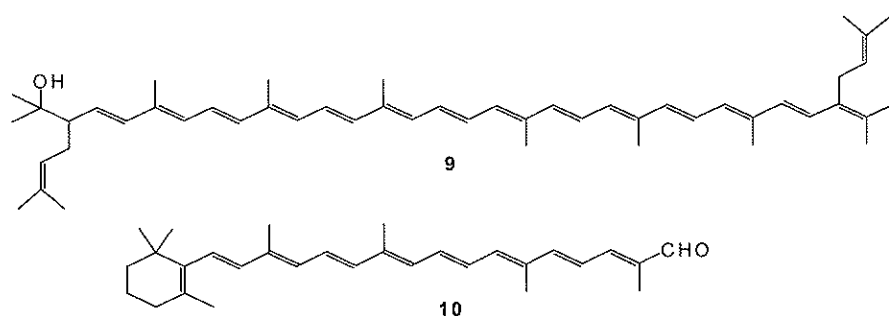


Figure 1.5 Trisanhydrobacterioruberin (9) and β -apo-8'-carotenal (10).

Natural products biosynthesized in suitable environments often incorporate heteroatoms such as S, Se, and halogens (e.g. S-sugars, Se-sugars, S-aminoacids, Se-aminoacids, Cl-steroids, and Br-fatty acids).⁴⁻¹⁰ In contrast, carotenoids biosynthesized by plants in halogen-rich sea-water, or on Se-enriched soil do not incorporate heteroatoms. Carotenoids utilize phosphates in their biosynthesis (e.g. prephytoene pyrophosphate (diphosphate) (11), Figure 1.6), but so far no carotenoids with P, S, Se, N, Cl, Br or I have been detected. The only natural heteroatom directly attached to the carotenoid skeleton is O. Natural functional groups containing oxygen atoms are epoxy, hydroxy (OH), carboxy (CO₂H), ester (CO₂R), aldehyde (CHO), keto (C=O), lactones, sulfates, peroxides, and pyrophosphate.^{3, 11} Heterocarotenoids with N, S, Se, and Cl have been synthesized and found stable.¹²⁻²¹

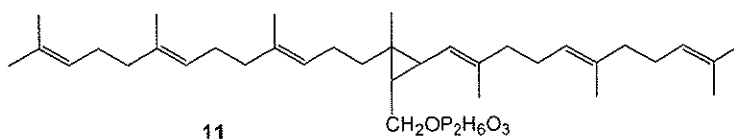


Figure 1.6 Prephytoene pyrophosphate (diphosphate) (11), an intermediate in the biosynthesis of carotenoids.

The approximately 740 naturally occurring carotenoids¹¹ are divided into two classes: the hydrocarbon carotenoids are named carotenes, while those containing oxygen are known as xanthophylls.²²

1.2 Functions of carotenoids

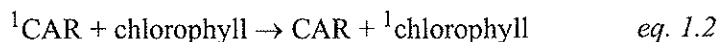
1.2.1 In nature

The conjugated double bond system of carotenoids gives rise to the beautiful colors of flowers, fruits, leaves, and birds. The pigments have several functions, such as indicators of maturity (in fruits) and as attractants for pollinating insects (in flowers). The feathers of many birds are yellow or red because of carotenoids ingested from food, and are important for recognition and attraction in the bird mating process.²³ The attractive red color of the flesh of salmon and trout comes from astaxanthin (Figure 1.7).²⁴ Tomatoes are rich in lycopene, while citrus fruits contain mostly β -cryptoxanthin (Figure 1.7).²³

Carotenoids have the capacity to both transfer and accept electronic energy. In photosynthesis they act as antennae pigments, absorbing visible light of wave length regions only weakly absorbed by chlorophylls (eq. 1.1).



The energy is then effectively transferred to chlorophyll, producing a singlet excited chlorophyll (eq. 1.2).



Carotenoids also protect green plants, algae, and photosynthetic bacteria from light damage.^{25, 26}

1.2.2 In human

About 40 carotenoids are present in a typical human diet, some of the most abundant are shown in Figure 1.7.^{23, 27, 28}

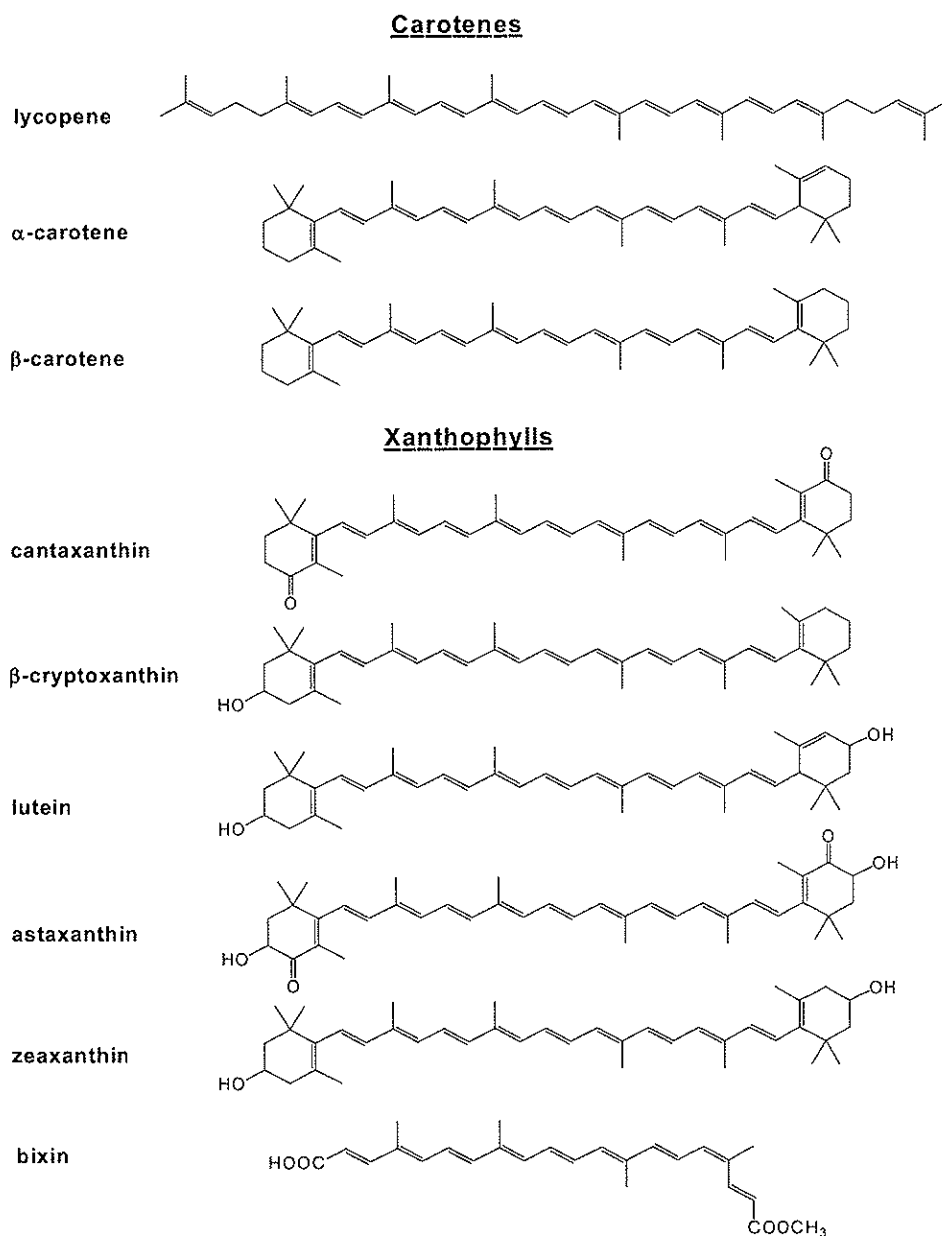


Figure 1.7 Structures of some of the carotenoids found in food.

In humans the most well-known function of carotenoids are as vitamin A precursors, about 50 are provitamin A active compounds, of which β,β -carotene (12) has the highest potential vitamin A activity.²⁹

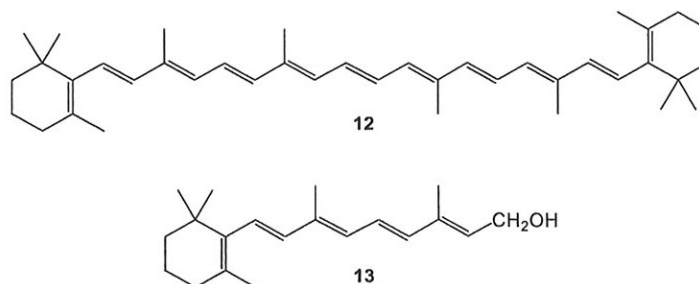


Figure 1.8 β,β -carotene (12) and retinol (vitamin A) (13).

Carotenoids possess several other important biological activities. They increase cell communication, act as immune enhancers, and increase tumor surveillance, all of which are important functions in cancer protection. Nevertheless, it is their antioxidant property which has given the carotenoids most attention^{23, 29, 30} Carotenoids have the ability to deactivate reactive molecules such as free radicals and toxic forms of oxygen, which cause damage in living systems.³¹

Free radicals and reactive oxygen species (*e.g.* $^1\text{O}_2$, OH, $\text{O}_2^{\cdot-}$, and H_2O_2) are produced during normal cellular respiration and metabolism in the human body. In addition, humans are exposed to exogenous sources of free radicals (*e.g.* tobacco smoke, radiation, organic solvents, and pesticides). Free radicals and singlet oxygen can be beneficial because they act as effective killers of pathogenic organisms which normally invade the body. However, if there is an overproduction of these highly reactive species they can attack fatty acids in cell membranes, enzymes, nucleic acids, and endothelial cells. This may lead to cellular lyses, mutations and inflammation. These damages are correlated with ageing and chronic diseases, such as heart diseases, arteriosclerosis, age-related macular degeneration, and certain types of cancer.^{27, 31} Several studies show that diets containing carotenoids are correlated with a reduced risk of these pathological conditions.^{27, 32}

1.2.3 In medicine

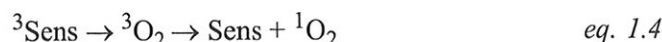
Vitamin A deficiency occurs in poorly developed countries and is treated with a dietary supplement of vitamin A.^{33, 34} Some other derivatives of retinoic acids are used for dermatological disorders such as psoriasis and eczema.³⁵ β,β -Carotene is effective in the treatment of erythropoietic protoporphyria, an illness where $^1\text{O}_2$ is produced via sensitization of free porphyrins accumulated in the skin.^{36, 37} The water-soluble carotenoid crocin (14) is effective in the treatment of arthritis in mammals³⁸, and aqueous ultramicroemulsions of xanthophyll esters have been developed for treatment of tumors.³⁹

1.2.4 In industry

Carotenoid-containing plant extracts have been used for coloring of food and feed for centuries. For example, the extracts from saffron, annatto, palm oil, and paprika make food yellow to dark red. Egg yolk, butter, cheese, salmon, trout, and chicken all get their colors indirectly from carotenoids.^{40,41} β,β -carotene (E160e) was the first synthetic carotenoid introduced as food colorant in 1954. Since then other carotenoids such as β -apo-8'-carotenoic acid ethyl ester (E 160f), β -apo-8'-carotenal (E 160e), canthaxanthin (E 161g), lycopene, and natural extracts of capsanthin and lutein have been approved for food use.^{40, 42, 43} β,β -carotene, β -apo-8'-carotenal, β -apo-8'-carotenoic acid ethyl ester, and canthaxanthin are used as feed additives, mainly for the pigmentation of egg yolk, plumage, and flesh of fowl.⁴⁰ In aquaculture, astaxanthin and canthaxanthin are added to the feed of salmon and trout.^{24, 44}

1.2.5 Antioxidant action of carotenoids

Reactive oxygen species, such as singlet oxygen, are most critical to biological systems.³¹ Singlet oxygen is formed in the presence of a sensitizer (Sens), e.g. chlorophyll, porphyrin, and bilirubin. Under light, Sens may be excited to its first excited state (1 Sens) and then undergo intersystem crossing (ISC) to a triplet state (3 Sens), see eq. 1.3 and eq. 1.4.^{25, 28}

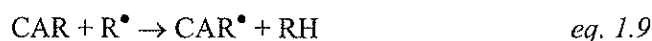


Quenching of singlet oxygen ($^1\text{O}_2$) is the best documented antioxidant property of carotenoids, and has especially been studied for β,β -carotene.^{36, 45-47} $^1\text{O}_2$ is highly reactive and capable of oxidizing nucleic acids, proteins, and unsaturated fatty acids. The quenching of singlet oxygen involves transfer of excited energy from $^1\text{O}_2$ to the carotenoids, resulting in a ground state oxygen ($^3\text{O}_2$) and a triplet excited carotenoid (^3CAR) (eq. 1.5). Carotenoids finally release the excess energy as heat via vibrational and rotational interactions with solvent (eq. 1.6).⁴⁷

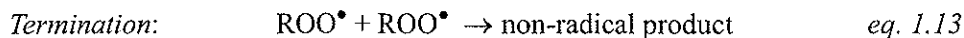
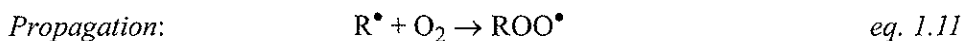
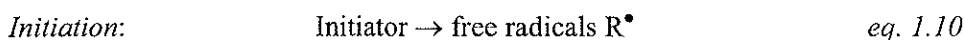


Each carotenoid molecule is estimated to quench about 1000 $^1\text{O}_2$ molecules.^{28, 47} The quenching rate constant increases with the number of double bonds in the polyene system, and varies with chain structure and functional groups.^{48, 49}

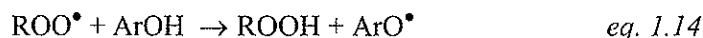
Carotenoids also effectively trap radical species. In theory, carotenoids can react with free radicals in three possible ways, *e.g.* by adduct formation (eq. 1.7), electron transfer (eq. 1.8), and allylic proton abstraction (eq. 1.9).²⁵



The prime targets for free radicals and singlet oxygen are the unsaturated fatty acids in cell membranes. Free radical and singlet oxygen attack of unsaturated acids may cause a loss in membrane fluidity, receptor alignment, and potential cellular lysis.³¹ Lipid peroxidation is a branching chain reaction, generally presented in the following three steps:



Mostly the initiator is hydrogen peroxide. ROO^\bullet and RH represent peroxy radical and hydrocarbon, respectively. Antioxidants can terminate lipid peroxidation in mainly two ways, by reacting with ROOH such as preventative antioxidants (*e.g.* the enzymes catalase and peroxidase) or by interfering with the chain propagation step, such as chain-braking antioxidants (*e.g.* vitamin E and superoxide dismutase). The conventional chain-braking antioxidants, such as vitamin E or other phenolic antioxidants, trap the peroxy radical ROO^\bullet by donating a hydrogen-atom, thus producing a resonance-stabilized aromatic radical (eq. 1.14).⁴⁵



Carotenoids are believed to act different. A suggested mechanism is an addition reaction between the carotenoid molecule and the peroxy radical, which produces a resonance-stabilized carbon centered radical (Figure 1.9 and eq. 1.7).^{28, 45} *In vitro* studies have verified that β, β -carotene is very reactive to peroxy radicals, but only at oxygen tensions below 150 mm Hg (the partial pressure found in most

tissues under physiological conditions) and lower concentrations. At high oxygen pressures, β,β -carotene loses its antioxidant activity and shows pro-oxidant properties. The carbon-centered radical (R-CAR \cdot) then reacts reversibly with oxygen to form a new peroxy radical, R-CAR-OO \cdot (see eq. 1.15). The new peroxy radical can initiate the process of lipid peroxidation (eq. 1.16, eq. 1.17). In addition, the concentration of carotenoids may effect their antioxidant properties. Carotenes such as β,β -carotene and lycopene exhibit a pro-oxidant character at high concentrations.^{27, 45} Carotenoid cation radicals, CAR $^{+\cdot}$ (eq. 1.8), have been formed *in vitro*, for instance in lipid membrane models.⁵⁰⁻⁵²

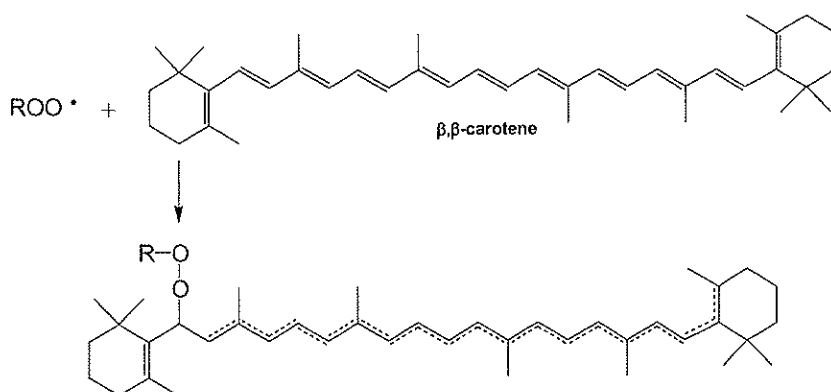
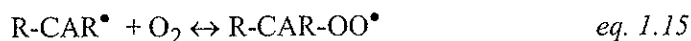


Figure 1.9 The formation of a resonance-stabilized carbon centered radical from trapping of a peroxy radical by β,β -carotene.



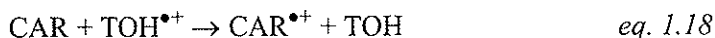
1.2.6 Antioxidant interactions

Carotenoids are only part of a large number of dietary and endogenous components that function as antioxidants in the human body.²⁹ Investigations of the antioxidant potential of carotenoids have mostly been performed *in vitro*; e.g. in organic solutions, micelles, or liposomes, and with individual carotenoids and radical species⁵³⁻⁵⁶ but indications of potent *in vivo* antioxidant activity are reported.⁵⁷ The action of carotenoids in living systems is much more complex.⁵⁸ Their function *in vivo* is dependent upon their chemical structure, but also from their localization and interaction with other antioxidants. The interaction of all of

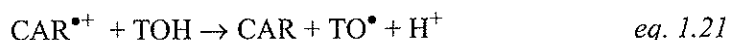
the digested antioxidant nutrients is responsible for the total antioxidant protection rather than one single antioxidant.⁵⁹ Many authors have discussed the effect of combination of various antioxidants.^{27, 60-63}

Selenium is a nutritional trace element, necessary for human health.⁶⁴ It is incorporated into selenoproteins as the amino acid selenocysteine serving as cellular antioxidants, and controlling the thyroid hormone T₃. Selenium is also important for the immune system.¹⁰ Selenium compounds, together with carotenoids have shown to inhibit carcinogenesis in rodents and humans.⁶⁵⁻⁶⁷ The combined application of selenium, β,β-carotene, and vitamin E have shown to reduce the risk of stomach cancer.³⁰

Vitamin E is the most important lipid-soluble antioxidant involved in the protection of biological membranes.⁶⁸ It is believed that β,β-carotene complements vitamin E in the protection of lipid tissues from peroxidation *in vivo*, in that β,β-carotene is actually more effective at lower oxygen pressures than vitamin E.^{45, 46, 58} Recently, it was reported that zeaxanthin in combination with ascorbic acid (vitamin C) and α-tocopherol (vitamin E) showed a synergistic protection of human retinal pigment epithelium cells against oxidation induced by photosensitizers.⁶⁹ Their synergistic interaction is thought to be a result of their different chemical properties and tissue localization. Vitamin C is water-soluble and traps peroxy radicals in the aqueous phase, *e.g.* in extracellular fluids such as plasma and cytosol. Carotenoids and vitamin E however, are present in the lipid phase of cell membranes.⁶⁸ Vitamin C enhances the activity of vitamin E by reducing the tocopheroxyl radicals.^{31, 68, 70} It has also been suggested that β,β-carotene can repair the vitamin E radical (TOH^{•+}) (eq. 1.18), while the resulting carotenoid cation radical (CAR^{•+}) is repaired by vitamin C (ASC-H),^{36, 70} shown by eq. 1.19 and eq. 1.20:



Contradictory reports show the opposite; α-tocopherol (TOH) can reduce carotenoid radical cations by the following reaction (eq. 1.21):



An antioxidant hierarchy was suggested, based on *in vitro* studies of the relative stability of tocopherol radicals and carotenoid radical cations:

a-tocopherol > lycopene > β,β -carotene > zeaxanthin > lutein > canthaxanthin > astaxanthin.

α -Tocopherol forms the most stable radical, while the astaxanthin radical is the less stable, hence, α -tocopherol can reduce carotenoid radical cations by the reaction in eq. 1.21.^{71, 72} However, the carotenoid radical cation has not yet been found *in vivo*.⁵⁰ Whether the individual carotenoid function as a scavenger of free radicals or as a recycler is probably dependent on chemical structure, chemical reactivity, concentration, oxygen pressure, site of radical generation, and localization in the cell membrane.^{36, 46, 72, 73}

1.2.7 Carotenoids in cell membranes

Carotenoids have been incorporated into phosphatidylcholine liposomes to imitate membrane biological systems.⁷⁴⁻⁷⁹ It was postulated that carotenoids may play a role as membrane stabilizers in bacteria, like cholesterol in eucaryotes.⁷⁴ β,β -carotene increases the freedom of motion of the lipid molecules in phosphatidylcholine membranes. The opposite, a rigidifying effect, is reported for bipolar carotenoids (xanthophylls) when incorporated in lipid membranes, shown by decreased water permeability, swelling properties, and increased hydrophobicity.⁷⁵⁻⁷⁸ An increase in hydrophobicity increases the energy required for small polar molecules (*e.g.* free radicals) to penetrate the membrane.⁷⁶

The cell membrane of thermophilic bacteria contain polar carotenoids, such as carotenoid glycoside esters. Carotenoid glycoside esters are believed to reinforce the membranes of thermophilic bacteria at high temperatures.^{80, 81} Additionally, their stabilizing effect on liposomes has been proved.⁸² The lengths of carotenoid molecules is similar to the thickness of a lipid bilayer. This suggests that they may stabilize both halves of a cell membrane.^{76, 81}

The xanthophyll pigments lutein and zeaxanthin are present in large amounts in the membranes of *macula lutea* of the human retina. Their role is still not fully understood, but they may filter short-wavelength (blue) light and protect the polyunsaturated lipids in the photoreceptor membranes against oxidative damage.⁸³ Lutein and zeaxanthin both act similarly in the protection against free radical attack in egg yolk membranes, but act differently upon UV exposure.⁸⁴ The reason may be a small difference in absorption and arrangement of the carotenoids in the membranes.⁸⁵

Non-polar carotenes, such as β,β -carotene, orient parallel to the membrane, thus lying in the hydrophobic core. On the other hand, the polar xanthophylls, such as the dihydroxy carotenoid zeaxanthin, orient antiparallel to the membranes, thus spanning the entire membrane (Figure 1.10).⁷⁷ Zeaxanthin can react with radical species entering from the aqueous phase, while the action of β,β -carotene and

other non-polar carotenoids are restricted to the hydrophobic core of the cell membrane. This may explain why β,β -carotene and zeaxanthin protect similarly against lipid peroxidation in organic solution, but differ in phosphatidylcholine liposomes. Zeaxanthin and β -cryptoxanthin are more effective against lipid peroxidation than β,β -carotene when the peroxy radicals are produced in the aqueous phase. This suggests that polar peroxy radicals probably migrate to the membrane surface. Therefore, zeaxanthin can act both as a membrane rigidifier and as an ideally localized antioxidant, effectively trapping the radicals entering the membrane surface.^{55, 79}

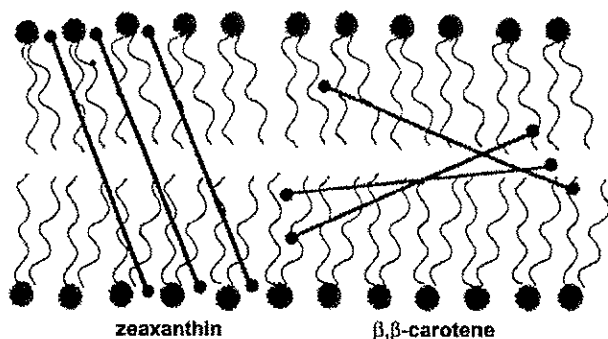


Figure 1.10 Schematic drawing of a lipid membrane with incorporated β,β -carotene and zeaxanthin (from ref. 36).

1.3 Absorption, metabolism, and transport of carotenoids

Although carotenoids have beneficial health effects and have been considered as safe, nutritious, and food additives for decades^{30, 40, 86, 87} many questions still remain regarding absorption, metabolism, and transport of carotenoids to tissues. However, it is known that carotenoids in general, are poorly absorbed by human and animals. Less than 17% of the β,β -carotene dose is absorbed by the intestine cells in humans. Before absorption, the ingested carotenoids must be released from the food matrix, where they are associated with proteins. This is carried out by digestive enzymes. The carotenoids are then dispersed in lipid emulsions and solubilized by bile salts to micellar particles, transported through the unstirred water layer (UWL) adjacent to the microvillus surface. The intestinal uptake of carotenoids from the micelles is believed to occur by passive diffusion. The carotenoids are further incorporated into chylomicrons and transported through lymph and blood (see Figure 1.11).⁸⁸⁻⁹⁰ The most abundant carotenoids in human plasma are lutein, zeaxanthin, β -cryptoxanthin, lycopene, α -carotene, and β,β -carotene, but many more are present in less amounts.⁹¹ Lipoprotein lipase effectively breaks down the chylomicrons, and the remnants are taken up by the

liver and other tissues. Some of the absorbed carotenoids are resecreted from the liver and carried by lipoproteins (LDL and HDL) to reach other tissues. Carotenoids are found in almost all tissues, but they are mostly distributed to the liver and adipose tissues.^{88, 89, 92}

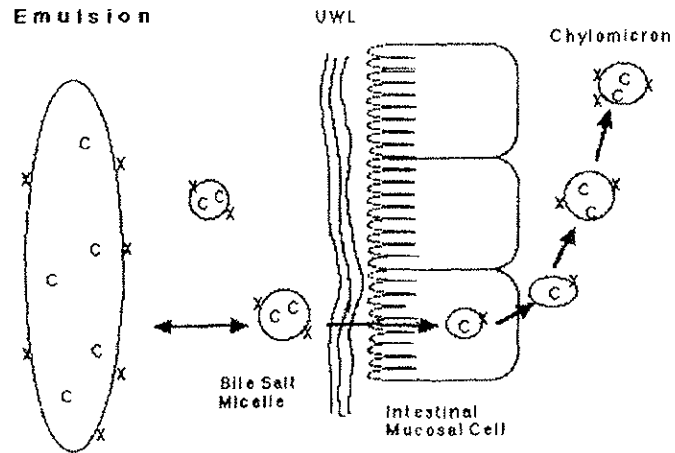


Figure 1.11 Intestinal uptake of carotenoids; from lipid emulsion in the small intestine to bile salt micelles, through the unstirred water layer (UWL) and enterocytes, with incorporation into chylomicrons. Nonpolar carotenes (c) are thought to be located in the hydrophobic core of lipid emulsions, bile salt micelles, and chylomicrons, while polar xanthophylls (x) are more likely surface components (*from ref. 90*).

Digestion and absorption are affected by dietary factors.^{89, 92} Carotenoids are better absorbed from micellar solutions, commercial beadlets, or in oil than from foods such as raw vegetables and tomato juice. Absorption of carotenoids from raw vegetables is highly improved after heating and grinding.^{90, 92} This effect was shown for lycopene, where the bioavailability of lycopene was better from tomato paste than from fresh tomatoes.⁹³ Absorption of carotenoids are enhanced when ingested with fat.⁹² Dietary fat was found to improve the absorption of β , β -carotene from green leafy vegetables in children.⁹⁴ Xanthophylls such as lutein, zeaxanthin, and β -cryptoxanthin occur in food as esters of long-chain fatty acids and are hydrolyzed to the more polar form before absorption.

The physical properties of carotenoids may also affect their absorption. It is believed that polar carotenoids are more efficiently absorbed than carotenes.⁹⁰ Contact between the lipid micelles and the mucosal cells of the duodenum is

important for carotenoid absorption.⁹² Since polar carotenoids most likely orient themselves at the micelle surface (see Figure 1.11), they get better contact with the hydrophilic surface of the duodenum, facilitating better absorption.

Additionally, the distribution among the lipoproteins is determined by the physical properties of the carotenoids.⁸⁹ Non-polar carotenes are mainly carried in low-density lipoproteins (LDL), while the polar xanthophylls are equally distributed between LDL and high-density lipoproteins (HDL). Since HDL contains more phospholipids than LDL, and LDL contains more triglycerides than HDL, polar carotenoids accumulate at the phospholipid surface, and carotenes in the triglyceride core.^{95, 96} This was evidenced by an *in vitro* study of carotenoids in biological emulsions.⁹⁷ The consequences of the different distribution are still not clear.⁹² Dietary capsanthin accumulates in appreciable amounts in human plasma lipoproteins, with a preference for HDL. The clearance of capsanthin in blood plasma after ingestion of parika juice was much faster than that of lycopene, indicating an increased metabolism of this polar carotenoid.⁹⁶

The interest in metabolism of carotenoids is due to their provitamin A function as well as their potential role in the prevention of chronic diseases.⁹⁰ Naturally, the predominant focus has been the transformation of β,β -carotene into retinol (vitamin A)⁹², mainly because of this vitamin's role in vision (see Figure 1.12 for further details).⁹⁸ Several pathways have been proposed for the biotransformation of β,β -carotene and other provitamin A carotenoids to vitamin A.^{89, 92} One pathway is the central cleavage by β -carotenoid-15,15'-dioxygenase, an enzyme localized in the intestine. It is specific for the central double bond, but can also cleave other carotenoids or apo-carotenoids with at least one β -ionone ring (*e.g.* β -cryptoxanthin and β -apo-8'-carotenal).⁹⁹ From β,β -carotene this pathway yields two molecules of retinal which is reduced to retinol. Retinol is transported in blood by a specific retinol-binding protein, and transported to the tissues or stored in the liver as retinylesters. Another model of the biotransformation of provitamin A carotenoids is an asymmetric cleavage to β -apo-8'-carotenal which is further cleaved into other β -apocarotenoids (*e.g.* β -apo-10'-carotenal, β -apo-12'-carotenal) or retinal and retinylesters (Figure 1.12).⁴⁰

Not much is known about the metabolism of carotenoids other than β,β -carotene in humans. The ethyl ester of β -apo-8'-carotenoic acid is absorbed, but is not metabolized, while β -apo-8'-carotenal is actively metabolized in the intestine, converted to the corresponding acid, alcohol, or palmitate ester. Recently, it was suggested that oxidative cleavage reactions occur with any carotenoid with a polyene chain system¹⁰⁰, meaning that any carotenoid could be metabolized in the body. Nevertheless, absorption, metabolism, and plasma transport are affected by structural differences and physical properties among the individual carotenoids.^{88, 92}

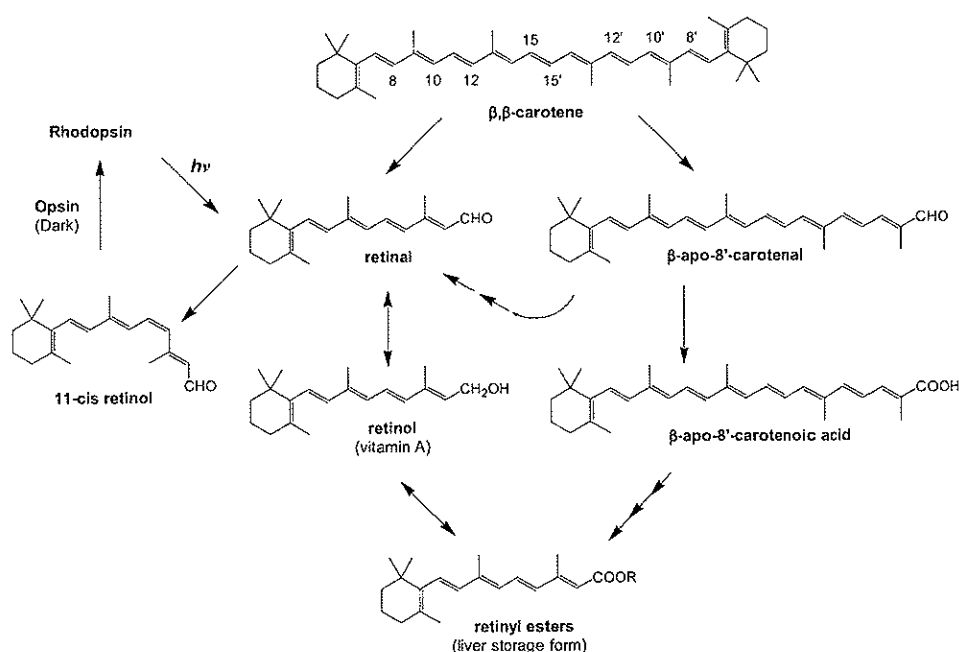


Figure 1.12 Bioconversion of β,β -carotene to retinol* (vitamin A), β -apocarotenoids and retinylesters.
 (*Retinol is oxidized to retinal, then isomerized to the biologically active 11-*cis* retinal, which reacts with the protein opsin to form rhodopsin. Rhodopsin absorbs light, transforming the *cis* double bond to *trans*, which in turn triggers a nerve impulse in the eye⁹⁸).

1.4 Industrial synthesis of carotenoids

The first industrial production of β,β -carotene began in 1954. Hoffman-La Roche and BASF AG are today the two major industrial producers of chemically synthesized carotenoids. They produce 8 different carotenoids, β,β -carotene, canthaxanthin, astaxanthin, lycopene, (*R,R*)-zeaxanthin, and the apocarotenoids β -apo-8'-carotenal, β -apo-8'-carotenoic acid ethyl ester and citranaxanthin.¹⁰¹ The total annual sale in 1995 was about US \$300 millions, most of the carotenoids are used as food and feed additives. Current market prices (1995, US \$ per kilo) were 600 for β,β -carotene, 900 for β -apo-8'-carotenoids, 1300 for canthaxanthin and 2500 for astaxanthin.¹⁰² The worldwide carotenoid market is estimated to reach US \$935 millions by 2005.¹⁰³

A significant source of lutein and zeaxanthin produced for the pigmentation of poultry and egg yolk is Marigold extracts. Carotenoids are also being produced by biosynthetic methods, utilizing microalgae. Micro Gaia Inc. and Cyanotech Corp.,

Hawaii both produce astaxanthin by the green microalgae *Haematococcus pluvialis*. This microalgae is believed to be the world's richest known source of astaxanthin (30,000 mg or more per kilo dry weight).¹⁰⁴ β,β -Carotene, under appropriate conditions, can be produced in large amounts by the two strains of the algae *Dunaliella* (*D. bardawil* and *D. salina*). Betatene Ltd., Australia produces crystalline β,β -carotene by growing *D. salinas* in lakes covering a total area of 300 hektars.¹⁰⁵ Simultaneous production of β,β -carotene, glycerol and algae meal are effected by the cultivation of *D. bardawil* in Israel (Nature Betatene Technologie, Ltd.). The content of β,β -carotene may reach 50-90 mg per gram dry weight of algae.^{106, 107}

The production of carotenoids by genetic engineering through cloning of bacterial genes represents an alternative approach in producing natural or novel carotenoids. By incorporation of carotenoid-producing genes from different parent organisms into *E. coli*, new carotenoids (e.g. C₄₅ and C₅₀ carotenoids) were biosynthesized, which are not found in the organisms where the parent genes came from.^{108, 109}

It is most likely that the production and application of carotenoids in cosmetics, medicine, as food and feed colors, as drug additives, and other applications will continue to increase in the future.

1.5 Water-dispersible/soluble carotenoids

1.5.1 Naturally water-dispersible/soluble carotenoids

Generally, hydrophilicity is imparted by hydrophilic substituents of the carotenoids. To date 732 naturally occurring carotenoids are listed.¹¹ Only a few of these are described as water-soluble* carotenoids, like the diacids crocetin (**15**) and norbixin (**16**), shown in Figure 1.14, and the sugarester crocin (**14**) (Figure 1.14). Norbixin is a saponification product of bixin, extracted from the annatto tree, *Bixa orellana*. The water-dispersible/soluble preparations consist mainly of norbixin, and are used for the coloring of cheese, cereals, and ice cream.¹¹⁰

*. In this work we understand water-solubility to mean a predominance of monomers in aqueous carotenoid solutions, and water dispersibility to mean a predominance of aggregates in aqueous carotenoid solutions.

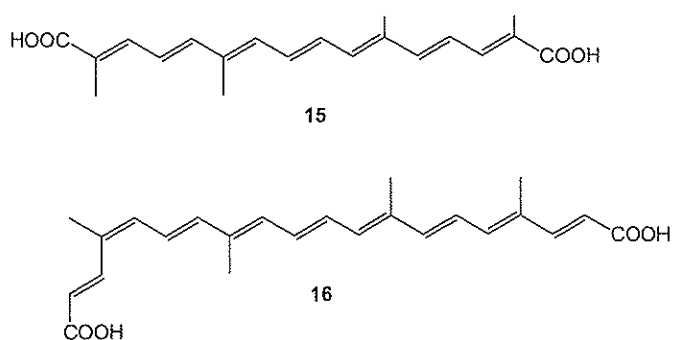


Figure 1.13 Water-dispersible carotenoid diacids; crocetin (**15**) and norbixin (**16**).

Crocetin (**14**), the di-gentobiose ester of crocetin (**15**), is found in saffron (*Crocus sativus*),^{11, 110} and other plants.¹¹¹ In ancient times saffron was used as a cosmetic, specifically for coloring womens' skin, and as a medication against chest pains, plague, and for relieving coughs.¹¹² This water-soluble carotenoid is now used as a colorant in beverages and food such as risotto and curry.¹¹⁰

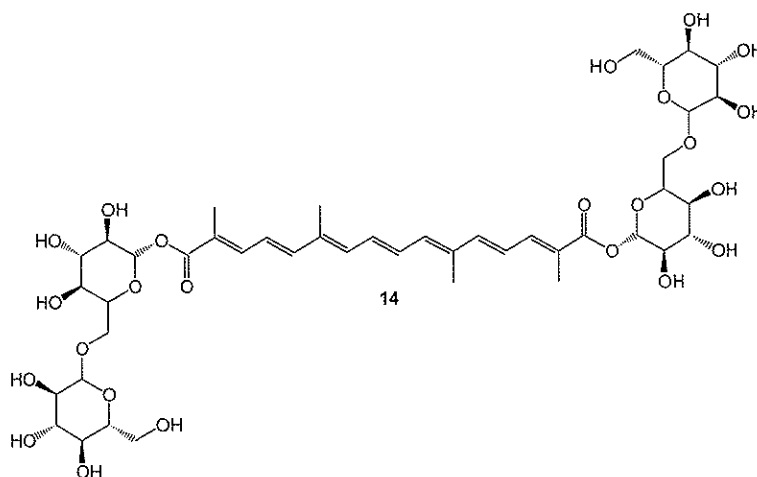


Figure 1.14 The water-soluble sugarester crocin (**14**), the major pigment in saffron.

Several other glycosyl esters of crocetin have been identified. Mono-, di-, and mixed esters of glucose, the disaccharide gentobiose, and the trisaccharide neapolitanose (e.g. crocetin dineapolitanosyl ester (**17**), Figure 1.15) have been

isolated. Glucosylesters of a C_{30} -dicarboxylic acid (e.g. diapolycopenedioic acid diglucosyl ester (**18**), Figure 1.15) were found in bacteria (e.g. *Methylobacterium rhodinum*).^{11, 111}

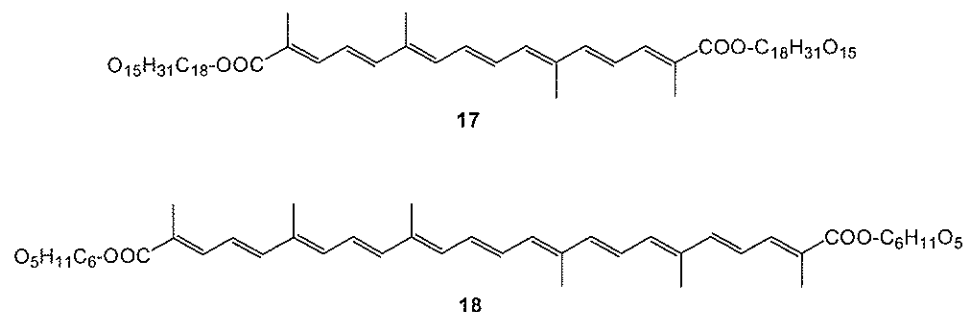


Figure 1.15 Naturally occurring carotenoid glycosyl esters; crocetin dineapoltanosyl ester (**17**) and dipolycopenedioic acid diglucosyl ester (**18**).

The carotenoid sugar ethers (carotenoid glycosides), are structurally related to the carotenoid glycosylesters. They have been extracted mainly from bacteria and blue-green algae.^{11, 111} One example is astaxanthin glucoside (**19**), see Figure 1.16. The occurrence of water-soluble carotenoid glycosides and glycosyl esters other than crocin is probable but not reported.^{113, 114}

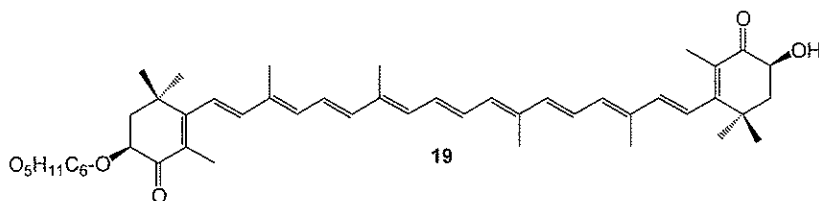


Figure 1.16 A carotenoid glycoside; astaxanthin glucoside (**19**).

Another hydrophilic class of carotenoids are the carotenoid sulfates, extracted from various marine microorganisms, bacteria, and sponges. About 12 naturally occurring carotenoid sulfates have been detected (e.g. bastaxanthin (**20**) and ophioxanthin (**21**), Figure 1.17)^{11, 115, 116} Incorporation of the ionized sulfate group gives carotenoids a strongly polar character and unusual solubility properties. However, the degree of water-dispersibility/solubility is low^{113, 116, 117} and consequently, the carotenoid sulfates have not found commercial interest.

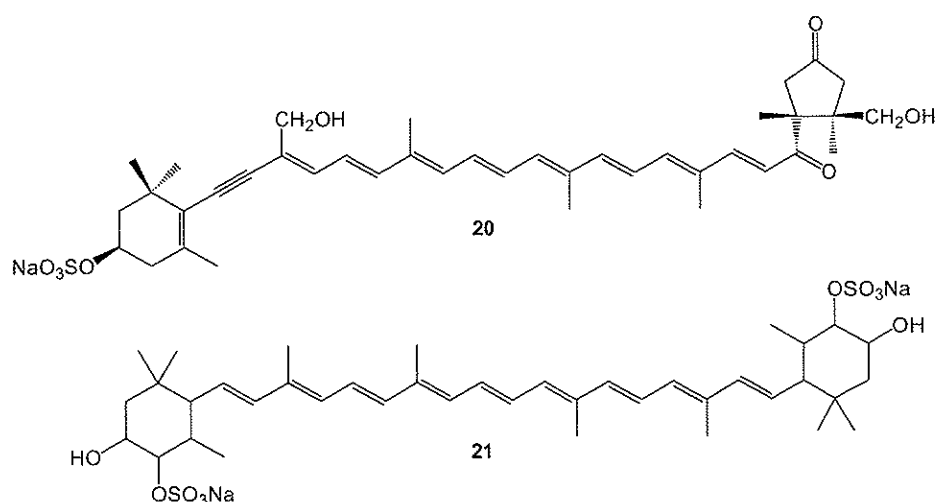


Figure 1.17 Carotenoid sulfates, bastaxanthin C (20) and ophioxanthin (21).

1.5.2 Water-dispersible/soluble carotenoids by inclusion and additives

The fact that free carotenoids are generally not soluble in water and poorly soluble in fats and oils limits their use. Water-dispersible/soluble carotenoids are utilized not only for use in feed or foodstuff, but also as drug additives,¹¹⁸ in nutrition,¹¹⁹ and in cosmetic and pharmaceutical products.¹²⁰⁻¹²² In addition, water-dispersible/soluble carotenoid formulations are useful in studies of *in vitro* cell supplementation.¹²³

Although nearly all of the natural carotenoids are lipophilic, they are present in aqueous systems in nature. This is a result of their association with lipid-protein complexes. For example, the colors of carrots, oranges, and tomatoes arise from finely dispersed carotenoids present as complexes with proteins or lipoproteins.¹²⁴⁻¹²⁶ Such chromophore-protein interactions are also responsible for the green, purple, and blue colors of marine invertebrates.^{125, 127} A well-known example is the blue-green color of the lobster *Homarus gammarus* formed by the astaxanthin-protein complex crustacyanin. The sudden colorshift of lobsters to red upon cooking has fascinated scientists for more than 50 years.^{128, 129} The interest might have been the result of the demand for water-soluble, natural blue pigments as food colorants.¹³⁰ In contrast to free carotenoids, the carotenoid-protein complexes are soluble in aqueous buffered solutions.¹³¹ Other water-dispersible/soluble carotenoproteins have been isolated from cyanobacteria, starfish, mango, and carrots.¹³²⁻¹³⁴

Carotenoproteins perhaps inspired the inclusion of carotenoids into macromolecules such as β -cyclodextrin (Figure 1.18), which improves water-dispersibility/solubility significantly.^{120, 135-137} Cyclodextrins are cyclic oligosaccharides formed by the enzymatic cyclization of starch. They are built up by six, seven, or eight α -D-glucopyranose units, forming a cone-shaped structure, with a non-polar interior and a polar exterior. These structural features give the polymer water-solubility with the ability to transport non-polar materials.¹³⁸ Inclusion of β , β -carotene has been confirmed by NMR.¹³⁹ Astaxanthin was much more water-dispersible/soluble after complexation with a highly water-soluble sulfobutyl ether of β -cyclodextrin (Captisol®).¹³⁵ The pigmentation of salmon was enhanced by incorporation of an astaxanthin-cyclodextrin complex in fish feed.¹⁴⁰

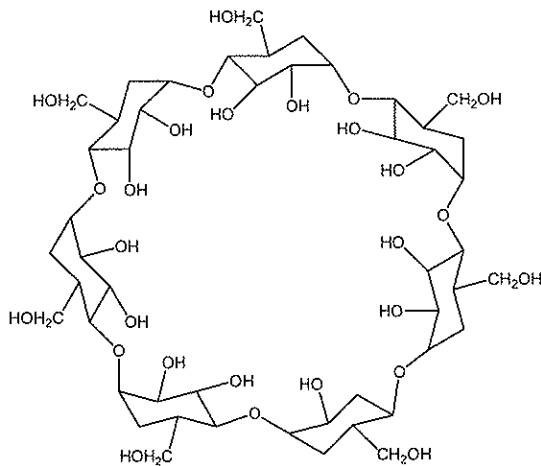


Figure 1.18 β -cyclodextrin is formed by seven α -D-glucopyranose units.

Water-soluble or water-dispersible carotenoid formulations have also been made by dispersing carotenoids into macromolecules like polyethylene glycol,¹⁴¹ dextran,¹⁴¹ lignin,¹¹⁹ albumin,¹⁴² and gelatin.¹⁴³

Coloring properties, absorbability, and bioavailability are improved by reducing the carotenoid particle size.^{41, 144} Emulsification and grinding of oily solutions of carotenoids give preparations with particle sizes in the range of 1-5 μm ,^{145, 146} which is sufficient for the coloring of fat-based food.¹⁴⁶ So-called "beadlets", which are spray-dried micro-colloidal oily dispersions of canthaxanthin, β -apo-8'-carotenal, or β , β -carotene, were developed for use in water-based food in the 1950's.^{42, 126} By further reduction of the particle size by various micronization processes, the coloring properties and probably also the bioavailability increase.¹⁴⁶ For use in aqueous solutions, one needs to reduce the particle size to

below 1 μm . Therefore, other elaborate methods are used. To obtain particle size distribution in the nanometer size range, the mixing chamber was developed for micronization,¹⁴⁵⁻¹⁴⁷ Figure 1.19.

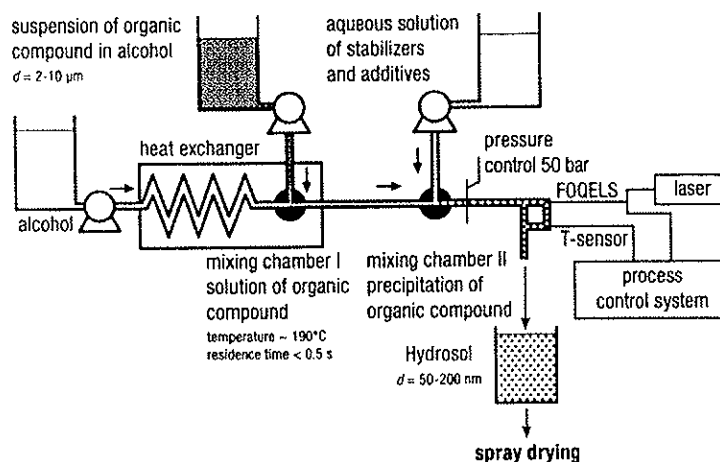


Figure 1.19 Scheme of the micronization process for the preparation of nanoparticle sized carotenoid hydrosols (from ref. 147).

Micronization is a continuous two-step process consisting of the dissolution and a controlled precipitation of the particular carotenoid. A molecularly dispersed solution of a carotenoid in alcohol (or another water-miscible solvent) is obtained in a mixing chamber at ca 200°C for 0.5 sec. In a second mixing chamber, containing an aqueous solution with a polymer stabilizer, e.g. gelatin, the precipitation generates fine hydrosol nanoparticles (Figure 1.20). The growth of the carotenoid nanoparticles, in the range of 50-200 nm, is induced by the changes in the solvent and the temperature drop. The polymer, a hydrophilic matrix, serves as a protective shield for the carotenoid against oxidation and preventing agglomeration. The hydrosol particles are concentrated and transferred to dry powders normally by spray-drying and can be used directly for the coloring of beverages.¹⁴⁵⁻¹⁴⁸ The colors are not only dependent upon the carotenoid polyene chain, but also on particle size and agglomeration behavior of the powders.¹⁴⁹

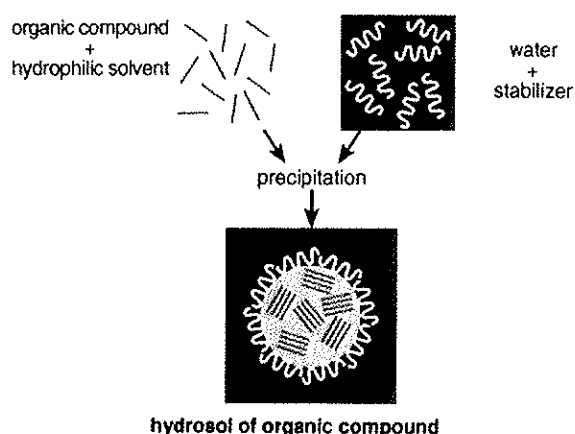


Figure 1.20 Principle of the preparation of organic hydrosol nanoparticles (from ref. 147)

The colors obtained from natural or synthetic carotenoids such as canthaxanthin, β -apo-8'-carotenal, β,β -carotene, lutein, and astaxanthin range from yellow to dark red, depending on the concentrations and formulation methods used. There have been continuous efforts to develop new formulations, basically to obtain new shades of colors. Light yellow colored water-soluble preparations for food use was obtained from crocetin diesters.¹⁵⁰ Addition of an organosulfur compound (*e.g.* cysteine) to formulations of carotenoids such as β,β -carotene, β -apo-8'-carotenal, and canthaxanthin tuned the colors to darker red, due to a bathochromic shift of the carotenoid absorption maxima in the UV/VIS spectrum.¹⁵¹ Similarly, a complexation of norbixin to a protein led to a color change from orange to magenta.¹⁵²

1.5.3 Water-dispersible/soluble carotenoid derivatives by synthesis

To prepare water-dispersible formulations, it is necessary to add stabilizers (*e.g.* gelatin) and emulsifiers (*e.g.* ascorbyl palmitate) and then to heat the carotenoid mixtures at high temperatures (Figure 1.19). Attaching hydrophilic substituents to carotenoids is an alternative pathway to obtain water-soluble or water-dispersible carotenoids. Not all polar substituents give rise to hydrophilic carotenoids. Salts of enolized β -diketones (partial structure **a**) and diosphenols (partial structure **b**) (Figure 1.21) exhibit limited water-solubilities.¹¹³

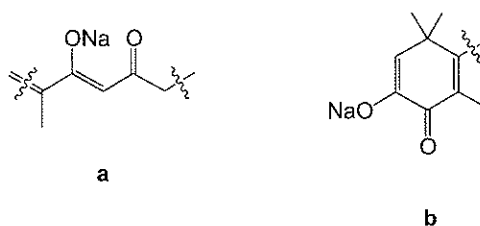


Figure 1.21 Partial structures of salts of enolized β -diketones (a) and diosphenols (b)

Also one or more hydroxy moieties do not give sufficient water-dispersibility/solubility.¹¹³ The carotenoid monoglyceride **22a** (Figure 1.22) synthesized by esterification of β -apo-8'-carotenoic acid with glycerol¹⁵³ did not show a significant water-dispersibility.

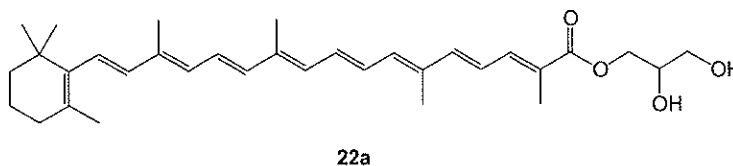


Figure 1.22 Carotenoid monoglyceride **22a**.

The first carotenoid sulfate was isolated in 1981.¹⁵⁴ Since then about 22 carotenoid sulfates have been synthesized (*e.g.* zeaxanthin disulfate (**23**), Figure 1.23).^{116, 117} Introduction of a sulfate group to carotenoids gives low water-dispersibility (up to 0.4 mg/ml).^{113, 116, 117}

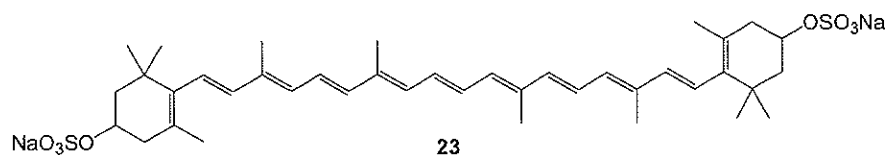


Figure 1.23 Zeaxanthin disulfate (**23**).

Also the vitamin C-carotenoid **24** obtained from esterification of ascorbic acid with β -apo-8'-carotenoic acid exhibits only low water-dispersibility (0.5 mg/ml).¹⁵⁵

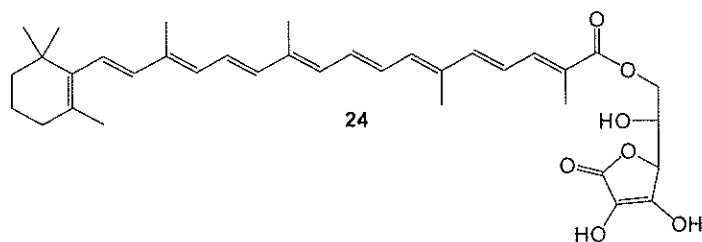


Figure 1.24 Vitamin C carotenoid ester **24** from reaction of ascorbic acid with β -apo-8'-carotenoic acid.

Lipophilic compounds (e.g. α -tocopherol) with practical water-solubility have been achieved by introducing sugar moieties.¹⁵⁶ Possible water-soluble carotenoid glycosylesters **25** and **26** (Figure 1.25) of β -apo-8'-carotenoic acid were synthesized as potential additives in food and pharmaceuticals. However, the solubilities were not reported.¹⁵⁷

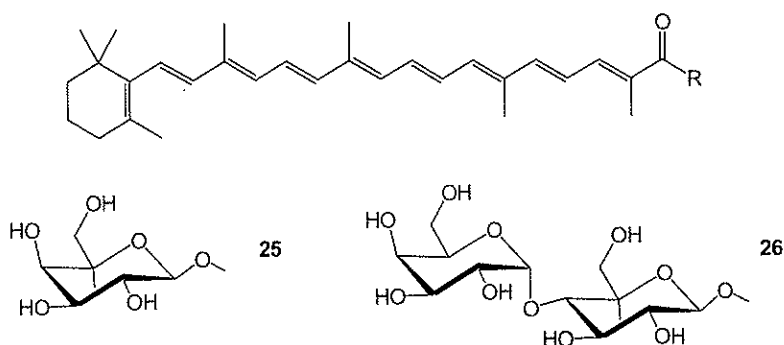


Figure 1.25 Glycosyl esters **25** and **26** synthesized from β -apo-8'-carotenoic acid esterified with β -D-galactose and β -D-maltose, respectively.

Water-soluble/dispersible, artificial pyridinium carotenoids **27** and **28** (Figure 1.26) and a glycoside amide carotenoid **29** (Figure 1.27) were obtained merely by accident as "by products" in the synthesis of "electron wires", in model vesicle membranes. Compounds **28** and **29** are both derivatives of bixin. No values for water-dispersibility/solubility were reported.¹⁵⁸⁻¹⁶⁰

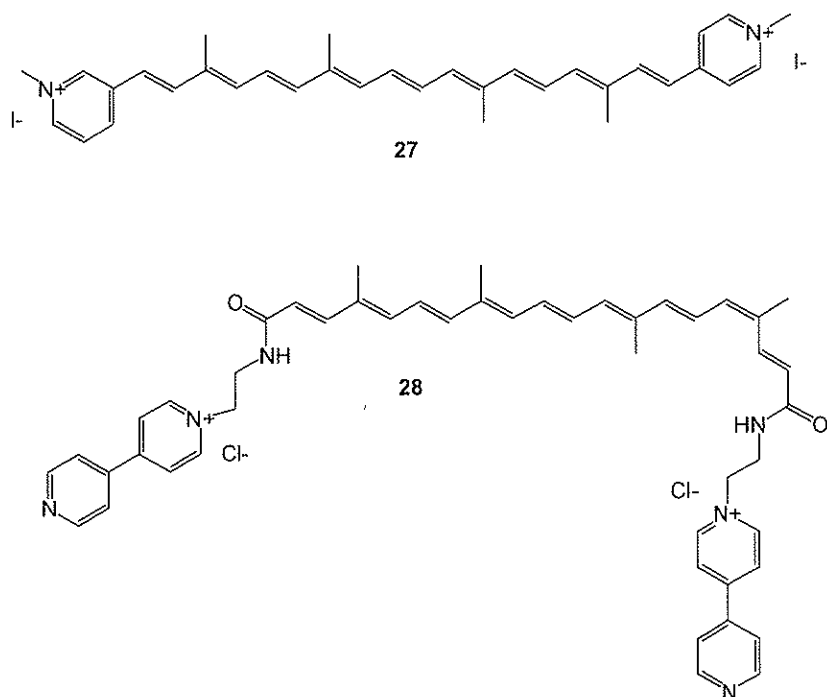


Figure 1.26 Water-soluble/dispersible pyridinium carotenoids **27** and **28**.

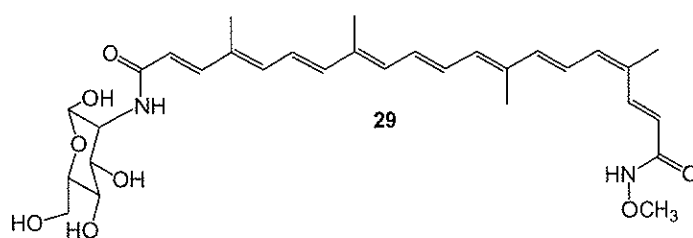


Figure 1.27 A water-soluble/dispersible glycoside amide carotenoid **29**.

The disodium dissuccinate astaxanthin derivative (CardaxTM) (**30**) and the tetracationic astaxanthin-amino acid conjugate **31** synthesized by Hawaii Biotech, Inc. are highly water-dispersible. The reported water-dispersibilities of these novel carotenoid derivatives **30** and **31** were 9 and 182 mg/ml, respectively.^{161, 162}

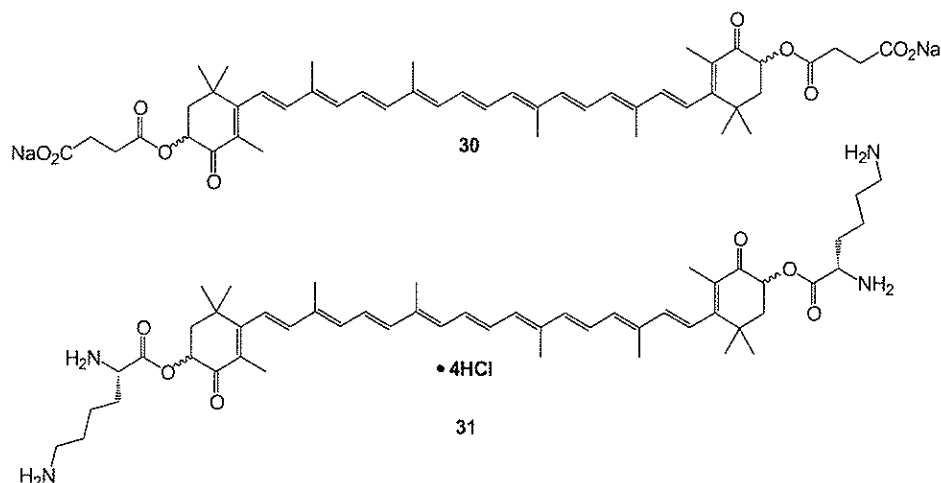


Figure 1.28 Disodium salt of a disuccinate diester (CardaxTM) (30) and tetrahydrochloride salt of a dilysinate diester of astaxanthin 31.

High water-dispersibility or water-solubility allow for aqueous delivery of carotenoids both *in vitro* and *in vivo*. This could enhance their potential clinical utility as chemopreventive agents against cancer and heart diseases. The disodium disuccinate diester of astaxanthin (CardaxTM) (30) showed an increased bioavailability in rodents after oral administration of the compound in a lipophilic emulsion.¹⁶³ The highly hydrophilic astaxanthin-amino acid conjugate 31 and CardaxTM (30) were both potent aqueous-phase scavengers of superoxide anion ($O_2^{\cdot-}$) *in vitro*.^{162, 164} CardaxTM (30) also showed an upregulation of connexin 43 protein and an increased gap junctional communication *in vitro*, both indicating possible potent cancer chemopreventive properties *in vivo*.¹⁶⁵ An animal study of rats dosed with CardaxTM (30) prior to induced heart infarction, showed a significant correlation between reduced infarct size and plasma-levels of non-esterified, free astaxanthin.¹⁶⁶

Hydrophilic, water-dispersible, or water-soluble carotenoid derivatives may represent the “new generation” of carotenoids. Their polar character is similar to the naturally occurring xanthophylls, hence, they can interact easier with the polar free radicals entering from the aqueous phase. Their hydrophilicity may give a broader application to carotenoids, both as therapeutic agents and as additives in food, feed, and cosmetics.

1.6 Multifunctional carotenoid derivatives

Modifying carotenoids by connecting new types of substituents to their polyenic chains will give rise to new carotenoid derivatives. Depending on the substituent used, it is possible to design a compound that exhibits new properties^{156, 160} or possesses multifunctional activity.¹⁶⁷ In the last two decades, several new carotenoid derivatives have been developed, based on these ideas.^{14-21, 153, 155, 168-173}

By direct attachment of two antioxidants, it is possible to combine their biological and physiological properties. Polyunsaturated fatty acids are known for their beneficial health effects¹⁷⁴, but also their limited practical use due to their high susceptibility to autooxidation.¹⁷⁵ Industrial applications of carotenoids are also restricted because of their rapid degradation when exposed to air, heat or light.¹⁶⁸ Addition of antioxidants like vitamin E, ascorbic acid and BHT are common methods to inhibit degradation of polyunsaturated fatty acids and carotenoids.¹⁷⁶⁻¹⁷⁸ This method may not be effective, since the antioxidant and the fatty acids or carotenoids have different physical properties.¹⁶⁸ Alternatively, by linking the molecules they are brought closely together. This will increase their contact and may enhance their activity. Eicosapentaenoic acid (EPA, C20:5) and docosahexaenoic acid (DHA, C22:6) were esterified with ascorbic acid in order to design stable polyunsaturated fatty acids.¹⁷⁵ The same method was used for the carotenoids β -apo-8'-carotenoic acid, bixin and norbixin (see Figure 1.24 and Figure 1.29 for examples).^{155, 168}

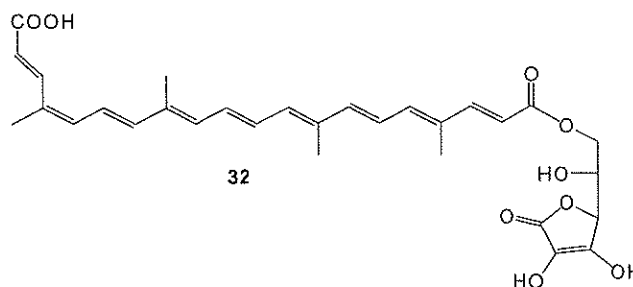


Figure 1.29 32: norbixin linked to ascorbic acid.

Three naturally vitamin E-carotenoids (e.g. pitosporumxanthin B (**33**)) have been isolated from plants.¹¹ A synthetic vitamin E-carotenoid **34** was obtained by a direct linkage of β -apo-8'-carotenoic acid to α -tocopherol, Figure 1.30.¹⁶⁹

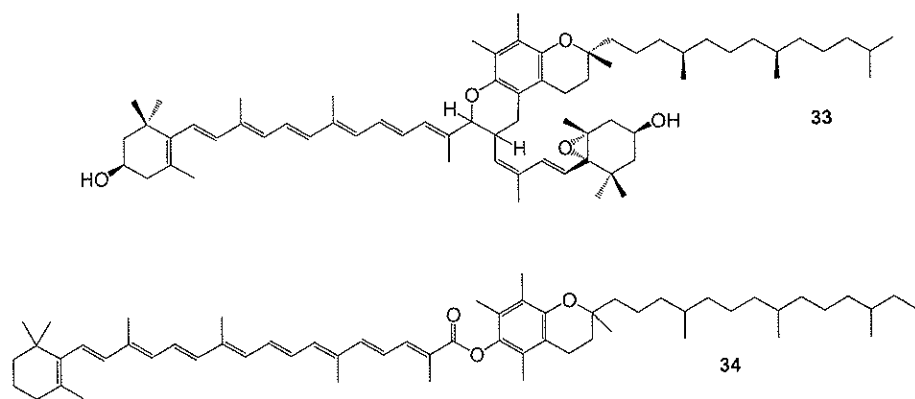


Figure 1.30 A natural (33) and a new, synthetic (34) vitamin E-carotenoid.

Other multifunctional carotenoids were obtained from esterification of β -apo-8'-carotenol with trolox (a water-soluble vitamin E derivative) and BHT (Figure 1.31).¹⁷⁰

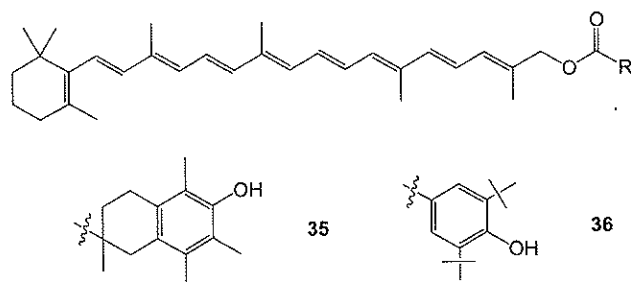


Figure 1.31 Examples of new multifunctional carotenoid derivatives; 35: β -apo-8'-carotenol linked to trolox and 36: BHT.

Another approach in designing new derivatives of bioactive compounds is to incorporate the bioactive moieties into naturally occurring carrier molecules, such as glycerol and phospholipids.^{153, 169, 171, 172, 179} A stable, highly unsaturated fat (37) (Figure 1.32) was obtained by connecting β -apo-8'-carotenoic acid and an unsaturated fatty acid ($C_{18:2}$). This polyfunctional carotenoid derivative 37, in which the antioxidant moiety potentially can protect the unsaturated fatty acid, may be more easily absorbed as a triglyceride,¹⁵³ a class of important fats in human nutrition.¹⁸⁰

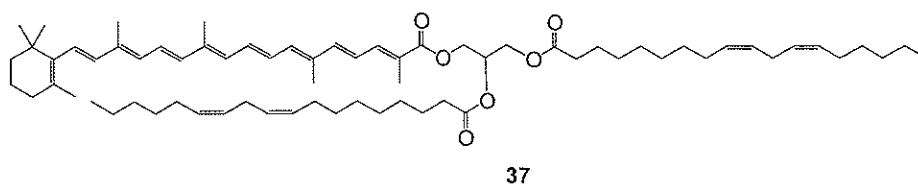


Figure 1.32 A stable, highly unsaturated fat (**37**).

Mixtures of antioxidants (e.g. selenium, β , β -carotene, vitamin E) are available as food supplements. Glycerol can serve as an excellent tool to link such bioactive compounds together. A triantioxidant (**38**) was synthesized by connecting β -apo-8'-carotenoic acid, selenacapyloic acid, and trolox to produce a triglyceride (Figure 1.33).¹⁷¹ A seleno fatty acid and a seleno fatty alcohol were also connected with β -apo-8'-carotenoic acid by esterification using glycerol (Figure 1.33).¹⁷²

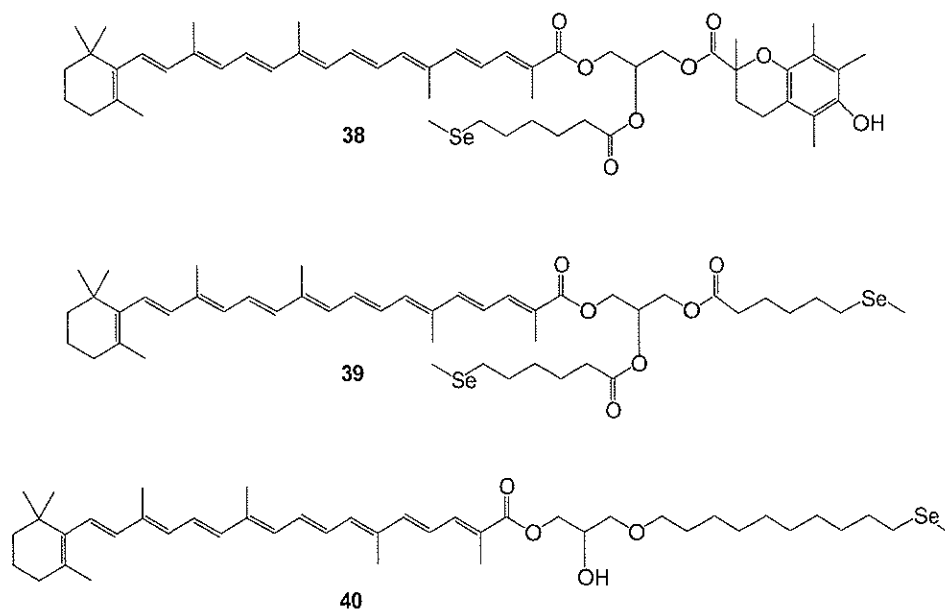


Figure 1.33 β -apo-8'-carotenoic acid, selenacapyloic acid, and trolox were combined to produce a triantioxidant (**38**). A seleno fatty acid and a seleno fatty alcohol were combined with β -apo-8'-carotenoic acid by esterification using glycerol, to obtain the glycerides **39** and **40**, respectively.

Synthetic combinations of antioxidants may also increase the chemopreventive activity of the individual compounds due to synergistic effects. The triantioxidant compound **38** revealed in a DPPH (1,1-diphenyl-2-picrylhydrazyl) radical test an additive effect consisting of the quenching activity of both the carotenoid and trolox (the test was not sensitive to the selenium moiety).¹⁷¹ The caro-trolox antioxidant behavior during oxidative light exposure was slightly better than of the carotenoids β,β -carotene, β -apo-8'-carotenoic acid, and ethyl β -apo-8'-carotenoate.¹⁷⁰

1.7 Phospholipids

Phospholipids are found in all living organisms and are the major constituents of cell membranes and membranous organelles. Among the enormous variety of phospholipids existing in nature, the phosphatidylcholines are most studied.^{181, 182} Phosphatidylcholines were discovered by the French chemist Gobley around 1850. Gobley isolated a phosphorus-containing lipid from egg-yolk and named it lecithin (from the Greek word for egg yolk, *lekithos*). Gobley obtained glycerophosphoric acid and fatty acids from the lipid while Strecker and Diakanow isolated choline. Lecithin and phosphatidylcholine are two trivial names for the same compound, 1,2-diacyl-*sn*-glycero-3-phosphocholine, Figure 1.34.¹⁸³

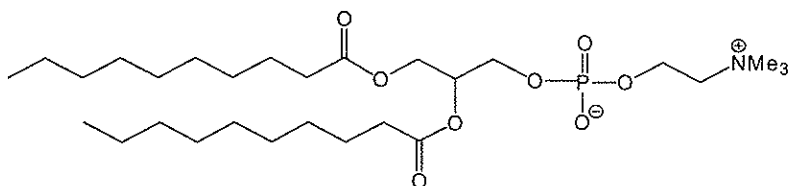


Figure 1.34 1,2-didecanoyl-*sn*-glycero-3-phosphocholine (diacylphosphatidylcholine).

Phosphatidylcholine and phosphatidylethanolamine dominate quantitatively amongst the many classes of phospholipids.¹⁸⁴ Most phospholipids have two aliphatic chains, and a polar or a zwitterionic head group, while lysophospholipids have a single aliphatic chain.¹⁸² Lysolecithins are intermediates in the metabolic pathways of lecithins. They have one free glycerol hydroxyl at either *sn*-1 or *sn*-2, thus they are 1- or 2-acyl-*sn*-glycero-3-phosphocholines, see Figure 1.35. Lysolecithins also occur in tissues, though in smaller amounts than lecithin.¹⁸³ They are more water soluble and have higher surface activity (see Chapter 3.5) than their parent diacylphosphatidylcholines.¹⁸⁵⁻¹⁸⁷

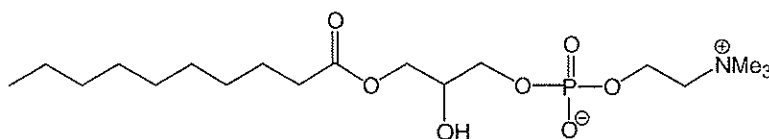


Figure 1.35 Lysolecithin (1-acyl-*sn*-glycero-3-phosphocholine or lysophosphatidylcholine).

1.7.1 Functions of phospholipids

The phospholipid molecule is amphiphilic, meaning that one end is polar (hydrophilic, water-friendly) and one end is unpolar (lipophilic, fat-friendly).¹⁸² This structure gives the phospholipids their unique emulsifying and wetting properties. For example, in the bile digestive fluid, phospholipids ensure fine dispersion of fatty molecules in the water phase, thus improving digestion and absorption.^{88, 180} In the lungs, 1,2-dipalmitoyl-glycero-3-phosphocholine, is the main active component of the lung surfactant, ensuring miscibility at the air-liquid interface.^{188, 189}

Commercial lecithin is a mixture of phospholipids from animal, vegetable or microbial sources, also containing other kinds of lipids like fatty acids and triglycerides.¹⁸⁵ Phospholipids are excellent emulsifiers and surfactants and have been used in paints, dyes, and foods, as well as in creams and lotions for many years. They can serve as nutrients supplying fatty acids, organic phosphate and choline.¹⁸⁸ Choline seems to have beneficial effects in psychiatric disorders and on memory function in relation to ageing.^{188, 190} Phospholipid molecules can spontaneously form structured aggregates such as micelles, vesicles (liposomes) and lamellar structures in aqueous media (Figure 1.36). Such aggregation properties, combined with the biodegradable nature of phospholipids, allows for their utilization in several applied fields, for example biotechnology (liposomal delivery of genetic materials), food industry (microencapsulation of food components for better stability and distribution control), and pharmaceutical industry (drug formulations).¹⁸⁸

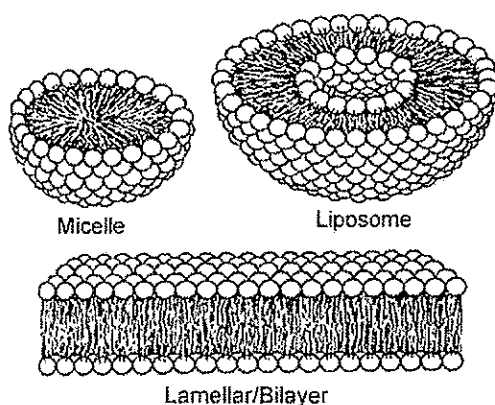


Figure 1.36 Micelles, vesicles (liposomes), and lamellar structures formed by phospholipids in aqueous media.

Phospholipids can act as suitable, non-toxic carriers of pharmaceuticals into cells.¹⁸⁹ Phospholipids are the major constituents of cell membranes, therefore, a phosphatidyl moiety will possess affinity for the membranes. α -Tocopherol and ascorbic acid have been combined to phospholipids.^{179, 191, 192} The phosphatidyl moiety can facilitate the insertion of the antioxidant molecule into cellular membranes,¹⁹³ which in turn may enhance antioxidant activity.¹⁹²

1.7.2 The role of phospholipids in the absorption of carotenoids

Free carotenoids need to be taken with fat to form micelles for absorption.⁸⁹ Lycopene is commercially available in a proliposomal form ("Lyco-Sorb") in which the carotenoid is emulsified with phospholipids.¹⁹⁴ Recent studies have shown that lysophosphatidylcholine enhanced the uptake of lutein and β , β -carotene from micelles by human intestine cells,¹⁹⁵ additionally increasing the accumulation of lutein in the liver of mice.¹⁹⁶ This suggests that not only do phospholipids play an important role in the solubilization of carotenoids in lipid emulsions, but also that hydrolysis of phospholipids to lysophospholipids is required for the efficient uptake of carotenoids into intestinal cells. Due to their more polar character, lysophospholipids might facilitate the carotenoids diffusion across the water layer from micelles to the membrane of intestinal cells.¹⁹⁶ The same effect was shown for α -tocopherol.¹⁹⁷

1.7.3 The role of unsaturated fatty acids in phospholipids

Fatty acids may be accessed more effectively from phospholipids than from triglycerides.¹⁸⁰ In most naturally occurring lecithins, the 1-position is esterified with a saturated fatty acid, and the 2-position with an unsaturated fatty acid.¹⁸³

There are two types of unsaturated fatty acids (Figure 1.37), the unconjugated, polyunsaturated fatty acids, such as eicosapentanoic (EPA) (C20:5), and docosahexaenoic acid (DHA) (C22:6), and the conjugated fatty acids, such as trienoic (3 double bonds) and tetraenoic (4 double bonds) conjugated fatty acids. EPA and DHA account for 50% of the fatty acid constituents of marine phospholipids.¹⁹⁸ Phospholipids from purified soy constitutes of about 8% C18:3 fatty acids.¹⁹⁹ The most conjugated, unsaturated phosphatidylcholine isolated contains parinaric acid (C18:4).²⁰⁰ In marine species, polyunsaturated fatty acids increase membrane fluidity and mobility, maintaining the membrane integrity and function at lower temperatures.¹⁹⁸ Polyunsaturated phosphatidylcholines show beneficial effects in human health.¹⁸⁴ Several methods have been developed to produce polyunsaturated phospholipids¹⁹⁸⁻²⁰⁵ and lysophospholipids.²⁰⁶ Phospholipids or phospholipid formulations enriched with unsaturated fatty acids are useful in foods, cosmetics, and pharmaceuticals.^{207, 208}

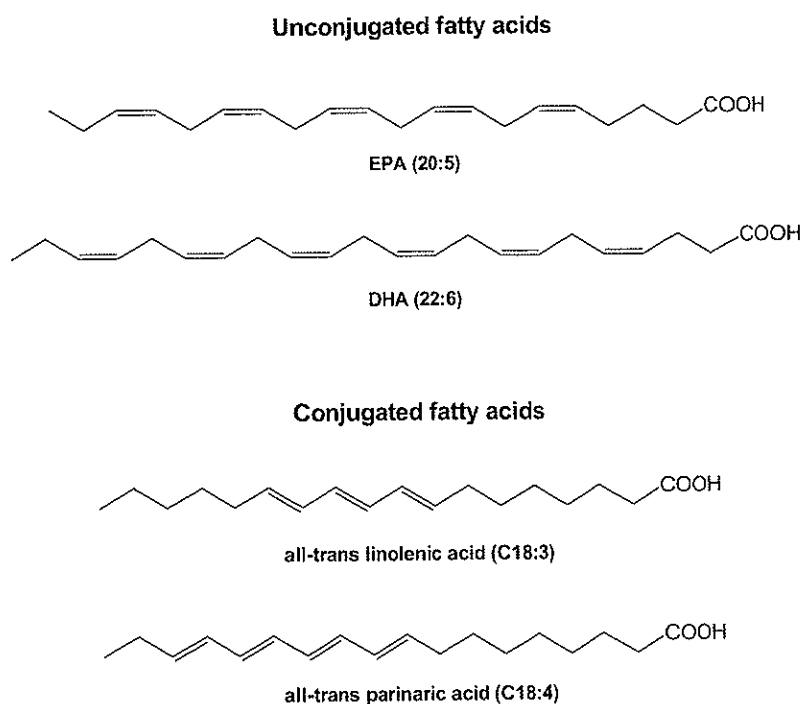


Figure 1.37 Examples of naturally occurring unconjugated and conjugated polyunsaturated fatty acids.

1.8 Aggregates and self-assembly monolayers (SAMs)

1.8.1 Self-assemblies in water

Amphiphilic molecules such as phospholipids form aggregates, which are self-assembled systems, when dissolved in water.¹⁸⁸ Aggregates of carotenoids were first observed in 1931. These were formed after addition of water to an acetone solution of α - and β,β -carotene.²⁰⁹ Aggregates of other carotenoids were later studied.^{210, 211} Most carotenoids in polar solutions (*e.g.* acetone, ethanol, and methanol) display a 3-peak absorption curve in the visible spectral region (420-480 nm). When water is added to such solutions there is generally a characteristic change in the absorption spectra, due to aggregation of the carotenoids.²¹⁰ Aggregation of α - and β,β -carotene lead to a broadening of the absorption peaks, in addition to a loss of the 3-peak fine structure.^{212, 213} The xanthophylls (*e.g.* lutein, zeaxanthin, astaxanthin), give even more pronounced changes; a new absorbance peak (a blue shift) arises usually in the area 370-410 nm depending on the carotenoid, and the fine structured 3-peak diminishes or disappears totally if more water is added to the solution.²¹⁰ Sometimes a red-shifted minor absorption band near 510 nm has also been observed. The least polar xanthophylls (*e.g.* zeaxanthin) have a greater tendency for aggregation than the most polar ones (*e.g.* neoxanthin).²¹⁴

Aggregates of carotenoids in aqueous solution are held together by weak non-covalent forces, and can be disrupted by an increase in the temperature or by addition of organic solvents.²¹¹ The blue shift is believed to be due to a “card-pack” orientation of the polyene chains, while the red-shift is due to a “head-to-tail” orientation, see Figure 1.38. These orientations are referred to as H- and J-aggregates, respectively.²¹⁴⁻²¹⁶ The aggregation type observed for each carotenoid cannot be predicted utilizing nearly identical experimental conditions. Astaxanthin form J-aggregates, lycopene form H-aggregates. Both types of aggregates are photostable, whereas the parent compounds are easily destroyed by irradiation. H-aggregated, and in particular J-aggregated carotenoids, may be used as a tool for varying the color characteristics of carotenoids as colorants in food, cosmetics, and pharmaceuticals.²¹⁷

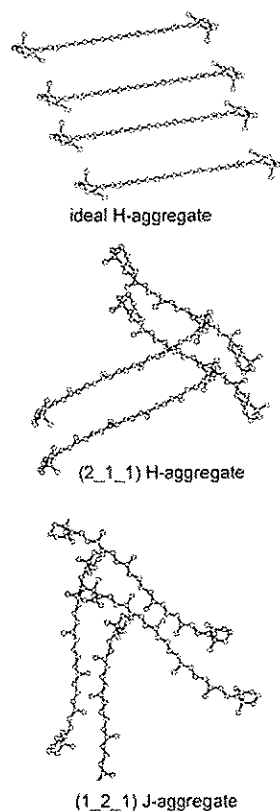


Figure 1.38 Models of H- and J-aggregates (from ref. 148).

marked aggregation for lutein than for β,β -carotene and zeaxanthin.⁵⁰

The color of a yellow protein, isolated from lobster shell, containing 20 molecules of astaxanthin per unit protein, was suggested to come from carotenoid-carotenoid interactions similar to the interactions in aggregates.^{215, 218} A temperature and time dependent study of astaxanthin in aqueous solutions showed red-shifted absorption bands at 560 nm above 21°. These “head-to-tail” aggregates were believed to arise from “card-packed” aggregates. Further, they were suggested to consist of less of an amount of molecules than the aggregates producing the absorption peak near 510 nm.²¹⁶ Blue-shifted absorption spectra have also been induced by carotenoid aggregation in bile acid solutions,²¹⁹ sodium dodecyl sulfate solutions,²²⁰ and in cholate micelles,²²¹ while red-shifted bands were induced by encapsulation of carotenoids in rigid-rod β -barrels²²¹ or by dispersing carotenoids into linear macromolecules (e.g. dextran and polyethylene glycol).¹⁴¹ Aggregates from β,β -carotene complexes with cyclodextrins were evidenced by light scattering and NMR spectroscopy.¹³⁹ β,β -carotene and the two xanthophylls zeaxanthin and lutein were incorporated into liposomes of dipalmitoyl phosphatidylcholine, showing a more

The water-dispersible vitamin C-carotenoid **24** (Figure 1.24) exhibited a marked red absorption shift of approximately 50 nm when dissolved in water.¹⁵⁵ The highly water-dispersible astaxanthin-amino acid conjugate **31** (Figure 1.28) does not aggregate spontaneously in aqueous solution, but show a continuous decrease in the absorption intensity and exhibits a blue shift of 22 nm after 24 hours.¹⁶² The water-soluble pyridinium carotenoid **27** (Figure 1.26) also did not show a spontaneous shift in the absorption spectrum when changing from organic to aqueous solution (no time-dependent study was done).^{158, 159} However, when longer polyene homologues were dispersed in water, a marked hypsochromic shift was seen in the absorption spectra. Similar to the non water-dispersible/soluble carotenoids, the initial spectrum is restored after adding organic solvent.^{158, 162}

Aggregation behavior is clearly dependent on the degree of hydrophilicity, a result of the nature of the polar substituent(s) and the polyene chain length.

1.8.2 Self-assemblies on surfaces

Many surface active organic molecules in dilute solutions self-assemble into oriented monolayers on metal surfaces (Figure 1.39). The driving forces are chemical bond formation of the molecules with the surface and intermolecular interactions.^{222, 223} In 1983, it was shown that oriented monolayers of dialkyl disulfides on gold could be formed by adsorption of di-*n*-alkyl sulfides in dilute solutions. Since then, many self-assembly systems have been studied, including thiols and disulfides on gold and silver, silanes on silicon dioxide, fatty acids on metal oxide surfaces, phosphonates on phosphate surfaces, and isocyanides on platinum.^{222, 224}

Although both sulfur and selenium compounds have a strong affinity to transition metal surfaces, the most studied SAMs have been thiol/disulfide monolayers on gold.²²² The Au-S bond in SAMs of alkanethiolates is strong (40 kcal/mol) and long-chain alkane-thiols form compact monolayers on gold.²²⁴ However, in the recent past there have been several reports on organoselenium monolayers as alternatives for organothiol monolayers on gold.²²⁵⁻²³³ They are interesting because a number of organoselenium compounds are found in living tissues, and because selenium can substitute or accompany sulfur compounds in the organism.²³⁴ Alkaneselenols and dialkylselenides form stable incommensurate monolayers on gold, whereas the alkanethiols form ordered, compact structures.²³³ Diselenides form stable monolayers due to facile Se-Se cleavage.²²⁶

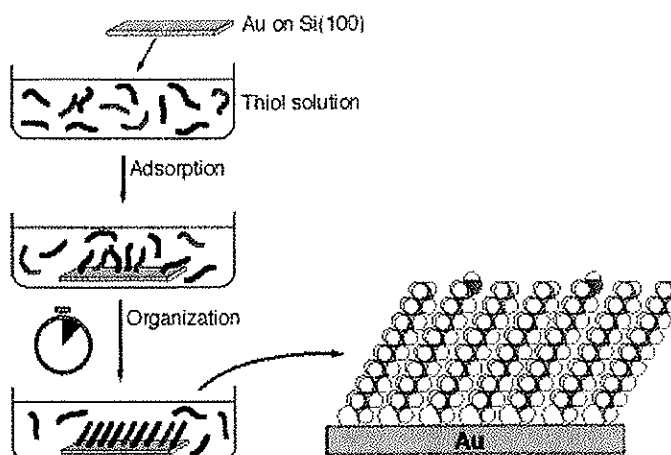


Figure 1.39 Schematic illustration of the preparation of self-assembled monolayers (SAMs) on gold from a thiol solution (from ref. 235).

SAMs are in general highly ordered structures; the degree of order is determined by three main interactions between: 1) the head group of the surfactant and the metal surface, 2) the alkyl chains, and 3) the terminal functional groups and the outer medium.²²⁴ By varying the alkyl chain and the terminal groups, or by modifying the monolayer by organic reactions with functional groups (e.g. hydroxyl, carboxyl, and amino groups), a variety of organic surfaces with a well-defined composition, structure, and thickness can be formed.^{222, 223} SAMs may be utilized as biomimetic films, lubricants, protective coatings, components in electronic devices, functionalized gold nanoparticles, and other interesting applications.^{222, 233}

Although SAMs are interesting as biomimetic films, there have been few reports of monolayers containing unsaturated alkyl chains.²³⁶ Some SAMs with unsaturated hydrocarbon thiols, and aromatic disulfides and diselenides on gold have been reported.^{226, 228, 230, 231} SAMs formed from electroactive organic compounds have become more and more interesting because of their potential applications as molecular devices.²³⁷ The large, delocalized π -electron system of carotenoids have therefore been a natural choice, and their electrochemical properties are now studied.²³⁸ A synthetic thiol substituted carotenoid polyene (**41**) (Figure 1.40) embedded in SAMs of 1-docosanethiol was shown to be over a million times more electronically conductive than the alkane chain of similar length 173. The same compound formed stable SAMs on gold, but they were less ordered than alkanethiols due to steric hindrance.²³⁷

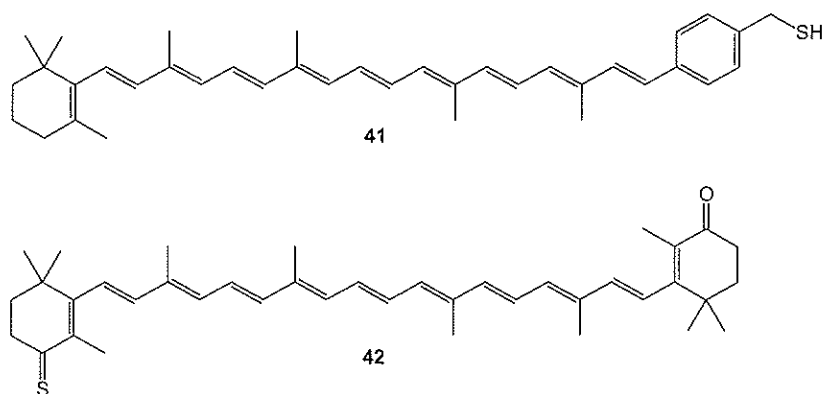


Figure 1.40 Synthetic sulfur-containing carotenoids 7'-apo-7'-(4-mercaptomethylphenyl)-β,β-carotene (**41**) and 4'-thioxo-β,β-carotene-4-one (**42**), both of which form self-assembled monolayers (SAMs) on gold.

A carotenoid self-assembled monolayer was also obtained by dipping a gold electrode into a solution of the carotenoid thion derivative **42** (Figure 1.40) in acetonitrile, and the electrochemical properties were studied by cyclic voltammetry (CV) in aqueous solution. The surface layer was electrochemically stable within the potential region between 0.5 and -0.6 V vs. SCE, but an electron transfer from the polyene chain occurred at 0.9 V vs. SCE.²³⁹ The studies of these carotenoids showed that sulfur-substituted carotenoids form hydrophobic interfaces at the gold surfaces and may have potential applications as molecular wires. For the study of SAMs of selenium-containing carotenoids, see Chapter 7.4.

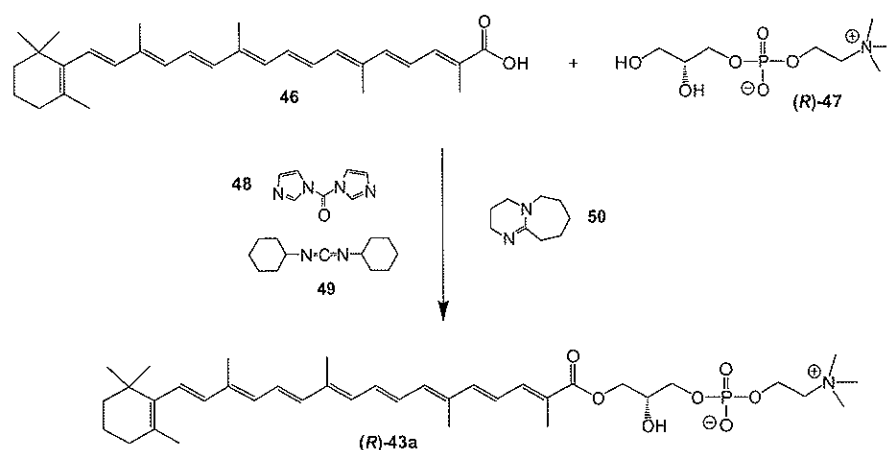
The first carotenoid thiol was synthesized in 1990.¹⁵ Also, optically active thiols have been known for some time. Unfortunately, synthesis produced the thiol in only low yield, including many byproducts, which demanded laborious work-up procedures. These shortfalls have so far prevented the preparation of optically active carotenoid SAMs.¹⁶

2 Synthesis of hydrophilic, water-dispersible carotenoid derivatives

2.1 Synthesis of carotenoid lysophosphocholine *R*-43a and 43a/43b/43c (paper nr. 1, 2, and 9)

Lysophospholipids are natural compounds with high water-activity.^{183, 185-187} A hydrophobic carotenoid appearing as lysophospholipid may have improved bioavailability compared to corresponding free carotenoid (see also Chapters 1.5.3 and 1.7.2). There have been few reports on chemical synthesis of unsaturated (lyso)phosphocholines.^{206, 240} The synthesis is challenging due to the sensitivity of the unsaturated chain.^{241, 242}

In a first attempt, β -apo-8'-carotenoic acid (**46**) was reacted with an excess of *sn*-glycero-3-phosphocholine (GPC) (*R*-47) ($p = 0.88$), in the presence of CDI (**48**), DCC (**49**), and DBU (**50**), according to a previously described method (Scheme 2.1).²⁴³ The enantiomer *R*-43a was isolated by chromatographic methods in low yield (< 5 %). The optical activity of *R*-43a is described in Chapter 8.



Scheme 2.1 First synthesis of the carotenoid lysophosphocholine *R*-43a, starting from *sn*-glycero-3-phosphocholine (GPC) (*R*-47) in the presence of CDI (**48**), DCC (**49**), and DBU (**50**).

In a second synthesis (Scheme 2.2) direct esterification of glycerol with β -apo-8'-carotenoic acid chloride (**51**) resulted in the two carotenoid monoglycerides, 1-(β -apo-8'-carotenoyl)-glycerol (**22a**) (Figure 1.22) and its 2-acyl isomer 2-(β -apo-8'-carotenoyl)-glycerol (**22b**) in 26% yield. Chromatographic separation of the two components of the mixture by reported methods (*e.g.* TLC impregnated with 1.2 % boric acid in chloroform/acetone (96/4, v/v%) or chloroform/methanol (98/2, v/v%)^{244, 245} were not successful. Acyl migration (Figure 2.1) in monoacylglycerols occurs during chromatography on silicic acid or under acidic, basic, or thermal conditions. The mixture composition, 88 % of the 1-acyl isomer **22a** and 12% of the 2-acyl isomer **22b**, was in agreement with the literature^{246, 247} and is speculated to arise from the synthesis and/or acyl migration.

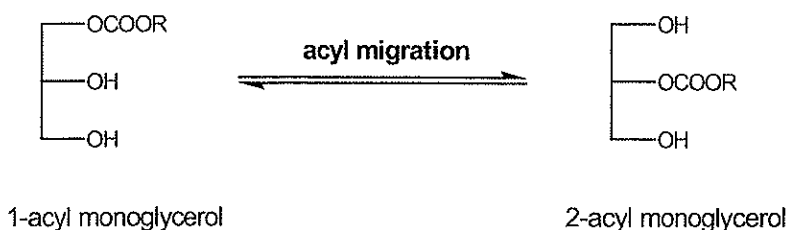
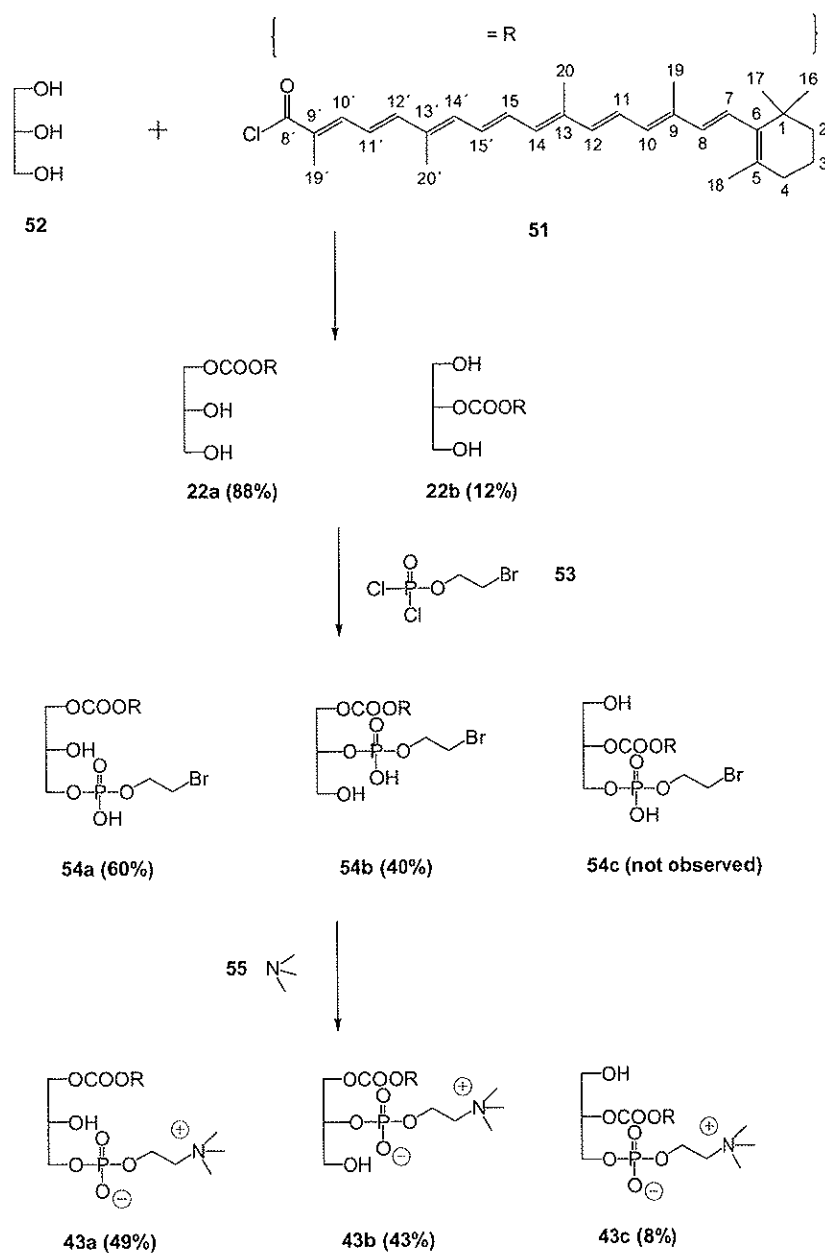


Figure 2.1 Acyl migration in monoacylglycerols.



Scheme 2.2 Second synthetic pathway of the carotenoid lysophosphocholine, resulting in a regioisomeric mixture of **43a**, **43b**, and **43c**.

Aware of the possibilities of obtaining regioisomeric mixtures in the subsequent synthetic steps, the synthesis was continued by introducing the phosphoryl group to the mixture of the two carotenoid monoglycerides **22a/22b**. This step resulted in the bromine adducts **54a/54b** in a ratio 60:40%, respectively. A small amount of isomer **54c** was anticipated, but was not detected in the product mixture. The absence of **54c** may be a result of negligible formation in addition to low resolution in the ^1H and COSY spectra and the broadened ^{13}C and ^{31}P spectra (see Chapter 2.5.2).

Finally, after amination with trimethylamine (**55**) a regioisomeric racemic mixture of the carotenoid lysophospholipid **43a/43b/43c** was finally obtained in 33% yield. In addition to acyl migration in (lyso)phosphocholines²⁴⁸⁻²⁵⁰ there has been some reports on phosphoryl migration (Figure 2.2) observed mostly under drastic conditions (e.g. high temperatures and in alkaline solutions).²⁵¹⁻²⁵³ No acyl or phosphoryl migration was observed for the regioisomer **R-43a** after purification on preparative TLC, nor observed during the time scale of the NMR measurements. The ratio of **43a/43b/43c** (49%/43%/8%, respectively) may therefore originate mostly from the synthesis.

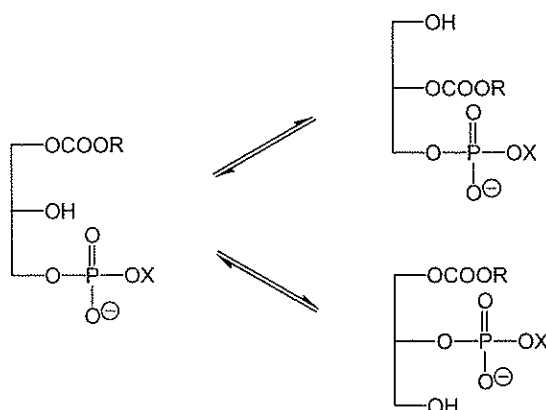
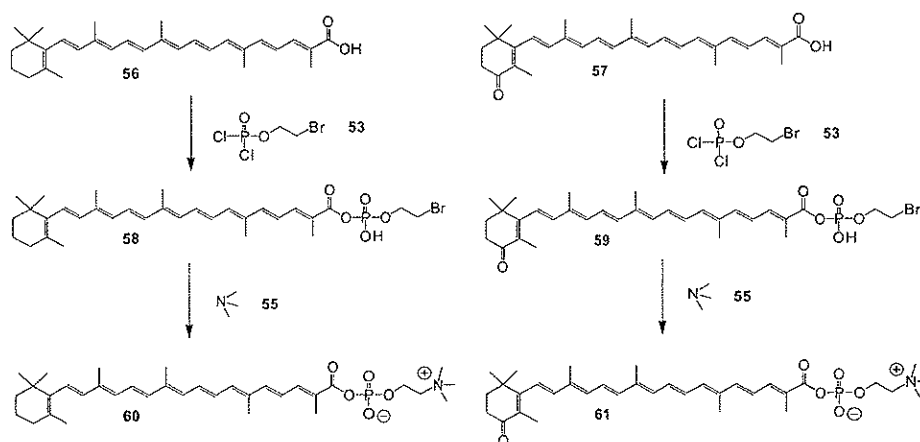


Figure 2.2 Acyl and phosphoryl migration in lysophosphocholines.

2.2 Synthesis of phosphocholine esters from β -apo-8'-carotenoic acid (**56**) and 4-oxo- β -apo-8'-carotenoic acid (**57**)

Phosphate, phosphatidyl, and phosphorylcholine derivatives of lipophilic compounds (e.g. vitamin E and fatty acids) have been synthesized to improve water-solubility of the parent compounds,^{179, 254, 255} for use in pharmaceuticals

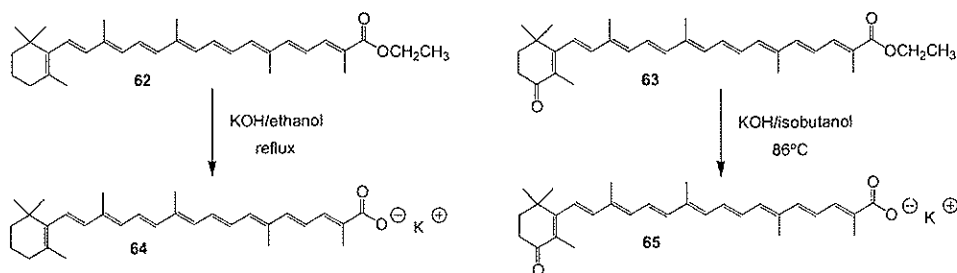
and food, or as moisturizers in cosmetics.^{256, 257} In order to obtain hydrophilic, water-dispersible carotenoids, phosphocholine esters were synthesized from β -apo-8'-carotenoic acid (**56**) and 4-oxo- β -apo-8'-carotenoic acid (**57**)²⁵⁸ (Scheme 2.3). After the esterification of the acids with 2-bromoethyl dichlorophosphate (**53**), the bromine intermediates **58** and **59** were isolated in 20 and 12% yield, respectively. Amination with trimethylamine (**55**) gave the final carotenoid phosphocholine esters **60** and **61** in 88 and 78% yield, respectively.



Scheme 2.3 Synthesis of carotenoid phosphocholine esters **60** and **61**.

2.3 Synthesis of potassium salts of β -apo-8'-carotenoic ethyl ester (**62**) and 4-oxo- β -apo-8'-carotenoic ethyl ester (**63**)

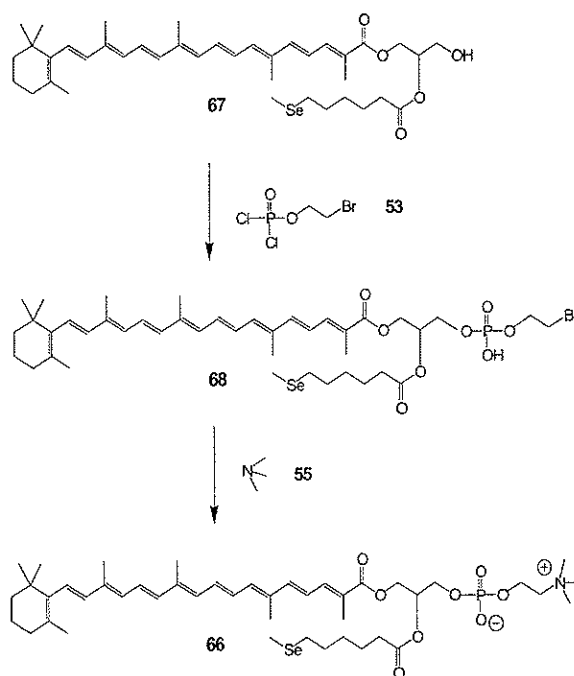
Sodium salts of carotenoids have been shown to impart high degrees of water-dispersibility to the compounds, as well as improved bioavailability.¹⁶³ High concentrations of the corresponding potassium salts may not be used for *in vivo* purposes, due to toxicity issues.²⁵⁹ However, potassium salts are in general more water-soluble than the sodium salts. Therefore, the potassium salts of β -apo-8'-carotenoic ethyl ester (**62**) and 4-oxo- β -apo-8'-carotenoic ethyl ester²⁵⁸ (**63**) were made by the methods outlined in Scheme 2.4. The solid crude product, obtained after solvent evaporating, was washed with ice-cold CH_2Cl_2 . The products **64** and **65** were obtained in approximately 70 and 40 % yield, respectively.



Scheme 2.4 Synthesis of the carotenoid potassium salts **64** and **65**.

2.4 Synthesis of carotenoid-selena-phosphocholine **66**

The synthesis of the carotenoid-selena-glyceride **67** has previously been described.¹⁷¹ Analogous to the method outlined in Scheme 2.2 and 2.3, 2-bromoethyl dichlorophosphate (**53**) was introduced to the carotenoid-selena-glyceride **67** which, after purification on preparative TLC, afforded the bromine intermediate **68** in 16% yield. Amination with trimethylamine (**55**) gave the carotenoid-selena-phosphocholine **66** in 45% yield.



Scheme 2.5 The synthesis of the carotenoid-selena-phosphocholine **66**.

The polar, hygroscopic carotenoid-selena-phosphocholine **66** forms a self-assembled-monolayer (SAM) on gold. This behavior was investigated by electrochemical methods (see Chapter 7).

2.5 Structural elucidation by 1D and 2D NMR

2.5.1 Structural elucidation of the carotenoid monoglycerides **22a/22b**

From the ^1H - ^1H -COSY spectrum of **22a/22b** in Figure 2.3, it is seen that characteristic glyceryl and carotenoyl ^1H and ^{13}C NMR shifts were obtained for both the two carotenoid monoglycerides **22a** and **22b**. A 3-spin system is seen at 4.35-4.26 ppm (H_2COOR) - 4.02-3.98 ppm (HCOH) - 3.73-3.60 ppm (H_2COH) for the 1-acyl isomer **22a**, and a 2-spin system at 5.03-5.00 ppm (H_2COOR) - 4.10-3.97 ppm (H_2COH) for the 2-acyl isomer **22b**, according to previous reported ^1H NMR data of monoacyl glycerol isomers.²⁶⁰

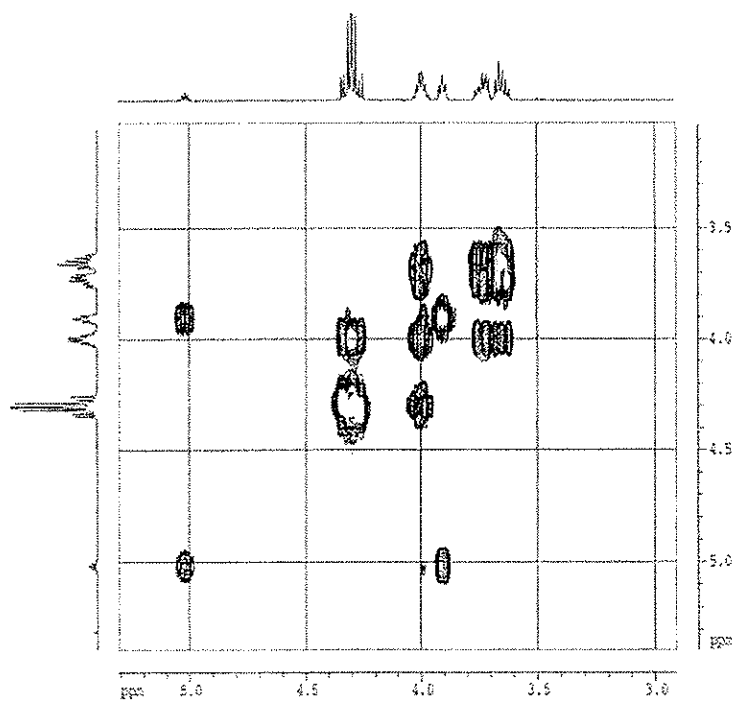


Figure 2.3 1D ^1H and 2D ^1H - ^1H -COSY spectra of the glyceryl region of the carotenoid monoglyceride mixture **22a/22b**.

2.5.2 Structural elucidation of the carotenoid lysophosphocholines R-43a and 43a/43b/43c and their 2-bromoethyl derivatives (paper 2)

Typical 1D ^1H spectra of the three positional isomers of lysophosphocholines are shown in Figure 2.4.

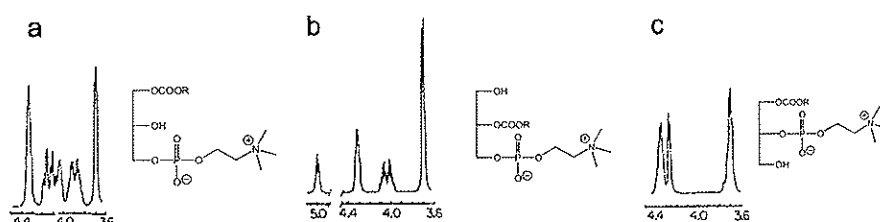


Figure 2.4 Typical 1D ^1H spectra of individual regioisomers of lysophosphocholines (taken from ref. 251).

By analyzing high resolution ^1H and H,H-COSY spectra of the regioisomeric mixture of the carotenoid lysophosphocholine **43a/43b/43c**, it was possible to identify the characteristic glyceryl and phosphocholine proton shifts of all three isomers in the mixture (Figure 2.5). A 3-spin system is seen for both isomers **43a** and **43b** at 4.19-4.22 ppm (H_2COOR) - 4.04 ppm (HCOH) - 3.89-3.92 ppm (H_2COP) and 4.26-4.31 ppm (H_2COH) - 4.40 ppm (HCOP) - 3.72-3.78 ppm (H_2COH), respectively. The typical spin system for the 2-acyl minor isomer **43c** appear at 3.75-3.78 ppm (H_2COH) - 5.02 ppm (HCOOR) - 4.06-4.09 ppm (H_2COP).

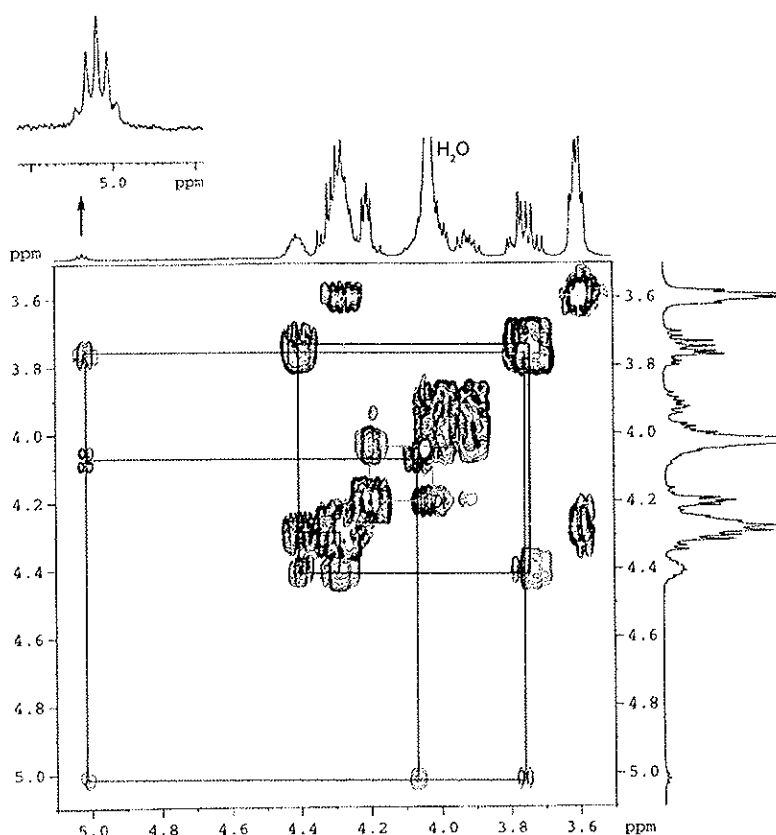


Figure 2.5 ^1H and H,H-COSY spectrum of the lysophosphocholine mixture **43a/43b/43c**. Only the glyceryl (1a: red, 1b: green, 1c: blue) and phosphocholine moiety (yellow) correlations are shown.

^{13}C DEPT 135 spectra revealed the ^{13}C signals of the glyceryl and the phosphocholine chain signals for **43a** and **43b**, analogous to the signals for the bromine adducts **54a/54b** in Figure 2.6. No glyceryl or phosphocholine ^{13}C signals for the minor isomer **43c** were detected due to low concentration.

Due to partial aggregation of the bromine adducts **54a** and **54b** 1D ^1H and 2D H,H-COSY spectra revealed low resolution for the glyceryl and 2-bromoethyl phosphoryl moieties in different solvent systems. However, all the characteristic glyceryl and 2-bromoethyl ^{13}C signals of both isomers **54a** and **54b** were identified from the ^{13}C DEPT 135 spectrum (Figure 2.6). A difference in chemical shifts between the two $-\text{CH}_2\text{Br}$ groups (31.5 ppm and 31.7 ppm) for **54a** and **54b**, respectively indicate that not only the glyceryl chemical shifts, but also the 2-

bromoethyl chemical shifts are sensitive to the position of the unsaturated acyl chain.

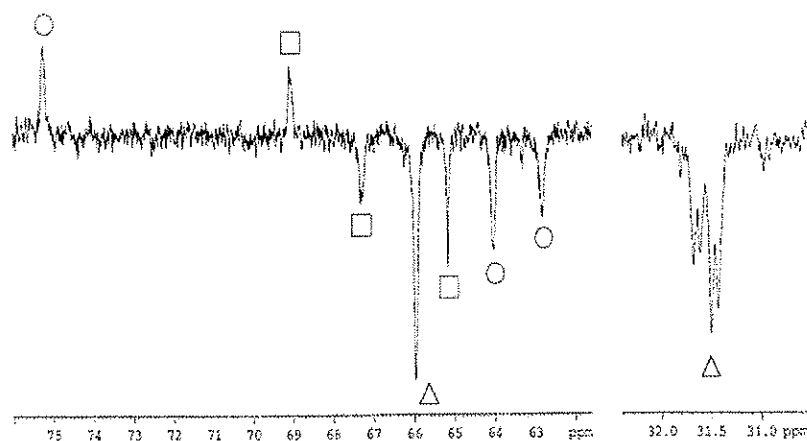


Figure 2.6 ^{13}C DEPT 135 spectrum of the isomeric mixture **54a/54b**. Only the glyceryl \square (**54a**), \circ (**54b**) and the 2-bromoethyl phosphoryl \triangle moiety signals are shown.

^{31}P NMR can be used to distinguish regioisomers of lysophosphocholines.²⁵¹ 1D ^{31}P spectra of **R-43a** and the mixture **43a/43b/43c** confirmed the presence and determined the ratio of the three isomers in the mixture (Figure 2.7). Contrary to ^{13}C -NMR, the ^{31}P NMR spectra allowed the detection of the minor isomer **43c**.

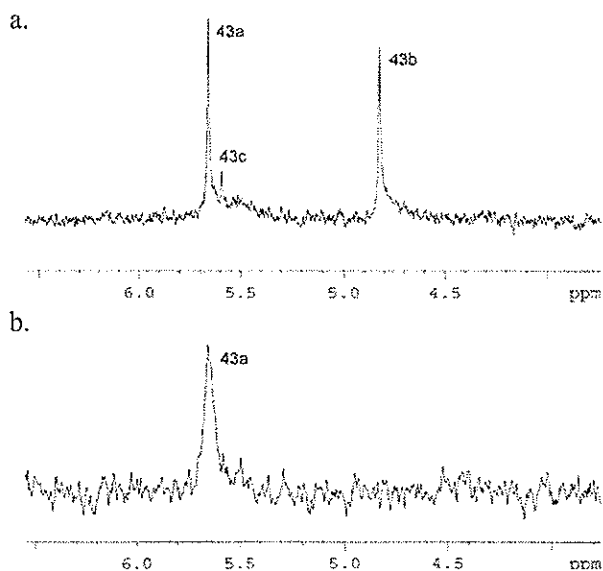


Figure 2.7 1D ^{31}P NMR signals for the a) lysophosphocholine mixture 43a/43b/43c and b) the pure regioisomer *R*-43a.

High resolution 1D ^1H and 2D H,H-COSY spectra could not distinguish between the carotenoyl moiety of the regioisomers. However, a 1D ^1H NMR subtraction spectrum of the mixture and the pure isomer [(43a/43b) - *R*-43a] could be used to determine the ^1H shifts of the carotenoyl chain for the individual regioisomers, Figure 2.8. The most pronounced deviation of *R*-43a compared to 43b is seen for the H10' which gives a doublet of doublets at about 7.32 ppm. In the isomeric mixture a multiplet at 7.32 ppm is observed, indicating that the isomers 43a and 43b each give one doublet of doublets with a small chemical shift difference. By similar subtraction, the other proton signals for isomer 43b could also be determined, as seen for H11 and H15 in Figure 2.9, (the concentration of 43c was too low to give significant signals in the polyene chain region).

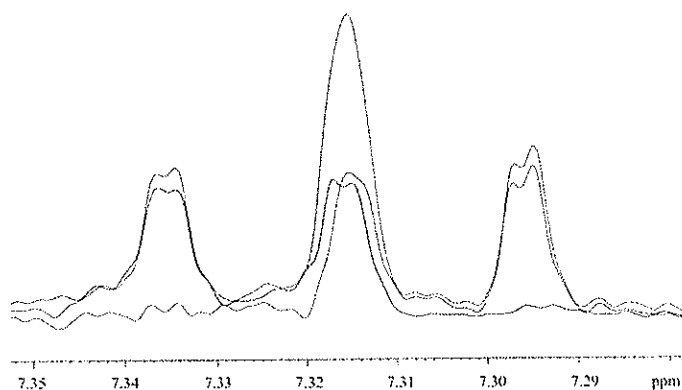


Figure 2.8 H10' signal for **43a/43b** (red) and pure **R-43a** (blue) and the signal for **43b** (green) after subtraction [(43a/43b) - **R-43a**].

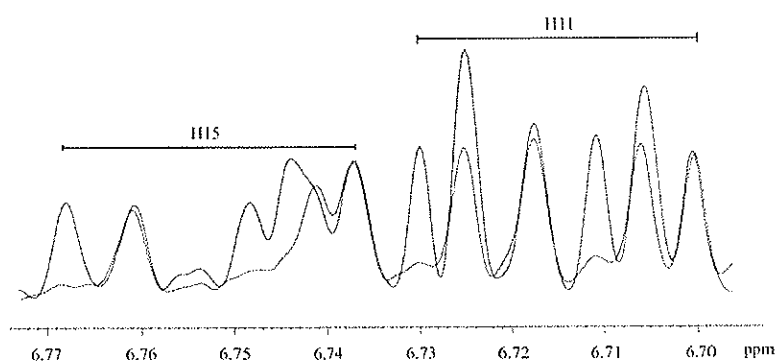


Figure 2.9 H15 and H11 signals for **43a/43b** (blue) and pure **R-43a** (red).

The observation of double ^{13}C signals in the polyene chain region of the mixtures **43a/43b** and **54a/54b** confirmed that the chemical shifts in the unsaturated chain are affected by their position on the glycerol backbone. In conclusion, in NMR spectra of glycerol(phospho)lipids from unsaturated conjugated polyenic acids, the ^1H and ^{13}C signals of the unsaturated part of the acyl chain appear in regions normally not occupied by other lipid signals. It was shown that ^1H and ^{13}C polyenic NMR signals having characteristic shifts, depending on the position in the glycerol backbone, may be used to distinguish between positional isomers of (lyso)phosphocholines and their 2-bromoethyl derivatives.

2.5.3 Structural elucidation of seleno-carotenoid-phosphocholine 66

The glyceryl protons of 1,2-diacyl-glycero-3-phosphocholines (Figure 2.10) give an ABMX_Y spin system in the 1D ¹H and H,H-COSY spectra.^{261, 262} This is shown for the carotenoid-selena-phosphocholine **66** in Figure 2.11. The H_A and H_B signals both appear as doublets of doublets at 4.48-4.41 ppm (dd, 1H, CHOP) and 4.27-4.16 ppm (dd, 1H, CH₂OP), respectively. The coupling constant between H_A and H_B is 12.23 Hz. The multiplet at 5.23-5.32 ppm (m, 1H, -CH-) arise from H_M and H_X and H_Y appear as one multiplet at 3.98-4.06 (m, 2H, CH₂COO). The glyceryl proton signals for the 2-bromoethyl derivative **68** showed a similar pattern.

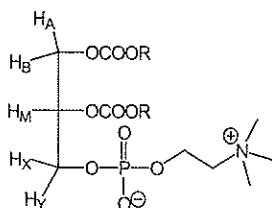


Figure 2.10 The ABMX_Y glyceryl protons of 1,2-diacyl-3-glycero-3-phosphocholines.

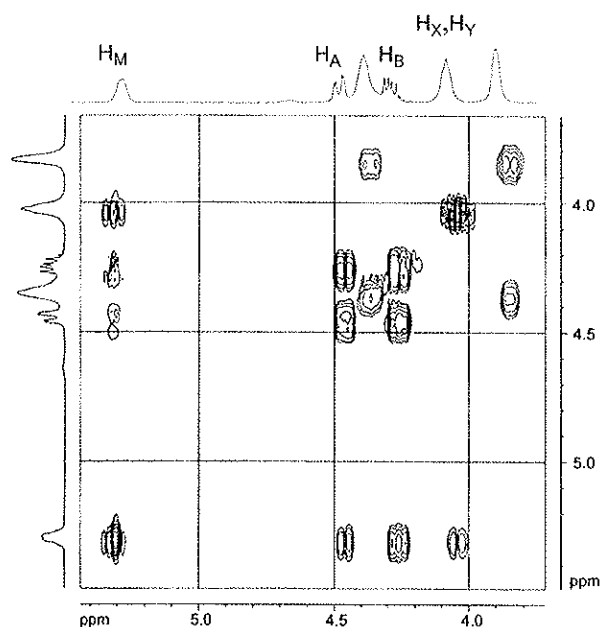


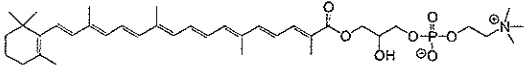
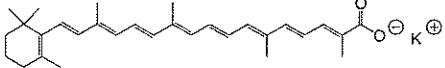
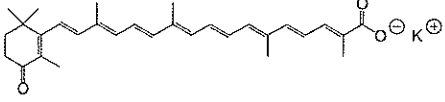
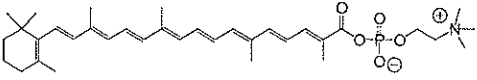
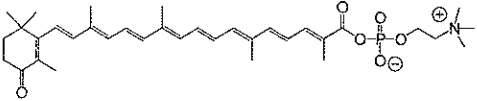
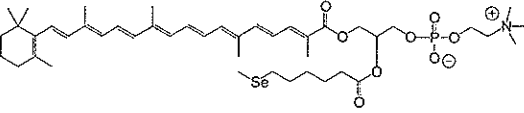
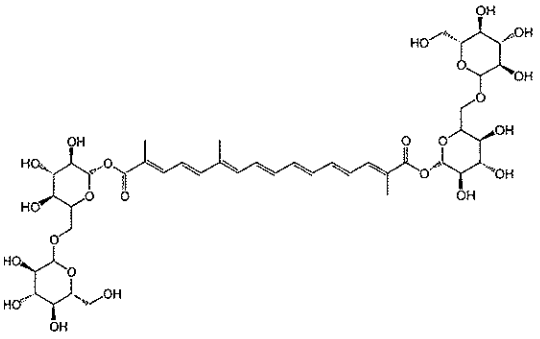
Figure 2.11 1D ¹H and 2D H,H-COSY spectrum of the glyceryl (ABMX_Y) and phosphocholine region of carotenoid-selena-phosphocholine **66**.

2.6 Water-dispersibility, water-solubility

The polar character of xanthophylls was early determined by extraction techniques. The carotenoid was partitioned from a solution of known concentration in a polar solvent (*e.g.* methanol) into a non-polar solvent (*e.g.* hexane). The amount of carotenoid could then be determined by UV-VIS absorption.²⁶³ Water-dispersibility/solubility of low hydrophilic carotenoids such as the carotenoid sulfates, was determined by dissolving a spectrophotometrically (in MeOH) determined amount of carotenoid in water. The solution was then centrifuged and decanted. Excess carotenoid was quantitatively measured by UV-VIS absorption in MeOH, and the weight difference was used to estimate the carotenoid concentration in water.¹¹⁷ These methods are not suitable for highly water-dispersible carotenoids.

In this work, the hydrophilic carotenoids were dried under reduced pressure over night. A certain amount of distilled, filtered (0.22 μm) water was added and the solution/dispersion was stirred until no visible solid was left. All compounds dissolved either in pure water (**43a/43b/43c**, **64**, **65**, **66**, **14**) or in 1% methanol/water (**60**, **61**). The water solubility varied from 1.5 mg up to more than 60 mg/ml, see Table 1. Because of limited amount of samples, the real values for solubilities summarized in Table 2.1 may be higher. For crocin (**14**) no saturation limit was previously reported.²⁶⁴

Table 2.1 Water-dispersibility/solubility of hydrophilic carotenoids

Chemical Structure	Compound Nr.	Water solubility (mg/ml)
	43a/43b/43c	> 60
	64	> 5.0
	65	> 4.5
	60	in 1% methanol
	61	in 1% methanol
	66	> 1.5
	14	> 150

2.7 Experimental

2.7.1 Synthesis of the phosphocholine esters of β -apo-8'-carotenoic acid (**56**) and 4-oxo- β -apo-8'-carotenoic acid (**57**)

(The synthesis is analogous to the method described by Hansen *et al.*²⁶⁵) To an ice-cooled solution of 2-bromoethyl dichlorophosphate (**53**) (175.0 mg, 1.4 mmol) (prepared and freshly distilled as described 265) in anhydrous diethyl ether (Et₂O) (10 ml) under N₂-atmosphere was added dropwise pyridine (1.5 ml), followed by β -apo-8'-carotenoic acid (**56**) (86 mg, 0.2 mmol) dissolved in Et₂O (15 ml). The solution was allowed to reach room temperature and then refluxed for 5 h under nitrogen. After cooling in an ice-bath, water (1 ml) was added dropwise, and the mixture was stirred at room temperature for 12 h. The solvents were removed under reduced pressure. The residue was taken up in a mixture of CHCl₃/CH₃OH (2:1, v/v%) (10 ml) and 2 drops H₂SO₄ (aq, 25%) was added. The organic phase was washed with H₂O (3ml). The combined organic phase was dried over anhydrous Na₂SO₄ and filtered. The solvents were removed under reduced pressure, and the crude product was dissolved in CHCl₃/CH₃OH (2:1, v/v%). After purification on preparative TLC in CHCl₃/CH₃OH (2:1, v/v%), **58** was obtained in 20% yield (25 mg).

R_f (CHCl₃/CH₃OH) (3:1, v/v%) = 0.3. UV-VIS: λ_{\max} = 447 nm (methanol). MS (ESI): m/z 663 [M - H + 2Na]⁺.

(This step was performed in accordance to the method described by Stamatov.¹⁹¹) The bromine adduct **58** was taken up in a mixture of CHCl₃/2-propanol/dimethylformamide (20 ml, 3:5:5 v/v/v%) and treated with a 45% solution of trimethylamine (**55**) (45% in H₂O, 1.5 ml) at room temperature for 4 h. The volatile solvents were removed, the residue dissolved in CHCl₃/CH₃OH (2:1, v/v%), and washed with H₂O. The organic phase was dried over anhydrous Na₂SO₄ and filtered. The solvents were removed under reduced pressure, the crude product was dissolved in CHCl₃/CH₃OH (2:1, v/v%), and purified by preparative TLC in CHCl₃/CH₃OH/H₂O (4:5:1, v/v/v%). **60** was obtained in 88% yield (20 mg).

R_f (CHCl₃/CH₃OH/H₂O (4:5:1, v/v/v%)) = 0.45. UV-VIS: λ_{\max} = 452 nm (methanol), 453 nm (CH₂Cl₂). MS (ESI): m/z 620 [M - H + Na]⁺. ¹H-NMR (400 MHz, CDCl₃ (75%)/CD₃OD (25%); carotenoyl moiety: 7.33 ppm (d, 1H, H10'), 6.76 ppm (m, 1H, H15), 6.72 ppm (m, 1H, H11), 6.69 ppm (m, 1H, H12'), 6.64 ppm (m, 1H, H15'), 6.49 ppm (dd, 1H, H11'), 6.44 ppm (m, 1H, H14'), 6.37 ppm (m, 1H, H12), 6.28 ppm (m, 1H, H14), 6.19 ppm (m, 1H, H7), 6.11 ppm (m, 1H, H8), 6.16 ppm (m, 1H, H10), 2.009 ppm (s, 3H, H20), 1.999 ppm (s, 3H, H19'), 1.982 ppm (s, 3H, H20'), 1.985 ppm (s, 3H, H19), 1.97 ppm (m, 2H, H4), 1.72 ppm (s, 3H, H18), 1.59 ppm (m, 2H, H3), 1.43 ppm (m, 2H, H2), 1.03 ppm (s, 6H,

CH₃, C5); phosphocholine moiety: 4.52-4.58 ppm (m, 2H, CH₂OP), 3.72-3.78 ppm (m, 2H, CH₂N⁺), 3.25 ppm (s, 9H, [CH₃]₃N⁺).

The bromine intermediate **59** was prepared from 4-oxo-β-apo-8'-carotenoic acid (**57**) (89 mg, 0.20 mmol) by the same procedure as for **58**. After chromatographic work up by preparative TLC in CHCl₃/CH₃OH/H₂O (4:5:1, v/v/v%), **59** was obtained in 12% yield (15 mg).

R_f (CHCl₃/CH₃OH/H₂O (7:3:0.3, v/v/v%) = 0.48. UV-VIS: λ_{max} = 464 nm (CH₂Cl₂). MS (ESI): m/z 402 [(M - C₂H₅O₃PBr) - CO₂]⁺. ¹H-NMR (400 MHz, CDCl₃ (75%)/CD₃OD (25%); carotenoyl moiety: 7.40 ppm (d, 1H, H10'), 6.76 ppm (m, 1H, H15), 6.70 ppm (m, 1H, H11), 6.66 ppm (m, 1H, H12'), 6.65 ppm (m, 1H, H15'), 6.51 ppm (dd, 1H, H11'), 6.43 ppm (m, 1H, H12), 6.41 ppm (m, 1H, H14'), 6.36 ppm (m, 1H, H8), 6.30 ppm (m, 1H, H14), 6.27 ppm (m, 1H, H10), 6.24 ppm (m, 1H, H7), 2.49 ppm (m, 2H, H3), 1.991 ppm (s, 3H, H19), 1.990 ppm (s, 3H, H20), 1.966 ppm (s, 3H, H20'), 1.947 ppm (s, 3H, H19'), 1.84 ppm (m, 2H, H2), 1.83 ppm (s, 3H, H18), 1.20 ppm (s, 6H, CH₃, C5); 2-bromoethyl moiety: 4.24-4.29 ppm (m, 2H, CH₂OP), 3.54-3.57 ppm (m, 2H, CH₂Br).

The final carotenoid phosphocholine ester **61** was isolated after chromatographic work up by preparative TLC in CHCl₃/CH₃OH/H₂O (4:5:1, v/v/v%) in 78% yield (9 mg).

R_f (CHCl₃/CH₃OH (4:5:1, v/v/v%) = 0.38. UV-VIS: λ_{max} = 464 nm (CH₂Cl₂); λ_{max} = 461 nm (methanol). MS (ESI): m/z 612 M⁺, 634 [M - H + Na]⁺. ¹H-NMR (400 MHz, CDCl₃ (75%)/CD₃OD (25%); carotenoyl moiety: 7.43 ppm (d, 1H, H10'), 6.76 ppm (m, 1H, H15), 6.72 ppm (m, 1H, H11), 6.69 ppm (m, 1H, H12'), 6.66 ppm (m, 1H, H15'), 6.53 ppm (dd, 1H, H11'), 6.44 ppm (m, 1H, H12), 6.42 ppm (m, 1H, H14'), 6.38 ppm (m, 1H, H8), 6.31 ppm (m, 1H, H14), 6.28 ppm (m, 1H, H10), 6.26 ppm (m, 1H, H7), 2.48 ppm (m, 2H, H3), 2.064 ppm (s, 3H, H19'), 1.994 ppm (s, 3H, H19), 1.986 ppm (s, 3H, H20), 1.967 ppm (s, 3H, H20'), 1.84 ppm (m, 2H, H2), 1.83 ppm (s, 3H, H18), 1.20 ppm (s, 6H, CH₃, C5); phosphocholine moiety: 4.46-4.40 ppm (m, 2H, CH₂OP), 3.64-3.58 ppm (m, 2H, CH₂N⁺), 3.20 ppm (s, 9H, [CH₃]₃N⁺).

2.7.2 Synthesis of potassium salts of β-apo-8'-carotenoic ethyl ester (**62**) and 4-oxo-β-apo-8'-carotenoic ethyl ester (**63**)

β-apo-8'-carotenoic ethyl ester (**62**) (345.5 mg, 0.75 mmol) was dissolved in a KOH-ethanolic solution (5.7% KOH; 29.7 mg in 50 ml EtOH). The solution was refluxed for 12 h, and the solvent removed under reduced pressure. The solid crude product was washed with ice-cooled CH₂Cl₂, while unreacted KOH was

precipitated and removed by filtration. The pure potassium salt **64** was finally dried *in vacuo* and obtained in 70% yield.

UV-VIS: $\lambda_{\max} = 438$ nm (methanol). MS (ESI): m/z 431 [M - K]⁻. ¹H-NMR (400 MHz, CD₃OD): 7.07 ppm (d, 1H, H10'), 6.70 ppm (m, 1H, H11), 6.69 ppm (m, 1H, H15), 6.67 ppm (m, 1H, H15'), 6.55 ppm (dd, 1H, H11'), 6.51 ppm (m, 1H, H12'), 6.37 ppm (m, 1H, H12), 6.32 ppm (m, 1H, H14'), 6.27 ppm (m, 1H, H14), 6.19 ppm (m, 1H, H7), 6.14 ppm (m, 1H, H10), 6.11 ppm (m, 1H, H8), 2.03 ppm (m, 2H, H4), 1.986 ppm (s, 3H, H20), 1.988 ppm (s, 3H, H19'), 1.979 ppm (s, 3H, H20'), 1.974 ppm (s, 3H, H19), 1.72 ppm (s, 3H, H18), 1.64 ppm (m, 2H, H3), 1.48 ppm (m, 2H, H2), 1.03 ppm (s, 6H, CH₃, C5).

4-oxo- β -apo-8'-carotenoic ethyl ester (**63**) (159.0 mg, 0.34 mmol) was dissolved in a mixture of aqueous KOH (8.9% KOH; 1.29 g in 107 ml H₂O) and isobutanol (15 ml). The solution was heated to 86 °C and stirred for 12 h. The solvents were removed under reduced pressure, the crude solid product was washed with ice-cooled CH₂Cl₂, and unreacted KOH was precipitated and removed by filtration. The pure potassium salt **65** was dried *in vacuo* and obtained in 40% yield.

UV-VIS: $\lambda_{\max} = 455$ nm (methanol). MS (ESI): m/z 483 [M - H]⁺, 445 [M - K]⁻. ¹H-NMR (400 MHz, CD₃OD): 7.06 ppm (d, 1H, H10'), 6.78 ppm (m, 1H, H15), 6.74 ppm (m, 1H, H11), 6.69 ppm (m, 1H, H15'), 6.60 ppm (dd, 1H, H11'), 6.53 ppm (m, 1H, H12'), 6.51 ppm (m, 1H, H12), 6.39 ppm (m, 1H, H14), 6.36 ppm (m, 1H, H10), 6.34 ppm (m, 1H, H14'), 6.33 ppm (m, 1H, H8), 6.26 ppm (m, 1H, H7), 2.51 ppm (m, 2H, H3), 2.047 ppm (s, 3H, H20), 2.016 ppm (s, 3H, H20'), 1.978 ppm (s, 3H, H19), 1.975 ppm (s, 3H, H19'), 1.88 ppm (m, 2H, H2), 1.85 ppm (s, 3H, H18), 1.23 ppm (s, 6H, CH₃, C5).

2.7.3 Synthesis of the carotenoid-selena-phosphocholine **66**

(The synthesis is analogous to the method described by Hansen *et.al.*²⁶⁵) To an ice-cooled solution of 2-bromoethyl dichlorophosphate (**53**) (10.3 mg, 0.08 mmol) (prepared and freshly distilled as described 265) in anhydrous diethyl ether (Et₂O) (4 ml) under N₂-atmosphere was added dropwise pyridine (0.03 ml), followed by carotenoid-selena-glyceride **67** (11.5 mg, 0.02 mmol) dissolved in Et₂O (8 ml). The solution was allowed to come to room temperature before refluxing for 6 h under nitrogen. After cooling in an ice-bath, water (0.5 ml) was added dropwise, and the mixture was stirred at room temperature for 12 h. The solvents were removed under reduced pressure. The residue was taken up in a mixture of CHCl₃/CH₃OH (2:1, v/v%) (8 ml) and 1 drop of H₂SO₄ (aq, 10%) was added. The organic phase was washed with H₂O (2 x 4ml). The combined organic phase was dried over anhydrous Na₂SO₄ and filtered. The solvents were removed under reduced pressure and the crude product was dissolved in CHCl₃/CH₃OH (2:1, v/v)

v%). After purification on preparative TLC with CHCl₃/CH₃OH (2:1, v/v%) as eluent, the bromine intermediate **68** was obtained in 16% yield (2.1 mg).

R_f (CHCl₃/CH₃OH (3:1, v/v%)) = 0.3. UV-VIS: λ_{max} = 456 nm (methanol). MS (ESI): m/z 883 [M - CH₃ - H]⁻. ¹H-NMR (400 MHz, CDCl₃); carotenoyl moiety: 7.28 ppm (d, 1H, H10'), 6.71 ppm (m, 1H, H15), 6.68 ppm (m, 1H, H11), 6.60 ppm (m, 1H, H12'), 6.60 ppm (m, 1H, H15'), 6.47 ppm (dd, 1H, H11'), 6.37 ppm (m, 1H, H14'), 6.34 ppm (m, 1H, H12), 6.23 ppm (m, 1H, H14), 6.17 ppm (m, 1H, H7), 6.11 ppm (m, 1H, H8), 6.14 ppm (m, 1H, H10), 2.02 ppm (m, 2H, H4), 1.974 ppm (s, 3H, H20), 1.966 ppm (s, 3H, H19), 1.944 ppm (s, 3H, H20'), 1.937 ppm (s, 3H, H19'), 1.72 ppm (m, 3H, H18), 1.62 ppm (m, 2H, H3), 1.48 ppm (m, 2H, H2), 1.03 ppm (s, 6H, CH₃, C5); glyceryl moiety: 5.39-5.28 ppm (m, 1H, -CH-), 4.55-4.30 ppm (d, 2H, CH₂OP), 4.15-4.05 ppm (m, 2H, CH₂COO); 2-bromoethyl moiety: 4.38-4.27 ppm (m, 2H, CH₂-O), 3.64-3.54 ppm (m, 2H, CH₂Br); selena-acyl moiety: 2.52-2.48 ppm (t, 2H, CH₂; C2), 2.43-2.26 ppm (m, 2H, CH₂; C6), 1.98 ppm (s, 3H, CH₃), 1.73-1.65 ppm (m, 6H, CH₂; C3, C4, C5).

(This step was performed in accordance to the method described by Stamatov.¹⁹¹) The bromine adduct **68** (2.11 mg, 0.003 mmol) was dissolved in a CHCl₃/2-propanol/dimethylformamide (10 ml, 3:5:5 v/v/v%) and treated with a solution of trimethylamine (**55**) (45% in H₂O, 0.3 ml) at room temperature under N₂-atmosphere for 12 h. The volatile solvents were removed, and the residue was dissolved in CHCl₃/CH₃OH (3:1, v/v%) and washed with H₂O (3 x 5ml). The organic phase was dried over anhydrous Na₂SO₄ and filtered. The solvents were removed under reduced pressure, the crude product was dissolved in CHCl₃/CH₃OH (3:1, v/v%), and purified by preparative TLC in CHCl₃/CH₃OH/H₂O (7:3:0.3, v/v/v%). **66** was obtained in 45% yield (1.0 mg).

R_f (CHCl₃/CH₃OH/H₂O (7:3:0.3, v/v/v%)) = 0.25. UV-VIS: λ_{max} = 456 nm (CH₂Cl₂). MS (ESI): m/z 863 [M - H]⁻, 886 [M + Na]⁺. ¹H-NMR (400 MHz, CDCl₃); carotenoyl moiety: in accordance with compound **68**; glyceryl moiety: 5.23-5.32 ppm (m, 1H, -CH-), 4.48-4.41 ppm (dd, 12.23 Hz, 1H, CH₂OOR), 4.27-4.16 ppm (dd, 12.23 Hz, 1H, 1CH₂OOR), 3.98-4.06 ppm (m, 2H, CH₂COP); phosphocholine moiety: 4.38-4.27 ppm (m, 2H, CH₂-O), 3.88-3.80 ppm (m, 2H, CH₂N⁺), 3.41-3.32 ppm (s, 9H, [CH₃]₃N⁺); selena-acyl moiety: 2.52-2.47 ppm (t, 2H, CH₂; C2), 2.36-2.25 ppm (m, 2H, CH₂; C6), 1.98 ppm (s, 3H, CH₃), 1.67-1.56 ppm (m, 6H, CH₂; C3, C4, C5).

3 Determination of surface properties

Surfactants modify the surface of liquids or solids on which they are adsorbed. This capacity is utilized in several different industrial applications (*e.g.* as wetting, dispersing, antisticking, and antispattering agents).¹⁸⁵ If adsorption takes place at the liquid/gas interface, the surface tension of the liquid decreases. Surface tension is the cohesive energy present at an interface. Polar liquids such as water have strong intermolecular interactions and therefore high surface tension. When amphiphilic molecules are dissolved in polar solvents they arrange on the air/liquid surface, with the hydrophilic component anchored in water, while the hydrophobic component points out in the air. This disrupts the intermolecular interactions of the water molecules and therefore decreases the surface tension of water (72 mN/m²⁶⁶). As the concentration (C) of a surfactant increases, the surface tension drops because more molecules are adsorbed to the surface and decrease the interfacial free energy of water. At a certain concentration the water surface becomes saturated and the surface tension does not change, even if the compound concentration in the bulk solution increases. At this concentration, a typical surfactant will self-assemble into molecular aggregates, often into micelles, and consequently the surface saturation concentration is called the critical micellar concentration (cmc).^{182, 267, 268}

The critical micellar concentration (cmc) characterizes the surface behavior of a surfactant and is therefore a highly valuable parameter.²⁶⁹ Cmc can be determined by analyzing several different physical properties (*e.g.* detergency, viscosity, density, conductivity, light scattering, and surface tension) of a particular surfactant in aqueous solution at different concentrations.^{267, 270} The measurement of surface tension is performed with a tensiometer, an instrument which measures the force of interaction between a surface and a probe connected to a balance. There are several different methods or probes to choose between, for example the Wilhelmy plate, the Du Noüy ring, and the Pendant/Sessile drop method.²⁷¹ Here, the Wilhelmy plate and the Pendant drop method will be discussed.

3.1 The Wilhelmy Plate Method

A vertical thin plate made of platinum of known perimeter is attached to a balance through a wire. The solution is raised to the plate so that it just touches the bottom of it. Surface tension (γ) is the force (F) measured by the balance divided by the perimeter (L) of the plate, Figure 3.1. The plate must be completely wetted to ensure that the contact angle (θ) is zero.²⁷¹

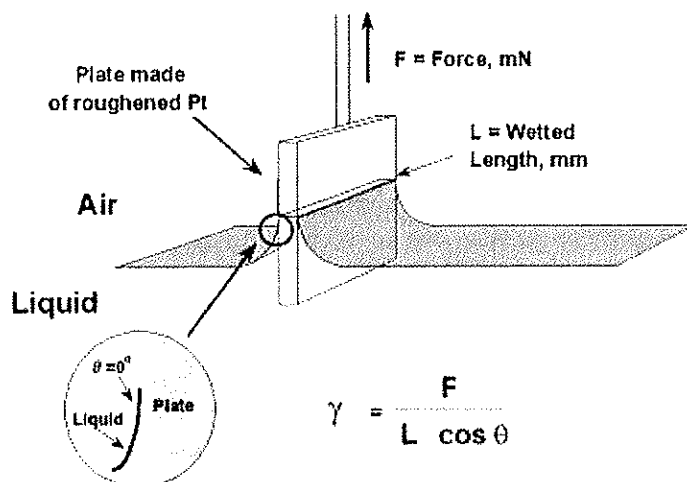


Figure 3.1 The Wilhelmy plate method (from ref. 272).

3.2 The Pendant Drop Method

The pendant drop method utilizes the geometry of a sample drop to analyze the surface tension. Like the Wilhelmy plate method it is a static process. The sample liquid is injected from a needle, thus forming a drop hanging from the tip of the needle. The drop is optically observed by a camera and the surface tension is then calculated by a computer program from the shape of the drop, based on a numerical solution of the theoretical Young-Laplace equation.^{273, 274} The surface tension is related to the drop shape through the following equation (eq. 3.1):

$$\gamma = \frac{\Delta\rho \cdot g \cdot R_0^2}{\beta} \quad \text{eq. 3.1}$$

where γ is the surface tension, $\Delta\rho$ is the density difference between the drop and the surrounding medium, R_0 radius of the drop curvature at apex, and β is the shape factor. The shape factor (β) is found from eq. 3.2 - eq. 3.4, which are derived from the Young-Laplace equation,²⁷³⁻²⁷⁵ see also Figure 3.2:

$$(d\theta)/(dS) = 2 - \beta Y - \frac{\sin \theta}{X} \quad \text{eq. 3.2}$$

$$(dX)/(dS) = \cos \theta \quad \text{eq. 3.3}$$

$$(dY)/(dS) = \sin \theta \quad \text{eq. 3.4}$$

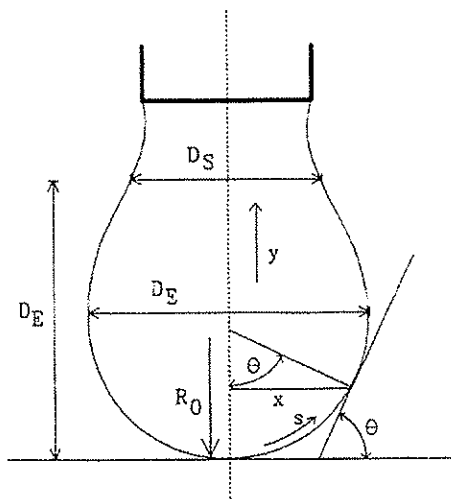


Figure 3.2 Illustration of a pendant drop and the co-ordinates x , y , s and θ from the Young-Laplace equation (from ref. 273).

3.3 Graphical determination of cmc

By measuring the surface tension (γ) of a series of increasingly concentrated solutions of a particular surfactant, a graph of γ vs. C is plotted (Figure 3.3). At low concentrations, only a small change in surface tension will be observed (I). At higher concentrations, the surface tension decreases with increasing concentration (II), until the surface is occupied, resulting in no or small changes in surface tension (III). Cmc is found at the discontinuity of the graphs.²⁷⁶ The graphs are obtained by regression analysis (e.g. polynomial, exponential, geometric, and Szyzkowski equation²⁷⁷). Further, the discontinuity is somewhat dependent on how the regression is performed (Figure 3.4).

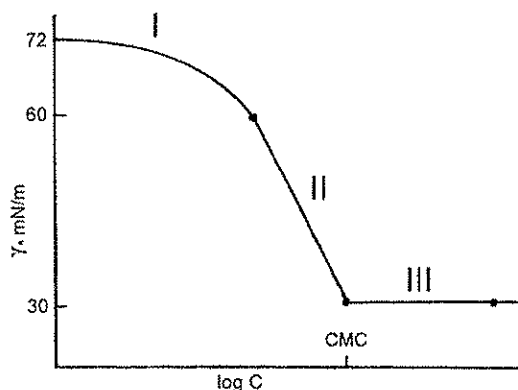


Figure 3.3 Schematic plot of surface tension (γ) versus logarithm of the surfactant concentration (C) (taken from ref. 276).

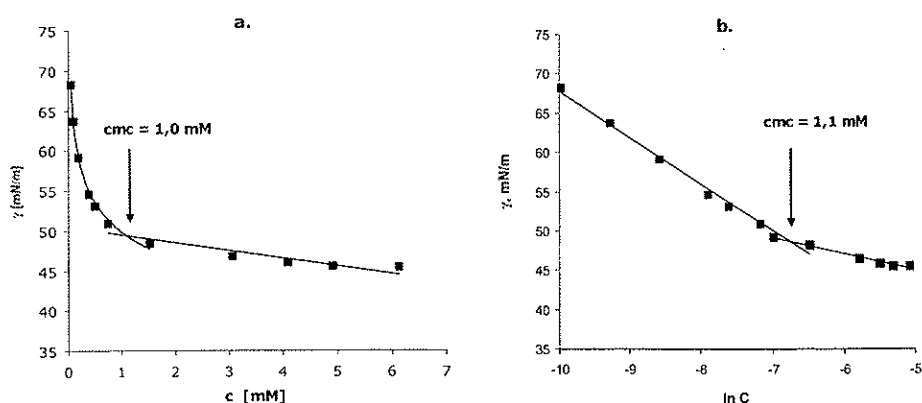


Figure 3.4 Graphical determination of cmc; **a**: geometric (γ vs. C), **b**: linear (γ vs. $\ln C$). Data from surface tension measurements of crocin (14) in water (paper 5).

3.4 Calculation of thermodynamic data

When surfactants disperse/dissolve in water, the molecules are in equilibrium between three states: as dispersed monomers in the solution, as self-assembled aggregates, and as adsorbed monomers at the air/water interface (Figure 3.5). The equilibrium is depending on temperature, pressure, and concentration.

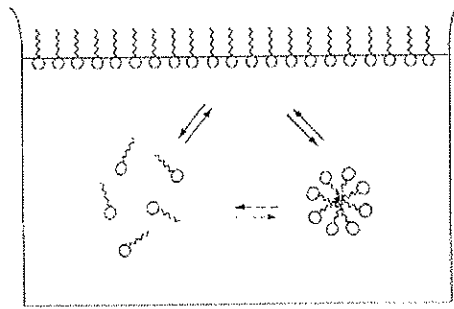


Figure 3.5 Schematic representation of the three states of surfactant molecules in water; monomers adsorbed at the air/water interface, monomers in the solution, and micelles (from ref. 269).

The thermodynamic data for the processes can be calculated from the surface tension (γ) versus log concentration (C) curves. The surface concentration (Γ), which is the number of moles per unit area (mol/m^2), is calculated from the declining slope ($d\gamma/d\ln C$):

$$\Gamma = \frac{1}{n \cdot R \cdot T} \cdot \left(\frac{d\gamma}{d\ln C} \right)_{cmc} \quad \text{eq. 3.5}$$

where n is the number of species in solution, R is the gas constant, and T is the absolute temperature.²⁶⁹ Γ indicates the maximum number of molecules at the surface and is a measure of the effectiveness of the adsorption, a useful factor for determining surface properties like wetting and emulsification.²⁷⁸

The area per molecule (a_m) (in $\text{\AA}^2/\text{molecule}$) at the surface saturation is obtained from:

$$a_m = \frac{10^{20}}{N \cdot \Gamma} \quad \text{eq. 3.6}$$

where N is the Avogadro number.²⁶⁹

The change in standard free energy per mole when associating in micelles, ΔG_m^0 (J/mol) is given by:

$$\Delta G_m^0 = n \cdot R \cdot T \cdot \ln cmc \quad \text{eq. 3.7}$$

Standard free energy of adsorption ΔG_{ad}^0 (J/mol) is the change in energy when a molecule in the bulk phase adsorbs to the surface. ΔG_{ad}^0 is found from eq. 3.8:

$$\Delta G_{ad}^0 = \Delta G_m^0 - \left(6,023 \cdot 10^{-3} \cdot \Pi \cdot a_m \right) \quad \text{eq. 3.8}$$

where Π is the surface pressure or the change of surface tension caused by the substrate ($\gamma^0 = 73$ mN/m);²⁷⁹

$$\Pi = \gamma^0 - \gamma \quad \text{eq. 3.9}$$

The equilibrium constant k^{280} is given by:

$$k = e^{-\frac{\Delta G}{n \cdot R \cdot T}} \quad \text{eq. 3.10}$$

3.5 Surface properties of water-dispersible/soluble carotenoids (paper 3, 4, and 5)

The surface tension was measured and thermodynamic data calculated for the water-dispersible carotenoid lysophosphocholine mixture **43a/43b/43c** (paper 3), CardaxTM (**30**) (paper 4), and crocin (**14**) (paper 5). In addition, the surface tension of the carotenoid potassium salts C30:9-K **64** and C30:9-cantha-K **65** were measured. Cmc for carotenoid potassium salts **64** and **65** were determined from linear regression (Figure 3.6), and the minimum and maximum values were obtained from different fitting of the graphs.

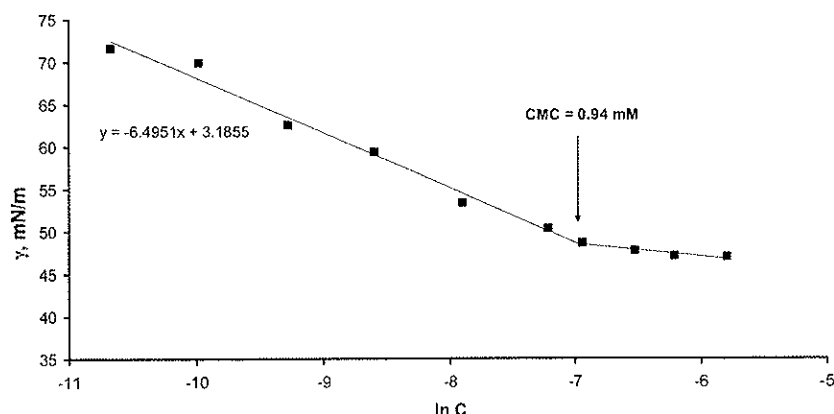


Figure 3.6 Graphical determination of cmc for C30:9-cantha-K **65**. The graphs were obtained by linear regression analysis determined from surface tension measurements by the Wilhelmy plate method. Cmc is found from the discontinuity of the graphs.

Thermodynamic data (Table 3.1) were calculated from eq. 3.5 - eq. 3.10, and showed comparable results for the two carotenoid potassium salts **64** and **65**. The surface concentration (Γ) was calculated from both $n = 1$ and $n = 2$. The value of n depends on the dissociation of the adsorbed surfactant. For zwitterionic or ionic surfactants with strong, counterion binding (ion pairing), $n = 1$. For completely dissociated surfactants with monovalent counterions, $n = 2$.²⁸¹⁻²⁸³ Dissociation is favored at low concentrations, and $n = 1$ is considered to be the most probable value at the determined cmc for the carotenoid potassium salts **64** and **65**.

Surfactants with one hydrophilic group normally orient themselves in a vertical or tilted manner with respect to the the liquid/air surface. This usually give a_m values between 40-60 Å²/molecule. Bola surfactants with two ionic polar groups, such as CardaxTM (**30**), are oriented in a horizontal manner, resulting in large a_m values (>200).²⁸⁴ The a_m data calculated for the mono polar surfactants **64** and **65** indicate an oblique orientation (66 ± 2 and 65 ± 2 Å²/molecule, $n = 1$) for both carotenoids, as observed for the glycoside carotenoid crocin (**14**) ($a_m = 67$) and C12:0-SO₄Na (SDS) ($a_m = 66$) (Table 3.2). When assuming full dissociation ($n = 2$), $a_m = 132 \pm 4$ and 125 ± 4 Å²/molecule is obtained, a molecular surface which is not in accordance with a horizontal orientation.

The surface concentration ($\Gamma = 2.5 \pm 0.1$ and $\Gamma = 2.7 \pm 0.1 \cdot 10^{-6}$ mol/m², for $n = 1$), indicates a packing of the surface film and a surface activity similar to crocin (**14**) and SDS (Table 3.2). Both carotenoid potassium salts **64** and **65** and crocin (**14**)

form more dense layers at the surface than CardaxTM (30), but less dense than the zwitterionic carotenoid lysophosphocholine 43a/43b/43c. The greater Γ , the more surface-active is the compound. The carotenoid lysophosphocholine 43a/43b/43c is the most surface-active of the carotenoid surfactants so far investigated.

The high equilibrium constants k_m (900/1100) and k_{ad} (52000/53000) of 64 and 65 demonstrate a high preference for surface adsorption compared with the other carotenoid surfactants (Table 3.1).

The absorption micellar energy ratio (AMER) was suggested as an indicator of a surfactant's performance, and values close to unity indicates dense monolayer formation, enhanced micelle concentration, and good cleansing and wetting properties.²⁸⁵ The AMER values of 64 and 65 (1.6 for both) resemble that of crocin (14) (1.7).

Thermodynamic data, except cmc values, of the potassium salts of saturated and unsaturated fatty acids are sparingly reported in literature^{284, 286} Some values are listed in Table 3.2. In a series of homologous (e.g. potassium salts of fatty acids) the cmc decreases linearly with increasing number of carbon atoms in the hydrophobic chain, according to eq. 3.11.

$$\log \text{cmc} = A - Bn \quad \text{eq. 3.11}$$

where A and B are constants and n is the number of carbon atoms. Double bonds with their shorter bond length (versus single bonds) reduce the effective chain length, in that a *cis* double bond is equivalent to the removal of 1-1.7 carbon atoms, a *trans* double bond removes 0.5-0.85 chain atoms.^{287, 288} Cmc values (at 25°C) for saturated potassium salts of chain length C11-C14, calculated from values obtained from ref. 287, give the equation:

$$\log \text{cmc} = 2.12 - 0.31n \quad \text{eq. 3.12}$$

where n is the number of carbon atoms. Cmc of the carotenoid potassium salts 64 and 65 place them between C16:0 and C17:0 fatty acids (Figure 3.7), indicating no significant effect of the somewhat polar double bonds for the effective chain length. This may show that their polar head group are the main contributors to their surfactant properties. In contrast, the double bonds in CardaxTM (30) and the carotenoid lysophosphocholine 43a/43b/43c had a chain reducing effect.

Crocin (14), the carotenoid potassium salts 64 and 65, CardaxTM (30), and the carotenoid lysophosphocholine 43a/43b/43c may all be called "efficient" surfactants, meaning that they reach the cmc at relatively high concentrations, but

still lower the surface tension markedly. This is in contrast to “effective” surfactants, such as SDS, which are effective at very low concentrations.²⁸¹

Table 3.1 Thermodynamic data (21°C) for water-dispersible/soluble carotenoids.

	Carotenoid lysophospho- choline 43a/43b/43c	Cardax™ (30)	C30:9-K 64	C30:9- cantha-K 65	Crocin (14)
γ_{cmc} (mN/m)	57	60	48	48	50
Π (mN/m)	16	13	25	25	23
cmc (mM)	1.3 ± 0.2	0.45 ± 0.05	1.10 ± 0.2	0.94 ± 0.2	0.90 ± 0.1
Γ 10^{-6}molm^{-2}	4.5 ± 1	0.7 ± 0.1	2.5 ± 0.1	2.7 ± 0.1	2.7 ± 0.1
a_m Å^2 / molecule	39 ± 9	240 ± 30	66 ± 2	63 ± 2	62 ± 2
ΔG_m^o kJ/mol	-16.2 ± 0.4	-54.8 ± 0.8	-16.6 ± 0.3	-17.0 ± 0.3	-11.5 ± 0.3
ΔG_{ad}^o kJ/mol	-20.1 ± 1.4	-73.6 ± 3.2	-26.5 ± 0.6	-26.4 ± 0.5	-20.0 ± 0.6
k_m	750	1800	900	1100	100
k_{ad}	3500	23000	52000	53000	3500
AMER $(\Delta G_{ad}^o)/(\Delta G_m^o)$	1.2	1.3	1.6	1.6	1.7

Table 3.2 Thermodynamic data (21-25°C) of the carotenoid potassium salts C30:9-K **64**, C30:9-cantha-K **65**, and related compounds.

Chain length	cmc (mM)	ΔG_{ad}° (kJ/mol)	Γ (10^{-6}molm^{-2})	a_m ($\text{\AA}^2/\text{molecule}$)	γ_{cmc} (mN/m)
C30:9-K 64	1.10 ± 0.2	-26.5 ± 0.6	2.5 ± 0.1	66 ± 2	48
C30:9-cantha-K 65	0.94 ± 0.2	-26.4 ± 0.5	2.7 ± 0.1	63 ± 2	48
C8:0-K	430 ^a	-	-	-	-
C10:0-K	100 ^a 93.3 ^b	- -8.1 ^b	-	-	38 ^b
C12:0-K	25.5 ^{a,d}	-	3.8 ^c	43 ^c	-
C14:0-K	6.0 ^{a,d}	-	-	-	-
C16:0-K	3.2 ^d	-	-	-	-
C18:0-K	0.35 ^a 0.70 ^{b*}	-18.2 ^{b*}	-	-	66 ^{b*}
C18:1-K (oleat)	1.0 ^e 6.3 ^b	-12.2 ^b	-	-	49 ^b
C12:0-SO ₄ Na	8.2 ^d	-27 ^f	2.5 ^d	66 ^d	39 ^d

a Calculated from values obtained from *ref. 287*, b *ref. 286*; * at (60°C), c *ref. 284*, d *ref. 289*, e *ref. 287*, f *ref. 285*.

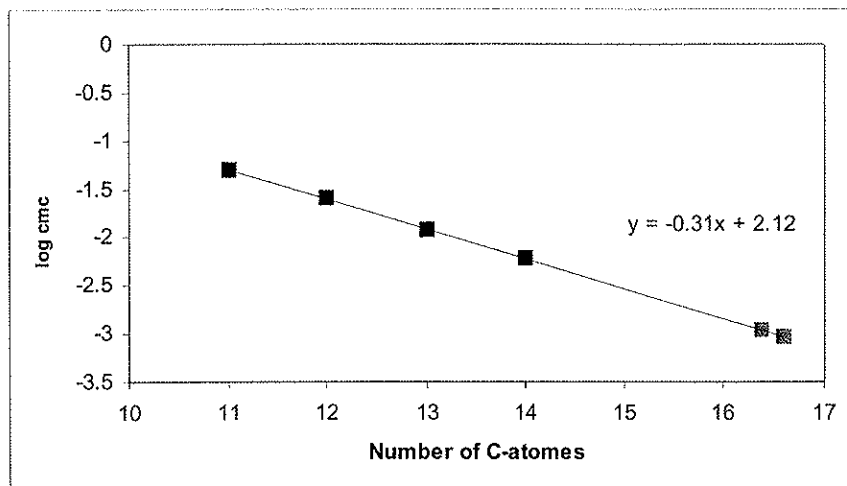


Figure 3.7 Number of chain carbon atoms for C11:0 - C14:0 versus log cmc. Extrapolating the measured cmc values (at 21°C) for **64** and **65** (■) places them in the range of C16:0 and C17:0 fatty acids.

3.5.1 Sample preparation and recording

Stock solutions were made from dry compounds (dried under reduced pressure at 1-3 mbar overnight) and distilled, filtered (0.22 μm) water. The stock solutions were stirred, then diluted to the appropriate concentrations. All samples were prepared the same day or the day before measuring. For the Wilhelmy method, the solutions were poured into the measuring vessel (each sample, approximately 20 ml). Four to eight measurements were performed for each sample, and the values were recorded immediately after the initial equilibrium was reached. After each measurement, the plate was rinsed with distilled water and acetone, then briefly heated to glowing by holding it above a Bunsen burner. The plate was brought back to room temperature before it was attached to the hook projecting from the headpiece of the instrument. Before changing samples, the measuring vessel was cleaned with soap and rinsed thoroughly with distilled water and acetone, then dried with a hair dryer. The same procedure for making the aqueous solutions was followed for the pendant drop method. The solution was injected through the needle. One hundred measurements were recorded within two seconds, the mean value (mN/m) was used, and standard deviation was between 0.01-0.02. Only the carotenoid lysophosphocholine mixture **43a/43b/43c** was measured by both the pendant drop and the Wilhelmy plate method, and both methods gave comparable data.

4 Aggregation behavior

Aggregation behavior of non hydrophilic carotenoids in aqueous/organic solutions have traditionally been investigated by UV-VIS spectroscopy (see Chapter 1.8.1). In this work UV-VIS spectroscopy and dynamic light scattering (DLS) were used to characterize and measure aggregates formed by water-dispersible/soluble carotenoids upon addition of water.

4.1 UV-VIS spectroscopy of water-dispersible/soluble carotenoids (*paper 3, 4, and 5*)

UV-VIS spectra in water of the carotenoid lysophosphocholines *R-43a* and *43a/43b/43c*, carotenoid phosphocholine esters **60** and **61**, carotenoid potassium salts **64** and **65**, carotenoid-selena-phosphocholine **66**, CardaxTM (**30**), and crocin (**14**) show different aggregation behavior. However, most of the compounds give hypsochromic shifts in water ranging from 10 to 75 nm from the monomer absorption in organic solutions (Table 4.1). The shifts are likely the result of H-aggregate formation.²¹⁴⁻²¹⁶ In addition, the small shoulders observed around 500-520 nm (for crocin (**14**) at 480 nm) are thought to arise from J-aggregates. Spectra of carotenoid phosphocholine ester **60** both in water and in organic solution do not differ much, although a small shoulder at 380 nm (H-aggregates) from the λ_{\max} in organic solution is observed (Figure 4.1). The aqueous solution of potassium salt **65** gives a minor hypsochromic shift (10 nm) compared to the monomer solution in methanol (Figure 4.2). Additionally, the peak at 338 nm is occasionally observed. This is in contrast to **64**, which in water indicates a clear hypsochromic shift from 439 to 364 nm (H-aggregates), as seen in Figure 4.3.

Table 4.1 λ_{\max} of the water-dispersible/soluble carotenoids in organic and aqueous solution. The hypsochromic shifts (nm) resulting from aggregated solutions are given.

Compound	λ_{\max} in organic solution (nm)	λ_{\max} in aqueous solution (nm)	Hypsochromic shift (nm) H-aggregates	Shoulder J-aggregates (nm)
<i>R-43a</i>	450 ^a /446 ^b	380-400	50-70	500(s)
43a/43b/43c	450 ^a /446 ^b	380-400	50-70	500(s)
60	453 ^c	380(s)	73	520(s)
61	460 ^c	386	74	520(s)
64	437 ^c	364	73	520(s)
65	455 ^c	445/338	10/117	520(s)
66	447 ^c	402	45	520(s)
30	490 ^a	440	50	-
14	440 ^c	420	20	480(s)

^a in acetonitril, ^b ethanol, ^c methanol, s = small peak/shoulder

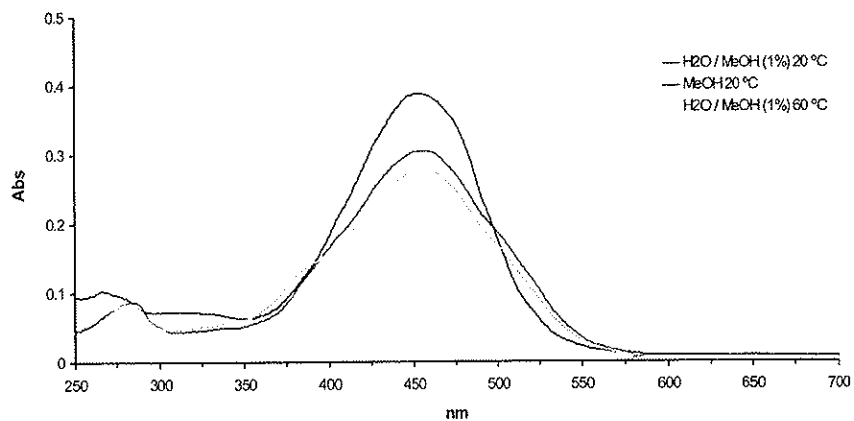


Figure 4.1 UV-VIS of carotenoid phosphocholine ester **60** in methanol (at 20 °C) and water/methanol (99/1%, v/v), at 20 and 60 °C.

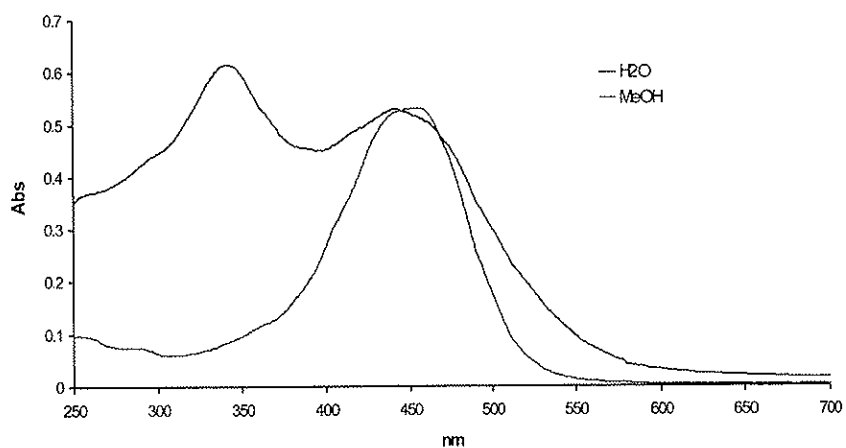


Figure 4.2 UV-VIS of carotenoid potassium salt **65** in water and methanol.

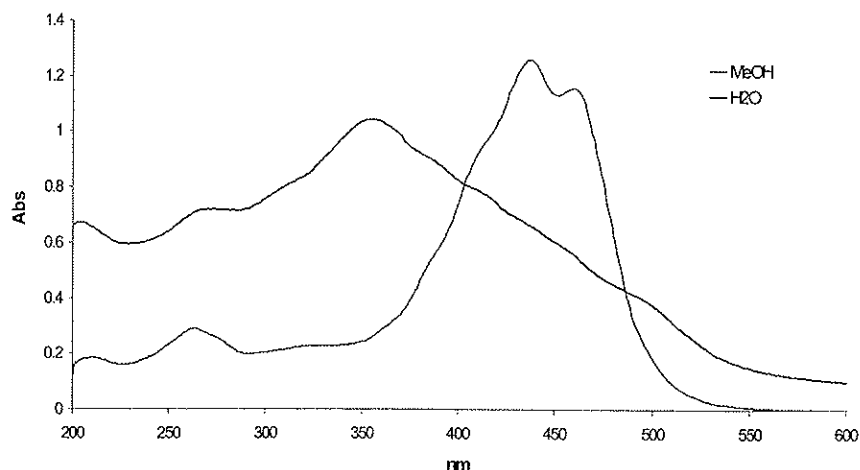


Figure 4.3 UV-VIS of carotenoid potassium salt **64** in water and methanol.

The temperature-dependent stability of the aggregates in water was examined for carotenoid phosphocholine esters **60** and **61** and lysophosphocholine **43a/43b/43c**. It was found that these compounds form stable aggregates up to 60°C (Figure 4.1).

When organic solvents (*e.g.* methanol, ethanol, and acetonitrile) were added to the aqueous solutions, small or no changes in the absorption spectra are observed at first. After addition of significant amounts, an abrupt change in solution from aggregates to monomers is evident, in accordance with previous observations^{158, 162}. The complete disruption of aggregation was achieved by adding: 27% methanol to the aqueous solution of carotenoid phosphocholine ester **61** (Figure 4.4), 41% ethanol to the aqueous solution of carotenoid lysophosphocholine **43a/43b/43c**, 44% methanol to the aqueous solution of carotenoid-selenaphosphocholine **66** (Figure 4.5), and 47 % methanol to the aqueous solution of carotenoid potassium salt **64**.

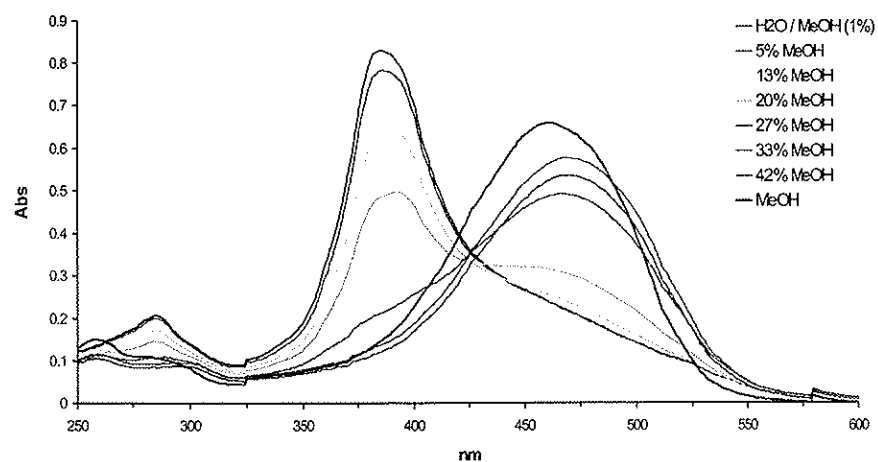


Figure 4.4 UV-VIS of carotenoid phosphocholine ester **61** in water/methanol (99/1%, v/v) vs. dropwise addition of methanol.

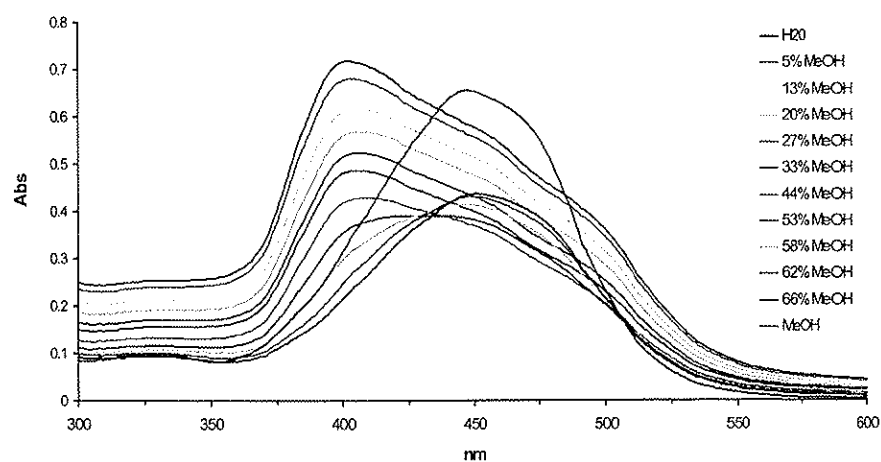


Figure 4.5 UV-VIS of carotenoid-selena-phosphocholine **66** in water vs. dropwise addition of methanol.

4.2 Dynamic light scattering

Light scattering is an important technique for the study of the size of aggregates, polymers, and particles.²⁹⁰ This method is a non-destructive technique, and

artifacts associated with particle isolation, sample drying, and sample loss can be avoided. Dynamic light scattering (DLS), also referred to as quasi-elastic light scattering or photon correlation spectroscopy, is applicable over a wide size range.²⁹¹ The main components of a light scattering instrument are shown in Figure 4.6.²⁹²

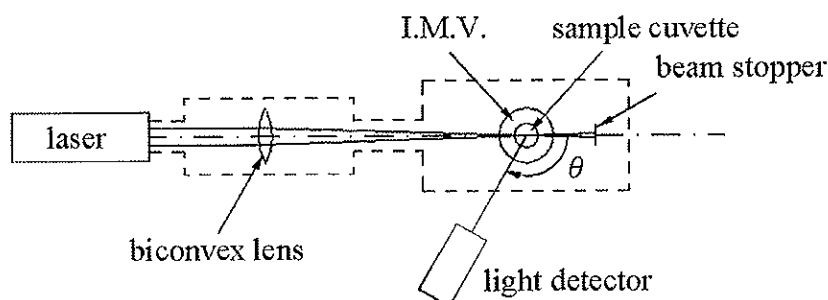


Figure 4.6 The main components of a light scattering instrument. The index matching vat is denoted I.M.V.

When a beam of light passes through a particle suspension, the particles scatter the light in all directions. If the light is coherent and monochromatic, as from a laser, it is possible to observe time-dependent fluctuations in the scattered intensity using a detector (Figure 4.7). These fluctuations arise from the particles thermal, random (Brownian) motions and contain information about the particle's translational and rotational motion. Analysis of the time dependence of the intensity fluctuations can therefore give the translational and rotational diffusion coefficients of the particles.²⁹³

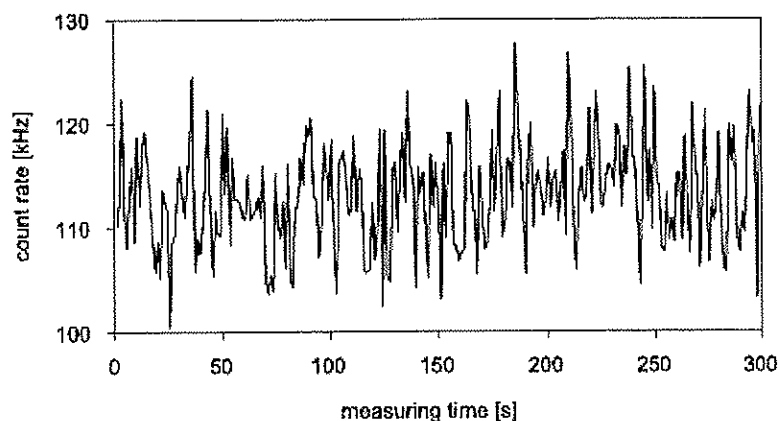


Figure 4.7 Illustration of the intensity fluctuations of scattered light. The count rate is plotted against measured time.

The time dependence of the intensity fluctuation is most commonly analyzed using a digital correlator. Such a device determines the intensity autocorrelation function of the scattered light:

$$g_2(\tau) = \frac{\langle I(t)I(t+\tau) \rangle}{\langle I(t) \rangle^2} \quad \text{eq. 4.1}$$

where $I(t)$ and $I(t+\tau)$ are the intensity of the scattered light at time t and $t+\tau$, respectively.

Over time, as particles diffuse, the correlation diminishes. Fast decay results from rapid diffusion of small particles, while slow decay is the result of the motions of larger particles.²⁹¹ The exponential decay of the correlation function is characteristic for the diffusion coefficient (D) of the particles.²⁹⁴ Data are typically collected over a delay range from 200 ns to several seconds, depending on the particle size and viscosity of the solution.

The diffusion coefficient of the particle is closely related to particle size, expressed by the Stokes-Einstein relation:

$$D = \frac{k_B \cdot T}{6 \cdot \pi \cdot \eta \cdot R_h} \quad \text{eq. 4.2}$$

where k_B is the Boltzmann constant, T is the absolute temperature, η is the viscosity of the solvent, and R_h is the hydrodynamic radius of the particles.²⁹¹

For spheres $R_h = R$, and for non-spherical particles, the equation above gives the equivalent hydrodynamic radius of the particles (example given in Figure 4.8). For non-spherical particles with defined geometry such as ellipsoids and rods, analytical expressions for D are available.²⁹⁵

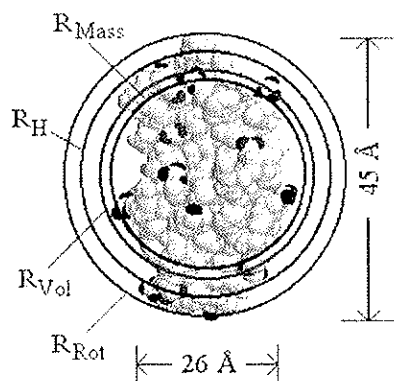


Figure 4.8 Hydrodynamic radius (R_h) of a non-spherical particle ($l = 45 \text{ \AA}$). R_{rot} stands for rotational radius.

Several methods exist for analyzing the correlation functions. The Fortran program Contin is one of the most widely used methods. A typical distribution function obtained by Contin analysis is shown in Figure 4.9. Additionally, there are different methods used to define the particle size distribution (*e.g.* number-, mass-, and intensity-weighted distribution). The number-weighted distribution gives the number ratio between the different populations of particles in the solution.

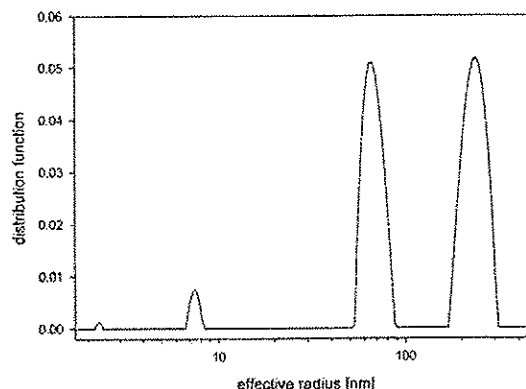


Figure 4.9 A typical plotted intensity distribution function for a sample versus the effective hydrodynamic radius (R_h).

4.3 Aggregation properties of water-dispersible/soluble carotenoids (paper 3, 4, and 5)

The hydrodynamic radius (R_h) and proposed shape of the aggregates of the water-dispersible carotenoid lysophosphocholine **R-43a** and **43a/43b/43c**, CardaxTM (**30**), and crocin (**14**), upon addition of water, are shown in Table 4.2 Carotenoid lysophosphocholine **R-43a** and **43a/43b/43c** spontaneously form stable, yellow dispersions in water. Aggregation starts far below cmc, as confirmed by UV-VIS spectroscopy. It has previously been suggested that lysophosphocholines with long chain fatty acids exist as monomers or small aggregates at concentrations below cmc. At concentration over cmc, larger aggregates are assumed to appear.²⁹⁶

The number-weighted distribution of **R-43a** and **43a/43b/43c** indicate a dominance of nanometer-sized aggregates of 6 and 8 nm, respectively. In addition, some larger aggregates (30-500 nm and 40-600 nm, respectively) are formed. The pure isomer **R-43a** and the isomeric mixture **43a/43b/43c** show similar aggregation behavior. This has earlier been reported for other regioisomeric (lyso)phosphocholines.²⁹⁷

The anionic bolaamphiphile CardaxTM (**30**) aggregated at concentrations below cmc, as did **R-43a** and **43a/43b/43c**. The rigid spacer and the charge of the polar groups in CardaxTM (**30**) prevent the formation of small, curved aggregates. Aggregates of CardaxTM (**30**) are dominated by the formation of large, extended

monolayer structures. DLS measured both in water and in 0.15 M NaCl, displayed a fast formation of aggregates of 1.2-1.3 μm size (Table 4.3). In 0.5 M and 2.0 M NaCl, a slow association of the aggregates to larger ones was observed. This behavior is thought to be a result of the shielding of charges and binding of counterions due to the higher salt concentration, thus, the repulsion between the particles is reduced and aggregation is favored.

A different behavior was observed for neutral crocin (**14**) in water. At $C < \text{cmc}$, only monomers occur. At $C > \text{cmc}$, aggregates of size 1.6 nm were observed, together with few aggregates in the region 6-200 nm.

Table 4.2 Hydrodynamic radius (R_h) and shape of aggregates formed by water-dispersible carotenoids in water (measured by DLS).

Compound/ Concentration	Hydrodynamic radius (R_h) in water	Assumed shape of particle
R-43a 0.05 mg/ml, $C < \text{cmc}$	6 nm 30-500 nm	lamellar
43a/43b/43c 0.05 mg/ml, $C < \text{cmc}$	8 nm 40-600 nm	lamellar
14 0.06 mg/ml, $C < \text{cmc}$	0.7 nm 6-200 nm	monomer/ vesicle
2.0 mg/ml, $C > \text{cmc}$	1.6 nm 6-200 nm	vesicle
30 0.06 mg/ml, $C < \text{cmc}$	1.3 μm	non-spherical vesicle

Table 4.3 Hydrodynamic radius (R_h) of CardaxTM (**30**) in water and in different NaCl concentrations (measured by DLS).

Compound/ Concentration	Hydrodynamic radius (R_h)			
	Water	NaCl (0.155 M)	NaCl (0.5 M)	NaCl (2.0 M)
30 0.06 mg/ml	1.3 μm	1.2 μm	3 μm	10 μm

5 Biological activity

5.1 General

Free radicals and reactive oxygen species, such as singlet oxygen ($^1\text{O}_2$) and superoxide anion ($\text{O}_2^{\bullet-}$), are the major contributors to the process of oxidative stress in the human body. In model systems, carotenoids are potent quenchers of singlet oxygen ($^1\text{O}_2$) as well as direct radical scavengers, and strong evidence suggests that they are important antioxidants *in vivo* as well²⁷ (see also Chapter 1.2.5).

Radical reaction kinetics depends on the individual carotenoids and the model systems (solvent and radical species) used.^{79, 298, 299} Most of the biological reactions occur in aqueous systems in the form of emulsions or aggregates. Yet few data on the radical scavenging or singlet oxygen quenching ability of carotenoids, in aqueous or micellar systems, are found in the literature. However, aqueous singlet oxygen ($^1\text{O}_2$) quenching abilities have been evaluated for crocetin (**15**), crocin (**14**), and β,β -carotene (**12**). The water-dispersible/soluble carotenoids crocetin and crocin showed $^1\text{O}_2$ quenching capacities in water comparable to other carotenoids in organic solution.^{300, 301} The non-polar β,β -carotene did not quench $^1\text{O}_2$ ³⁰², nor inhibit autooxidation of linoleic acid³⁰³ in an aqueous micelle system. This is likely to be the result of aggregation of β,β -carotene in water.³⁰² Supramolecular assemblies of carotenoids in water seem to inhibit scavenging of radicals and reactive oxygen species.¹⁶⁴ Therefore, both the dispersibility/solubility and behavior of the individual molecules of a carotenoid in water, have to be taken into consideration when their antioxidant properties are evaluated.

Spin trap electron paramagnetic resonance (spin trap-EPR) spectroscopy provides direct evidence of the presence of radicals in a reaction system. EPR spectroscopy detects the resonance absorption of microwave radiation by paramagnetic ions or molecules (with at least one unpaired electron spin), in the presence of a static, magnetic field. EPR spectroscopy has a wide range of applications in chemistry, physics, biology, and medicine. Most commonly, EPR spectra are recorded in the range of 9-10 GHz (X-band).³⁰⁴ In the spin-trapped method, the transient radical is reacted with a diamagnetic reagent to form a more persistent radical, which can be detected by EPR.³⁰⁵

5.2 Direct superoxide anion ($\text{O}_2^{\bullet-}$) scavenging of carotenoid lysophosphocholine 43a/43b/43c evaluated by EPR spectroscopy (*paper 6*)

In this work, direct superoxide anion ($\text{O}_2^{\bullet-}$) scavenging by the highly water-dispersible carotenoid lysophosphocholine 43a/43b/43c was measured by EPR

spectroscopy using the spin trap DEPMPO (Oxis, Portland, OR). The assay used is a standard *in vitro* test system, where $O_2^{\bullet-}$ is produced from isolated human neutrophils.

The experiments were performed in ethanolic/water (prepared from 41% ethanol stock solution), to ensure a monomeric solution, as evidenced by UV-VIS spectroscopy, and in water, where the carotenoid self-assembles into vesicles (Chapter 4). The results are summarized in Table 5.1, and compared with recently reported values for both the novel highly water-dispersible tetrahydrochloride salt of the dilysinate diester of astaxanthin (**31**)¹⁶² and CardaxTM (**30**).¹⁶⁴ Included is also the mean inhibition (%) of non-esterified astaxanthin (reference standard) in a DMSO test system.

Table 5.1 Mean inhibition (%) of aqueous superoxide anion ($O_2^{\bullet-}$) production for increasing concentration of aqueous and ethanolic solutions of water-dispersible carotenoids. Non-esterified astaxanthin was used as a reference standard.

Carotenoid	Solvent	Concentration (mM)	Mean inhibition (%)
carotenoid lysophosphocholine 43a/43b/43c	water	0.5	18.2
	water	1.0	24.6
	water	3.0	51.8
	water	10.0	94.3
	EtOH (41%)	0.1	13.3
	EtOH (41%)	0.3	31.3
	EtOH (41%)	0.5	61.7
	EtOH (41%)	1.0	79.3
	EtOH (41%)	3.0	98.7
	Cardax TM (30) ^a	water	0.1
EtOH (33%)		0.1	38.0
EtOH (33%)		0.5	60.1
EtOH (33%)		1.0	78.0
EtOH (33%)		3.0	95.0
astaxanthin-amino acid conjugate 31 ^b	water	0.001	10.3
	water	0.01	46.7
	water	0.05	86.0
	water	0.1	95.7
astaxanthin ^a	DMSO	0.1	28.0

^a from ref. 164, ^b from ref. 162.

The positional isomers of carotenoid lysophosphocholine **43a**, **43b** and **43c** are expected to behave identically, as the structure of their hydrophobic chain is identical. For the different stereoisomers of the disodium disuccinate diester of astaxanthin (CardaxTM) (**30**), no significant differences related to radical scavenging properties were observed.¹⁶⁴

From Table 5.1, it is seen that the scavenging ability of water-dispersible carotenoids (**43**, **30**, and **31**) are concentration-dependent, and the quenching of the induced superoxide anion signal can be near completed. Over 90% of the superoxide anion is scavenged by **43a/43b/43c** and **31** in 10mM and 0.1 mM water solution, respectively. Identical scavenging capacity was obtained by **43a/43b/43c** and **30** in 3mM ethanol/water solution (prepared from 41% and 33 % ethanol stock solutions). Using same concentrations (0.5, 1.0, and 3.0 mM) in either water or 41% ethanol, the scavenging ability was found to be superior in ethanol (Figure 5.1), as was also observed for CardaxTM (**30**).

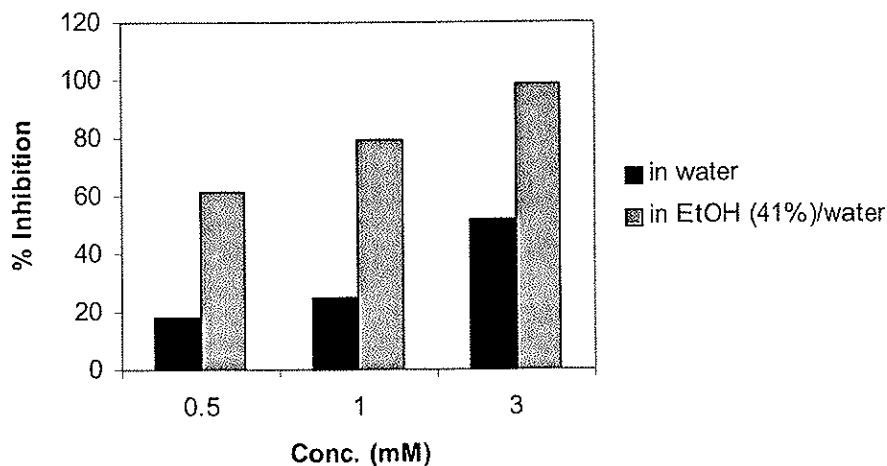


Figure 5.1 Comparison of the superoxide anion ($O_2^{\bullet -}$) scavenging ability of carotenoid lysophosphocholine **43a/43b/43c** at various concentrations in water and ethanol/water solutions, detected by spin-trap EPR spectroscopy.

Because water-dispersible carotenoids aggregate in water, and occur as monomers in aqueous ethanol solutions, it can be concluded that the radical scavenging ability of self-assembled aggregates are less than that of a monomeric solution of the same carotenoid. This phenomenon is also attributed to the absence of a linear

relationship between the concentration and the scavenging properties in both water and ethanol/water solutions. Only at concentrations ≤ 0.5 mM in ethanol (no aggregation), an almost linear increase is seen.

In ethanol/water at 100 μ M, the mean scavenging ability of carotenoid lysophosphocholine **43a/43b/43c** (13.3%) is less than of CardaxTM (**30**) (38.0%). This is believed to be the result of their difference in effective chromophore length (dependent on the total number of polyene bonds; 9 vs. 11, and λ_{max} ; 446 vs. 481 nm).³⁰⁶ However, this can be compensated by the higher water-dispersibility of carotenoid lysophosphocholine **43a/43b/43c** (>60 mg/mL) compared to CardaxTM (**30**) (9 mg/mL).

Of the hydrophilic carotenoids investigated so far, the highly water-dispersible tetrahydrochloride salt of dilysinate diester of astaxanthin (**31**) (>182 mg/mL), synthesized by Hawaii Biotech, Inc., shows the most effective superoxide anion scavenging properties in aqueous solutions, as tested by spin trap-DEMPO EPR spectroscopy. Total scavenging (95.7%) is reached with only a 100 μ M water solution without addition of a co-solvent (Table 5.1).

In conclusion, water-dispersible carotenoids, such as carotenoid lysophosphocholine **43a/43b/43c**, are potent aqueous-phase, direct scavengers of superoxide anion ($\text{O}_2^{\bullet -}$) produced from isolated human neutrophils. Carotenoid lysophosphocholine **43a/43b/43c** may also be a potent scavenger of other reactive oxygen species and free radicals in biological systems.

6 Laser flash photolysis of radicals and triplet states of carotenoids

6.1 General

Laser flash photolysis (LFP) is a useful method for the investigation of reactive species (*e.g.* excited states and radicals), which, as a function of time, are generated by a laser pulse. Pulse radiolysis was introduced after LFP, and both techniques do not differ much from conventional UV spectroscopy. The experimental setup is shown in the illustration below (Figure 6.1).

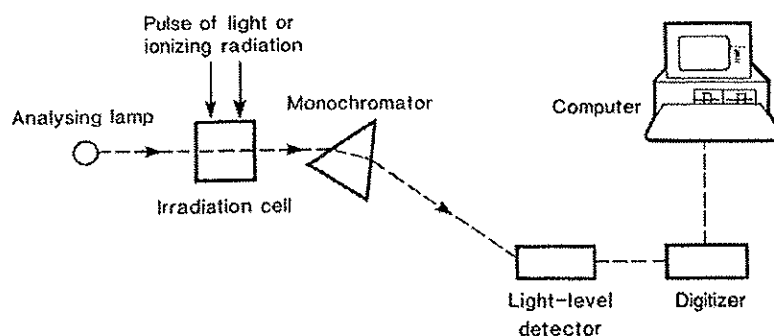


Figure 6.1 Principle of flash photolysis and pulsed radiolysis (*from ref. 35*).

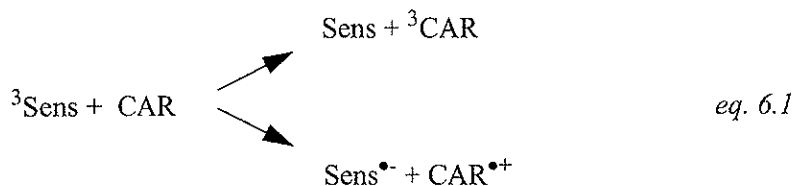
LFP and pulse radiolysis have been used to study excited states and radical cations of carotenoids. Carotenoids can act both as an acceptor of triplet energy and as an electron donor (see also Chapter 1.2.5), which result in either a triplet state (^3Car) or radical cation ($\text{Car}^{\bullet+}$).³⁵ The majority of the studies of triplet states and radical cations have been performed in organic solutions. However, the triplet state of water-dispersible crocetin (**15**) was studied in aqueous solutions by LFP.³⁰⁷ The triplet and radical absorption of carotenoids resembles that of carotenoids in the ground state, *i.e.* increasing absorption coefficients and bathochromic shifts with increasing number of double bonds. The triplet states and radical cations absorb at higher absorption maxima than the parent carotenoids, an example is given in Table 6.1. There is an upper absorption limit for ground state (S) and ^3Car spectra after a certain number of double bonds is reached. There is no such convergence limits for $\text{Car}^{\bullet+}$ absorption.³⁵

Table 6.1 Absorption maxima (nm) for ground state, triplet state, and radical cations of septapreno- β,β -carotene and β,β -carotene (n is the number of double bonds).

Carotenoid	n	Species	Solvent	λ_{\max} (nm)
Septapreno- β,β -carotene ^a	9	neutral	hexane	410
		triplet state	hexane	495
		radical cation	hexane	915
β,β -carotene ^a	11	neutral	pet.ether	445
		triplet state	hexane	515
		radical cation	hexane	1050

^a From ref. 35.

The sensitizer 1-nitronaphthalene in the triplet state ($^3\text{Sens}$) has the ability to either donate triplet energy to carotenoids (eq. 6.1), or accept an electron from carotenoids. Since $^3\text{Sens}$ can produce singlet oxygen ($^1\text{O}_2$) (see Chapter 1.2.5), these reactions indirectly quench the formation of $^1\text{O}_2$. The ratio of the probabilities for energy- or electron transfer is called the bifurcation ratio, and depends upon the polarity of the solvent used. By using 1-nitronaphthalene as a sensitizer, both the energy- or electron-transfer reactions of a carotenoid can be investigated in the same experiment.³⁰⁸



6.2 The antioxidant properties of water-dispersible/soluble carotenoids (paper 7)

The antioxidant properties of carotenoid lysophosphocholine **43a/43b/43c**, CardaxTM (**30**), and crocin (**14**) were investigated by laser flash photolysis using 1-nitronaphthalene as the sensitizer. All compounds were investigated as monomers in MeCN possessing a dielectric constant of 36, and water/MeCN (5:1) having an estimated dielectric constant of 75.

The wavelength absorption maxima (nm) of triplet states and cation radicals of all three compounds are shown in Table 6.2. Except for the differences expected from the number of double bonds, consistent results were obtained for all three carotenoids. The collision between 1-nitronaphthalene ($^3\text{Sens}$) and the carotenoids either leads to energy or electron-transfer, and the ratio of the reactions changes with solvent polarity. In MeCN (lowest dielectric constant), energy-transfer is favored, while in aqueous solution (highest dielectric constant), electron-transfer is dominant (Table 6.3). The decay of $^3\text{Sens}$ matches the increase in both ^3Car and $\text{Car}^{\bullet+}$, but is best seen by the increase in $\text{Car}^{\bullet+}$, since the lifetime of ^3Car is small. The lifetime of $^3\text{Sens}$ is slightly longer in the mixed solvent (15 μs) than in MeCN (7 μs). In the case of crocin (**14**), a stronger shift of the bifurcation ratio toward energy-transfer is seen in MeCN, in comparison with carotenoid lysophosphocholine **43a/43b/43c** and CardaxTM (**30**).

Table 6.2 Absorption maxima (nm) of triplet state and radical cations of water-dispersible/soluble carotenoids in organic and aqueous solvents (n is the number of double bonds).

Carotenoid	n	Species	Solvent	λ_{max} (nm)
crocin (14)	7	triplet state radical cation	MeCN or water/MeCN	490 680
carotenoid lysophospho- choline 43a/43b/43c	9	triplet state radical cation	MeCN or water/MeCN	505 820
Cardax TM (30)	11	triplet state radical cation	MeCN or water/MeCN	550 850

Table 6.3 The energy-/electron-transfer ratio (bifurcation ratio) of water-dispersible carotenoids in organic and aqueous solvents.

Carotenoid	Solvent	Energy-/electron transfer ratio ($^3\text{Car} : \text{Car}^{\bullet+}$)	
		bifurcation	peak heights
carotenoid lysophosphocholine 43a/43b/43c	MeCN	7.6	3.33
	water/MeCN	0.6	0.41
Cardax TM (30)	MeCN	2.7	2.2
	water/MeCN	-	0.4
crocin (14)	MeCN	-	-
	water/MeCN	-	0.61

6.3 Aggregation vs. formation of ^3CAR and $\text{CAR}^{\bullet+}$ (paper 7)

Crocin (**14**) is perhaps one of the few water-soluble carotenoids, which at modest concentrations, exists only as monomers in water. The aggregation of carotenoids in water has been shown to exert autoprotective properties, the photodegradation of carotenoid aggregates was significantly reduced compared to the photobleaching of the monomers.²¹⁷ Some investigations of aggregated $\text{CAR}^{\bullet+}$ have been performed, in that aggregated CAR in TX-100 micelles prevented electrochemical oxidation.³⁰⁹

Of the three carotenoids investigated in water, carotenoid lysophosphocholine **43a/43b/43c** and CardaxTM (**30**) did not react with the triplet sensitizers 1-nitronaphthalene, rose bengal, and methylene blue. The aggregation of carotenoids prevents the sensitizer from reaching the polyene chain, which is located in the interior of the aggregate. Addition of melittin, a natural membrane opener^{310, 311} also had no effect. Carotenoid molecules only become available when the aggregates are disrupted to monomers by addition of organic solvents (Table 6.2). In conclusion, both the water-dispersible carotenoid lysophosphocholine **43a/43b/43c** and CardaxTM (**30**) exhibit self-protecting properties due to aggregate formation in water.

7 SAM formation investigated by electrochemical methods

7.1 General

Self-assembled monolayer (SAM) formation provides a rational route to the preparation of well-defined, organized, monomolecular assemblies on solid surfaces (e.g. gold and silver) (see Chapter 1.8.2). The degree of organization depends on the structure of the adsorbed species due to geometry, interactions within the monolayer, and affinity to the metal surface. As a result, SAMs can be slightly disordered (liquid like) or well-packed (crystal-like). Not only the choice of adsorbed species, but also introduction of two different groups to the monolayer (mixed monolayers) can be used to control the composition and properties of self-assembled monolayers.²²³

SAMs are characterized by substrate rugosity, molecular conformation, molecular orientation, monolayer structure, and monolayer morphology (e.g. stability, thickness, coverage degree, and pinhole defect density).²²⁴ The formation and characterization of SAMs have been studied and elucidated by several methods, including contact angle measurements, X-ray photoelectron spectroscopy (XPS), Raman and infrared spectroscopy, scanning-tunneling microscopy (STM), and electrochemical techniques, such as cyclic voltammetry (CV), electrochemical impedance spectroscopy (EIS), and electrochemical quartz crystal microbalance (EQCM).^{224, 225, 228, 231} The electrochemical techniques will be discussed in the next section.

7.2 Electrochemical techniques

7.2.1 Cyclic voltammetry (CV)

Voltammetry refers to the measurement of current as a function of applied potential (voltage). In cyclic voltammetry (CV), the potential of an electrode in solution is linearly cycled between a starting potential and a final potential (multiple cycles can take place). During this process the electrochemical reaction of the species in the solution is continually cycled. The basic shape of the current response for a CV experiment performed on a redox couple (R/O), is shown in Figure 7.1. At the start of the experiment (point A), the initial potential is too low for an oxidation ($R \rightarrow O$) to take place. At a critical potential of the forward scan, the oxidation of R will take place. At point B the potential is sufficiently positive that any R that reaches the electrode surface will be oxidized. After reversal of the potential scan direction (C) and upon depletion of the oxidized species, the reverse reaction ($O \rightarrow R$) (D) takes place.^{312, 313}

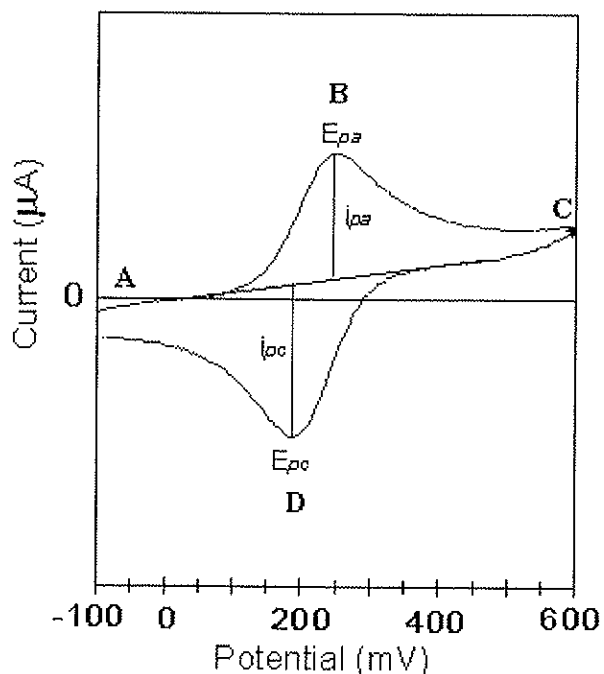


Figure 7.1 The basic shape of the current response for a cyclic voltammetry experiment performed on a redox couple R/O (taken from ref. 312)

If the electron-transfer reaction remains at equilibrium throughout the potential scan, the electrochemical process is said to be reversible. The peak current ratio (i_{pa}/i_{pc}) is then equal to 1 for all scan rates whereas the difference of peak potentials ($E_{pa} - E_{pc}$) is $0.059/n$ V at 25 °C (n stands for the number of electrons involved in the electrochemical reaction). For irreversible reactions or if adsorption of species take place, the voltammogram shape will change.^{312, 314}

CV can monitor chemical reactions and provide useful information about the stability, number of oxidation states, and rate constants of the reactive species, as well as the surface coverage and pinhole defects of SAMs.³¹⁵

7.2.2 Electrochemical impedance spectroscopy (EIS)

Electrochemical impedance is usually measured by applying an alternate current (AC) potential to an electrochemical cell and measuring the current through the cell. Impedance is therefore analogous to resistance for a direct current (DC) system, and may result from solution (electrolyte) resistance, double layer capacitance, charge transfer resistance, diffusion (Warburg impedance), and more.

Any frequency can be applied, and the impedance of a circuit element is represented as a function of frequency.

EIS is commonly analyzed by fitting the acquired data to equivalent electrical circuit models, including common circuit elements such as resistors, capacitors, and inductors. When a model is found which gives an impedance spectrum that is in agreement with the measured spectrum, it is possible to calculate charge transfer resistance, diffusion coefficients, coverage degree, and pinhole parameters.³¹⁶ Such parameters give insight into the morphology (e.g. packing density and distribution of pinhole defects) of self-assembled monolayers.

7.2.3 Electrochemical quartz crystal microbalance (EQCM)

Electrochemical quartz crystal microbalance (EQCM) is an efficient method to investigate the adsorption and desorption of SAMs of organic compounds on metal surfaces. EQCM has a high sensitivity (± 1 ng) toward mass changes. A change in the resonance frequency is inverse to a change in the mass.²²⁸ Simultaneous electrochemistry and piezoelectric microgravimetry is possible on minute amounts of mass of substances attached to an electrode, with the use of EQCM and CV (example given in Figure 7.2).

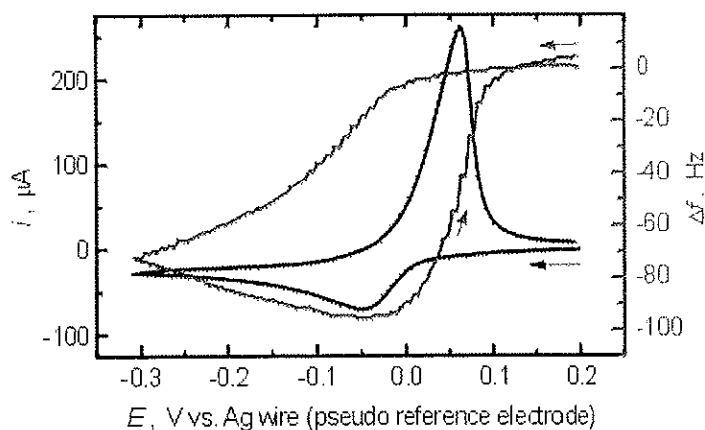


Figure 7.2 Simultaneous cyclic voltammetry and piezoelectric microgravimetry (at electrochemical quartz crystal microbalance (EQCM)) of the Ag/Ag^+ redox couple (taken from ref. 317).

7.2.4 Electrochemical studies on carotenoids

Electrochemical techniques, and CV in particular, have been widely used to investigate the production and study of reactive intermediates (*e.g.* excited states and radicals) of carotenoids in organic solvents.²³⁸ In 1991, the first observation of carotenoid polymerization on gold was noticed during CV investigations of the electrooxidation of β,β -carotene in organic solvents.³¹⁸ This is actually not a self-assembly process. Adsorption of a carotenoid to a metal surface (*e.g.* gold and mercury), allows the study of electrochemistry and SAM formation of the carotenoid in aqueous solution, mimicking the natural environment of carotenoids in living systems.

So far, only two publications have described the electrochemistry of carotenoid self-assembled monolayers, *i.e.* SAM formation by a carotenoid thiol²³⁷ and carotenoid thion.²³⁹ This work brings about new results regarding the self-assembly of seleno-glyceride **69** at gold surfaces. The seleno-glyceride **69** SAM was investigated by cyclic voltammetry, phase-sensitive AC voltammetry, electrochemical impedance spectroscopy, and piezoelectric microgravimetry. Seleno-glyceride **69** was later used as a bridge to form more complex carotenoid SAMs. The SAMs of carotenoid-seleno-glyceride **67** and carotenoid-seleno-phosphocholine **66** were studied by CV in aqueous solutions. These data will be discussed in the following sections.

7.3 Investigation of the SAM formation of seleno-glyceride **69** on a gold surface (*paper 8*)

The preparation of the seleno-glyceride **69** (O^1 -[6-methylselenanyl]hexanoyl]-glycerol) was performed by previously described methods.^{319, 320} In order to achieve the chemisorption of seleno-glyceride **69**, the gold electrode was immersed into a 4.6 mM solution of seleno-glyceride **69** in acetonitrile under nitrogen atmosphere, then rinsed carefully with acetonitrile and water. As shown in Figure 7.3, CV runs of the modified electrode in 0.1M HClO₄ solution in the anodic region from 0 to 1.5V, evidenced the adsorption of seleno-glyceride **69**. The first scan (curve 1) displays the anodic peak A, which is assigned to the oxidative desorption of the organic surface layer. This is alike the desorption of short-chain alkane-thiol SAMs.³¹⁵ The anodic desorption occurs almost completely during the first scan, as proved by a comparison of curves 1 and 2. The 3rd and 4th scans (not shown) are identical and do not differ much from the second one. Hence, a steady state is attained during the 3rd scan. Simultaneous to desorption, gold oxidation takes place at peak A, while gold oxide reduction occurs in the region of the cathodic peak B. These results demonstrate that **69** adsorbs irreversibly to the gold surface. Desorption occurs only if the system is shifted far from equilibrium by imposing a positive enough electrode potential.

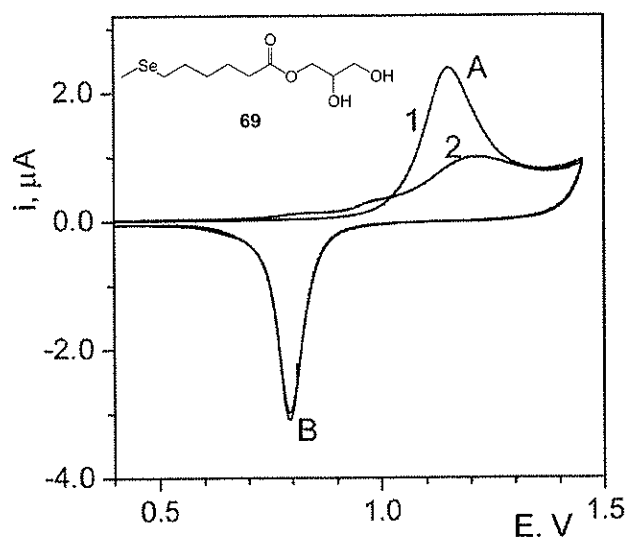


Figure 7.3 CV of a seleno-glyceride **69**-modified gold electrode in the anodic potential region, in 0.01 M HClO₄; scan speed 20 mV/s. Adsorption time 60 min. 1) 1st scan; 2) 2nd scan. Peak A: anodic desorption and gold oxidation; peak B: gold oxide reduction.

The anodic desorption process was monitored by EQCM (Figure 7.4a) with simultaneous CV runs (Figure 7.4b) between 0.375 and 1.450 V. Curve 1 in Figure 7.4a shows the shift in the resonance frequency during the first scan and displays a positive maximum in the region of peak A. The occurrence of this maximum is the result of two simultaneous processes with opposite effects: desorption of the monolayer (positive frequency shift) and gold surface oxidation (negative frequency shift). Curve 2 was recorded during the 4th CV scan and is typical of a plain gold electrode. Therefore, curve 2 displays only gold oxidation and gold oxide reduction. By subtracting curve 2 from curve 1, curve 3 results, which represents the desorption process only. Curve 3 shows that the negative mass change is the effect of an irreversible desorption process that occurs under the direct scan, and no readsorption occurs during the reverse potential sweep (evidenced by the horizontal part of the reverse curve). The data in Figure 7.4 demonstrate that the seleno-glyceride-generated SAM is stable in the anodic region up to about 1.0 V, *i.e.* where gold oxide formation is initiated.

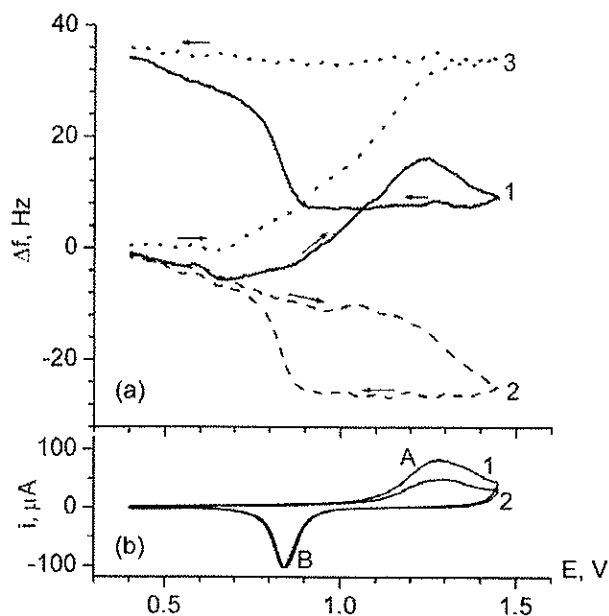


Figure 7.4 EQCM (a) and CV data (b) for the anodic desorption at a selenoglyceride **69**-modified gold piezoelectrode in 0.1 M HClO_4 , adsorption time 17 min, scan speed 50 mV s^{-1} . 1) first scan; 2) 4th scan; 3) the result of subtracting curve 2 from curve 1 in (a).

As shown in Figure 7.5, it was found from the capacity current recorded by AC voltammetry, that the adsorption process reaches a saturation point after 30 minutes. This was shown by a decrease in the capacity current ($i_{\text{SAM}}/i_{\text{Au}}$) with increasing modification time, reaching a limiting value after 30 minutes. In this experiment, the variability of the surface was accounted for by normalizing the AC current for the modified electrode (i_{SAM}) to the AC current measured after performing anodic desorption (i_{Au}).

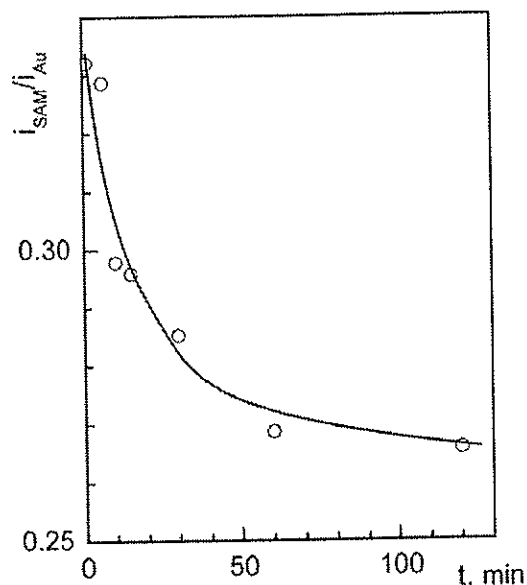
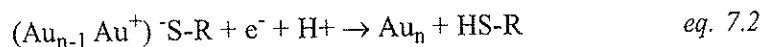
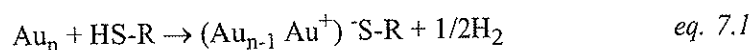


Figure 7.5 Effect of the adsorption time on the AC capacity current at 0.00V.

Selena-glyceride may undergo some chemical transformation as a consequence of the adsorption process, particularly at the Se site which interacts with gold. Consequently, the adsorbed product could be different from selena-glyceride itself. In order to determine the state of the adsorbate, the cathodic behavior of the modified electrode was studied by successive cathodic CV scans in 0.5M KOH, in the potential region from 0 to -1.5 V. As a working hypothesis, it was assumed that adsorption results in the splitting of a Se-C bonding and the actual adsorbate was the selenol form (O¹-(6-selenaylhexanoyl)-glycerol) (SeR). In order to check this assumption, it was necessary to compare the cathodic behavior of the selena-glycerol modified electrode with that of alkanethiol and thioester SAMs. Thiol (HS-R) adsorption on gold is an oxidative process (eq. 7.1), whereas the cathodic reaction (eq. 7.2) consists of gold reduction accompanied by the release of the adsorbate:



In contrast, thioethers undergo a physical adsorption with no modification in the oxidation state of gold.³¹⁵ That is why no cathodic reaction occurs with thioether modified electrodes.

Since a cathodic response of the seleno-glyceride **69**-monolayer was observed, it was inferred that the adsorbed species was in the selenol form as predicted. This was further confirmed by EQCM investigations, which demonstrated that the cathodic reaction is accompanied by a mass loss of 266g/F, which is close to the molecular weight of the proposed desorbed species (268 g/mol). The SAM formation by seleno-glyceride **69** adsorption is therefore believed to take place via a Se-CH₃ cleavage, as outlined in Figure 7.6.

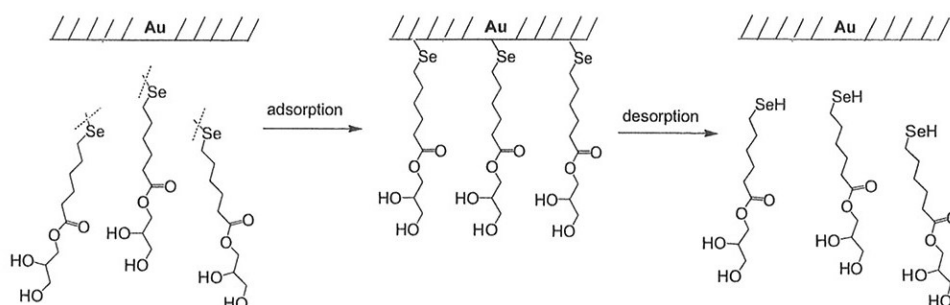


Figure 7.6 A schematic illustration of the adsorption of seleno-glyceride **69** onto the gold electrode surface, via the cleavage of the Se-CH₃ bond, and desorption of the SeHR state.

Coverage degree and surface layer morphology was investigated by electrochemical impedance spectroscopy (EIS) in a $[\text{Fe}(\text{CN})_6]^{3-}/[\text{Fe}(\text{CN})_6]^{4-}$ solution. It was assumed that the surface is not covered by a continuous layer but contained disk-shaped pinholes, which are non-covered islets. This results in direct contact between the gold surface in the islets and the $[\text{Fe}(\text{CN})_6]^{3-}/[\text{Fe}(\text{CN})_6]^{4-}$ solution. Fitting of the EIS data to a model whose impedance matched the measured data confirmed the presence of the defect sites (pinholes), and gave information about the surface coverage degree (θ), radius of pinholes (r_a), and half-distance between the pinholes (r_d). The overall data indicate a compact surface layer with a coverage degree close to unity for an adsorption time of 30-80 min. The monolayer exhibits uniform pinholes ($r_a = 1-3 \mu\text{m}$) and spacing of the islets ($r_d = 6-50 \mu\text{m}$). It was also found that both r_a and r_d increase with increasing modification time, while θ did not change significantly. This may indicate a coalescence of pinholes into larger islets at a greater distance from each other, in accordance to previous observations for organoselenium compounds.²²⁷

7.4 SAM formation of carotenoid derivatives with selenoglyceride **69** as an anchor (*paper 8*)

Gold electrodes modified by the hydrophilic carotenoid-selena-glyceride **67** and carotenoid-selena-phosphocholine **66** were obtained by chemisorption in a 4 mM acetonitrile and 3.9 mM methanol solution, respectively. Their anodic behavior were investigated in 0.1M HClO₄ solution, in the anodic region from 0 to 1.5V. The presence of each compound at the gold electrode surface was demonstrated by the anodic peak A on the CV voltammogram, as shown in Figure 7.7. The peak is similar to that obtained for selena-glyceride **69** (Figure 7.3), proving that both **67** and **66** adsorb to the surface via the selenium function. Peak D was assigned to the anodic oxidation of the carotenoid moiety, in accordance with the similar anodic response detected with a gold electrode modified by a sulfur-containing carotenoid (see Chapter 1.8.2).²³⁹ As a direct consequence of water inclusion into the surface organic layer, this peak (D) develops at a less positive potential for the highly hydrophilic carotenoid-selena-phosphocholine **66** compared to carotenoid-selena-glyceride **67**. Water-molecules are believed to react with the cation-radical which is the primary product of carotenoid anodic reaction. In this way, the anodic process is facilitated by the presence of water molecules close to the reaction site.

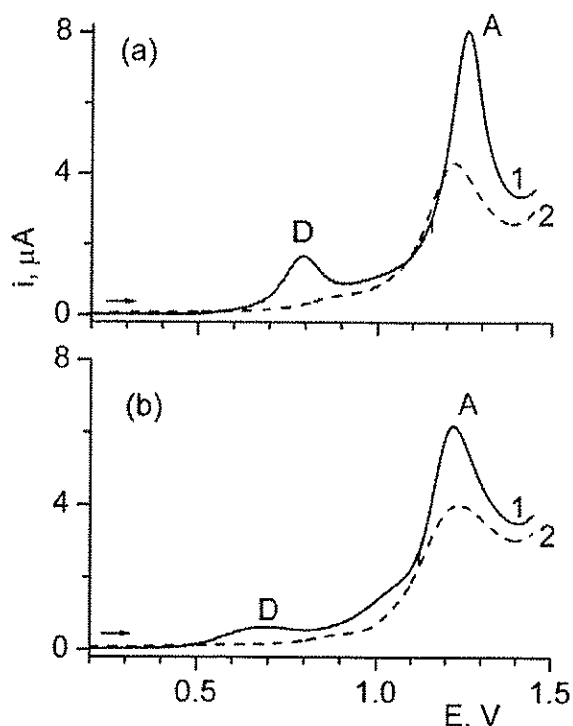


Figure 7.7 Anodic reactions at the gold electrode modified by carotenoid-selena-glyceride **67** (a) and carotenoid-selena-phosphocholine **66** (b). Same conditions as in Figure 7.1. 1) 1st scan, 2) 2nd scan, adsorption time 30 min.

From Figure 7.7 it is seen that both carotenoid derivatives desorb during the first anodic scan (curve 1), the response in the second scan (curves 2) is close to that for pure gold oxide formation. A steady state was obtained for both compounds after the third scan (not shown), which is similar to the anodic behavior of selena-glyceride **69**.

Carotenoid-selena-phosphocholine **66** forms a less compact monolayer than carotenoid-selena-glyceride **67**. This is seen by the difference in intensities of the anodic peaks A and D, and may be due to steric hindrance from the choline moiety.

Summing up, in the presented work, it was demonstrated that selena-glyceride **69** binds irreversibly to the gold surface. The adsorption is accompanied by the cleavage of the Se-CH₃ bond, and the adsorbed layer consists mainly of the selenol form (SeR). The free OH groups in selena-glyceride **69** or its 2-acyl isomer can be

used to attach carotenoids and prepare carotenoid-containing SAMs on gold. This possibility was demonstrated for carotenoid-selena-glyceride **67** and carotenoid-selena-phosphocholine **66**. Also, other functional groups may be attached to the surface by means of the ester function. Binding of a second moiety to glycerol, as for the carotenoid-selena-phosphocholine **66**, allows the possibility to form mixed self-assembly monolayers. Finally, it was shown that carotenoid electron-transfer reactions in the SAM form can be studied in aqueous solutions.

8 Optical activity

8.1 Optical activity of monomeric carotenoids

Optical activity refers to a molecule's ability to interact with polarized light. Until now, only polarized UV/VIS light has been applied to the investigation of optically active carotenoids and consequently, activity refers in this chapter only to electronic optical activity. All optically active molecules have an asymmetric constituent (atom, plane, axis), but not all chiral molecules are optically active. The optical properties of most chiral carotenoids originates from asymmetric carbon atoms of the head groups, *e.g.* (3*R*, 3'*R*)-zeaxanthin (Figure 8.1). The steric hindrance across the C6-C7 bond results in a twist of the chromophore system, *i.e.* the double bonds of the end-ring point out of plane of the polyene. Whenever there exists an asymmetric C-atom in the end-ring, the twist achieves a handedness in the associated polyene, which in turn results in a chiral π -system.

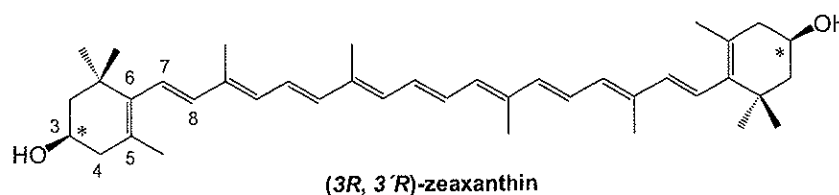


Figure 8.1 (3*R*, 3'*R*)-zeaxanthin.

The chiroptical methods that have been used to determine the absolute configuration of chiral carotenoids are: 1) measurement of the angle (α) of rotation of the plane of polarized light at different wavelengths (optically rotary dispersion, ORD) and 2) circular dichroism (CD). CD spectroscopy is now the most widely used technique when chirality of carotenoids is reported.

Circular dichroism (CD) spectroscopy measures the difference in the absorption of left-handed circular polarized light versus right-handed circular polarized light, $\Delta A = A(l) - A(r)$, and is a function of wavelength. The molar unit used in CD spectra is:

$$\Delta \epsilon = (\Delta A \times MW) / (C \times d) \quad \text{eq. 8.1}$$

where MW is molecular weight, C is concentration, and d is cell length.

Absorption maxima and minima in CD spectra and ORD are referred to as Cotton effects (CE). The CD intensity of optically active, monomeric carotenoids is strong in the UV range (200-380 nm) and represents the butadiene chromophore

of C5-C8, which is twisted out of plane by CH₃-C5 and chirally perturbed by the substituent at C3 (Figure 8.1). The chiral perturbation of the polyene chain by the substituent at C3 is not sufficient to create CE in the visible region (380-500 nm).^{20, 321} However, conformational changes in the carotenoid chromophore due to incorporation in phospholipid aggregates⁷⁴, upon binding to proteins (*e.g.* human serum albumin^{322, 323}), or inclusion using chiral hosts (*e.g.* rigid-rod β -barrels²²¹), have been shown to induce strong CD bands in the visible region.

8.2 Supramolecular induced exciton chirality of carotenoids

Carotenoids aggregate into supramolecular assemblies in aqueous solutions. This behavior results in either card-packed type (H-aggregate) or head-to-tail (J-aggregates) arrangements, which can be detected by blue or red shifted UV-VIS absorption maxima, respectively (see Chapters 1.8.1 and 4.1). Such supramolecular structures may exhibit CE in the visible region, giving values up to several hundred times greater than the individual molecules. These CE are a result of a special alignment of chirally perturbed neighboring polyene chains held together by secondary chemical forces, *e.g.* van der Waals and H-bonds (exciton signals). CE generated by the interaction of individual, chiral molecules are expressed as "supramolecular exciton chirality". Small structural differences may result in significant changes in the structure of the assembly.^{322, 324}

The chiral carotenoid lysophosphocholine **R-43a** has an asymmetric C-atom (*sn*-2-atom) in its glycerol backbone. The optical activity of **R-43a** will be discussed in the following section.

8.3 Optical activity of carotenoid lysophosphocholine **R-43a** (*paper 9*)

The *R*-enantiomer of carotenoid lysophosphocholine **43a**, was obtained starting from *sn*-glycero-3-phosphocholine (GPC) (**R-47**) ($p = 0.88$) by the method outlined in Scheme 2.1, Chapter 2.1. A small amount of its 2-acyl isomer was anticipated, but was not detected during high resolution 1D ¹H and 2D H,H-COSY NMR measurements. In water, carotenoid lysophosphocholine **R-43a** disperses into clear, orange colored aggregate dispersions. From Figure 8.2 (b), it is seen that the self-assembly in water results in a 65 nm hypsochromic (blue) shifted UV-VIS absorption maxima, compared to the monomeric solution in methanol.

Weak CE from the ester chromophore of saturated glycerides have been observed in the 215-220 nm region.³²⁵ The CD spectra of monomeric solutions of carotenoid lysophospholipid **R-43a** in methanol detected no CE in this region (not shown), nor in the visible chromophore region (300-600 nm) (Figure 8.2 (a)). The asymmetric *sn*-2-atom in the glycerol backbone of **R-43a** does not chirally disturb

the polyene chain. While the CD-spectrum of *R-43a* in methanol proved the optical inactivity of the monomeric solution, the CD spectra in water show strong CE. A positive band is seen at 410 nm, a strong negative band at 445 nm, and a positive band at 520 nm. This indicates that the aggregation of *R-43a* in water produces a chiral association of individual molecules. Hence, an induced optical activity is generated upon addition of water. The higher intensity of CE at 35 °C suggests that the association of monomers into aggregates can be accelerated at higher temperature.

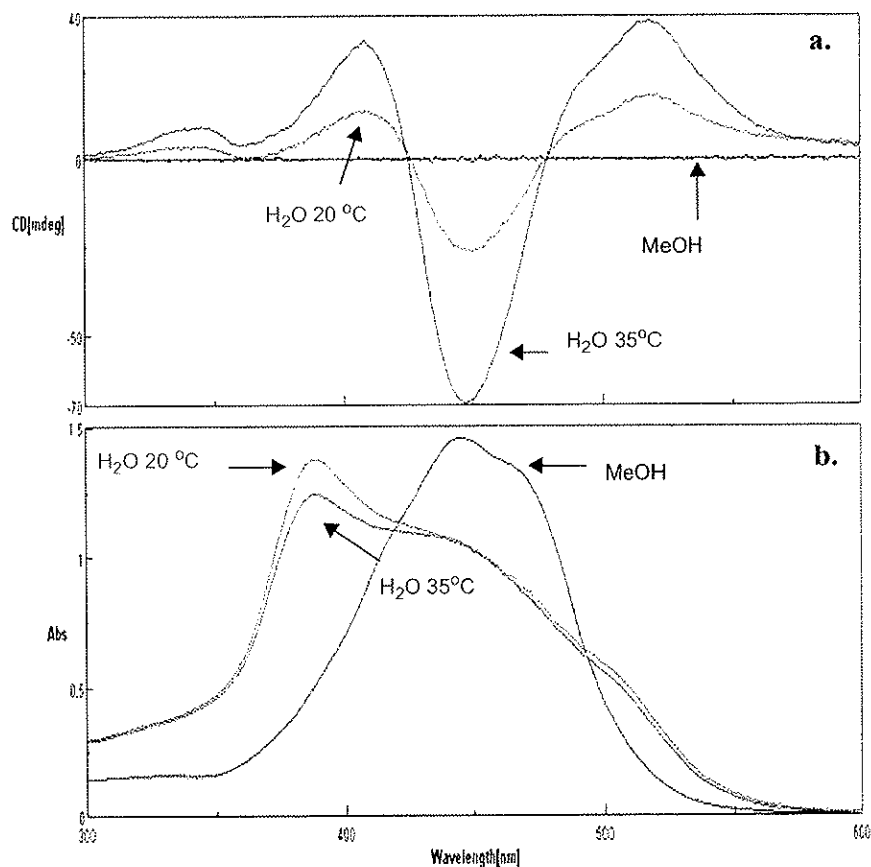


Figure 8.2 a) CD-spectrum, and b) UV-VIS spectrum of *R-43a*, in the 300 - 600 nm region. Path length = 1 cm, $c = 2 \times 10^{-5}$ M.

The origin of the optical activity of the aggregates was obtained by molecular mechanics programs and force field (CVFF) calculations, proposing an enantiomeric oligomer composed of approximately 8 monomers as the basic unit

of the aggregates (Figure 8.3). The calculated absorption and CD spectra for the oligomer (not shown) are in accordance with the experimental spectra of **R-43a** in water. It is evident from Figure 8.3 that ordered arrangements caused by defined H- and J-aggregates do not exist in aggregates of **R-43a**. The alignment of the chromophores results in a shift of the absorption maxima to shorter and longer wavelengths.

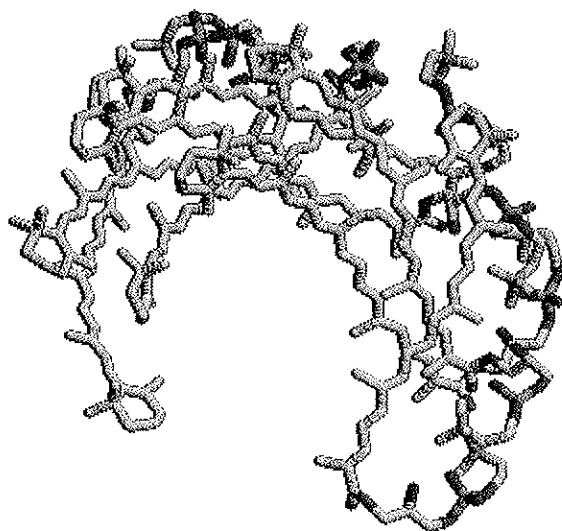


Figure 8.3 Optically active P-oligomer unit, built from eight inactive **R-43a** monomers.

Dynamic light scattering (DLS) investigation of **R-43a** in water did not detect aggregates indicative of an oligomer of 8 monomers. The oligomer unit is therefore speculated to represent the smallest aggregation unit. Several times it was observed that the absorption maximum of the aggregates varied between 380 and 400 nm. This may indicate a high sensitivity to subtle experimental conditions in aggregate formation. It seems, however, that the chiroptical properties of the **R-43a** aggregates are retained.

It is concluded that carotenoid lysophosphocholine **R-43a** is optical inactive in the monomer form, but forms chiral aggregates upon addition of water. Based on molecular mechanics calculations, an oligomeric basic unit was proposed, satisfactorily explaining the spectroscopic properties of **R-43a**.

References

1. Isler, O. in *Carotenoids* (Ed.: O.Isler), Birkhäuser, Basel, **1971**, pp 11-28.
2. Weedon, B. C. L. in *Carotenoids* (Ed.: O.Isler), Birkhäuser, Basel, **1971**, pp. 29-59.
3. Weedon, B. C. L., Moss, G. P. in *Carotenoids Volume 1A: Isolation and Analysis* (Eds.: Britton, G., Liaaen-Jensen, S., Pfander, H.), Birkhäuser, Basel, **1995**, pp. 27-34.
4. Gribble, G. W. *J. Nat. Prod.* **1992**, *55*, 1353-1395.
5. Daniels, L. A. *Biol. Trace Elem. Res.* **1996**, *54*, 185-199.
6. Ernst, W. H. O. *Biodegradation.* **1998**, *9*, 311-318.
7. Ellis, D., R., Salt, D. E. *Curr. Opin. Plant Biol.* **2003**, *6*, 273-279.
8. Suzuki, U., Mori, T. *Biochem. Z.* **1925**, *162*, 413-424.
9. Zhang, X., Wang, L., Li, G., Zhu, Y. *Haiyang Yu Huzhao.* **2000**, *31*, 643-646.
10. Tapiero, H., Townsend, D. M., Tew, K. D. *Biomed. Pharmacother.* **2003**, *57*, 134-144.
11. Britton, G., Liaaen-Jensen, S., Pfander, H. *Carotenoids: Handbook*, Birkhäuser Verlag, Basel, **2004**.
12. Pfander, H., Leuenberger, U. *Chimia.* **1976**, *30*, 71-73.
13. Brahmana., Katsuyama, K., Inanaga, J., Katsuki, T., Yamaguchi, M. *Tetrahedron Lett.* **1981**, *22*, 1695-1696.
14. Inanaga, J., Yamaguchi, M. *Ser. C.* **1989**, *17*, 109-112.
15. Sliwka, H.-R., Liaaen-Jensen, S. *Acta Chem. Scand.* **1990**, *44*, 61-66.
16. Sliwka, H.-R., Liaaen-Jensen, S. *Tetrahedron: Asymmetry.* **1993**, *4*, 361-368.
17. Sliwka, H.-R., Liaaen-Jensen, S. *Acta Chem. Scand.* **1994**, *44*, 679-683.
18. Sliwka, H.-R., Liaaen-Jensen, S. *Tetrahedron: Asymmetry.* **1993**, *4*, 2377-2382.
19. Sliwka, H.-R., Liaaen-Jensen, S. *Acta Chem. Scand.* **1995**, *49*, 428-432.
20. Sliwka, H.-R., Liaaen-Jensen, S. *Helv. Chim. Acta.* **1995**, *82*, 161-169.
21. Sliwka, H.-R., Liaaen-Jensen, S. *Acta Chem. Scand.* **1997**, *51*, 345-347.
22. Davies, B. H. in *Chemistry and Biochemistry of Plant Pigments, Volume 2* (Ed.: T. W. Goodwin), Academic Press, London, 2nd ed., **1976**, pp. 38-165.
23. Faulks, R. M. *Educ. Chem.* **2004**, *41*, 21-24.
24. Foss, P., Storebakken T., Schiedt, K., Liaaen-Jensen, S., Austreng, E., Streiff, K. *Agriculture.* **1984**, *41*, 213-226.
25. Krinsky, N. I. *NATO ASI Series, Series A: Life Sciences.* **1998**, *296*, 323-332.
26. Krinsky, N. in *Carotenoids* (Ed.: O.Isler), Birkhäuser Verlag, Basel, **1971**, pp. 669-716.
27. Kiokias, S., Gordon, M. H. *Food Rev. Int.* **2004**, *20*, 99-121.
28. Yanishlieva, N. V., Aitzetmüller, K., Raneva, V. G. *Lipid.* **1998**, *10*, 444-462.
29. Olson, J. A., Krinsky, N. I. *FASEB J.* **1995**, *9*, 1547-1550.
30. Russel, R. M. *Internat. J. Vit. Nutr. Res.* **1998**, *68*, 349-353.

31. Bendich, A. *Adv. Exp. Med. Biol.* **1990**, 262, 1-12.
32. Tapiero, H., Townsend, D. M., Tew, K. D. *Biomed. Pharmacother.* **2004**, 58, 100-110.
33. Filteau, S. M., Tomkins, A. M. *Lancet.* **1999**, 353, 1458-1459.
34. Haskell, M. J., Brown, K. H. *J. Mammary Gland Biol.* **1999**, 4, 243-257.
35. Bensasson, R. V., Land, E. J., Truscott, T. G. in *Excited states and free radicals in biology and medicine; Contributions from flash photolysis and pulsed radiolysis*. Oxford University Press, **1999**, pp 65, 201-224.
36. Young, A. J., Lowe, G. M. *Arch. Biochem. Biophys.* **2001**, 381, 20-27.
37. Mathews-Roth, M. M. *Ann. N. Y. Acad. Sci.* **1993**, 691, 127-138.
38. Gainer, J. L. US4176179, Virginia University, USA, **1979**.
39. Eugster, C., Eugster, C. H., Haldemann, W., Rivera, G. US5536504, Marigen S. A., Switzerland, **1994**.
40. Bauernfeind, J. C. *J. Agr. Food. Chem.* **1972**, 20, 456-473.
41. Paust, J. *Pure Appl. Chem.* **1991**, 63, 45-58.
42. Emodi, A., Scialpi, L., Antoshkiw. *Food Technology.* **1976**, 30, 58-60.
43. Haila, K. M., Lievonon, S. M., Heinonen, M. I. *J. Agr. Food Chem.* **1996**, 44, 2096-2100.
44. Bauernfeind, J. C. *Prog. Fish Cult.* **1976**, 38, 180-183.
45. Burton, G. W., Ingold, K. U. *Science.* **1984**, 224, 569-573.
46. Tsuchihashi, H., Kigoshi, M., Iwatsuki, M., Niki, E. *Arch. Biochem. Biophys.* **1995**, 323, 137-147.
47. Krinsky, N. I. *Ann. N. Y. Acad. Sci.* **1998**, 854, 443-447.
48. Lee, S.-H., Min, D. B. *J. Agric. Food Chem.* **1990**, 38, 1630-1634.
49. Hirayama, O., Nakamura, K., Hamada, S., Kobayasi, Y. *Lipids.* **1994**, 29, 149-150.
50. Burke, M., Edge, R., Land, E. J., Truscott, T. G. *J. Photoch. Photobio. B.* **2000**, 60, 1-6.
51. Tinkler, J. H., Tavender, S. M., Parker, A. W., McGarvey, D. J., Mulroy, L., Truscott, T. G. *J. Am. Chem. Soc.* **1996**, 118, 1756-1761.
52. Edge, R., Land, E. J., McGarvey, D., Mulroy L., Truscott, T. G. *J. Am. Chem. Soc.* **1998**, 120, 4087-4090.
53. Woodall, A. A., Lee, S. W.-M., Weesie, R. J., Jackson, M. J., Britton, G. *Biochim. Biophys. Acta.* **1997**, 1336, 33-42.
54. Tatsuzawa, H., Yoshio, U., Minoru, N. *Photomed. Photobiol.* **1996**, 18, 61-62.
55. Woodall, A. A., Britton, G., Jackson, M. L. *Biochim. Biophys. Acta.* **1997**, 1336, 575-586.
56. Lim, B. P., Nagao, A., Terao, J., Tanaka, K., Suzuki, T., Takama, K. *Biochim. Biophys. Acta.* **1992**, 1126, 178-184.
57. Nakagawa, K., Fujimoto, K., Miyazawa, T. *Biochim. Biophys. Acta.* **1996**, 1299, 110-116.
58. Krinsky, N. I. *Nutrition.* **2001**, 17, 815-817.

59. Yeum, K.-J., Aldini, G., Chung, H.-Y., Krinsky, N. I., Russel, R. M. *J. Nutr.* **2003**, *133*, 2688-2691.
60. Tesoriere, L., Bongiorno, A., Pintaudi, A. M., D'Anna, R., D'Arpa, D., Livrea, M. A. *Arch. Biochim. Biophys.* **1996**, *326*, 57-63.
61. Edge, R., McGarvey, D. J., Truscott, T. G. *J. Photoch. Photobio. B.* **1997**, *41*, 189-200.
62. Alaejos, M. S., Romero, F. J. D., Romero, C. D. *Nutrition.* **2000**, *16*, 376-383.
63. Stahl, W., Sies, H. *Mol. Aspects Med.* **2003**, *24*, 345-351.
64. Nève, J. *Experientia.* **1991**, *47*, 187-193.
65. Appel, M. J., Woutersen, R. A. *Carcinogenesis.* **1996**, *17*, 1411-1416.
66. Duffield-Lillico, A. J., Dalkin, B. L., Reid, M. E., Turnbull, B. W., Slate, E. H., Jacobs, E. T., Marshall, J. R., Clark, L. C. *BJU Int.* **2003**, *91*, 608-612.
67. Combs, G. F., Clark, L. C., Turnbull, B. W. *Met. Ions Biol. Med.* **2002**, *7*, 600-603.
68. Sies, H., Stahl, W., Sundquist, A. R. *Ann. N. Y. Acad. Sci.* **1992**, *669*, 7-20.
69. Wrona, M., Rózanowska, M., Sarna, T. *Free Radical Bio. Med.* **2004**, *36*, 1094-1101.
70. Edge, R., Truscott, T. G. *Nutrition.* **1997**, *13*, 992-994.
71. Palozza, P., Krinsky, N. I. *Arch. Biochem. Biophys.* **1992**, *297*, 184-187.
72. Mortensen, A., Skibsted, L. H. *FEBS Lett.* **1997**, *417*, 261-266.
73. Mortensen, A., Skibsted, L. H., Truscott, T. G. *Arch. Biochem. Biophys.* **2001**, *385*, 13-19.
74. Milon, A., Wolff, G., Ourisson, G., Nakatani, Y. *Helv. Chim. Acta.* **1986**, *69*, 13-25.
75. Lazrak, T., Milon, A., Wolff, G., Albrecht, A.-M., Miché, M., Ourisson, G., Nakatani, Y. *Biochim. Biophys. Acta.* **1987**, *903*, 132-141.
76. Wisniewska, A., Subczynski, W. K. *Biochim. Biophys. Acta.* **1998**, *1368*, 235-246.
77. Gabrielska, J., Gruszecki, W. I. *Biochim. Biophys. Acta.* **1996**, *1285*, 167-174.
78. Milon, A., Lazrak, T., Albrecht, A. M., Wolff, G., Weill, G., Ourisson, G., Yoichi, N. Y. *Biochim. Biophys. Acta.* **1986**, *859*, 1-9.
79. Woodall, A. A., Britton, G., Jackson, M. L. *Biochem. Soc. T.* **1995**, *23*, 133S.
80. Kull, D. R., Pfander, H. *J. Nat. Prod.* **1997**, *60*, 371-374.
81. Burgess, M. L., Barrow, K. D., Gao, C., Heard, G. M., Glenn, D. *J. Nat. Prod.* **1999**, *62*, 859-863.
82. Yamano, Y., Sakai, Y., Hara, M., Ito, M. *J. Cem. Soc., Perkin Trans.* **2002**, *1*, 2006-2013.
83. Billsten, H. H., Bhosale, P., Yemelyanov, A., Bernstein, P. S., Polívka, T. *Photochem. Photobiol.* **2003**, *78*, 138-145.
84. Sujak, A., Gabrielska, J., Grudziński, W., Borc, R., Mazurek, P., Gruszecki, W. I. *Arch. Biochem. Biophys.* **1999**, *371*, 301-307.
85. Krinsky, N. I. *J. Nutr.* **2002**, *132*, 540S-542S.

86. Manz, V. U. *Chimia*. **1967**, *21*, 329-335.
87. Gordon, H. T., Bauernfeind, J. C., *Crit. Rev. Food Sci.* **1982**, *18*, 59-97.
88. Parker, R. S. *FASEB J.* **1996**, *10*, 542-551.
89. van Vliet, T. *Eur. J. Clin. Nutr.* **1996**, *50*, S32-S37.
90. Furr, H. C., Clark, R. M. *J. Nutr. Biochem.* **1997**, *8*, 364-377.
91. Khachik, F., Beecher, G. R., Smith, J. C. *J. Cell Biochem.* **1995**, *22*, 236s-246s.
92. Olson, J. A. *Pure Appl. Chem.* **1994**, *66*, 1011-1016.
93. Gartner, C., Stahl, W., Sies, H. *Am. J. Clin. Nutr.* **1997**, *66*, 116-122.
94. Jayarajan, P., Reddy, V., Mohanram, M. *Indian J. Med. Res.* **1980**, *71*, 53-56.
95. Goulinet, S., Chapman, M. J. *Arterioscl. Throm. Vas.* **1997**, *17*, 786-796.
96. Oshima, S., Sakamoto, H., Ishiguro, Y., Terao, J. *J. Nutr.* **1997**, *127*, 1475-1479.
97. Borel, P., Grolier P., Armand, M., Partier, A., Lafont, H., Lairon, D., Azais-Braesco, V. *J. Lipid Res.* **1996**, *37*, 250-261.
98. Pitt, G. A. J. in *Carotenoids* (Ed.: O. Isler), Birkhäuser, Basel, **1971**, pp. 717-732.
99. Lakshman, M. R. *J. Nutr.* **2004**, *134*, 241S-245S.
100. Nagano, A. *J. Nutr.* **2004**, *134*, 237S-240S.
101. Ernst, H. *Pure Appl. Chem.* **2002**, *74*, 2213-2226.
102. Britton, G., Liaaen-Jensen, S., Pfander, H. in *Carotenoids Volume 1A: Isolation and Analysis* (Eds.: Britton, G., Liaaen-Jensen, S., Pfander, H), Birkhäuser, Basel, **1995**, pp. 13-26.
103. Net information from <http://www.bccresearch.com/editors/RGA-110.html>, 09.08.2004.
104. Net information from: <http://www.astafactor.com/algae.htm>, 18.10.2004.
105. Schlipalius, L. *Bioresource Technol.* **1991**, *38*, 241-243.
106. Mordhay, A., Ben-Amotz, A. US4199895, Yeda Research and Development Co. Ltd., Israel, **1980**.
107. Net information from <http://www.aquacarotene.com/corporate.html>, 09.08.2004.
108. Schmidt-Dannert, C., Umeno, D., Arnold, F. H. *Nat. Biotechnol.* **2000**, *18*, 750-753.
109. Umeno, D., Arnold, F. H. *J. Bacteriol.* **2004**, *186*, 1531-1536.
110. Bauernfeind, J. C., Brubacher, G.B., Kläui, H.A., Marusich, W.L. in *Carotenoids* (Ed.: O. Isler), Birkhäuser, Basel, **1971**, pp. 743-764.
111. Meyer, P., Riesen, R., Pfander, H. in *Carotenoids Volume 1A: Isolation and Analysis* (Eds.: Britton, G., Liaaen-Jensen, S., Pfander, H), Birkhäuser, Basel, **1995**, pp. 277-282.
112. Net information from *Antica Azienda Agricola Peltuinum*, http://www.peltuinum.it/inglese/home_eng.htm, 09.08.2004.

113. Liaaen-Jensen, S., Hertzberg, S., Rønneberg, H. *Int. Conf. Chem. Biotechnol. Biol. Act. Nat. Prod.* **1981**, *2*, 150-164.
114. Pfander, H. in *Carotenoids Volum 2: Synthesis*. (Eds.: G. Britton, S. Liaaen-Jensen, Pfander, H.), Birkhäuser, Basel, **1996**, pp. 293-294.
115. Yokoyama, A., Izumida, H., Shizuri, Y. *Biosci. Biotech. Biochem.* **1996**, *60*, 1877-1878.
116. Liaaen-Jensen, S. in *Carotenoids Volum 2: Synthesis*. (Eds.: G. Britton, S. Liaaen-Jensen, Pfander, H.), Birkhäuser, Basel, **1996**, pp. 295-300.
117. Hertzberg, S., Liaaen-Jensen, S. *Acta Chem. Scand. B.* **1985**, *39*, 629-638.
118. Auweter, H., Bohn, H., Lüddecke, E. WO9826008, BASF A.-G., Germany, **1998**.
119. Leuenberger, B. US5668183, Roche Vitamins Inc., US, **1997**.
120. Fortier, N. E. WO9639870, The Procter and Gamble Company, US, **1996**.
121. Auweter, H., Bohn, H., Haberkorn, H., Horn, D., Lüddecke, E., Rauschenberger, V. DE19637517, BASF A.-G., Germany, **1998**.
122. Kläui, von H., Münzel, K. *Pharm. Acta Helv.* **1964**, *40*, 153-157.
123. Pfitzner, I., Francz, P. I., Biesalski, H. K. *Biochim. Biophys. Acta.* **2000**, *1474*, 163-168.
124. Vishnevetsky, M., Ovadis, M., Vainstein, A. *Trends Plant Sci.* **1999**, *4*, 232-235.
125. Goodwin, T. W., in *The Biochemistry of the Carotenoids; volume II Animals* (Ed. T. W. Goodwin), Chapman and Hall, London, 1984, pp 1-19.
126. Bunnell, R. H., Driscoll, W., Bauernfeind, J. C. *Food Technology.* **1958**, *12*, 536-541.
127. Weesie, R. J., Merlin, J. C., De Groot, H. J. M., Britton, G., Lugtenburg, J., Jansen, F. J. H. M., Cornard, J. P. *Biospectroscopy*, **1999**, *5*, 358-370.
128. Chayen, N. E., Cianci, M., Grossmann, J. G., Habash, J., Helliwell, J. R., Nneji, G. A., Raftery, J., Rizkallah, P. J., Zagalsky, P. F. *Acta Cryst.* **2003**, *D59*, 2072-2082.
129. Kildahl-Andersen, G., Lutnaes, B. F., Liaaen-Jensen, S. *Org. Biomol. Chem.* **2004**, *2*, 489-498.
130. Britton, G., Weesie, R. J., Askin, D., Warburton, J. D., Gallardo-Guerrero, L., Jansen, F. J., de Groot, H. J. M., Lugtenburg, J., Cornard, J.-P., Merlin, J.-C. *Pure Appl. Chem.* **1997**, *69*, 2075-2084.
131. Zagalsky, P. F. in *Carotenoids Volum 1A: Isolation and analysis*. (Eds.: G. Britton, S. Liaaen-Jensen, Pfander, H.), Birkhäuser, Basel, 1995.
132. Shone, C. C., Britton, G., Goodwin, T. W. *Comp. Biochem. Physiol. B.* **1979**, *62B*, 507-513.
133. Lakshman, M. R., Okoh, C. *Methods Enzymol.* **1993**, *214*, 74-86.
134. Kerfeld, C. A., Sawaya, M. R., Brahmandam, V., Cascio, D., Ho, K. K., Trevithick-Sutton, C. C., Krogmann, D. W., Yeates, T. O. *Structure.* **2003**, *11*, 55-65.

135. Lockwood, S. F., O'Malley, S., Mosher, G. L. *J. Pharm. Sci.* **2003**, *92*, 922-926.
136. Lancrajan, I., Diehl, H. A., Socaciu, C., Engelke, M., Zorn-Kruppa, M. *Chem. Phys. Lipids.* **2001**, *112*, 1-10.
137. Leuenberger, B., Stoller, H. US 5,221,735, Hoffmann-La Roche Inc., **1993**.
138. Loftsson, T., Friðriksdóttir, H. *Int. J. Pharm.* **1998**, *163*, 115-121.
139. Mele, A., Mendichi, R., Selva, A. *Carbohydr. Res.* **1998**, *310*, 261-267.
140. Jansson, S. T. K., Mortensen, B. WO2004005353, Poltec AS, Norway, **2004**.
141. Inamura, I., Isshiki, M., Araki, T. *Bull. Chem. Soc. Jpn.* **1989**, *62*, 1671-1673.
142. Shibata, H., Kurosaki, C., Kawashima, T., Ochiai, H. *Agric. Biol. Chem.* **1987**, *51*, 3261-3266.
143. Isager, P. P., Winning, M. US 6190686, CHR. Hansen A/S, Denmark, **2001**.
144. Bohn, H., Auweter, H., Lüddecke, E. WO9826008, BASF A.-G., Germany, **1998**.
145. Horn, D., Lüddecke, E. *NATO ASI Ser., Ser. 3: High Technology.* **1996**, *12*, 761-775.
146. Horn, D. *Angew. Makromol. Chem.* **1989**, *166*, 139-153.
147. Horn, D., Rieger, J. *Angew. Chem. Int. Ed.* **2001**, *40*, 4330-4361.
148. Auweter, H., Haberkorn, H., Heckmann, W., Horn, D., Lüddecke, E., Rieger, J., Weiss, H. *Angew. Chem. Int. Ed.* **1999**, *38*, 2188-2191.
149. Wegmann, J., Krucker, M., Bachmann, S., Fischer, G., Zeeb, D., Lienau, A., Glaser, T., Runge, F., Lüddecke, E., Albert, K. *J. Agric. Food Chem.* **2002**, *50*, 7510-7514.
150. Kläui, H., Ulrich, M., Rigassi, N., Ryser, G., Schwieter, U. CA966147, Hoffman-La Roche Inc., Switzerland, **1975**.
151. Auweter, H., Bohn, H., Horn, D., Krämer, K., Paust, J., Weiss, H. US6271396, BASF, Germany, **2000**.
152. Todd, P. H. US5053240, Kalamazoo Holdings, Inc., US, **1991**.
153. Partali, V., Kvittingen, L., Sliwka, H.-R., Anthonsen, T. *Angew. Chem. Int. Ed. Engl.* **1996**, *35*, 328-330.
154. Liaaen-Jensen, S., Hertzberg, S. in *Carotenoids Volume 1A: Isolation and Analysis* (Eds.: Britton, G., Liaaen-Jensen, S., Pfander, H), Birkhäuser, Basel, **1995**, pp. 283-286.
155. Lerfall, J. Diploma Thesis, Norwegian University of Science and Technology (NTNU); *Syntetisk kombinasjon av β -apo-8'-karotensyre, Vitamin C, EPA, Trolox og selenafettsyre*. Trondheim, Norway, **2002**.
156. Lahmann, M., Thiem, J. *Carbohydr. Res.* **1997**, *299*, 23-31.
157. Pfander, H., Dumont, R., Läderach, M. *Chimia.* **1980**, *34*, 20-23.
158. Blanchard-Desce, M., Arrhenius, T. S., Lehn, J. M. *Bull. Soc. Chim. Fr.* **1993**, *130*, 266-272.

159. Arrhenius, T. S., Blanchard-Desce, M., Dvolaitzky, M., Lehn, J. M., Malthete, J. *Proc. Natl. Acad. Sci. USA.* **1986**, *83*, 5355-5359.
160. Fuhrop, J.-H., Krull, M., Schulz, A., Möbius, D. *Langmuir*, **1990**, *6*, 497-505.
161. Frey, D. A., Kataisto, E. W., Ekmanis, J. L., O'Malley, S., Lockwood, S. F. *Org. Process Res. Dev.* **2004**, *8*, 796-801.
162. Jackson, H. L., Cardounel, A. J., Zweier, J. L., Lockwood, S. F. *Bioorg. Med. Chem. Lett.* **2004**, *14*, 3985-3991.
163. Showalter, L. A., Weinman, S. A., Østerlie, M., Lockwood, S. F. *Comp. Biochem. Phys. C.* **2004**, *137*, 227-236.
164. Cardounel, A. J., Dumitrescu, C., Zweier, J. L., Lockwood, S. F. *Biochem. Bioph. Res. Co.* **2003**, *307*, 704-712.
165. Hix, L., Lockwood, S. F., Bertram, J. S. *Cancer Lett.* **2004**, *211*, 25-37.
166. Gross, G. J., Lockwood, S. F. *Life Sci.* **2004**, *75*, 215-224.
167. Shimizu, K., Kondo, R., Sakai, K., Takeda, N., Nagahata, T., Oniki, T. *Lipids*, **2001**, *36(12)*, 1321-1326.
168. Humeau, C., Girardin, M. *Biotechn. Lett.* **2000**, *22*, 165-168.
169. Larsen, E., Abendroth, J., Partali, V., Schulz, B., Sliwka, H.-R., Quartey, G. K. *Chem. Eur. J.* **1998**, *4*, 113-117.
170. Karagiannidou, E., Størseth, T. R., Sliwka, H.-R., Partali, V., Malterud, K. E., Tsimidou, M. *Eur. J. Lipid Sci. Technol.* **2003**, *105*, 419-426.
171. Naalsund, T., Malterud, K. E., Partali, V., Sliwka, H.-R. *Chem. Phys. Lipids*, **2001**, *112*, 59-65.
172. Houte, H., Partali, V., Sliwka, H.-R., Quartey, E. G. K. *Chem. Phys. Lipids*, **2000**, *105*, 105-113.
173. Leatherman, G., Durantini, E. N., Gust, D., Moore, T. A., Moore, A. L., Stone, S., Zhou, Z., Rez, P., Liu, Y. Z., Lindsay, S. M. *J. Phys. Chem. B.* **1999**, *103*, 4006-4010.
174. Tapiero, H., Nguyen Ba, G., Couvreur, P., Tew, K. D. *Biomed. Pharmacother.* **2002**, *56*, 215-222.
175. Humeau, C., Girardin, M., Rovel, B., Miclo, A., *J. Mol. Catal. B: Enzym.* **1998**, *5*, 19-23.
176. Bauernfeind, J. C. *Int. J. Vitam. Nutr. Res.* **1985**, *27*, 307-333.
177. Lambert, C. R., Black, H. S., Truscott, T. G. *Free Radical Bio. Med.* **1996**, *21*, 395-400.
178. Papas, A. M. *Toxicol. Ind. Health.* **1993**, *9(1-2)*, 123-149.
179. Koga, T., Nagao, A., Terao, J., Sawada, K., Mukai, K. *Lipids*. **1994**, *29*, 83-89.
180. Ramirez, M., Amate, L., Gil, A. *Early Hum. Dev.* **2001**, *65*, S95-S101.
181. Bretscher, M. S. *Sci. Am.* **1985**, *253*, 100-108.

182. Small, D. M. in *Handbook of Lipid Research; The Physical Chemistry of Lipids* (Ed.: D. J. Hanahan), Volum 4. Plenum Press, New York, **1986**, pp. 475-476.
183. Ansell, G. B., Spanner, S. in *Phospholipids* (Eds.: J. N. Hawthorne and G. B. Ansell), Elsevier Biomedical, Amsterdam, **1982**, pp. 1-5.
184. Gundersman, K. J. in *Phospholipids: Characterization, Metabolism, and Novel Biological Applications* (Eds.: G. Cevc, F. Paltauf), AOCS Press, Illinois, **1995**, pp. 208-227.
185. Wendel, A. in *Encyclopedia of chemical technology* (Ed.: K. Othmer), Volume 15, 4th ed., Wiley, New York, **1995**, pp. 193-211.
186. Hayashi, H., Yamanaka, T., Miyajima, M., Imae, T. *Chem. Lett.* **1994**, *12*, 2407-2410.
187. Robinson, N. *J. Pharm. Pharmacol.* **1961**, *13*, 321-354.
188. New, R. R. C. in *Phospholipids Handbook* (Ed.: G. Cevc), Marcel Dekker, New York, **1993**, pp.885-878.
189. Namba, Y. in *Phospholipids Handbook* (Ed.: G. Cevc), Marcel Dekker, New York, **1993**, pp.879-894.
190. Szuhaj, B. F. in *Encyclopedia of food science and technology* (Ed.: Y. H. Hui), Volume 3, Wiley, New York, **1991**, pp. 1601-1604.
191. Stamatov, S. D. *Chem. Phys. Lipids.* **1998**, *91*, 129-134.
192. Nagao, A., Terao, J. *Biochim. Boph. Res. Co.* **1990**, *172*, 385-389.
193. Koga, T., Moro, K., Terao, J. *Lipids*, **1998**, *33*, 589-594.
194. Net information from <http://www.musclesurf.com/lycosorb.html>, 10.08.2004.
195. Sugawara, T., Kushiro, M., Zhang, H., Nara, E., Ono, H., Nagao, A. *J. Nutr.* **2001**, *131*, 2921-2927.
196. Baskaran, V., Sugawara, T., Nagao, A. *Lipids.* **2003**, *38*, 705-711.
197. Koo, S. I., Noh, S. K. *J. Nutr.* **2001**, *131*, 717-722.
198. Haraldsson, G. G., Thorarensen, A. *J. Am. Oil Chem. Soc.* **1999**, *76*, 1143-1149.
199. Totani, Y., Hara, S. *J. Am. Oil Chem. Soc.* **1991**, *68*, 848-851.
200. Geiger, O., Thomas-Oates, J. E., Glushka, J., Spaink, H. P., Lugtenberg, B. J. J. *J. Biol. Chem.* **1994**, *269*, 11090-11097.
201. Schmitz, B., Egge, H. *Chem. Phys. Lipids.* **1984**, *43*, 139-151.
202. Yoshimoto, T., Nakata, M., Yamaguchi, S., Funada, T., Saito, Y., Inada, Y. *Biotechnol. Lett.* **1986**, *8*, 771-116.
203. Na, A., Eriksson, C., Eriksson, S.-G., Österberg, E., Holmberg, K. *J. Am. Oil Chem. Soc.* **1990**, *67*, 766-770.
204. Lilja-Hallberg, M., Härröd, M. *Biocatalysis.* **1994**, *9*, 195-207.
205. Lilja-Hallberg, M., Härröd, M. *Biocatal. Biotransfor.* **1995**, *12*, 55-66.
206. Bibak, N., Hajdu, J. *Tetrahedron Lett.* **2003**, *4*, 5875-5877.
207. Larson-Backström. US 5434183, Pharmacia AB, Sweden, **1995**.

208. Horrobin, D. F., McMordie, A., Manku, M. S. US5466841, Scotia Holdings PLC, England, **1995**.
209. Euler, H. V., Hellström, H., Klussmann, E. *Arkiv För Kemi. Mineralogi och Geologi*, **1931**, Bd 10 B. No 18., 1-4.
210. Hager, A. *Planta (Berlin)*, **1970**, 91, 38-53.
211. Salares, V. R., Young, N. M., Carey, P. R., Bernstein, H. J. *J. Raman Spectrosc.* **1977**, 6, 282-288.
212. Shibata, K. *Biochim. Biophys. Acta.* **1956**, 22, 398-399.
213. Karrer, von P., Strauss, W. *Helv.* **1938**, 21, 1624-1636.
214. Ruban, A. V., Horton, P., Young, A. J. *J. Photochem. Photobio. B.* **1993**, 21, 229-234.
215. Buchwald, M., Jencks, P. *Biochem.* **1968**, 7, 834-843.
216. Mori, Y., Yamano, K., Hashimoto, H. *Chem. Phys. Lett.* **1996**, 254, 84-88.
217. Lüddecke, E., Auweter, H., Schweikert, L. EP0930022, BASF A.-G., Germany, **1998**.
218. Salares, V. R., Young, N. M., Bernstein, H. J., Carey, P. R. *Biochem.* **1977**, 16, 4751-4756.
219. Takadi S., Ito T., Nakajima, A., Kimura, Y., Takeda, K. *Nippon Nogei Kagaku Kaishi.* **1993**, 67, 1055-1060.
220. Takagi, S., Takeda, K., Shiroishi, M. *Agric. Biol. Chem.* **1982**, 46(9), 2217-2222.
221. Baumeister, B. Matile, S. *Chem. Eur. J.* **2000**, 6, 1739-1749.
222. Ulman, A. *Chem. Rev.* **1996**, 96, 1533-1554.
223. Chechic, V., Crooks, R. M., Stirling, C. J. M. *Adv. Mater.* **2000**, 12, 1161-1171.
224. Xu, J., Li, H.-L. *J. Colloid Interf. Sci.* **1995**, 176, 138-149.
225. Huang, F. K., Horton, R. C., Myles, D. C., Garrell, R. L. *Langmuir*, **1998**, 14, 4802-4808.
226. Aslam, M., Bandyopadhyay, K., Vijayamohan, K., Lakshminarayanan, V. *J. Colloid. Interf. Sci.* **2001**, 234, 410-417.
227. Dishner, M. H., Hemminger, J. C., Feher, F. J. *Langmuir.* **1997**, 13, 4788-4790.
228. Bandyopadhyay, K., Vijayamohan, K. *Langmuir.* **1998**, 14, 625-629.
229. Reinerth, W. A., Burgin, T. P., Dunbar, T. D., Bumm, L. A., Arnold, J. J., Jackiw, J. J., Zhou, C.-W., Deshpande, M. R., Allara, D. L. Weiss, P. S., Reed, M. A. Tour, J. M. *Polymeric Materials Science and Engineering.* **1998**, 78, 178-179.
230. Bandyopadhyay, K., Vijayamohan, K. *Langmuir.* **1999**, 15, 5314-5322.
231. Han, S. W., Kim, K. *J. Colloid Interf. Sci.* **2001**, 240, 492-497.
232. Garg, N., Lee, R. T. *Langmuir*, **1998**, 14, 3815-3819.
233. Yee, C. K., Ulman, A., Ruiz, J. D., Parikh, A., White, H., Rafailovich, M. *Langmuir.* **2003**, 19, 9450-9458.
234. Jiøi L., Nygård, B. *J. Electroanal. Chem.* **1997**, 423, 1-11.

235. Net information from: <http://www.ifm.liu.se/applphys/biomaterial/research/sam.html>, 10.08.2004.
236. Schreiber, F., Leung, T. Y. B., Schwartz, P., Fenter, P., Kahn, A., Eisenberger, P., Scoles, G. *Book of abstracts, 214th ACS National Meeting, Phys-347*, Las Vegas, USA, **1997**.
237. Liu, D., Szulczewski, G. J., Kispert, L. D. *J. Phys. Chem. B.* **2002**, *106*, 2933-2936.
238. Liu, D., Gao, Y., Kispert, L. D. *J. Electroanal. Chem.* **2000**, *488*, 140-150.
239. Ion, A., Partali, V., Sliwka, H.-R., Banica, F. G. *Electrochem. Commun.* **2002**, *4*, 674-678.
240. Onyango, A. N., Inoue, T., Nakajima, S., Baba, N., Kaneko, T., Matsuo, M., Shimizu, S. *Angew. Chem. Int. Ed.* **2001**, *40*, 1755-1757.
241. Hopper, D. W., Catalano, J. G., Macdonald, T. L. *Tetrahedron Lett.* **1996**, *37*, 7871-7874.
242. Eibl, H., Lands, W. E. M. *Biochemistry.* **1970**, *9*, 423-428.
243. Tomoi, M., Inomata, K., Kakiuchi, H., Tokuyama, S. *Synthetic Commun.* **1989**, *19*, 907-915
244. Thomas, A. E., Scharoun, J. E., Raltson, H. *J. Am. Oil Chem. Soc.* **1965**, *42*, 789-792.
245. Lyubachevskaya, G., Boyle-Roden, E. *Lipids.* **2000**, *35*, 1353-1358.
246. Martin, J. B. *J. Am. Chem. Soc.* **1953**, *75*, 5482-5486.
247. Serdarevich, B. *J. Am. Oil Chem. Soc.* **1967**, *44*: 381-393.
248. Lands, W. E. M., Merkel, I. *J. Biol. Chem.* **1963**, *238*, 898-904.
249. De Haas, G. H., Van Deenen, L. L. M. *Biochim. Biophys. Acta.* **1965**, *106*, 315-325.
250. Slotboom, A. J., Bensen, P. P. M. *Chem. Phys. Lipids.* **1970**, *5*, 301-398.
251. Plückerthun, A., Dennis, E. A. *Biochemistry.* **1982**, *21*, 1743-1750.
252. Lammers, J. G., Liefkens, T. J., Bus, J., Vandermeer, J. *Chem. Phys. Lipids.* **1978**, *22*, 293-305.
253. Eibl, H. *Chem. Phys. Lipids.* **1980**, *26*, 405-429.
254. Miyamoto, S., Koga, T., Terao, J. *Biosci. Biotechnol. Biochem.* **1998**, *62*, 2463-2466.
255. Kanetani, F., Negoro, K., Okada, E. *J. Chem. Soc. Jp.* **1984**, *9*, 1452-1458.
256. Kaneko, A., Suzuki, T. JP 62126192, Pola Chemical Industries, Inc., Japan, **1987**.
257. Nakamoto, K., Kitano, S., Nakano, Y., Suzuki, H. JP 2001181289, NOF Corporation, Japan, **2001**.
258. 4-oxo- β -apo-8'-carotenoic acid (C30 cantha acid) and its ethyl ester have been synthesized by H. Ernst, BASF A.-G., Germany.
259. Net information from: http://members.tripod.com/~charles_W/arthritis11.html, 14.10.2004.
260. Haraldsson, G. G., Gudmundsson, B. Ö., Almarsson, Ö. *Tetrahedron.* **1995**, *51*, 941-952.

261. Ponpipom, M. M., Bugianesi, R. L. *J. Lipid Res.* **1980**, *21*, 136-139.
262. Kriat, M., Vion-Dury, J., Confort-Gouny, S., Favre, R., Viout, P., Sciaky, M., Sari, H., Cozzone, P. J. *J. Lipid Res.* **1993**, *34*, 1009-1019.
263. Petracek, F. J., Zechmeister, L. *Anal. Chem.* **1956**, *28*, 1484-1485.
264. Merck Index, 13th Edition (Eds. P. Heckelman, A. Smith, M. J. Oneil). Merck Publishing Group, **2001**, p. 2617.
265. Hansen, W. J., Murari, R., Wedmid, Y., Baumann, W. J. *Lipids.* **1982**, *17*, 453-559.
266. Pallas, N. R., Pethica, B. A. *Colloid Surface.* **1983**, *6*, 221-227.
267. Dionisio, M., Sotomayor, J. *J. Chem. Educ.* **2000**, *77*, 59-62.
268. von Rybinski, W. in *Handbook of Applied Surface and Colloid Chemistry*; Vol. 1 (Ed.: K. Holmberg), Wiley, Chichester, **2001**, pp. 53-72.
269. Patist, A. in *Handbook of Applied Surface and Colloid Chemistry* Vol. 2, (Ed.: K. Holmberg), Wiley, Chichester, **2002**, pp. 239-249.
270. Mukerjee, P., Mysels, K. J. *Critical micelle concentrations of aqueous surfactant systems*, Nat. Stand. Ref. Data Ser., Nat. Bur. Standards, Washington, D.C. **1971**, pp. 13-17
271. Mulqueen, M., Huibers, P. D. T. in *Handbook of Applied Surface and Colloid Chemistry* Vol. 2, (Ed.: K. Holmberg), Wiley, Chichester, **2002**, pp. 217-224
272. Net information from www.surfchem.co.kr/tech/plate.htm, 16.08.2004.
273. Hansen, F. K., Rødsrud, G. *J. Colloid Interf. Sci.* **1991**, *141*, 1-9.
274. Hansen, F. K. *J. Colloid Interf. Sci.* **1993**, *160*, 209-217.
275. Net information from Prof. Finn Knut Hansen, University of Oslo, Norway; <http://folk.uio.no/fhansen/dropbroc.html>, 09.08.2004.
276. Schott, H. *J. Pharm. Sci.* **1980**, *69*, 852-854.
277. von Szyszkowski, B. *Z. Phys. Chem.* **1908**, *64*, 385-414.
278. Rosen, M. J. *Surfactants and interfacial phenomena*. 2nd ed., Wiley, New York, **1989**, pp. 431.
279. Bian, J., Roberts, M. F. *J. Colloid Interf. Sci.* **1992**, *153*, 421-428.
280. Lindman, B. in *Handbook of Applied Surface and Colloid Chemistry*; Vol. 1 (Ed.: K. Holmberg), Wiley, Chichester, **2001**, p. 432.
281. Kosswig, K., Marl, H. A. G. in *Ullmann's Encyclopedia of Industrial Chemistry*, Vol. A 25, **1994**, pp.747-761.
282. Lange, von H. *Kolloid Z. Z. Polym.* **1957**, *152*, 155-156.
283. Razafindralambo, H., Blecker, C., Delhay, S., Paquot, M. *J. Colloid Interf. Sci.* **1995**, *174*, 373-377.
284. Rosen, M. J. *Surfactants and interfacial phenomena*, 2nd ed., Wiley, New York, **1989**, pp 64-136.
285. Skrylev, L. D. *Russ. J. Appl. Chem.* **2000**, *73*, 1364-1367.
286. Zajic, Von Doz J., Bareš, M., Kaufman, K. *Fett. Wiss. Technol.* **1970**, *72*, 865-870.
287. Klevens, H. B. *J. Am. Oil Chem. Soc.* **1953**, *30*, 74-80.

288. Nagakaki, M., Komatsu, H., Handa, T. *Chem. Pharm. Bull.* **1986**, *34*, 4479-4485.
289. Malik, W. U., Srivastava, S. K., Gupta, D. *J. Electroanal. Chem.* **1972**, *34*, 540-542.
290. Nydén, M. in *Handbook of Applied Surface and Colloid Chemistry* Vol. 2, (Ed.: K. Holmberg), Wiley, Chichester, **2002**, pp. 294-296.
291. Borkovec, M. in *Handbook of Applied Surface and Colloid Chemistry* Vol. 2, (Ed.: K. Holmberg), Wiley, Chichester, **2002**, pp. 365-367.
292. Berne, B. J., Pecora, R. *Dynamic Light Scattering*. Wiley, New York, **1976**, p. 6.
293. Lewis, R. J., Huang, J. H., Pecora, R. *Macromolecules*. **1985**, *18*, 944-948.
294. Brown, W. *Dynamic Light Scattering*. Clarendon, Oxford, **1993**, pp. 272-277.
295. Lapham, J., Rife, J. P., Moore, P. B., Crothers, D. M. *J. Biomol. NMR*. **1997**, *10*, 255-262.
296. Robinson, N., Saunders, L. *J. Pharm. Pharmacol.* **1958**, *10*, 384-391.
297. Haftendorn, R., Schwarze, G., Ulbrich-Hofmann, R. *Chem. Phys. Lipids*. **2000**, *104*, 57-66.
298. Yanishlieva, N. V., Marinova, E. M., Raneva, V. G., Partali, V., Sliwka, H.-R. *J. Am. Oil Chem. Soc.* **2001**, *78*, 641-644.
299. Mortensen, A., Skibsted, L. H., Sampson, J., Rice-Evans, C., Everett, S. A. *FEBS Lett.* **1997**, *418*, 91-97.
300. Matheson, I. B. C., Rodgers, M. A. J. *Photochem. Photobiol.* **1982**, *36*, 1-4.
301. Manitto, P., Speranza, G., Monti, D., Gramatica, P. *Tetrahedron Lett.* **1987**, *36*, 4221-4224.
302. Lindig, B. A., Rodgers, M. A. J. *Photochem. Photobiol.* **1981**, *33*, 627-634.
303. Pryor, W. A., Strickland, T., Church, D. F. *J. Am. Chem. Soc.* **1988**, *110*, 2224-2229.
304. Net information from: <http://ierc.scs.uiuc.edu/epr.html>, 17.09.2004.
305. Net information from: <http://www.dartmouth.edu/~eprctr/highlights/high8.htm>, 17.09.2004.
306. Miki, W. *Pure Appl. Chem.* **1991**, *63*, 141-146.
307. Craw, M., Lambert, C. *Photochem. Photobiol.* **1983**, *38*, 241-243.
308. Fournier, T., Tavender, S. M., Parker, A. W. *J. Phys. Chem. A*. **1997**, *101*, 5320-5326
309. Edge, R., Land, E. J., McGarvey, D. J., Burke, M., Truscott, T. G. *FEBS Lett.* **2000**, *471*, 125-127.
310. Strom, R., Crifo, C., Viti, V., Guidoni, L., Podo, F. *FEBS Lett.* **1978**, *96*, 45-50.
311. Talbot, J. C., Bernard, E., Maurel, J. P., Faucon, J. P., Dufourq, J. *Toxicol.* **1982**, *20*, 199-202.
312. Net information from: http://www-biol.paisley.ac.uk/marco/Enzyme_Electrode/Chapter1/Cyclic_Voltammetry1.htm, 27.09.2004.

313. Bard, A. J., Faulkner, L. R. *Electrochemical methods: fundamentals and applications*. 2nd ed., Wiley, New York, 2001, p. 226.
314. Brett, C. M. A., Brett, A. M. O. *Electroanalysis*, Oxford University press, New York, **1998**, p. 52.
315. Finklea, H. O. in *Electroanalytical Chemistry* (Eds.: Bard, A. J., Rubinstein, I.), M. Dekker, New York, **1996**, p.109.
316. Macdonald, J. R. *Impedance spectroscopy: emphasizing solid materials and systems*. Wiley, New York, **1987**.
317. Net information from: <http://ichf.edu.pl/offers/instrum/quartz.htm>, 27.09.2004.
318. Otero, L., Silber, J. J., Sereno, L. *J. Electroanal. Chem.* **1991**, 319, 415-422.
319. Kodali, D. R. *J. Lipid Res.* **1987**, 28, 464-469.
320. Oghi, T., Kondo, T., Goto, T. *Tetrahedron Lett.* **1977**, 46, 4051-4054.
321. Buchecker, R., Noack, K. in *Carotenoids Volume 1B: Spectroscopy* (Eds.: Britton, G., Liaaen-Jensen, S., Pfander, H), Birkhäuser, Basel, **1995**, pp. 63-75.
322. Simonyi, M., Bikádi, Z., Zsila, F., Deli, J. *Chirality*. **2003**, 15, 680-698.
323. Zsila, F., Simonyi, M., Lockwood, S. F. *Bioorg. Med. Chem. Lett.* **2003**, 13, 4093-4100.
324. Zsila, F., Bikádi, Z., Deli, J., Simonyi, M. *Chirality*. **2001**, 13, 446-453.
325. Gronowitz, S., Herslöf, B., Ohlson, R., Töregård, B. *Chem. Phys. Lipids*. **1975**, 14, 174-188.

References

Appendices

Article 1

B. J. Foss, S. N. Næss, H.-R. Sliwka and V. Partali

**Stable and highly water-dispersible, highly unsaturated
carotenoid phospholipids – surface properties and
aggregate size**

Angew. Chem. Int. Ed. **2003**, *42*, 5237-5240.

Article 1 is not included due to copyright

Article 2

B. J. Foss and J. Krane

Structural elucidation by 1D and 2D NMR of three isomers of a carotenoid lysophosphocholine and its synthetic precursors

Magn. Reson. Chem. **2004**, *42*, 373-380.

Article 2 is not included due to copyright

Article 3

B. J. Foss, H.-R. Sliwka, V. Partali, S. N. Næss, A. Elgsæter,
T.-B. Melø and K. R. Naqvi

**Hydrophilic carotenoids: surface properties and aggregation behavior of a highly
unsaturated carotenoid lysophospholipid**

Chem. Phys. Lipids 2004, accepted

Hydrophilic carotenoids: surface properties and aggregation behavior of a highly unsaturated carotenoid lysophospholipid

Bente Jeanette Foss^a, Hans-Richard Sliwka^{a*}, Vassilia Partali^a, Stine Nalum Næss^b, Arnljot Elgsæter^b, Thor-Bernt Melø^b, K. Razi Naqvi^b

^aDepartment of Chemistry, ^bDepartment of Physics, Norwegian University of Science and Technology, N-7491 Trondheim, Norway.

*Corresponding author: Tel.: +47 73 59 5600; fax: +47 73 59 6255. E-mail address: hrs@nvg.ntnu.no

Keywords: carotenoids, surfactants, aggregates, phospholipids, fatty acids

Abstract

The water dispersibility of a hydrophobic carotenoid has been greatly enhanced by using it as the acyl part in the synthesis of a highly unsaturated lysophospholipid. Dynamic light scattering has revealed the formation of stable aggregates with an average hydrodynamic radius of a few nanometers, and absorption spectra show that the aggregates can withstand the addition of ethanol or acetonitrile until the volume fraction of water falls below 70% and 62%, respectively. The properties of the carotenoid phospholipids have been characterized by determining surface tension, critical micelle concentration, surface concentration, molecular area, free energy of adsorption and micellation, adsorption-micellar energy relationship, and equilibrium constants.

1. Introduction

The immense importance of the cell membrane is widely recognized and well documented. This explains why phospholipids, which are essential constituents of membranes, have been so thoroughly investigated, and why carotenoids have attracted just as much attention, since they provide structural stability to, and perform a host of other beneficial functions within, biological membranes (Milon et al., 1986, Gabrielska and Gruszecki, 1996; Gruszecki, 1999). Conjugated phospholipids are rarely encountered in nature; the most unsaturated natural example **12** contains parinaric acid (C18:4) (Schmitz and Egge, 1984). Saturated medium chain lysophosphatidylcholine isomers **11** occur as minor constituents in most tissues (Gunstone, 1994). The vast majority of the about 750 naturally occurring carotenoids are hydrophobic (Britton et al., 2004); water dispersibility has only been reported for the alkali salts of the carotenoid diacids crocetin (C20:7) and norbixin (C24:9) (Gainer, 2000; colorMaker 2004), for carotenoid sugar esters (Pfander, 1996), carotenoid sulfates (Liaaen-Jensen, 1996; Oliveiros, 1994), carotenoproteins (Palmer and Eckles, 1914; Zagalsky, 1995; Zsila et al., 2003) and for synthetic pyridinium carotenoids (Fuhrhop et al., 1990; Blanchard-Desce et al., 1993). In order to be absorbed in the intestine, dietary carotenoids undergo various processes, such as dispersion in lipid emulsion droplets. A recent study has shown that emulsification and, consequently, uptake of carotenoids can be enhanced by the presence of lysophosphatidylcholine (Sugawara et al., 2001).

Diet is not the only source of carotenoids. Orally administered supplements have often been claimed to provide greater benefits. Eight carotenoids are produced in appreciable amounts, and some of these commercially available hydrophobic carotenoids are frequently used to color water-based soft drinks (März, 2000; Kläui, 1965, Lüddecke et al., 1998). Water-dispersible carotenoids act as $^1\text{O}_2$ -quencher (Matheson and Rodgers, 1982; Speranza et al., 1990) and radical scavengers (Cardounel et al., 2003; Foss et al., 2004a) and have also found pharmaceutical application (Balakhovskii, 1934; Gross and Lockwood, 2004; Gainer, 1979). In order to achieve solubilization, elaborate preparation procedures have been developed, e.g. micronisation (Balakhovskii and Rachevskii, 1938) with consecutive coating by hydrophilic agents (sugar, gum arab), incorporation or encapsulation in water-soluble carriers (dextrin, starch, gelatin, protein) and addition of detergents (monoglycerols, polyethylene glycols) (Zagalsky, 1995; Horn and Rieger, 2001; Lockwood et al., 2003; Gellenbeck, 1999; Schlipalius, 1994; Werner, 1994). Formulation is the art of handling mixtures and the currently used solubilization procedures for carotenoids are therefore basically mechanical in nature (Horn and Rieger, 2001).

Synthesizing carotenoids with new functional groups, and thereby improving their desirable properties, is a topic of considerable academic and commercial interest. A carotenoid phosphate ester has been described previously (Sliwka, 1997). Carotenoid acids have also formerly been used for the synthesis of highly unsaturated lipids (Partali et al., 1996; Schaeren and Moreland, 1959; Naalsund et al., 2001; Houte et al., 2000; Larsen et al., 1998). For the current study, we have synthesized neutral (zwitterionic) carotenoid lysophospholipid isomers, which in water spontaneously disperse to nanometer-sized supramolecular self-assemblies. We present here data on the surface properties, critical micelle concentration and the aggregate size of the carotenoid lysophospholipids (**R**)-**7**, **7a**, **7b**, **7c**, **Schemes 1, 2**. A preliminary account of this comprehensive biophysical investigation has been reported (Foss et al., 2003).

We report similar observations on a water dispersible, highly unsaturated bolaamphiphile elsewhere (Foss et al., 2004b).

2. Experimental

2.1 Synthesis

The syntheses of (*R*)-1-(β -apo-8'-carotenoyl)-3-glycerophosphocholine [(*R*)-7] will be described separately (Foss et al., unpublished data). The synthesis and characterization of the (β -apo-8'-carotenoyl)-glycerophosphocholine isomers (7a/7b/7c) have been published (Foss et al., 2003; Foss and Krane, 2004).

2.2 Surface properties

The *contact angle* θ was determined with a goniometer (Fibro DAT 1122). For sample preparation, one drop of a solution of 7a/7b/7c in CH₂Cl₂ was placed on a glass plate and dried to a thin film before the water drop was added.

Surface tension γ and critical micelle concentration c_M were determined at 22 °C with a Wilhelmy plate tensiometer (Krüss K10 T digital tensiometer) and with a pendant drop instrument (Ramé-Hart, Inc.) with DROPimage software, developed by F.K. Hansen, University of Oslo (Hansen, 1993). A stock solution of 7a/7b/7c was prepared with distilled, filtered (0.22 μ m) water by stirring overnight. The stock solution was then diluted with distilled, filtered water to the final solutions with the required concentrations for the measurements. The values of the Wilhelmy and the drop method were recorded immediately after the initial equilibrium was obtained.

2.3. Determination of particle size by Dynamic Light Scattering (DLS)

The measurements were performed using an ALV DLS/SLS-5022F compact goniometer system and an ALV-5000/E multiple τ digital correlator (ALV, Langen, Germany). The light source was a 22 mW He-Ne laser (Uniphase, Witney Oxon, U.K.). The temperature of the sample was 23 °C and the scattering angle 90°. The sample was purified with 5 μ m filters. In order to obtain reliable decay time distribution functions, data from 14 successive 5-min measurements were averaged and then analyzed with the CONTIN-method (Bian and Roberts, 1992) (Provencher, 1984). In the absence of consistent information on the particle shape, we related the translational diffusion coefficient, D_T , to the equivalent hydrodynamic radius, r_H , through the Stokes-Einstein relation $r_H = \frac{k_B T}{6\pi\eta D_T}$, where k_B is Boltzmann's constant,

T the absolute temperature and η the solvent viscosity. For the number-weighted distribution we have assumed spherical particles.

2.4 Calculation of thermodynamic data:

Surface pressure (change of tension caused by the substrate) $\pi = \gamma^\circ - \gamma_{c_M}$, $\gamma^\circ = 73$, mN m⁻¹ (H₂O).

Surface concentration $\Gamma = \frac{-1}{nRT} \left[\frac{d\gamma}{d(\ln c)} \right]_{c_M} = \frac{-1}{nRT} \left(c \frac{d\gamma}{dc} \right)_{c_M}$, $n = 1$. When γ is

measured in N m⁻¹ = 10⁻³ J m⁻², R in J mol⁻¹ K⁻¹, and T in K (in our case 294 K), Γ comes out in mol m⁻².

Area per molecule in a filled monolayer $a_m = 10^{20} \Gamma^{-1} N_A^{-1} [\text{\AA}^2]$, where N_A is the Avogadro constant.

Free energy of micellation (energy change for a molecule from the monomer to the micelle state) $\Delta G_{mic}^\circ = RT \ln c_M$ [J mol⁻¹]. Free energy of adsorption (energy change of a molecule in the bulk and at the surface) $\Delta G_{ad}^\circ = RT \ln c_M - 6.023 \pi a_m$ [J mol⁻¹].

Equilibrium constants

aggregated molecules/monomer in bulk $K_{mic} = \exp(-\Delta G_{mic}^\circ / RT)$,

molecules at surface/monomer in bulk $K_{ad} = \exp(-\Delta G_{ad}^\circ / RT)$,

molecules at surface/aggregated molecules $K_{ad-mic} = \exp[-(\Delta G_{ad}^\circ - \Delta G_{mic}^\circ) / RT]$.

Aggregate geometry

The critical packing parameter (Israelachvili et al., 1992) $c_{pp} = \frac{v_L}{l_L \cdot a_m}$ predicts the

aggregate morphology. The hydrophobic portion is considered to be a cylinder with $d = 6 \text{ \AA}$ (Chifu et al., 1983), $l_L = 16 \text{ \AA}$ (C11-hydrophobic chain portion attached to the β -ring) and $v_L \approx 450 \text{ \AA}^3$, Fig. 1. With $a_m = 39 \text{ \AA}^2$ $c_{pp} \approx 0.7$; $0.5 > c_{pp} < 1.0$ denotes lamellar structures (Israelachvili et al., 1992).

Surface area unilamellar vesicle $S = 4\pi r_H^2 + 4\pi r_0^2$, where r_0 denotes the radius of the aqueous core. From DLS $r_H = 60 \text{ \AA}$ [(R)-7], $r_H = 80 \text{ \AA}$ (7a/7b/7c), $r_0 = 28 \text{ \AA}$ ($= 60 \text{ \AA} - 2l_L$), $r_0 = 48 \text{ \AA}$ ($= 80 \text{ \AA} - 2l_L$), $l_L = 16 \text{ \AA}$. Aggregation number $N = S/a_m$.

3. Results and discussion

3.1. Synthesis

We have synthesized the carotenoid lysophosphatidylcholines by two chemical methods (Foss et al., 2002; Paltauf and Hermetter, 1994), since the advantage of stereoselective enzymatic syntheses is devaluated by the rigid experimental conditions (Vitro and Adlercreutz, 2000; Partali et al., 1996): A. by esterification of a carotenoid fatty acid (C30-acid 2) with (+)-(R)-glycerolphosphorylcholine (GPC) ((R)-1), resulting in enantiomeric (R)-7 (p = 90%) in very low yield (4%) (Foss et al., unpublished data), Scheme 1, B. by introducing the choline group into the carotenoid monoglyceride mixture 8a, 8b, giving an isomeric mixture of 7a/7b/7c (49:43:8) in an acceptable yield (33%), (Foss et al., 2003) Scheme 2.

Phospholipids (R)-7, 7a, 7b, 7c are isomers with identical head groups and hydrocarbon chains, and are, therefore, expected to show similar surface and aggregation properties (Arnett and Gold, 1982; Robinson, 1961; Arnold et al., 1967; Haftendorn et al., 2000), Fig. 1. Both synthetic methods (Schemes 1, 2) allow, in principle, "tuning" of the color of the carotenoid dispersions to a desired tint - from fade yellow to red - by replacing the carotenoid acid C30:9 (2) with other known carotenoid acids, e.g. C20:5 (retinoic acid), C23:6, C25:7 etc. up to C40:13 (Schwieter et al., 1966; Dobler et al., 1996).

3.2. Contact angle, surface tension, critical micelle concentration (c_M)

The contact angle ($\theta \approx 25^\circ$) of a water drop on a dry film of **7a/7b/7c** and its lifetime (0.1 s) before spreading revealed noticeable surfactant properties for these isomers (Lam et al., 2002). Since measurements of the surface tension γ are notoriously error-prone, (Mukerjee and Mysels, 1971), see **Table 1**, we decided to use two tensiometers: one using the Wilhelmy plate technique (Mulqueen and Huibers, 2002) and the other the pendant drop method (Hansen, 1993). The results, plotted in **Fig. 2**, show that though each data set suffers from wide scatter, there is overall agreement between the two sets. The values of the retrieved parameters (the critical micelle concentration c_M and the slope, $d\gamma/dc$ or $d\gamma/d \ln c$, depending on how the data are plotted) are rather sensitive to the choice of the function used for fitting the data on either side of the discontinuity. Using linear approximations, we obtained $c_M = 1.1$ or 1.4 mM according to c or $\ln c$ plotted along the horizontal axis. When the data were fitted (with $c \leq 10^{-3}$ M) to the Szyszkowski equation (Szyszkowski, 1908), $\gamma = \gamma^0 - a \log(1 + bc)$, we found $c_M = 1.3$ mM. To take into account these variations, we have set $c_M = 1.3 \pm 0.2$ mM. All three methods gave $\gamma = 57$ mN m⁻¹. The final result for the surface concentration Γ reflects the uncertainties in c_M and $d\gamma/dc$, and was calculated to be 5.6×10^{-6} or 5.2×10^{-6} mol m⁻² for the first two choices, and 3.5×10^{-6} for the third: accordingly we set $\Gamma = (4.5 \pm 1) \times 10^{-6}$ mol m⁻². The values of γ , Γ , a_m (area of the molecule at the filled air-water interface), and other thermodynamic data are listed in **Table 1**. The surface area of **7a/7b/7c** suggests a vertical position of the isomers at the air/water interface. We will use the symbols c_s , c_a , and c_b to denote the concentration at the surface, in the aggregated form, and in bulk, respectively. The equilibrium constant $c_s/c_a = K_{ad-mic} = 5$ points to the low contribution of molecules from aggregates to the monolayer at the surface, whereas the equilibrium constants $c_s/c_b = K_{ad} = 3500$ and $c_a/c_b = K_{mic} = 750$ for **7a/7b/7c** demonstrate the predominance of molecules on the surface and in aggregates relative to monomers in the bulk, **Fig. 3**. The 5:1 concentration ratio (molecules at the surface : molecules in micelles) for these compounds signifies a ratio in favoring micelles; this is in contrast with the ratio of approximately 34:1 found for saturated C8-, C10-, C12- and C14-lysophospholipids. Similarly, the adsorption-micelle energy difference $\Delta G_{ad}^\circ - \Delta G_{mic}^\circ$ for **7a/7b/7c** is about half the reported value of the medium chain lysophospholipids. The adsorption-micellar energy ratio (AMER) (Skrylev et al., 2000) $\Delta G_{ad}^\circ / \Delta G_{mic}^\circ$ has been proposed as a surfactant performance indicator. AMER values close to unity imply dense monolayer formation, enhanced micelle concentration and high ability for flotation, cleansing and wetting. The AMER for **7a/7b/7c** demonstrates an improved ratio when compared with medium chain lysophospholipids, **Table 1**.

The dissimilarities in surface properties of **7a/7b/7c** compared with the saturated lysophospholipids are likely the result of an increased wettability and solubility of the unsaturated compounds (Robinson and Saunders, 1958a). Within a series of homologues, c_M depends primarily on the chain length of the hydrophobic group; methyl groups and rings attached to the chain exert little or no influence (Klevens, 1953). The hydrophobic portions in **7a**, **7b** and **7c** (C30:9) can therefore be visualized

as hypothetical, shorter *trans*-unsaturated chains, C17:8. Each *cis*-double bond present in an unsaturated chain of a lysophospholipid is equivalent to the removal of 1–1.7 carbon atoms (Klevens, 1953; Nagasaki et al., 1986), whereas the effect of a *trans*-double bond is approximately 50% less (Cevc, 1991). On a $\Delta G_{\text{mic}}^{\circ}$ -versus- n plot, where $\Delta G_{\text{mic}}^{\circ}$ is the free energy of micellation and n the chain carbon number of $Cn:0$ -lysophosphatidylcholine ($n = 8, 10, 12, 14, 16$), the $\Delta G_{\text{mic}}^{\circ}$ value for **7a/7b/7c** places it as C11:0, **Fig. 4**. An analogous plot of the free energy of adsorption $\Delta G_{\text{ad}}^{\circ}$ sets the surface absorption behavior of **7a/7b/7c** to C10:0. The data imply that a conjugated *trans* double bond is equivalent to the removal of 0.75–0.88 carbon atoms, which amounts to replacing C17:8 with C11:0 for aggregation, and with C10:0 for absorption. This signifies a significant reduction of the C30-carotenoid **2** to 1/3 of its carbon atoms as it relates to the effective chain length, **Fig. 4**. It can therefore be assumed that the hydrophilic effect of unsaturation is concentrated near the hydrophilic head group, dragging part of the polyene chain into water, **Fig. 1**. The medium chain lysophospholipids and **7a/7b/7c** show an a_m -value (area per molecule at the filled surface) in the range reported for surface films of the C30-ester **3** (Chifu et al., 1979; Zako et al., 1979), **Table 1**. At the air/water interface a_m is determined by the properties of the polar head group, whose size appears to be much smaller in **3** than in **7**, as judged from molecular models, **Fig. 1**.

The lysophospholipid isomer mixture **7a/7b/7c** formed yellow dispersions in water, which are clear and translucent at low concentrations but became viscous and turbid at higher concentrations. A saturation point could not be reached up to a solute concentration of 60 mg/ml (Robinson and Saunders, 1958b).

3.3 VIS spectroscopy, aggregate behavior

The absorption band of the monomer solution in organic solvent is characteristically displaced in aqueous solutions: one strong band appears in the H-aggregate region and a hardly visible shoulder is found around 500 nm, indicating J-aggregate formation. Since the absorption spectra of dilute aqueous dispersions of (*R*)-**7** (ca. 5×10^{-9} M in a cell of 10 cm path length) resemble the spectra recorded at higher concentrations, **Fig. 5**, it is evident that aggregation starts at exceedingly low concentrations, in line with previous observations of lysophospholipids (Robinson and Saunders, 1958b). The absorption spectrum of an aqueous dispersion of (*R*)-**7** is plotted in **Fig. 5**. The shape of the spectrum can vary from one dispersion to another, the peak wavelength lying between 380 to 400 nm with a shoulder in the vicinity of 500 nm. Variable peak wavelengths have also been observed for other carotenoid surfactants (Okamoto et al., 1989; Mori et al., 1996). When acetonitrile (MeCN) is gradually added to the sample, the spectrum undergoes only small variations at first. An abrupt change takes place when ρ , the volume fraction of MeCN, approaches 38%, and for $\rho \geq 66\%$, the spectrum is equivalent to that obtained with a solution of monomers. The corresponding values for an ethanol (EtOH)/water mixture are 30% and 38%, respectively. The spectrum of the aggregated form of (*R*)-**7** or of **7a/7b/7c** in water is similar to the absorption spectra of some other carotenoids in solvent-water mixtures (von Euler et al., 1931; Takagi et al., 1987; Zsila et al., 2001; Song and Moore, 1974).

3.4. Aggregate properties

Dynamic light scattering (DLS) allowed the determination of the equivalent hydrodynamic radius r_H of the aggregates (Santos and Castanho, 1996; Berne and Pecora, 1976). In water, (**R**)-**7** formed, at a concentration 0.05 mg/ml (below the c_M of 1 mg/ml), primarily aggregates with an average $r_H = 6$ nm, although some larger aggregates ($30 \leq r_H \leq 500$ nm) were also observed. The corresponding figures for **7a/7b/7c** are $r_H = 8$ nm and $40 \leq r_H \leq 600$ nm, **Fig. 6**. The virtually identical particle size denotes similar aggregation behavior for the pure isomer (**R**)-**7** and the isomer mixture **7a/7b/7c**. The larger particles appeared spherical in shape under light microscopy.

In general, single chain amphiphiles, such as lysophosphatidylcholines, aggregate as micelles (Nagarajan and Ruckenstein, 1979). In spherical micelles, the maximum radius cannot extend beyond the length of the extended oriented hydrocarbon chain $l_L \approx 20$ Å. [The length was estimated from published data (Drikos et al., 1988) and molecular models by reducing the chain with the three non-hydrophobic carbon atoms near the phosphatidylcholine group (Heerklotz and Epan, 2001)]. Micelles of (**R**)-**7** or **7a/7b/7c** certainly possess such an unfolded chain due to the stiffness induced by the conjugated double bonds. [In water, the length of the elongated chain of potassium octanoate (C8:0) and higher homologues (C8+n:0) is 30% reduced due to curling of the saturated, flexible chain (Elworthy 1963)]. However, particles with the predicted hydrocarbon chain size radius were not detected by DLS. The thermodynamic data suggest that the hydrocarbon chain (C17 + β -ring) in the aggregates of (**R**)-**7** or **7a/7b/7c** correspond to a hydrophobic chain of C11:0 attached to the β -ring (with its negligible effect on hydrophobic or hydrophilic properties). The hydrophobic chain portion with the β -ring occupies a cylinder whose volume (v_L) is determined by the diameter between the H-atoms at C4 and the H-atoms of the methyl groups at C1 ($d \approx 6$ Å) (Zako et al., 1979; Chifu et al., 1983), and the length between H-C2 and C14' ($l_L \approx 16$ Å), see **Fig. 1**. Using the length l_L , the volume v_L and with the molecule area a_m of **7**, the critical packing parameter (Israelachvili et al., 1992) $cpp = \frac{v_L}{l_L \cdot a_m} = 0.7$ was calculated, which predicts the formation of lamellar structures. The calculation is subject to certain caveats, as the cpp concept was actually developed for saturated molecules. The estimated aggregation number N for a spherical, unilamellar vesicle with $60 \text{ \AA} \leq r_H \leq 80 \text{ \AA}$ would be in the order of $N \approx 2000$. Aggregate shapes are known to fluctuate to a high degree (Bergström, 2000; Owenson and Pratt, 1984; Bogusz et al., 2000).

4. Conclusion

To sum up, the amphiphilic, highly unsaturated, conjugated, and surface active lysophosphatidylcholine isomers (**R**)-**7**, **7a**, **7b**, **7c** spontaneously form, upon the addition of water, clear, stable, yellow dispersions comprising aggregates mostly as small vesicles together with some big particles. The surface properties of the unsaturated lysophospholipid isomers are similar to saturated homologues with considerably lower carbon numbers in the acyl chain. The highly water-dispersible derivatives (**R**)-**7**, **7a**, **7b**, **7c** allow the investigation of a wide range of biological carotenoid properties in aqueous solutions without additional solubilizing agents.

We would like to conclude with additional relevant observations. First a remark about the possible lytic activity of the caroteno-lysophospholipid **7**: since the lytic activity of lysophosphatidylcholines **11** decreases, or is altogether lost, when the acyl chain contains less than 16 or more than 18 C-atoms, (Reman et al., 1969) none of the isomers **7** is expected to be lytically active. Secondly, the surface and aggregation properties of the few known hydrophilic carotenoid derivatives (see above) have not been investigated, which seems surprising, if one recalls that the aggregation behavior of other carotenoids with near zero aqueous affinity has attracted attention for quite some time (von Euler et al., 1931; Takagi et al., 1987; Zsila et al., 2001; Song and Moore, 1974; Karrer and Straub, 1938; Shibata, 1956; Buchwald and Jencks, 1968; Hager, 1970; Ruban et al., 1993; Salares et al., 1977).

In future publications, we plan to present surface data on crocin and other hydrophilic carotenoids (Foss et al., 2004b; Nalum Naess et al., unpublished data), and analysis of the spectral changes which accompany aggregate formation.

Acknowledgements

We thank F. K. Hansen and J. Vedde (Department of Chemistry, University of Oslo), for their advice and assistance concerning the use of the asymmetric drop shape analyzer, and electrospray mass spectra, respectively. We are also grateful to P. C. Mørk (Department of Chemical Engineering NTNU) for stimulating discussions on surface properties, A. Dyrli (SINTEF-Polymerkjemi, Trondheim) for assistance with surface tension measurements, H. Ernst (BASF AG Ludwigshafen) for C30-ester and S. Servi (Politecnico di Milano) for (+)-GPC. S. Nalum Næss thanks the Norwegian Research Council for a PhD-grant.

References

- Arnett, E.M., Gold, J.M., 1982. Chiral aggregation phenomena 4. A search for stereospecific interactions between highly purified enantiomeric and racemic dipalmitoyl phosphatidylcholines and other chiral surfactants in monolayers, vesicles, and gels. *J. Am Chem. Soc.* 104, 636-639.
- Arnold, D., Weltzien, H.U., Westphal, O., 1967. Über die Synthese von Lysolecithinen und ihrer Ätheranaloga. *J. Liebig Ann. Chem.* 709, 234-239.
- Balakhovskii, S.D., 1934. Significance of carotene in the living organism. *Compt. Rend. Acad. Sci URSS* 1, 28-29.
- Balakhovskii, S.D., F.A. Rachevskii, F.A., 1938. The preparation of colloidal solutions of carotene. *Byulleten Eksperimentalnoi Biologii i Meditsiny*, 5, 519-520.
- Bergström, M., 2000. Thermodynamics of anisotropic surfactant micelles I. The influence of curvature free energy on micellar size and shape. *J. Chem. Phys.* 113, 5559-5568.
- Berne, B.J., Pecora, R., 1976. *Dynamic Light Scattering*. Wiley, New York.
- Bian, J., Roberts, M.F., 1992. Comparison of surface-properties and thermodynamic behavior of lysophosphatidylcholines and diacylphosphatidylcholines. *J. Colloid Interf. Sci.* 153, 420-428.
- Blanchard-Desce, M., Arrhenius, T.S., J.M. Lehn, J.M., 1993. Caroviologens - Synthesis and optical-properties of A- Ω -bis-pyridine and A- Ω -bis-pyridinium polyenes. *B. Soc. Chim. Fr.* 130, 266-272.
- Bogusz, S., Venable, R.M., Pastor, R.W., 2000. Molecular dynamics simulations of octyl glucoside micelles: Structural properties. *J. Phys. Chem B* 104, 5462-5470.
- Britton G., Liaaen-Jensen, S., Pfander, H., Mercadante, A.Z., Egeland, E.S., 2004. *Carotenoids Handbook*, Birkhäuser, Basel 2004.
- Buchwald, M., Jencks, W.P., 1968. Optical properties of astaxanthin solutions and aggregates. *Biochemistry* 7, 834-43.
- Cardounel, A.J., Dumitrescu, C., Zweier, J.L., Lockwood, S.F., 2003. Direct superoxide anion scavenging by a disodium disuccinate astaxanthin derivative: relative efficacy of individual stereoisomers versus the statistical mixture of stereoisomers by electron paramagnetic resonance imaging. *Biochem. Biophys. Res. Commun.* 307, 704-712.
- Cevc, G., 1991. How membrane chain-melting phase-transition temperature is affected by the lipid chain asymmetry and degree of unsaturation: an effective chain-length model. *Biochemistry* 30, 7186-7193.

- Chifu, E., Tomoia-Cotisel, M., Andrei, Z., Bonciu, E., 1979. β -Apo-8'-carotenoic acid ethyl ester films at fluid interfaces. *Gazz. Chim. Ital.* 109, 365-369.
- Chifu, E., Zsako, J., Tomoia-Cotisel, M., 1983. Xanthophyll films. Single-component monolayers at the air/water interface. *J. Colloid Interface Sci.* 95, 346-354.
- colorMaker, Anaheim, California, 2004. Norbixin solutions over 5% can be achieved. Retrieved from company's home page
- Dobler, W., Krause, W., Paust, J., Wörz, O., Rheude, U., Brust, W., Däuwel, G., Bertram, A., Schulz, B., Wegner, G., Münster, P., Ernst, H., Kochner, A., Etzrodt, H., 1996. Verbessertes Verfahren zur Herstellung von Polyencarbonylverbindungen mit einem hohen Gehalt an dem all-E Isomeren, sowie von deren Acetalen oder Ketalen. BASF Ludwigshafen, EP 691329.
- Drikos, G., Dietrich, H., Ruppel, H., 1988. The polarized UV-absorption spectra and the crystal structure of two different monoclinic crystal forms of the retinal homologue β -8'-apocarotenal. *Eur. Biophys. J.* 16, 193-205.
- Elworthy, P.H., 1963. Estimation of deviations from Stoke's law for small molecules, and the shape of some organic ions in solutions. *J. Chem. Soc.* 388-392.
- Foss, B.J., Partali, V., Sliwka, H.R., Martin, H.-D., Mayer, B., 2002. This work, as part of the PhD thesis of Foss, B.J., has been partially reported at the 13th International Carotenoid Symposium, Hawaii, January 2002.
- Foss, B.J., Nalum Naess, S., Sliwka, H.R., Partali, V., 2003. Stable and highly water-dispersible, highly unsaturated carotenoid phospholipids – surface properties and aggregate size. *Angew. Chem. Int. Ed.* 42, 5237-5240; *Angew. Chem.* 115, 5395-5398.
- Foss, B.J., Krane, J., 2004. Structural elucidation by 1D and 2D NMR of three isomers of a carotenoid lysophosphocholine and its synthetic precursors. *Magn. Reson. Chem.* 42, 373-380.
- Foss, B.J., Sliwka, H.-R., Partali, V., Cardounel, A.J., Lockwood, S.F., 2004a. Direct superoxide anion scavenging by a highly water dispersible carotenoid phospholipid evaluated by electron paramagnetic resonance (EPR) spectroscopy. *Bioorg. Med. Chem. Letters* 14, 2807-2812.
- Foss, B.J., Sliwka, H.R., Partali, V., Nalum Naess, S., Elgsæter, A., Melø, T.B., Razi Naqvi, K., O'Malley, S., Lockwood, S.F., 2004b. Hydrophilic carotenoids: surface properties and aqueous aggregation of a rigid, long-chain, highly unsaturated dianionic bolaamphiphile with a carotenoid spacer. *Langmuir* xx, xxx-xxx.
- Foss, B.J., Sliwka, H.R., Partali, V., Meyer, B., Köpsel, C., Martin, H.-D., Bikadi, Z., Simonyi, M., 2004c. Optically active octamer units in aggregates of a highly unsaturated, optically inactive carotenoid phospholipid. To be submitted.

- Fuhrhop, J.H., Krull, M., Schulz, A., Möbius, D., 1990. Bolaform amphiphiles with a rigid hydrophobic bixin core in surface monolayers and lipid membranes. *Langmuir* 6, 497-505.
- Gabrielska, J., Gruszecki, W.I., 1996. Zeaxanthin (dihydroxy- β -carotene) but not β -carotene rigidifies lipid membranes: A H-1-NMR study of carotenoid-egg phosphatidylcholine liposomes. *Biochem. Biophys Acta-Biomembranes* 1285, 167-174.
- Gainer, J.L., 1979. Method for treating arthritis. US 4176179.
- Gainer, J.L., 2000. trans-Sodium crocetinate, methods of making and methods of use thereof, US 6060511.
- Gellenbeck, K.W., 1999. Dry carotenoid-oil powder and process for making same, Amway Corporation, Ada, MI. US5976575.
- Gross, G.J., Lockwood, S.F., 2004. Cardioprotection and myocardial salvage by a disodium disuccinate astaxanthin derivative (CardaxTM). *Life Sciences*, xx, xx-xx.
- Gruszecki, W.I., Carotenoids in membranes, 1999. *Advances Photosynthesis* 8, (Photochemistry of Carotenoids), 363-379.
- Gunstone, F.D., Harwood, J.L., Padley, F.B., (Eds.), 1994. *The Lipid Handbook*, Chapman & Hall, London, p. 25.
- Haftendorn, R., Schwarze, G., Ubrich-Hofmann, R., 2000. 1,3-diacylglycero-2-phosphocholines - synthesis, aggregation behaviour and properties as inhibitors of phospholipase D. *Chem. Phys. Lipids* 104, 57-66.
- Hager, A., 1970. Ausbildung von Maxima im Absorptionsspektrum von Carotinoiden im Bereich um 370 nm; Folgen für die Interpretation bestimmter Wirkungsspektren. *Planta* 91, 38-53.
- Hansen, F.K., 1993. Surface-tension by image-analysis - fast and automatic measurements of pendant and sessile drops and bubbles. *J. Colloid Interf. Sci.* 160, 209-217.
- Heerklotz, H., Epanand, R.M., 2001. The enthalpy of acyl chain packing and the apparent water-accessible apolar surface area of phospholipids. *Biophys. J.* 80, 271-9.
- Horn, D., Rieger, J., 2001. Organic nanoparticles in the aqueous phase - theory, experiment, and use. *Angew. Chem., Int. Edit.*, 40, 4331-4361.
- Houte, H., Partali, V., Sliwka, H.R., Quartey, E.G.K., 2000. Synthesis of structured lipids and etherlipids with antioxidants: combination of a seleno fatty acid and a seleno fatty alcohol with a carotenoid acid in glyceride molecules. *Chem. Phys. Lipids* 105, 105-113.

- Israelachvili, J.N., Mitchell, J.C., B.W. Ninham, B.W., 1992. Theory of self-assembly of hydrocarbon amphiphiles into micelles and bilayers. *J. Chem. Soc. Faraday Trans.* 72, 1525-1568.
- Karrer, P., Straub, W., 1938. Eigenschaften kolloider Carotinlösungen. *Helv. Chim. Acta* 21, 1624-1636.
- Klevens, H.B., 1953. Structure and aggregation in dilute solutions of surface active agents. *J. Am. Oil Chem. Soc.* 30, 74-80.
- Kläui, H., 1965. Waterdispersible carotenoid preparations and processes thereof, Hoffmann-La Roche, Nutley. US 3206316,
- Kumar, V.V., Baumann, W.J., 1991. Lanthanide-induced phosphorous-31 NMR downfield chemical shifts of lysophosphatidylcholines are sensitive to lysophospholipid critical micelle concentration. *Biophys. J.* 59, 103-107.
- Lam, C.N.C., Lu, J.J., Neumann, A.W., 2002. Measuring contact angle. In: Holmberg, K. (Ed), *Handbook of Applied Surface and Colloid Chemistry Vol. 2.* Wiley, Chichester, chpt. 14.
- Larsen, E., Abendroth, J., Partali, V., Schulz, B., Sliwka, H.R., Quartey, E.G.K., 1998. Combination of vitamin E with a carotenoid: alpha-tocopherol and trolox linked to β -apo-8'-carotenoic acid. *Chem. Eur. J.* 4, 113-117.
- Liaaen-Jensen, S., 1996. Partial synthesis of sulphates. In: Britton, G., Liaaen-Jensen, S., Pfander, H., Birkhäuser, (Eds.), *Carotenoids, Vol 2.* Birkhäuser, Basel 1996, pp. 295-300.
- Lockwood, S.F., O'Malley, S., Mosher, G.L., 2003. Improved aqueous solubility of synthetic astaxanthin (3,3'-dihydroxy- β , β -carotene-4,4'-dione) by Captisol (sulfobutyl ether β -cyclodextrin). *J. Pharm. Sci.* 92, 922-926.
- Lüddecke, E., Auweter, H., Schweikert, L., 1998. Verwendung von Carotinoidaggregaten als Färbemittel, BASF, Ludwigshafen. EP 930022.
- Matheson, I.B.C., Rodgers, M.A.J., 1982. Crocetin, a water soluble carotenoid monitor for singlet molecular oxygen. *Photochem. Photobiol.* 36, 1-4.
- Milon, A., Wolff, G., Ourisson, G., Nakatani, Y., 1986. Organization of carotenoid-phospholipid bilayer systems - incorporation of zeaxanthin, astaxanthin, and their C-50 homologs into dimyristoylphosphatidylcholine vesicles. *Helv. Chim. Acta* 69, 12-24.
- Mori, Y., Yamano, K., Hashimoto, H., 1996. Bistable aggregate of all-*trans*-astaxanthin in an aqueous solution. *Chem. Phys. Letters* 254, 84-88.
- Mukerjee, P., Mysels, K.J., 1971. Critical micelle concentrations of aqueous surfactant systems. *Nat. Stand. Ref. Data Ser., Nat. Bur. Standards, Washington, D.C.*, pp. 13-17.

Mulqueen, M., Huibers, P.D.T., 2002. Measuring equilibrium surface tensions. In: Holmberg, K., Shah, D.O., Schwuger, M.J. (Eds.), *Handbook of Applied Surface and Colloid Chemistry Vol. 2*. Wiley, Chichester, chpt. 12.

März, U., 2000. The global market for carotenoids, Business Communication Company, Norwalk: Astaxanthin, β , β -carotene, β -apo-8'-carotenal, β -apo-8'-carotenoid ethyl ester, capsanthin, cantaxantin, lycopene, lutein.

Nagakaki, M., Komatsu, H., Handa, T., 1986. Estimation of critical micelle concentration of lysolecithins with fluorescent probes. *Chem. Pharm. Bull.* 34, 4479-85.

Nagarajan, R., Ruckenstein, E., 1979. Aggregation of amphiphiles as micelles or vesicles in aqueous media. *J. Colloid Interface Sci.* 71, 580-604.

Naalsund, T., Malterud, K.E., Partali, V., Sliwka, H.R., 2001. Synthesis of a triantioxidant compound: combination of β -apo-8'-carotenoic acid, selenacapyloic acid and trolox in a triglyceride. *Chem. Phys. Lipids* 112, 59-65.

Okamoto, H., Hamaguchi, H., Tasumi, M., 1989. Resonance Raman studies on tetrademethyl- β -carotene aggregates. *J. Raman Spectroscopy* 20, 751-156.

Oliveiros, E., Braun, A.M., Aminian-Saghafi, T., Sliwka, H.R., 1994. Quenching of singlet oxygen ($^1\Delta_g$) by carotenoid derivatives - kinetic-analysis by near-infrared luminescence. *New J. Chem.*, 18, 535-539. (Describes an improved work-up procedure in the synthesis of carotenoidsulfates).

Owenson, B., Pratt, L.R., 1984. Molecular statistical thermodynamics of model micellar aggregates. *J. Phys. Chem.* 88, 2905-2915.

Palmer, L.S., Eckles, C.H., 1914. Carotin – the principal natural yellow pigment of milk fat: its relations to plant carotin and the carotin of the body fat, corpus lutetium, and blood serum. III. The yellow lipochrome of blood serum. *J. Biol. Chem.* 17, 223-236.

Paltauf, F., Hermetter, A., 1994. Strategies for the synthesis of glycerophospholipids. *Prog. Lipid Res.* 33, 239-328.

Partali, V., Kvittingen, L., Sliwka, H.R., Anthonsen, T., 1996. Stable, highly unsaturated glycerides - Enzymatic synthesis with a carotenoic acid. *Angew. Chem.* 108, 342-344; *Angew. Chem. Int. Edit.* 1996, 35, 329-330.

Pfander, H., 1996. Partial synthesis of glycosides and glycosyl esters. In: Britton, G., Liaaen-Jensen, S., Pfander, H., (Eds.), *Carotenoids*, Vol. 2. Birkhäuser, Basel, pp. 293-294.

Provencher, S.W., CONTIN (Version 2) Users manual, EMBL-technical report DA07. Max-Planck-Institut Biophysikalische Chemie, Göttingen 1984.

- Reman, F.C., Demel, R.A., de Gier, J., van Deenen, L.L., Eibl, H., Westphal, O., 1969. Studies on the lysis of red cells and bimolecular lipid leaflets by synthetic lysolecithins, lecithins and structural analogs. *Chem. Phys. Lipids* 3, 221-233.
- Robinson, N., 1961. Lysolecithin. *J. Pharm. Pharmacol.* 13, 321-354.
- Robinson, N., Saunders, L., 1958a. The surface activities of α - and β -(acyl) lysolecithins. *J. Pharm. Pharmacol.* 10 (Supp), 227 T-230 T.
- Robinson, N., Saunders, L., 1958b. Physical properties of lysolecithin and its sols. I. Solubilities, surface, and interfacial tensions. *J. Pharm. Pharmacol.* 10, 384-91.
- Ruban, A.V., Horton, P., Young, A.J., 1993. Aggregation of higher plant xanthophylls: Differences in absorption spectra and in the dependency on solvent polarity. *J. Photochem. Photobiol. B* 21, 229-234.
- Salares, V.R., Young, N.M., Carey, P.R., Bernstein, H.J., 1977. Excited state (exciton) interactions in polyene aggregates. Resonance Raman and adsorption spectroscopic evidence. *J. Raman Spectrosc.* 6, 282-288.
- Santos, N.C., Castanho, M.A.R.B., 1996. Teaching Light Scattering Spectroscopy: The Dimension and Shape of Tobacco Mosaic Virus. *Biophys. J.* 71, 1641-1650.
- Schaeren, S.F., Moreland, W.T., 1959. Bixin and norbixin esters, Pfizer. US 2891087.
- Schlipalius, L.E., 1994. Water-dispersible therapeutic composition for water-soluble drugs, Betatene Ltd. WO 9421232.
- Schmitz, H., Egge, H., 1996. 1-*trans*-Parinaroyl phospholipids: synthesis and fast atom bombardment/electron impact mass spectrometric characterization. *Chem. Phys. Lipids* 43, 139-151.
- Schwieter, U., Gutmann, Lindlar, H., Marbet, R., Rigassi, N., Rüegg, R., Schaeren, S.F., Isler, O., 1966. Synthesen in der Carotinoid-Reihe. Neue Synthesen von Apocarotinoiden. *Helv. Chim. Acta* 49, 369-390.
- Shibata, K., 1956. Absorption spectra of suspensions of carotene crystals. *Biochem. Biophys. Acta* 22, 398-399.
- Skrylev, L.D., Streltsova, E.A., Skryleva, T.L., 2000. Adsorption-micellar energy ratio as criterion for predicting surfactant performance. *Russian J. Appl. Chem.* 73, 1364-1367.
- Sliwka, H.R., 1997. Selenium carotenoids III: First synthesis of optically active carotenoid phosphates. *Acta Chem. Scand.* 51, 345-347.
- Song, P.S., Moore, T.A., 1974. Photoreceptor pigment for phototropism and photoaxis. Is a carotenoid the most likely candidate? *Photochem. Photobiol.* 19, 435-441.

Speranza, G., Manitto, P., Monti, D., 1990. Interaction between singlet oxygen and biologically active compounds in aqueous solution III. Physical and chemical $^1\text{O}_2$ -quenching rate constants of 6,6'-diapocarotenoids. J. Photochem. Photobiol. B: Biol. 8, 51-56.

Stafford, R.E., Fanni, T., Dennis, E.A., 1989. Interfacial properties and critical micelle concentration of lysophospholipids. Biochemistry 28, 5113-5120.

Sugawara, T., Kushiro, M., Zhang, H., Nara, E., Ono, H., Nagao, A., 2001. Lysophosphatidylcholine enhances carotenoid uptake from mixed micelles by Caco-2 human intestinal cells. J. Nutr. 131, 2921-2927.

Takagi, S., Nakano, S., Kameyama, K., Tagaki, T., 1987. Biochemical-studies on carotenoids 17. Lutein dispersed in acetone aqueous-solution – spectroscopic analysis and electron-microscope observation. Agric. Biol. Chem. 51, 1561-1566.

Vitro, C., Adlercreutz, P., 2000. Lysophosphatidylcholine synthesis with *Candida antarctica* lipase B (Novozym 435). Enzyme Microbiol. Technol. 26, 630-35.

von Euler, H., Hellström, H., Klussmann, E., 1931. Physikalisch-chemische Beobachtungen und Messungen an Carotenoiden I. Ark. Mineral. Geol. 10B, 1-4.

von Szyszkowski, B., 1908. Experimentelle Studien über kapillare Eigenschaften der wässrigen Lösungen von Fettsäuren. Z. phys. Chem. 64, 385-414.

Werner, M.T., 1974. Produits industriels nouveaux constitués par des caroténoïdes rendus hydrosolubles, leurs procédés de fabrication, les compositions les contenant et leurs applications. Quattrar SA, FR2187291.

Yamanaka, T., Ogihara, N., Ohhori, T., Hayashi, H., Maramutsa, T., 1997. Surface chemical properties of homologs and analogs of lysophosphatidylcholine and lysophosphatidylethanolamine in water. Chem. Phys. Lipids 90, 97-107.

Zagalsky, P.F., 1995. Carotenoproteines. In: Britton, G., Liaaen-Jensen, S., Pfander, H., Birkhäuser, (Eds.), Carotenoids Vol. 1A. Birkhäuser, Basel, pp. 287-294.

Zako, J., Chifu, E., Tomoia-Cotisel, M., 1979. Rotating rigid- plate model of carotenoid molecules and the behaviour of their monolayers at the air-water interface. Gazz. Chim. Ital. 109, 663-668.

Zsila, F., Deli, J., Bikadi, Z., Simonyi, M., 2001. Supramolecular assemblies of carotenoids. Chirality 13, 739-744.

Zsila, F., Simonyi, M., Lockwood, S.F., 2003. Interaction of the disodium disuccinate derivative of meso-astaxanthin with human serum albumin: from chiral complexation to self-assembly. Bioorg. Med. Chem. Letters 13, 4093-4100.

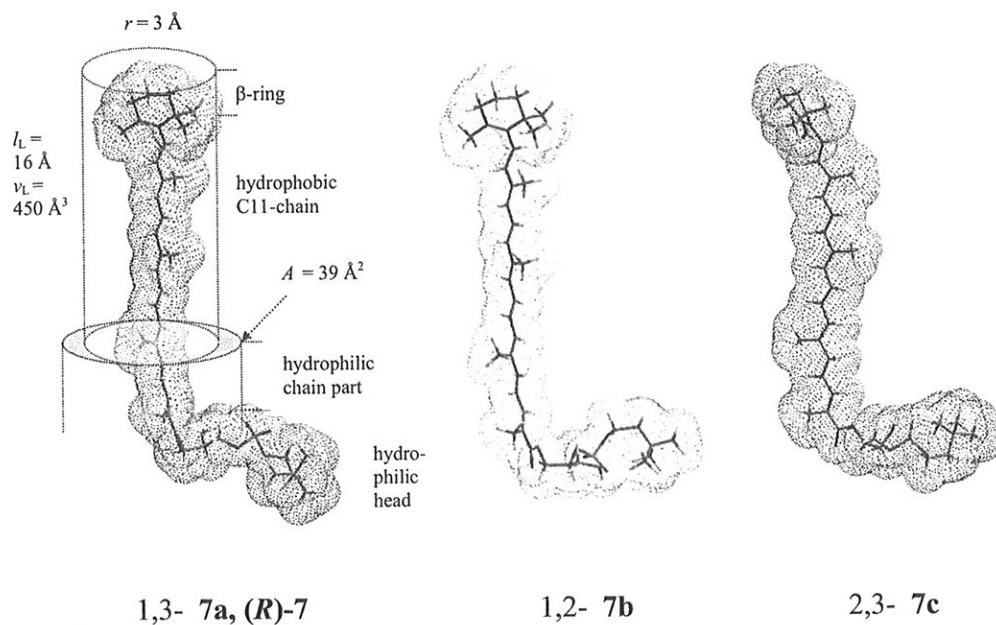


Fig. 1

Head group orientation and molecule parameters for 1,3-, 1,2-, 2,3-lysophosphatidylcholines **7a/7b/7c** (49:43:8). The molecular area a_m at the air/water interface is assumed not to change in the isomers. The hydrophilic effect of unsaturation is supposed to be located near the hydrophilic head.

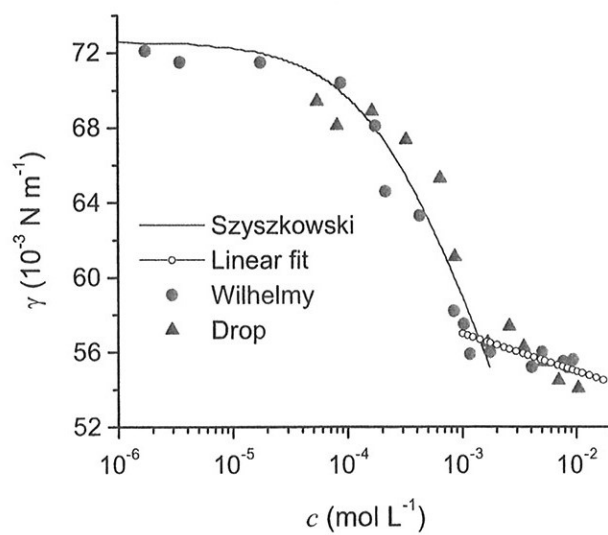


Fig. 2

The measured values of the surface tension plotted against the concentration of the surfactant. The solid curve is derived by fitting the data below 1 mM to the Szyszkowski equation (with $\gamma^0 = 72.6 \text{ mN m}^{-1}$, $a = 18.2 \text{ mN m}^{-1}$, and $b = 4.6 \times 10^3 \text{ L mol}^{-1}$).

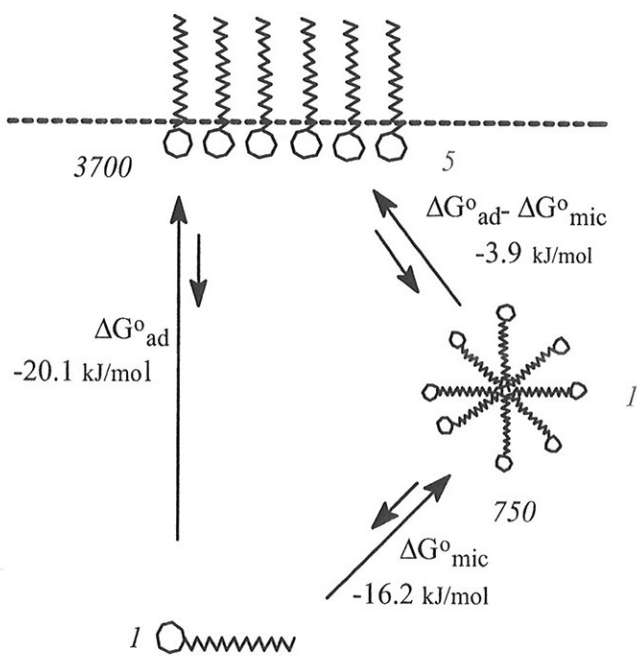


Fig. 3

Adsorption and micellation energy ΔG_{ad}° , ΔG_{mic}° and equilibrium constants K of **7a/7b/7c** for surface monolayer and aggregate formation.

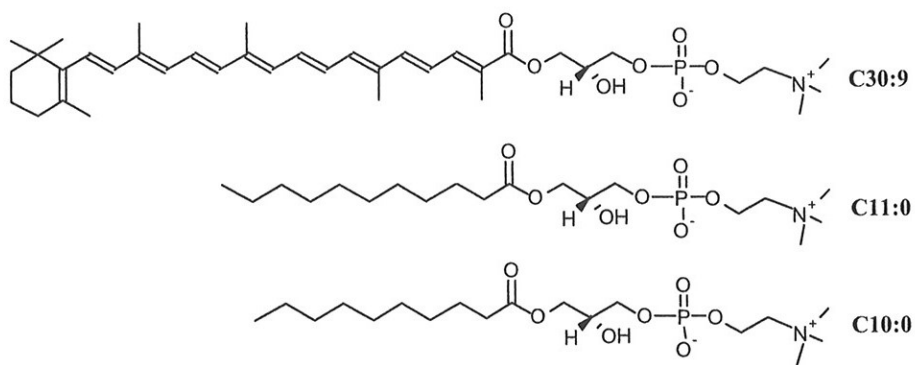
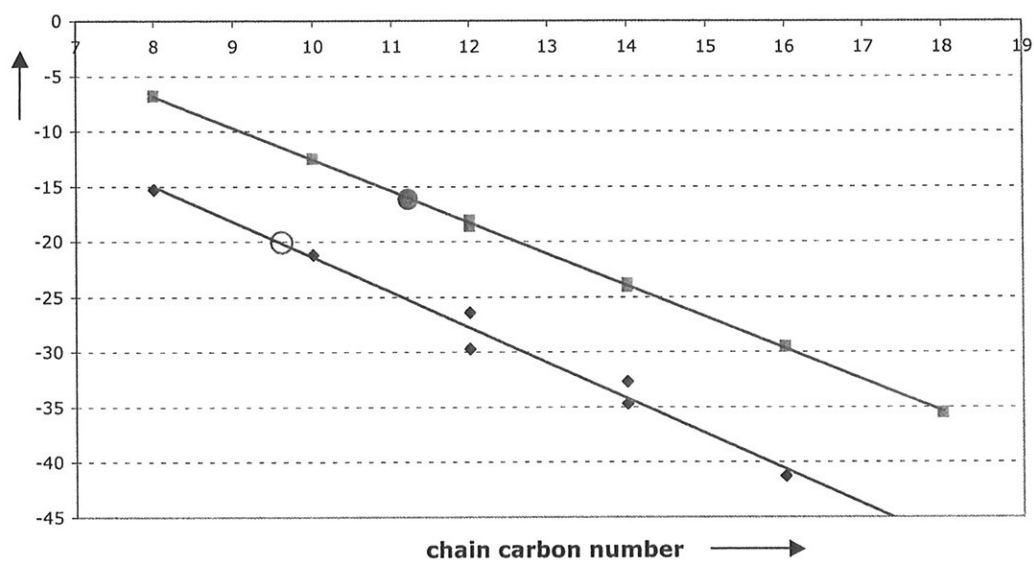


Fig. 4
Chain carbon number of saturated C8-, C10-, C12-, C14-, C16- and C18-lysophosphatidylcholines versus reported ΔG_{ad}^0 (\blacklozenge) and ΔG_{mic}^0 (\blacksquare). ΔG_{mic}^0 and ΔG_{ad}^0 of **7a/7b/7c** (C30:9) correspond to an effective chain length of C11:0 (\bullet) and C10:0 (\circ), respectively

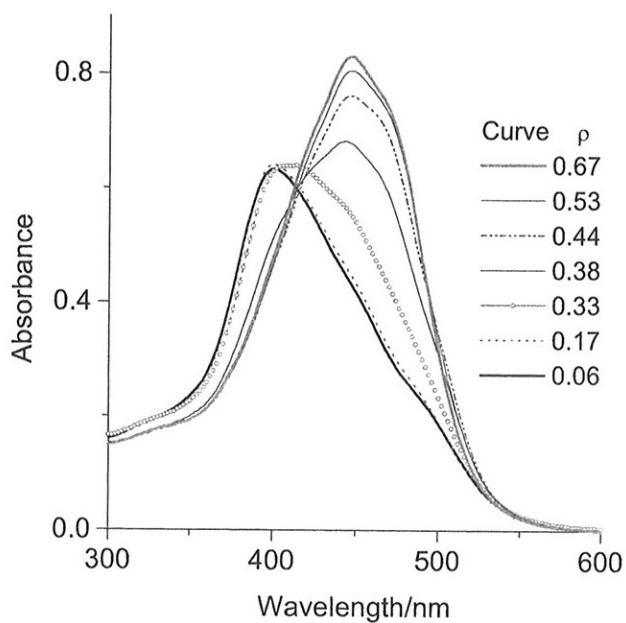


Fig. 5

UV-VIS absorption spectra of (*R*)-7 in various acetonitrile-water mixtures; ρ denotes the volume fraction of acetonitrile. The aggregates in the aqueous dispersion are stable until the solution reaches a concentration of 38% acetonitrile, at which point the aggregates disintegrate to monomers. Similarly, the aggregates are resistant to the addition of ethanol until the solution reaches 30%; at 38% EtOH only monomers exist in solution..

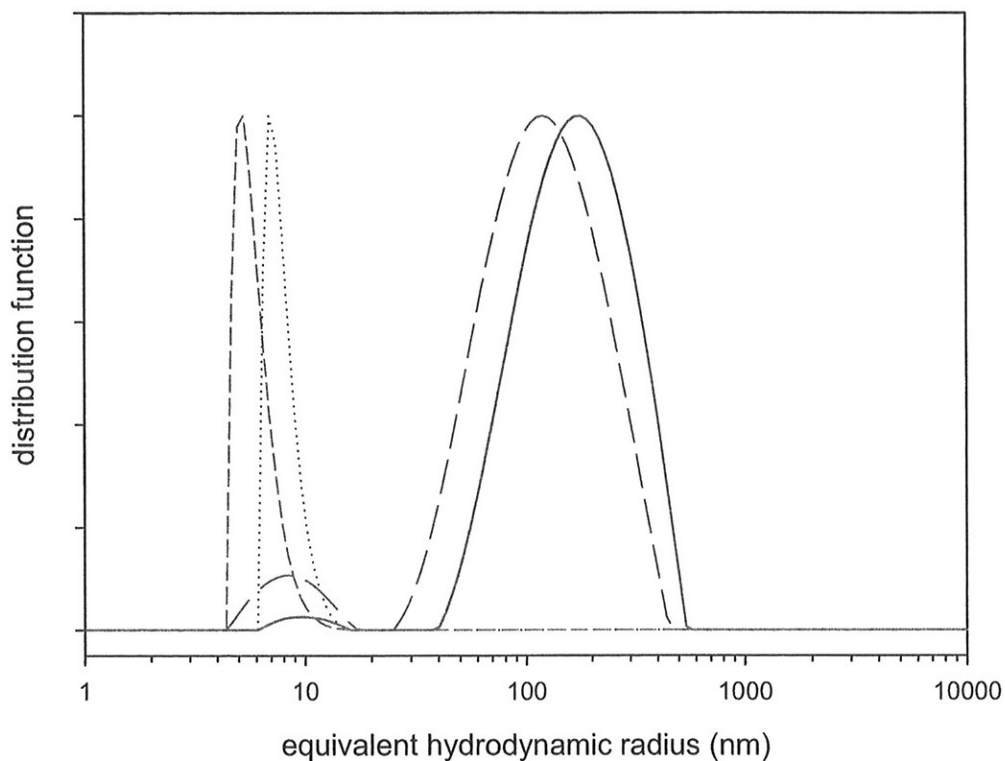
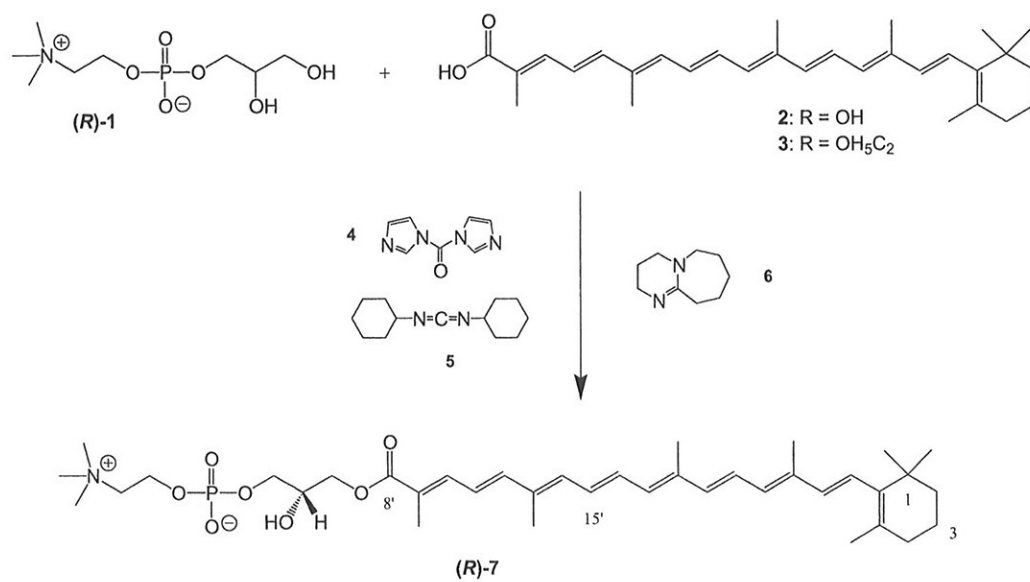
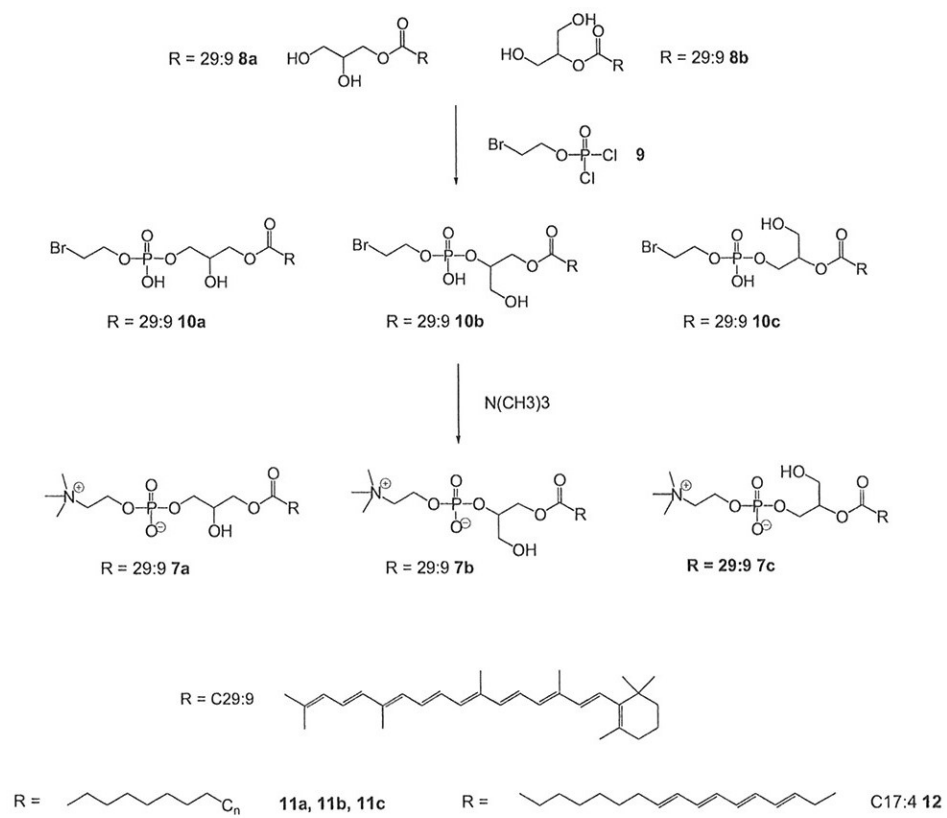


Fig. 6

Size determination of (*R*)-7- and 7a/7b/7c-aggregates in water at 23 °C by DLS. Intensity-weighted distribution (*R*)-7 (— — —), 7a/7b/7c (——) and number-weighted distribution (*R*)-7 (---), 7a/7b/7c (.....). Small aggregates with virtually identical hydrodynamic radii were formed in greatest proportion in both solutions: average $r_H = 6$ nm for (*R*)-7 and $r_H = 8$ nm for 7a/7b/7c. In addition, smaller amounts of large (*R*)-7-particles within the range $r_H = 30$ -500 nm and 7a/7b/7c-particles within the range $r_H = 40$ -600 nm were also observed.



Scheme 1



Scheme 2

lysophospholipid acyl	γ mN/m	π mN/m	c_M M 10^{-3}	Γ 10^{-6} mol/m ²	α_m Å ²	ΔG_{mic}° kJ/mol	ΔG_{ad}° kJ/mol	$\Delta G_{ad}^{\circ} - \Delta G_{mic}^{\circ}$ kJ/mol	K_{mic}	K_{ad}	K_{ad-mic}	AMER $\Delta G_{ad}^{\circ} / \Delta G_{mic}^{\circ}$
C30:9	57	16	1.3 ± 0.2	4.5 ± 1	39 ± 9	-16.2 ± 0.4	-20.1 ± 1.4	-3.9	750	3700	5	1.24
C 8:0	45.3 ^a	27.7 ^a	63 ^a	3.3 ^b	51 ^a	-6.85 ^a	-15.3 ^a	-8.45 ^b	15 ^b	500 ^b	32 ^b	2.23
C10:0	44.3 ^{a,c}	28.7 ^a	6.4 ^a	3.1 ^c	50.6 ^a	-12.5 ^a	-21.2 ^a	-8.7 ^b	170 ^b	5800 ^b	35 ^b	1.7
C12:0	43 ^a	30 ^a	0.67 ^{a,c}	3.7 ^c	45.7 ^a	-18.1 ^a	-26.4 ^a	-8.3 ^b	1600 ^b	49000 ^b	30 ^b	1.45
C12:0	40.1 ^d	33 ^b	0.55 ^d	2.9 ^d	56 ^d	-18.6 ^b	-29.7 ^b	-11.1 ^b	2000 ^b	190000 ^b	94 ^b	1.6
C14:0	42.8 ^{a,c}	30.2 ^a	0.067 ^{a,c}	4.8 ^c	41 ^a	-23.8 ^a	-32.7 ^a	-8.9 ^b	17000 ^b	646000 ^b	38 ^b	1.37
C14:0	39.4 ^d	34 ^b	0.059 ^d	3.2 ^d	52 ^d	-24.1 ^b	-34.7 ^b	-10.6 ^b	19000 ^b	1460000 ^b	76 ^b	1.44
C16:0	38.3 ^d	35 ^b	0.0083 ^d	3.0 ^d	56 ^d	-29.5 ^b	-41.3 ^b	-11.8 ^b	174000 ^b	22 10 ^{6b}	125 ^b	1.4
C18:0			0.0006 ^c			-35.5 ^b						
C30:9-ester ^f					46		-32					

a) 25 °C (Bian and Roberts, 1992), b) calculated from reported data, c) 30 °C (Stafford et al., 1989), d) 30 °C (Yamanaka et al., 1997), e) Kumar and Baumann, 1991), f) Langmuir film (Chifu et al., 1979; Zako et al., 1979).

Table 1 Thermodynamic data (22 °C) of carotenoid-lysophosphocholine **7a/7b/7c** (C30:9) and related compounds.

Article 4

B. J. Foss, H.-R. Sliwka, V. Partali, S. N. Næss, A. Elgsæter, T.-B. Melø, K. R. Naqvi,
S. O'Malley and S. F. Lockwood

**Hydrophilic carotenoids: surface properties and aqueous aggregation of
a rigid, long-chain, highly unsaturated dianionic bolaamphiphile
with a carotenoid spacer**

Chem. Phys. Lipids 2004, submitted

Hydrophilic carotenoids: surface properties and aqueous aggregation of a rigid, long-chain, highly unsaturated dianionic bolaamphiphile with a carotenoid spacer

Bente Jeanette Foss^a, Hans-Richard Sliwka^a, Vassilia Partali^a, Stine Nalum Naess^b, Arnljot Elgsaeter^b, Thor Bernt Melø^b, K. Razi Naqvi^b, Sean O'Malley^c, Samuel F. Lockwood^{c*}

^aDepartment of Chemistry, ^bDepartment of Physics, Norwegian University of Science and Technology (NTNU), N-7491 Trondheim, Norway, ^cHawaii Biotech, Inc., 99-193 Aiea Heights Drive, Suite 200, Aiea, Hawaii 96701, USA
*correspondence: slockwood@hibiotech.com

Abstract

The water dispersibility of astaxanthin has been greatly enhanced by converting it to a disodium disuccinate salt. This carotenoid salt behaves in water as a bolaamphiphile, forming aggregates in the μm range; dynamic light scattering has revealed the formation of stable aggregates with an average hydrodynamic radius close to one micrometer, and absorption spectra show that the aggregates can withstand the addition of 20% acetonitrile. The physicochemical properties of this astaxanthin derivative have been studied by measuring surface tension, critical aggregate concentration, surface concentration, molecular area, free energy of absorption and micellation, adsorption-aggregate energy relationship, and equilibrium constants.

Keywords: carotenoids, surfactants, aggregates, bolaamphiphile

Introduction

The poor water-solubility of most of the nearly 750 natural carotenoids limits considerably their use as food colorants,^[1,2] as pharmaceuticals,^[3,4] and as aqueous-based singlet oxygen quenchers and radical scavengers.^[5-8] With the exception of the carotenoid sugar ester crocin, and the diacids crocetin (C20:7), norbixin and isobixin (C24:9), the few other natural carotenoids with reported low water-solubilities have not yet found practical interest, e.g. carotenoid sulfates^[9] and carotenoid protein complexes.^[10,11] To satisfy the increasing demand for safe food colorants, highly sophisticated formulation methods have been developed to introduce the insoluble carotenoids in water-based systems: addition of detergents and solvents, micronisation, coating with hydrophilic agents, and incorporation in water-soluble carriers, e.g. with cyclodextrines.^[12-16] In most cases, the upper limit of solubility in the particular vehicle is quickly reached, and not always to the desired mg/ml range of solubility; toxicity of the solubilizing agent has also been demonstrated.^[17] Increasing the water-solubility or the water dispersibility of carotenoids by synthetic modification has been much less reliably achieved, and is sparingly reported in the literature. For pyridinium carotenoids water solubility has been reported, however, without giving details.^[18] Whereas a carotenoid monoglycerol conjugate only demonstrated a limited increase in solubility,^[19] a carotenoid lysophosphatidylcholine derivative was highly dispersible in water, and exhibited surface properties similar to other monopolar detergents.^[20,21] In contrast, bipolar detergents with two hydrophilic head groups attached to a hydrophobic spacer ("bolaamphiphiles") are expected to provide quite different properties. The properties in water of unmodified dihydroxy carotenoids such as astaxanthin (**1**), zeaxanthin, and lutein were investigated many years ago.^[22-24] The low water dispersibility limited applications of these carotenoids for the potential uses described in the current study.

In order to increase the water solubility or dispersibility of the dihydroxycarotenoid astaxanthin Hawaii Biotech, Inc. (HBI) successfully esterified each of the two hydroxyl groups of racemic (3*R*,3'*R*, 3*R*,3'*S*, 3*S*,3'*S*)-astaxanthin (**1**) (stereoisomeric ratio 1:2:1) with succinic acid to the acid-ester **2**, followed by neutralization of the free carboxyl groups with NaOH to disodium astaxanthin-3,3'-disuccinate (CardaxTM) **3**.^[25] **Scheme 1**. CardaxTM **3** exhibits substantial water dispersibility, ca. 9 mg/ml. This property allows the novel bolaamphiphilic derivative to be introduced into aqueous systems without additives or co-solvents, and to be delivered as a parenteral for in vivo whole animal experimentation, both advantages in the pre-clinical and clinical testing of the compound.^[4,26,27]

In the current study, the surface properties and the aqueous aggregation behavior of the dianionic bolaamphiphilic carotenoid derivative **3** were evaluated.

Results and Discussion

Surface properties

The surface tension of Cardax™ 3 in aqueous solutions was determined with the Wilhelmy plate method. At the critical aggregate (or micelle) concentration, $c_M = 0.45 \pm 0.05$ mM (= 0.3 mg/ml = 0.03%), the surface tension was $\gamma = 60$ mN m⁻¹,

Fig. 1. With the values of c_M and γ the surface concentration Γ , the surface pressure π , the molecule area at the interface a_m , the free energy of adsorption ΔG_{ad}° and micellation ΔG_{mic}° as well as the equilibrium constants for aggregation and surface adsorption were calculated, see **Table 1**. Γ and ΔG_{mic}° were derived from the

$$\text{equation } \Gamma = \frac{-1}{nRT} \left[\frac{d\gamma}{d(\ln c)} \right]_{c_M} = \frac{-1}{nRT} \left(c \frac{d\gamma}{dc} \right)_{c_M} \text{ and } \Delta G_{mic}^\circ = nRT \ln c_M + 2RT\beta \ln 2.$$

[28] These equations imply electro-neutrality of the surface-absorbed or aggregated compound and is, therefore, only valid for neutral and zwitterionic detergents or ionic surfactants with strong, counterion binding (ion pairing), factor $n = 1$. However, ionic surfactants dissociate into anions and cations, increasing the number of species: $n > 1$. Whereas for di-ionic detergents $n = 2$ has been established,^[29] the choice of n for tri-ionic surfactants, such as Cardax™ 3 is a matter of dispute.^[30-34] For bola and gemini surfactants, both full dissociation ($n = 3$) or monovalent ionpairing ($n = 2$) have been proposed. In the calculation of ΔG_{mic}° for ionic bolaamphiphiles, the prefactor $n = 1 + 2\beta = 3 - 2\alpha$ is obtained considering the degree of counterion dissociation β , or the ion association degree $\alpha = 1 - \beta$; $\beta = 1$ (or $\alpha = 0$) signifies no ionic association. The values of counterion attachment vary considerably according to the method of determination.^[35] At low c_M both complete ionic dissociation or association has been verified.^[34,36] Neutron reflectivity and conductivity measurements allow the determination of the prefactor n ; both methods gave in many cases contradictory results.^[32] In the absence of exact values for factor n , β , and α the results for complete, partial and non-ionic association are given in **Table 1**, entries 1-3. For the calculation of ΔG_{mic}° several equations have been proposed:

$$\Delta G_{mic}^\circ = (1 + 2\beta) RT \ln c_M + 2RT\beta \ln 2; \text{ Ref. [28]} \quad (1)$$

$$\Delta G_{mic}^\circ = (3 - 2\alpha) RT \ln c_M; \text{ Refs. [37, 38]} \quad (2)$$

$$\Delta G_{mic}^\circ = (2 - \alpha) RT \ln c_M = (1 + \beta) RT \ln c_M; \text{ Refs. [37, 39]} \quad (3)$$

$$\Delta G_{mic}^\circ = RT \ln c_M; \text{ Ref. [33]} \quad (4)$$

ΔG_{mic}° was calculated with equation (1) and the free energy of association was calculated with $\Delta G_{ad}^\circ = \Delta G_{mic}^\circ - 6.023 \times 10^{-3} \pi a_m$ [kJ/mol]. It remains to select a "reasonable result"^[31,40] from the calculated values given in **Table 1**, entry 1-3. Considering the low c_M of Cardax™ 3, taking into account that bolaamphiphiles with a rigid spacer prevent counter ion binding,^[31] and in view of the fact that the monosodium salt of succinic acid is a strong 1:1 electrolyte with high ion activity,^[41,42] the results for full dissociation with $n = 3$ ($\beta = 1$) appear more probable. The obtained low surface concentration Γ corresponds to a high molecule area $a_m = 240 \text{ \AA}^2$, **Tab. 1**, similar to other bolaamphiphilic diacids or diacid salts,^[43-45]

Fig. 2. The equilibrium constants reflect the high preference of the CardaxTM 3 molecule to be absorbed at the water surface, **Fig. 3.** The absorption-micellar energy ratio (AMER)^[46] $\Delta G_{ad}^{\circ}/\Delta G_{mic}^{\circ}$ has been proposed as a surfactant performance indicator. AMER values close to unity imply dense monolayer formation, enhanced micelle concentration and high ability in flotation, cleaning and wetting. The AMER-value for CardaxTM 3 expresses only slightly lower surfactant performance when compared to a highly water-soluble, monopolar carotenoid, **Table 1**, entry 9.^[20,21] The derived hydrophobic area $a_m = 240 \text{ \AA}^2$ (from Γ) is in accordance with $a \approx 220 \text{ \AA}^2$, calculated from the length of the hydrophobic part of CardaxTM 3 $l \approx 28 \text{ \AA}$ (C2-C2') and the width of the end groups $l \approx 8 \text{ \AA}$ (CH₃ C1 - C=O - H₂O).^[47] We propose therefore that the molecule adopts a horizontal orientation at the water surface with the succinic moieties anchored in water, **Fig. 2.** In contrast, the distance between the polar groups of saturated dicarboxylates at the water surface is reduced by looping of the now flexible spacer, e.g. a 20% distance reduction for tetradecane dicarboxylate, and a 25% reduction for octadecane dicarboxylate.^[48] The monolayer of CardaxTM 3 on the interface is estimated to be very thin, **Fig. 2.**

Comparison with similar compounds

For a saturated C6-disulfate a molecule area of 460 \AA^2 has been reported, **Tab. 1**, entry 10. The molecule areas of saturated C10- and C12-disulfates are still higher, **Tab. 1**, entries 11, 12. These elevated molecule areas are, at least in part, the result of c_M measurements at high temperatures due to an elevated Krafft point.^[49,50] The natural carotenoid *trans*-isobixin, a monomethylester, absorbs in Langmuir films with erected molecules at the air/water interface.^[51] The surface tension γ of CardaxTM 3 has about the same value as astaxanthin (1)^[52] and succinic acid,^[53-55] whereas the surface concentration Γ of CardaxTM 3 is four times lower, and the molecular area a_m four times higher than that reported for astaxanthin (1), **Table 1**, entries 1, 4, 13. In contrast to ionic CardaxTM 3 neutral astaxanthin (1) appears to adopt a vertical position at the water surface.^[47]

Aggregate behavior

Within a series of homologues, c_M depends predominantly on the chain length of the hydrophobic group,^[56] and double bonds reduce the effective chain length for monopolar surfactants.^[21] A plot of ΔG_{mic}° versus the chain carbon number of the potassium salts of saturated C16:0- and C18:0-diacids,^[57] places the aggregation properties of CardaxTM 3 similar to C22:0-dicarboxylate, **Fig. 4.** The resemblance of the molecular dimensions of CardaxTM 3 with docosanoate suggests that in the aggregates the β -rings of CardaxTM 3 are partly participating in the hydrophilic group. The membranes of both the saturated and unsaturated bolaamphiphile aggregates should consist of stretched carbon chains of $l \approx 28 \text{ \AA}$.^[58] Compared with the UV/VIS spectrum of CardaxTM 3 in acetonitrile ($\lambda_{max} = 490 \text{ nm}$) the absorption of aggregated CardaxTM 3 in water was shifted to $\lambda_{max} = 440 \text{ nm}$, indicating the formation of H-aggregates, **Fig. 5.**^[59] Astaxanthin (1) and the free acid 2 absorb in acetonitrile at $\lambda_{max} = 472 \text{ nm}$. The supramolecular assembly of astaxanthin (1) and other carotenoid derivatives has been reported using CD spectroscopy.^[11, 60] These aqueous supramolecular assemblies are sensitive to the addition of organic (*i.e.* less polar) solvents, and each drop of solvent gives rise to a steady change of the aggregate absorption, until only monomers prevail.^[61]

The rigid spacer and the charge of the polar groups in CardaxTM 3 do not favor the formation of small, curved aggregates. Therefore, aggregation of CardaxTM 3 is expected to be dominated by the formation of large, extended monolayer structures.^[62,63] Dynamic light scattering (DLS)^[64,65] measurements revealed that the intensity of the scattered light from CardaxTM 3 aggregates in water, in 0.155 M NaCl and 0.5 M NaCl did not change during the experiments. In these dispersions the aggregates quickly reached an equilibrium size. For CardaxTM-aggregates in 2.0 M NaCl the scattered intensity increased slowly during the experiment, suggesting a slow association process to larger aggregates. After several hours the aggregates became very large and precipitated from the solution. A small decrease in the decay time of the aggregates in 0.155 M NaCl is observed compared to the decay time of the aggregates in water, **Fig. 6**. This may be caused by osmotic shrinkage of the aggregate. The volume of the interior of the aggregate decreases by the egress of water molecules across the aggregate membrane to the outer environment. At higher salt concentrations fusion of the initial aggregates to overall larger association prevails. The intensity correlation function, **Fig. 6**, shows a significant increase in the decay time for CardaxTM 3 aggregates in 0.5 M and 2.0 M NaCl compared to the decay time of the aggregates in water. Screening of charges and binding of counter ions, i.e. reduction in the repulsion between particles, favor aggregation. The intensity-weighted distribution functions for CardaxTM-aggregates are shown in **Fig. 7**. The aggregates appeared non-spherical in shape under light microscopy. The distribution exhibits several peaks as expected for large non-spherical particles. The main peak expresses aggregate translation (slow decay time). The shoulder of the main peak and the smaller peaks in the left side of the Figure express aggregate rotation (fast decay times). The equivalent hydrodynamic radii for the slow decay times are given in **Fig. 8**. In water and 0.155 M NaCl CardaxTM-aggregates have a hydrodynamic radius $r_H \approx 1 \mu\text{m}$. The aggregates increase in size to $r_H \approx 3 \mu\text{m}$ and $r_H \approx 10 \mu\text{m}$ in 0.5 M and 2.0 M NaCl, respectively.

Conclusion

The water dispersible carotenoid derivative CardaxTM 3 behaves in water as a bolaamphiphile with a low c_M and a high surface tension. The derivative forms a horizontal layer at the air/water interface with an elevated molecule area. CardaxTM 3 also forms supramolecular assemblies in water consisting of non-spherical μm -sized aggregates that increase significantly in size in salt solutions of higher osmolarity.

Acknowledgement

S.N. Næss is grateful for financial support from the Norwegian Research Council.

Experimental

Surface tension γ and critical micelle (aggregate) concentration c_M were determined at 22 °C with a Wilhelmy plate tensiometer (Krüss K10 T digital tensiometer). A stock solution of Cardax™ 3 was prepared with distilled, filtered (0.22 μm) water by stirring overnight. The stock solution was then diluted with distilled, filtered water to the solution with the required concentrations for the measurements. The values were recorded immediately after the initial equilibrium was obtained.

Surface pressure (change of tension caused by the substrate) $\pi = \gamma^\circ - \gamma_{c_m}$, $\gamma^\circ = 73 \text{ mN m}^{-1}$ (H_2O).

Surface concentration $\Gamma = \frac{-1}{nRT} \left[\frac{d\gamma}{d(\ln c)} \right]_{c_M} = \frac{-1}{nRT} \left(c \frac{d\gamma}{dc} \right)_{c_M}$, $n=1-3$. When γ is

measured in $\text{N m}^{-1} = 10^{-3} \text{ J m}^{-2}$, R in $\text{J mol}^{-1} \text{ K}^{-1}$, and T in K (in our case 294 K),

Γ comes out in mol m^{-2} . For determining Γ , the surface tension data were fitted (with $c \leq 5 \times 10^{-4} \text{ M}$) to the Szyszkowski equation,^[66] $\gamma = \gamma^\circ - a \log(1 + bc)$,

we found $c_M = (4.5 \pm 0.5) \times 10^{-4} \text{ M}$.

Area per molecule $a_m = 10^{20} \Gamma^{-1} N_A^{-1} [\text{\AA}^2]$ where N_A is the Avogadro constant.

Equilibrium constants

aggregated molecules/monomer in bulk $K_{\text{mic}} = \exp(-\Delta G_{\text{mic}}^\circ/nRT)$, molecules at

surface/monomer in bulk $K_{\text{ad}} = \exp(-\Delta G_{\text{ad}}^\circ/nRT)$,

molecules at surface/aggregated molecules $K_{\text{ad-mic}} = \exp(-\Delta G_{\text{ad}}^\circ - \Delta G_{\text{mic}}^\circ/nRT)$

DLS measurements

Cardax™ 3 was dissolved in deionized water (Milli-Q). The stock-solution of 0.6 mg/ml Cardax™ 3 was stirred overnight and then diluted to approximately 1:10 in water and salt solutions of different osmolarity to give the final concentration ($c > c_M$). The water and the salt solutions were carefully filtered through 0.22 μm filters. The measurements were performed using an ALV DLS/SLS-5022F compact goniometer system and an ALV-5000/E multiple τ -digital correlator (ALV, Langen, Germany). The light source was a 22 mW He-Ne laser (Uniphase, Witney Oxon, U.K.). The temperature of the sample was 21.5 °C, the scattering angle 30° and the square of the scattering vector, q^2 , was $4.69 \times 10^{13} \text{ m}^{-2}$. The correlation functions (Fig. 7) are fitted to a double exponential consisting of the fast decay for rotation and the slow decay for translation. In order to obtain reliable decay time distributions functions, data from 15 successive 5-min measurements were averaged and then analyzed with the CONTIN-method.^[67]

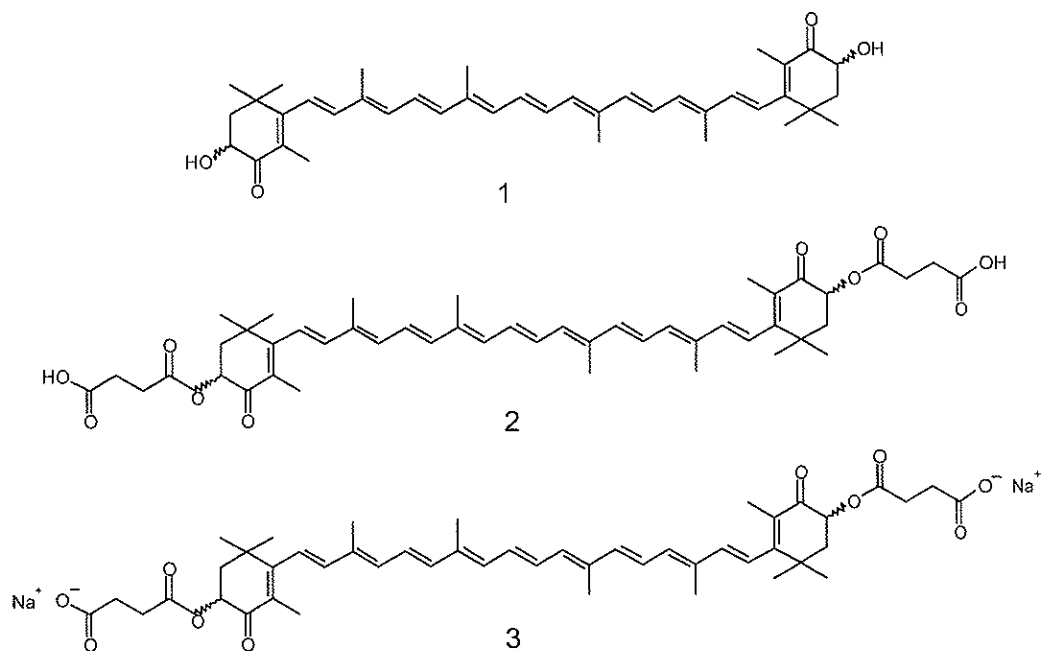
References

1. H. Kläui, Hofmann-La Roche, Nutley, US 3206316, **1965**.
2. E. Lüddecke, A. Auweter, L. Schweikert, BASF, Ludwigshafen EP 930022, **1998**.
3. J.L. Gainer, US 4176179, **1979**.
4. G.J. Gross, S.F. Lockwood. *Life Sci.* **2004**, *75*, 215-224.
5. I.B.C. Matheson, M.A.J. Rodgers. *Photochem. Photobiol.* **1982**, *36*, 1-4.
6. G. Speranza, P. Manitto, D. Monti. *J. Photochem. Photobiol. B: Biol.* **1990**, *8*, 51-56.
7. A.J. Cardounel, C. Dumitrescu, J.L. Zweier, S.F. Lockwood. *Biochem. Biophys. Res. Comm.* **2003**, *307*, 704-712.
8. B.J. Foss, H.-R. Sliwka, V. Partali, A.J. Cardounel, S.F. Lockwood. *Bioorg. Med. Chem. Letters* **2004**, *14*, 2807-2812.
9. Twelve natural sulfates are listed in: *Carotenoids Handbook*, Eds. G. Britton, S. Liaaen-Jensen, H. Pfander, A.Z. Mercadante, E.S. Egeland, Birkhäuser, Basel **2004**.
10. P.F. Zagalsky, in *Carotenoids Vol. 1A*, Eds.: G. Britton. S. Liaaen-Jensen, H. Pfander, Birkhäuser, Basel **1995**, pp 287-294.
11. F. Zsila, M. Simonyi, S.F. Lockwood. *Bioorg. Med. Chem. Letters* **2003**, *13*, 4093-4100.
12. D. Horn, J. Rieger. *Angew. Chem. Int. Edit.* **2001**, *40*, 4331-4361.
13. S.F. Lockwood, S. O'Malley, GL. Mosher. *J. Pharm. Sci.* **2003**, *92*, 922-926.
14. K.W. Gellenbeck. Amway Corporation, Ada, MI US5976575, **1999**.
15. L.E. Schlipalius. Betatene Ltd, WO 9421232, **1994**.
16. M.T. Werner, Quatrar SA, FR2187291, **1974**.
17. J.S. Bertram. *Nutr. Rev.* **1999**, *57*, 182-191.
18. M. Blanchard-Desce, TS. Arrhenius, J.M. Lehn. *B. Soc. Chim. Fr.* **1993**, *130*, 266-272.
19. V. Partali, L. Kvittingen, H.R. Sliwka, T. Anthonsen. *Angew. Chem. Int. Edit.* **1996**, *35*, 329-330.
20. B.J. Foss, S. Nalum Naess, H.R. Sliwka, V. Partali. *Angew. Chem. Int. Ed.* **2003**, *42*, 5237-5240..

21. B.J. Foss, H.R. Sliwka, V. Partali, S. Nalum Næss, A. Elgsæter, T.B. Melø, R.K. Naqvi. *Chem. Phys. Lipids*. **2004**, *xx*, xxx-xxx.
22. M. Buchwald, W.P. Jencks. *Biochemistry* **1968**, *7*, 834-843.
23. A. Hager. *Planta* **1970**, *91*, 38-53.
24. R. Douillard, C. Burghoffer, C. Costes. *Physiol. Vég.* **1982**, *20*, 123-126
25. L.M. Hix, H. Jackson, S. O'Malley, G. Nadolski, S.F. Lockwood, D.G. Watumull, Hawaii Biotech Inc, WO2004011423, **2004**.
26. L.A. Showalter, S.A. Weinman, M. Østerlie, S.F. Lockwood. *Comp. Biochem. Biophys. C*. **2004**, *137*, 227-236.
27. L.M. Hix, S.F. Lockwood, J.S. Bertram. *Cancer Letters* **2004**, *211*, 25-37.
28. R. Zana. *Langmuir* **1996**, *12*, 1208-1211.
29. H. Lange. *Kolloid-Zeitschrift* **1957**, *152*, 155-156.
30. E. Alami, G. Beinert, P. Marie, R. Zana. *Langmuir* **1993**, *9*, 1465-1467.
31. Z.X. Li, C.C. Dong, R.K. Thomas. *Langmuir* **1999**, *15*, 4392-4396.
32. R. Zana. *Adv. Coll. Interf. Sci.* **2002**, *97*, 205-253.
33. F. Devinsky, I. Lacko. *Tenside Surf. Det.* **1990**, *27*, 344-349.
34. Y. Yan, J. Huang, Z. Li, X. Zhao, B. Zhu, J. Ma. *Colloids and Surfaces A, Physicochem. Eng. Aspects* **2002**, *215*, 263-275.
35. T. Sasaki, M. Hattori, J. Sasaki, K. Nukina. *Bull. Chem. Soc. Jpn.* **1975**, *48*, 1397-1403
36. K.M. Kale, E.L. Cussier, D.F. Evans. *J. Phys. Chem.* **1980**, *84*, 593-598.
37. G. Bai, J. Wang, H. Yan, Z. Li, R.K. Thomas. *J. Phys. Chem. B.* **2001**, *105*, 9576-9580.
38. L. Grosmaire, M. Chorro, C. Chorro, S. Partyka, R. Zana. *J. Colloid Interface Sci.* **2002**, *246*, 175-181.
39. S.D. Wettig, P. Nowak, R.E. Verrall. *Langmuir* **2002**, *18*, 5354-5359.
40. K. Meguro, K. Ikeda, A. Otsuji, M. Taya, M. Yasuda, K. Esumi. *J. Colloid Interface Sci.* **1987**, *118*, 372-378.
41. J. Kielland. *J. Am. Chem. Soc.* **1937**, *59*, 1675-1678.

42. H. Høiland. *J. Chem. Soc. Faraday 1* **1975**, *74*, 797-802.
43. Q. Lu, Y. Luo, L. Li M. Liu. *Langmuir* **2003**, *19*, 285-291.
44. I. Weissbuch, R. Buller, K. Kjaer, J. Als-Nielsen, L. Leiserowitz, M. Lahav. *Colloids and Surface A, Physicochem. Eng. Aspects* **2002**, *208*, 3-27.
45. P.M. Jeffers, J. Daen. *J. Phys. Chem.* **1965**, *68*, 2368-2373.
46. L.D. Skrylev, E.A. Streltsova, T.L. Skryleva. *Russian J. Appl. Chem.* **2000**, *73*, 1364-1367.
47. J. Zsako, E. Chifu, M. Tomoaia-Cotisel. *Gaz. Chim. Ital.* **1979**, *109*, 663-668.
48. P.H. Elworthy. *J. Chem. Soc.* **1963**, 388-392.
49. M.J. Rosen, M. Baum, F. Kasher. *J. Am. Oil Chem. Soc.* **1976**, *53*, 742-745
50. If an ionic compound has a high Krafft point, c_M is not reached unless the temperature is raised to the Krafft temperature T_K (the Krafft temperature can be considered as the melting point of a surfactant in an aqueous environment). T_K is usually low in molecules with branched and unsaturated chains or when molecules associate in loose packings. Since we reached the c_M of CardaxTM at room temperature $T_K < 20$ °C.
51. J.H. Fuhrhop, M. Krull, A. Schulz, D. Möbius. *Langmuir* **1990**, *6*, 497-505.
52. A. Shibata, Y. Kiba, N. Akati, K. Fukuzawa, H. *Chem. Phys. Lipids* **2001**, *113*, 11-22.
53. A. Glagoleva. *Doklady Akademii Nauk SSR* **1952**, *86*, 103-106.
54. F.P. Maguna, M.B. Núñez, N.B. Okulik, E.A. Castro. *Chemistry Preprint Server* **2002**, physchem/0205006.
55. U.N. Dash, B.K. Mohanty. *Fluid Phase Equilibria* **1997**, *134*, 267-276.
56. H.B. Klevens. *J. Am. Oil Chem. Soc.* **1953**, *30*, 74-80.
57. I. Danielsson, Suomen Kemistiseuran Tiedonantoja – Finska Kemistsamfundets Meddelanden **1960**, *69*, 89-97. Other, much smaller $c_{M,cm}$ values in: P. H. Elworthy. *J. Pharm. Pharmacol.* **1959**, *11*, 557-564.
58. B. Gallot, A. Skoulios. *Kolloid Zeitschrift & Zeitschrift Polymere* **1968**, *222*, 51-55.
59. G. Britton, in *Carotenoids Vol. 1B*, Eds.: G. Britton, S. Liaaen-Jensen, H. Pfander, Birkhäuser, Basel **1995**, p. 13.

60. Z. Bikadi, F. Zsila, J. Deli, G. Mady, M. Simonyi. *Enantiomer* **2002**, *7*, 67-76.
61. Y. Mori, K. Yamano, H. Hashimoto. *Chem. Phys. Letters* **1996**, *254*, 84-88.
62. R. Nagarajan. *Chem. Eng. Comm.* **1987**, *55*, 251-273.
63. J.H. Fuhrhop, J. Mathieu. *Angew. Chem. Int. Ed.* **1984**, *23*, 100-113.
64. N.C. Santos, M.A.R.B. Castanho. *Biophysical Journal* **1996**, *71*, 1641-1650.
65. B.J. Berne, R. Pecora, *Dynamic Light Scattering*, Wiley, New York **1976**.
66. B. von Szyszkowki. *Z. phys. Chem.* **1908**, *64*, 385-414.
67. S.W. Provencher, CONTIN (Version 2) Users manual, technical report EMBL-DA07, Max-Planck-Institut Biophysikalische Chemie, Göttingen **1984**.
68. L. Zhang, S. Jiang, M. Liu. *J. Colloid Interface Sci.* **2003**, *261*, 417-422.
69. R.O. Sköld, M.A.R. Tunius. *J. Colloid Interface Sci.* **1992**, *152*, 183-189.

**Scheme 1**

Rac. astaxanthin (1), rac. astaxanthin-3,3'-disuccinic acid (2), and rac. disodium astaxanthin-3,3'-disuccinate (Cardax™) (3)

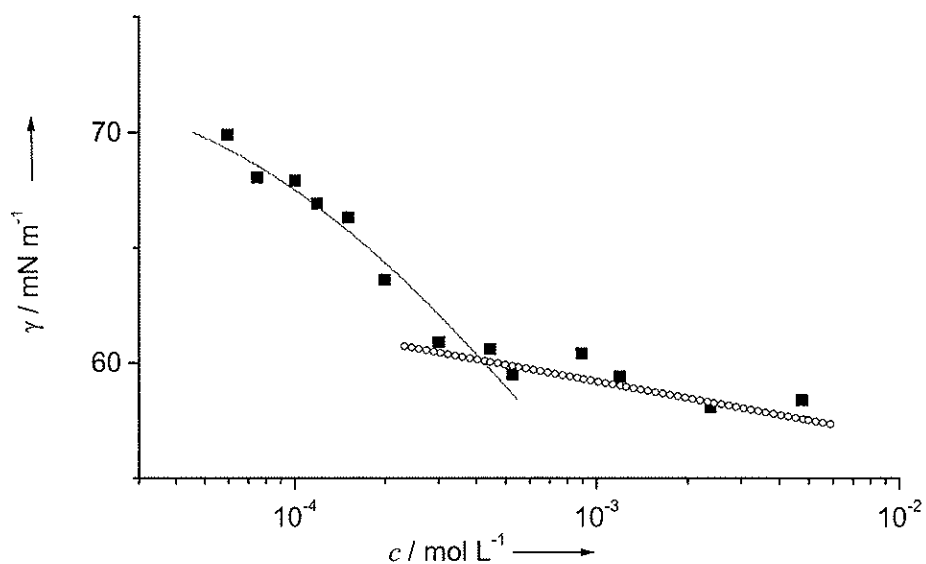


Fig. 1

The measured values of the surface tension plotted against the concentration of the surfactant. The solid curve is derived by fitting the data for $c < 0.5 \text{ mM}$ to the Szyszkowski equation (with $\gamma^0 = 72.6 \text{ mN m}^{-1}$, $a = 31.7 \text{ mN m}^{-1}$, and $b = 4.6 \times 10^3 \text{ L m}^{-1}$).

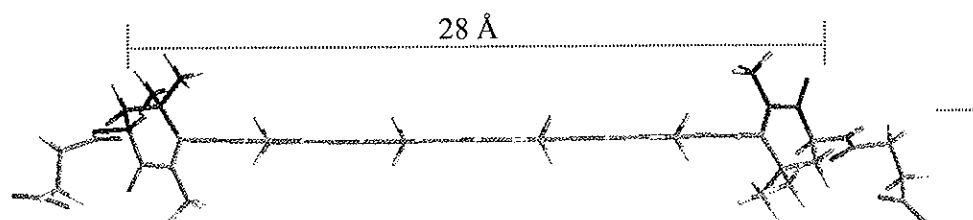


Fig. 2
Hypothetical, horizontal adsorption of Cardax™ 3 at the air/water interface with the hydrophilic succinate moieties anchored in water.

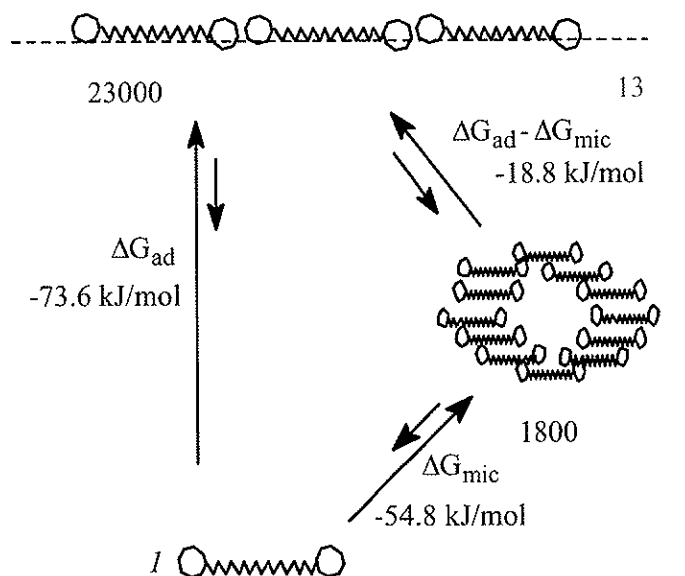


Fig. 3
Adsorption and aggregation energy ΔG_{ad}° , ΔG_{mic}° and equilibrium constants K of Cardax™ 3 for surface monolayer and aggregate formation.

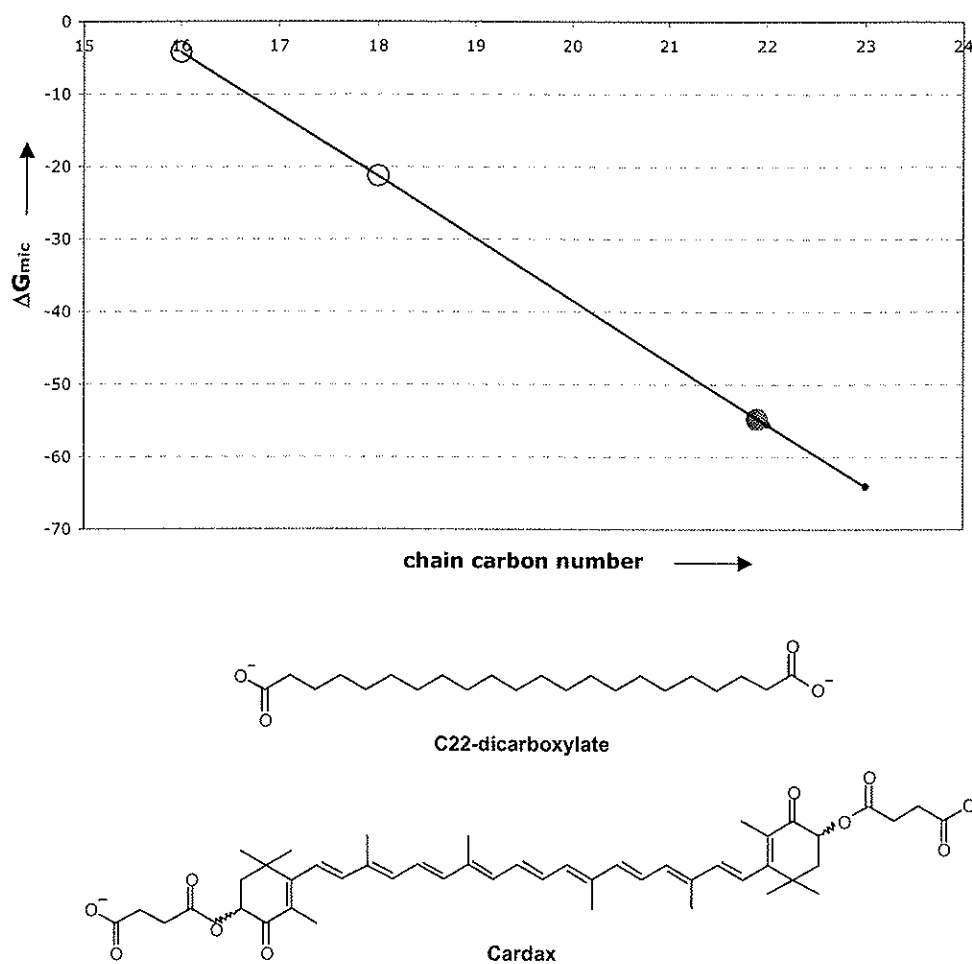


Fig. 4

Chain carbon number of C16:0 and C18:0 dicarboxylates versus ΔG_{mic}° ○ [calculated from reported c_M values at 25 °C [57id] with equation (1)] for K-C16-K $\Delta G_{mic}^{\circ} = -4.2$ kJ mol⁻¹ ○, K-C18-K $\Delta G_{mic}^{\circ} = -21.3$ kJ mol⁻¹ ○), extrapolating these values for C22- and C23-diacid salts ●. The measured ΔG_{mic}° -value (20 °C) of the disodium salt CardaxTM 3 ● is similar to the value of a stretched, saturated chain in an aggregate of C22-dicarboxylate (docosanoate).

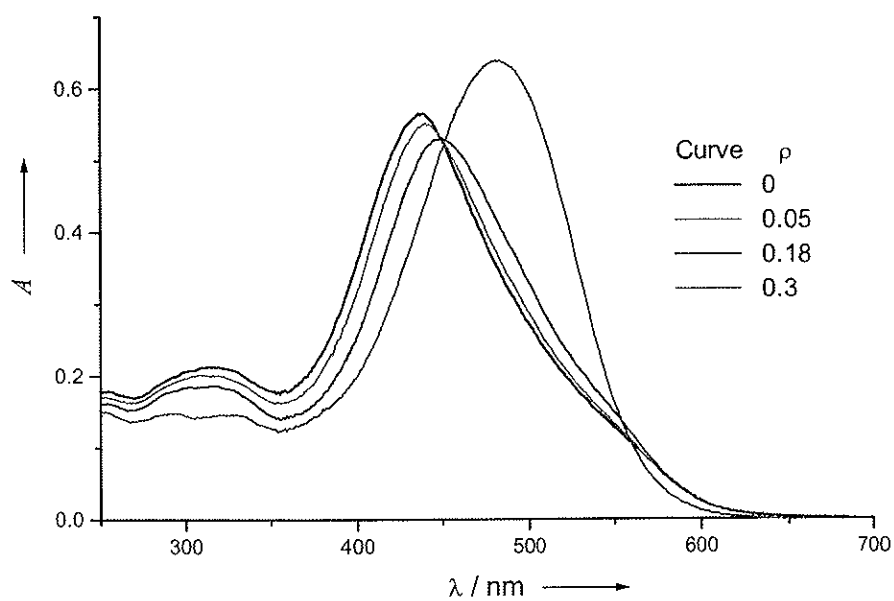


Fig. 5

UV/Vis absorption of monomeric CardaxTM ($\lambda_{\max} = 490$ nm, acetonitrile) and supramolecular assemblies (H-type aggregates) ($\lambda_{\max} = 440$, water). The aggregates in the aqueous dispersion are stable until the solution reaches a concentration of 20% acetonitrile, at which point the aggregates begin to disintegrate to monomers.

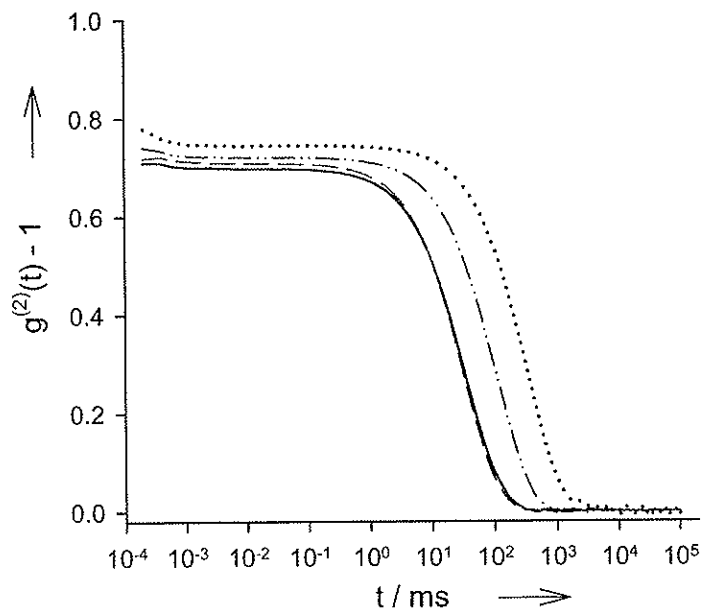


Fig. 6

Intensity autocorrelation functions, $g^{(2)}(t)$, for Cardax dissolved in water (**solid black line**), 0.155 M NaCl (dashed line), 0.5 M NaCl (dash-dotted line) and 2.0 M NaCl (dotted line) plotted versus the lag time, t . The measuring angle is 30° , and the square of the scattering vector, q^2 , is $4.69 \times 10^{13} \text{ m}^{-2}$.

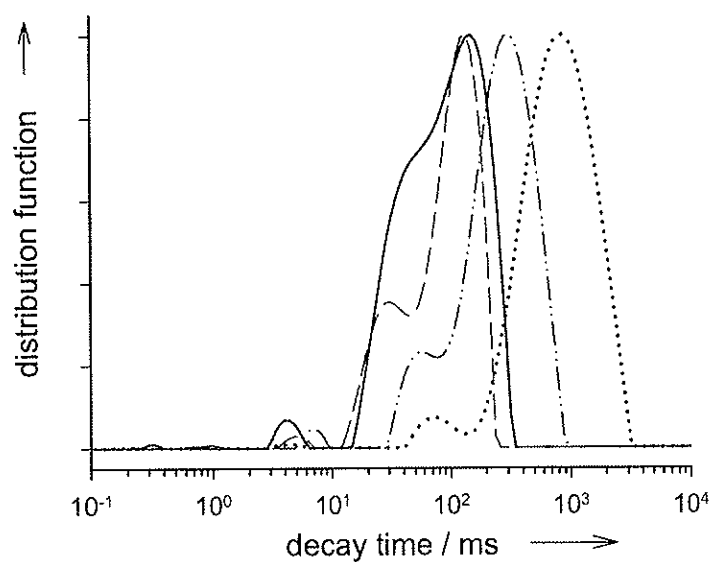


Fig. 7
Intensity-weighted distribution function for CardaxTM **3** dissolved in water (**solid black line**), 0.155 M NaCl (dashed line), 0.5 M NaCl (dash-dotted line) and 2.0 M NaCl (dotted line) plotted versus the decay time. The measuring angle and q^2 are as in **Fig. 6**.

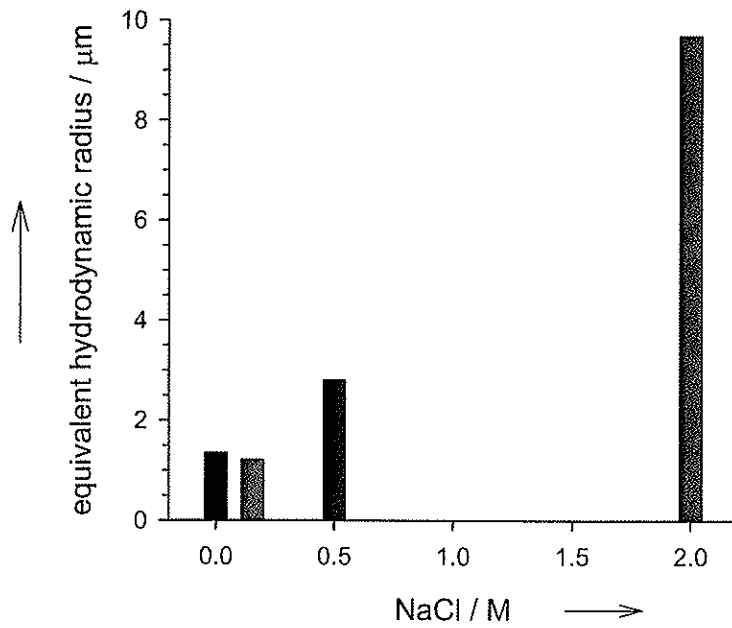


Fig. 8

The correlation functions of Figure 7 are fitted to a double exponential consisting of a fast decay time (rotation) and a slow decay time (translation). The equivalent hydrodynamic radii r_H for the slow decays are given. CardaxTM 3 forms non-spherical aggregates with an equivalent hydrodynamic radius $r_H = 1.3 \mu\text{m}$ (**water**), $r_H = 1.2 \mu\text{m}$ (0.155 M NaCl) (believed to osmotic shrinkage), $r_H = 3 \mu\text{m}$ (0.5 M NaCl) and $r_H = 10 \mu\text{m}$ (2.0 M NaCl).

	γ mN/m	π mN/m	C_M M 10^3	Γ 10^{-6} mol/m ²	α_m \AA^2	ΔG°_{mic} kJ/mol	ΔG°_{ad} kJ/mol	$\Delta G^{\circ}_{ad} - \Delta G^{\circ}_{mic}$ kJ/mol	K_{mic}	K_{ad}	$K_{ad/mic}$	AMER $\Delta G^{\circ}_{ad} / \Delta G^{\circ}_{mic}$
Cardax™ 3 n=3	60	13	0.45 ± 0.05	0.7 ± 0.1	240 ± 30	-54.8 ± 0.8	-73.6 ± 3.2	-18.8	1800	23000	13	1.34
Cardax™ 3 n=2	60	13	0.45 ± 0.05	1.1	150	-36.8	-48.6	-11.8				
Cardax™ 3 n=1	60	13	0.45 ± 0.05	2.1	80	-18.8	-25.0	-6.2				
astaxanthin 1	61.2 ^a	11.8		2.7 ^b	62.4 ^a							
NaOOC-C18-COONa	2 ^c	71		4 ^b	42 ^c							
NaOOC-C10-COONa	72 ^d	1	200 ^d	0.4 ^b	378 ^d							
bixin ^e				0.6	100							
isobixin					29 ^e							
C30-lysophospholipid ^f	57	16	1.3 ± 0.2	4.5 ± 1	39 ± 9	-16.2 ± 0.4	-20.1 ± 1.4	-3.9	750	3500	5	1.24
di-Na-C6-disulfate ^g			4.3	0.36	460							
di-Na-C10-disulfate ^g			2.0 (60 °C)	0.22	750							
di-Na-C12-disulfate ^g			1.0 (70 °C)	0.22	760							
succinic acid ^h	61.6	11										

a) Ref. 52, b) calculated from reported data, c) Ref. 68, d) Ref. 69, e) Ref. 63, f) Ref. 21, g) Ref. 49, h) Ref. 54

Table 1 Thermodynamic data for Cardax™ 3 and related compounds.

Article 5

S. N. Næss, A. Elgsæter, B. J. Foss, H.-R. Sliwka, V. Partali,
T.-B. Melø and K. R. Naqvi

**Hydrophilic carotenoids: Surface properties and aggregation of crocin, a natural,
rigid, long chain, highly unsaturated biosurfactant**

to be published

Hydrophilic carotenoids: Surface properties and aggregation of crocin, a natural, rigid, long chain, highly unsaturated biosurfactant

Stine Nalum Næss^a, Arnljot Elgsæter^a, Bente Jeanette Foss^b, Hans-Richard Sliwka^b, Vassilia Partali^{b*}, Thor-Bernt Melø^a, Razi K. Naqvi^a

^aInstitutt for Fysikk, ^bInstitutt for Kjemi, Norges Teknisk Naturvitenskapelige Universitet (NTNU), N-7491 Trondheim, Norway.

*correspondence: vassilia.partali@chem.ntnu.no

Abstract

The surface and aggregation properties of the naturally occurring pigment crocin have been examined through measurements of surface tension and optical absorption, and the following parameters have been determined: critical aggregate concentration, surface concentration, molecular area, free energy of adsorption- and micellation, adsorption-micellar energy relationship, equilibrium constants, and aggregate size. On structural grounds, the molecule should be classified as a bolaamphiphile, since it is the di-gentiobiose ester of the conjugated highly unsaturated diacid C20:7 carotenoid crocetin. However, our analysis of the data indicates that crocin does not behave like a typical bolaamphiphile: it adsorbs at the water surface with only one polar group; it aggregates only at rather high concentration, and it does not form vesicle-like aggregates.

Introduction

The highly unsaturated, conjugated polyenic carotenoids are biosynthesized in all plants. Although they appear only as minor constituents, the annual bioproduction of carotenoids is estimated to reach thousands of tons. Of about 750 different naturally occurring carotenoids so far been characterized, nearly all are hydrophobic, with the notable exception of a few diacids, sugaresters and sulfates.[1] Whereas the solubility of carotenoid sulfates is below the level (ca. 0.4 mg/ml) [2] of practical interest, the diacid norbixin affords solutions up to 5%, [3] and the sugarester crocin (1) has no saturation point in water.[4] The mentioned compounds possess hydrophilic and -phobic parts, which confer an amphiphilic character, accompanied with surfactant activity and aggregate formation. The surfactant properties of crocin (1), bixin and carotenoid sulfates have not yet been determined. Surprisingly, the aggregation behavior of other carotenoids with near zero aqueous affinity has found early interest.[5- 7] This academic curiosity was later merged with an important commercial perspective, when the few commercialized hydrophobic carotenoids were introduced as safe food colors for soft drinks.[8-10]

We report here on the surface activity and aggregate properties of crocin, β,β -digeantobiosyl 8,8'-diapocarotene-8,8'-dioate (1), the disugar ester of the highly unsaturated diacid crocetin C20:7,[11] **Scheme 1**. Crocin (1), a stable ingredient found to about 25% in saffron,[12-14] is actually the only really highly water-soluble natural carotenoid and the only highly unsaturated, conjugated sugar surfactant.[15] Crocin has antioxidant activities,[16] radical scavenging properties[17], acts as $^1\text{O}_2$ -oxygen quencher,[18, 19] inhibits human cancer cell growth,[20] arthritis[21] and prevents neurodegenerative disorders.[22] Other crocetin sugar esters are less biologically active.[23]

The presented results are part of investigations on synthetic water-soluble carotenoids and their biological and (photo)physical properties.[24-34].

Surface tension and critical micelle concentration

Crocetin dissolves in water to clear, yellow liquids. We did not find a saturation point up to 150 mg/ml. The surface tension γ of various concentrations of crocin (1) in water was determined with the Wilhelmy plate method.[35] By using the Szyszkowski equation[36]) for fitting the plot γ vs. $\ln c$ and γ vs. c we obtained at the point of discontinuity for the critical micelle concentration $c_M = 0.9 \pm 0.1$ mM and $\gamma = 50$ mN/m, **Fig. 1**. The concentration of crocin molecules, completely covering the surface, was calculated to be $\Gamma = (2.7 \pm 0.1) \times 10^{-6}$ mol m^{-2} , which corresponds to a molecular area at the interface $a_m = 62 \pm 2$ \AA^2 . Other thermodynamic data are listed in **Table 1**.

The surface area a_m of crocin suggests an erected or oblique orientation at the air/water interface, with only one polar group anchored in water, the other sugar group pointing outside, **Fig. 2**, Crocin does not, therefore, behave as a bolaamphiphile in the way forming horizontally oriented molecules on water surface. With c_s , c_a and c_b denoting the concentration at surface, in the aggregated form and in bulk, respectively, the equilibrium constants $c_s/c_b = K_{s-b} = 3500$ and $c_a/c_b = K_{a-b} = 100$ point to a high preference of crocin for surface absorption relative to aggregate formation. In addition, the relatively high equilibrium constant $c_s/c_a = K_{s-a} = 35$ (the

concentration ratio of molecules at the surface and in micelles) demonstrates a low aggregation preference, **Fig. 3**. The micellar energy ratio (AMER) [37] $\Delta G_{ad}^{\circ} / \Delta G_{mic}^{\circ}$ has been proposed as a surfactant performance indicator. AMER values close to unity imply dense monolayer formation, enhanced micelle concentration and high ability in flotation, cleaning and wetting.[25] Compared with other carotenoid surfactants, the AMER value of crocin indicates lower surfactant properties, **Table 1**. It has been found that small branching of the polyene chain has negligible influence on surface properties, Crocin C20:7 could therefore be regarded as C16:7 fatty diacid ester concerning surfactant and aggregation behavior. It has further been observed that double bonds with their small hydrophilic character reduce the effective chain length by pulling the polyene chain into the water. In a carotenoid lysophosphocholine one *trans* double bond was equivalent to the removal of about 0.8 carbon atoms,[25] which, if applicable to crocin, would reduce the polyene chain to C10:0. On the other hand, the free energy of surface absorption for crocin is $\Delta G_{ad}^{\circ} = -20$ kJ/mol. This is similar to the C8:0 monoester of the disaccharide maltose $\Delta G_{ad}^{\circ} = -19.8$ kJ/mol,[38] suggesting a reduction of the effective chain length in crocin from C16:7 to C8:0. The lack of data on sugar esters of saturated dicarboxylic acids did not allow verifying such a consideration.

The molecular area of crocin at the interface $a_m = 62 \text{ \AA}^2$ is comparable to the area of sucrose-C12:0 monoester $a_m = 56 \text{ \AA}^2$, **Table 1**, [39] and maltose-6-palmitate $a_m = 66 \text{ \AA}^2$ and -6-oleate $a_m = 61 \text{ \AA}^2$. [40] In sugar esters with saturated fatty acids one $-\text{CH}_2-$ group of the carbon chain is part of the hydrophilic group.[41] If the acid is unsaturated, the chain part of the hydrophilic group is increasing.[25] The molecule area of crocin should therefore principally be determined by the diameter of the polyene chain, enlarged by a hydration layer.[41] On the other hand, it is known that the molecule area of sugar esters expand with the sugar size, from $a_m = 40 \text{ \AA}^2$ for a C12:0 monosaccharide to $a_m = 70 \text{ \AA}^2$ for a C12:0 tetrasaccharide.[39] The molecular area at the interface is also dependent on the length of the fatty acid, *e.g.* lactose esterified with C14:0 has $a_m = 60 \text{ \AA}^2$, esterified with C16:0 $a_m = 68 \text{ \AA}^2$. [42] In opposition, the molecular area of maltose with a short acid is highest, with a long acid lowest: $a_m = 39 \text{ \AA}^2$ (C18:0), $a_m = 66 \text{ \AA}^2$ (C16:0), $a_m = \text{ \AA}^2$ (C14:0).[40] The reported data do not allow to locate exactly the hydrophilic-hydrophobic boundary of a sugar fatty ester molecule. The molecular area of crocin (**1**) at the interface is therefore arbitrarily positioned in **Fig. 2**.

Aggregation

The UV-VIS spectra of crocin in water at $c \leq c_M$ displays the monomer absorption ($\lambda_{max} = 440$ nm), similar to the spectrum of crocin in organic solvents, **Fig. 4**. Likewise, dynamic light scattering (DLS)-measurements show virtually only monomers at $c \leq c_M$, **Fig. 5**. Optical rotation slightly above c_M was similar to the value below c_M : $[\alpha]_{589}^{25} = -55$ and $[\alpha]_{589}^{25} = -53$, respectively, signifying the presence of monomers, since $[\alpha]_{644}^{22.5} = -55$ was measured for tetradecaacetylcrocine in chloroform.[40] We were not able to determine optical rotations at $c \gg c_M$ because of too strong absorption. High optical rotation $[\alpha]_{644}^{21} = -1760^{\circ}$ has been reported for $c < c_M$, which would imply aggregation prior reaching c_M . [43] At $c \geq c_M$ DLS detected aggregates, whereas UV-VIS spectra showed aggregate absorption bands only at high concentrations $c \gg c_M$. The absorption at $\lambda_{max} = 420$

nm indicates H-type and the small shoulder around 480 nm J-type arrangements of the monomers in the aggregates, **Fig. 4**. In order to assure that the absorption at 420 nm is not due to concentration effects, high concentrated crocin solutions in methanol (100mg/ml) were measured. These spectra did not show absorption shifts as observed in water, they were identical to the monomer spectra of crocin recorded at lower concentration. The detection of aggregates only after reaching the surface saturation concentration Γ and the critical micelle concentration c_M indicate that, for crocin, surface population and aggregation are consecutive processes. In contrast, carotenophospholipid molecules aggregate already at a very low concentration $c \leq 5 \times 10^{-9}$ M, [25] and aggregation and surface filling are thus immediate and parallel actions. Likewise, the anionic carotenoid bolaamphiphile (CardaxTM) aggregated and filled the surface simultaneously.[26] The different behavior of crocin, compared with the two other carotenoid surfactants, is reflected by the equilibrium constants, **Table 1**. Crocin molecules aggregate less easily than carotenophospholipid and CardaxTM molecules. Crocin molecules leave also more easily the aggregates than do molecules from aggregates of the two other surfactants, **Fig. 3**.

The intensity- and number weighted-distribution function from DLS for crocin plotted versus the equivalent hydrodynamic radius, r_H , is presented in **Fig. 5**. For $c = 0.6$ mg/ml crocin ($c < c_M$) most monomers of number-averaged $r_H = 0.7$ nm are present. Some few big aggregates in the range $r_H = 6$ -200 nm were also detected. For $c = 2.0$ mg/ml crocin ($c > c_M$) most aggregates of number-averaged $r_H = 1.6$ nm are present, again accompanied with an insignificant amount of big aggregates in the range $r_H = 6$ -200 nm.

Crocin monomers cannot appear as spheres: a prolate ellipsoid with semi axes $a = 1.7$ nm and $b = 0.4$ nm is an appropriate model for the crocin monomer, **Fig. 6**. Such an ellipsoid has an equivalent hydrodynamic radius of $r_H = 0.8$ nm (equation from Ref. [44]), which is in agreement with the measured value from DLS. The volume of the crocin ellipsoid $V_e = 1140 \text{ \AA}^3$ is in accordance with the volume obtained from molecular calculations $V_m = 924 \text{ \AA}^3$, taking into account the possibility of a hydrated sphere around the molecule (11 water molecules if $V_{H_2O} = 19 \text{ \AA}^3$) The size of the aggregates suggests monomer associations to a hexamere, forming an oblate ellipsoid with $r_H \approx 15 \text{ \AA}$, or a spherical octamere with $r_H \approx 17 \text{ \AA}$. [45] A significant amount of aggregates with a size indicating vesicle morphology and, consecutively, with high aggregation numbers, were not detected.

Conclusion

The natural, highly unsaturated, conjugated, surface active bolaamphiphile crocin (**1**) dissolves easily in water to monomer solutions. At higher concentrations the monomers associate to small, nanometer sized aggregates with a low aggregation number. At the water surface, crocin is absorbed with an oblique or erected orientation. Adsorption and aggregation behavior is at variance with typical bolaamphiphile properties.

Acknowledgement

S. Nalum Næss thanks the Norwegian Research Council for a PhD-grant.

Experimental

Crocin was purchased from Fluka (Fluka standard degree, Fluka AG, Buchs, Switzerland), and purified on a neutral alumina column eluted first with methanol/water/acetonitril 7:2:1 and then with pure water.

Surface tension γ and critical aggregate concentration c_M were determined with a Wilhelmy plate tensiometer (Krüss K10 T-digital tensiometer). A stock solution of **1** was prepared with distilled, filtered (0.22 μm) water by stirring overnight. The stock solution was then diluted with distilled, filtered water to the solution with the required concentrations for the measurements. The values were recorded immediately after the initial equilibrium was obtained.

Optical rotation were measured in water with a Perkin-Elmer 243B polarimeter in a 10 cm cell. $[\alpha]_{589}^{25} = -53$ ($c=0.38\text{mg/ml H}_2\text{O}$) $< c_M = 0.88\text{ mg/ml}$, $[\alpha]_{589}^{25} = -55$ ($c=1.1\text{g/ml H}_2\text{O} > c_M$). $[\alpha]_{589}^{25}$ -values at $c=2.2\text{ mg/ml}$ were not reproducible. Reference 41 reports $[\alpha]_{644}^{21} = -1760^\circ$ ($c = 1.06\text{ mg/ml H}_2\text{O} < c_M$).

UV-VIS spectra of the highly concentrated crocin solutions in water and MeOH (100 mg/ml) were recorded in a quartz cell with $d = 0.1\text{ cm}$ and as films between quartz plates, path lengths 0.08 to 0.2 mm.

Determination of particle size by Dynamic Light Scattering (DLS)

DLS measurements were performed using an ALV DLS/SLS-5022F compact goniometer system and an ALV-5000/E multiple τ -digital correlator (ALV, Langen, Germany). The light source was a 22 mW He-Ne laser (Uniphase, Witney Oxon, U.K.). Crocin was carefully filtered with 0.22 μm filters. The temperature of the sample was 21 $^\circ\text{C}$ and the scattering angle was 90 $^\circ$. Data analysis was performed using the CONTIN method available in the ALV software package.[46swp] In order to obtain reliable vesicle size distributions, long data acquisition times were required. This was achieved by averaging data from several runs. The measuring time was at least 30 minutes.

Calculation of thermodynamic data

Surface pressure (change of tension caused by the substrate) $\pi = \gamma^\circ - \gamma_{c_M}$, $\gamma^\circ = 73\text{ mN m}^{-1}$ (H_2O).

Surface concentration $\Gamma = \frac{-1}{RT} \left(\frac{d\gamma}{d \ln c} \right)_{c_M} = \frac{-1}{RT} \left(c \frac{d\gamma}{dc} \right)_{c_M}$ [m mol^{-2}]. When γ is

measured in $\text{mN m}^{-1} = \text{J m}^{-2}$, R in $\text{J mol}^{-1} \text{K}^{-1}$, and T in K (in our case 294 K), Γ comes out in mol m^{-2} . For determining Γ the surface tension data were fitted with the Szyszkowsky equation[30bvs] $\gamma = \gamma^\circ - a \log(1 + bc)$, we found

$$c_M = (0.9 \pm 0.1) \times 10^{-4} \text{ mM.}$$

Area per molecule in a filled monolayer $a_m = 10^{20} \Gamma^{-1} N_A^{-1}$ [\AA^2], where N_A is the Avogadro constant.

Free energy of micellation (energy change for a molecule from the monomer to the micelle state) $\Delta G_{mic}^\circ = RT \ln c_M$ [J mol^{-1}].

Free energy of adsorption (energy change of a molecule in the bulk and at the surface) $\Delta G_{ad}^{\circ} = \Delta G_{mic}^{\circ} - 6.023 \times 10^{-3} \pi a_m$ [J mol⁻¹].

Equilibrium constants

aggregated molecules/monomer bulk $K_{mic} = \exp(-\Delta G_{mic}^{\circ}/RT)$,

molecules at surface/monomer bulk $K_{ad} = \exp(-\Delta G_{ad}^{\circ}/RT)$,

molecules at surface/aggregated molecules $K_{ad-mic} = \exp(-\Delta G_{ad-mic}^{\circ}/RT)$.

References

1. *Carotenoid Handbook*, Eds. G. Britton, S. Liaaen-Jensen, H. Pfander, A.Z. Mercadante, E.S. Egeland, Birkhäuser, Basel **2004**.
2. S. Liaaen-Jensen. in *Carotenoids, Vol 2*, Eds. G. Britton, S. Liaaen-Jensen, H. Pfander, Birkhäuser, Basel **1996**, p 295-300.
3. Norbixin solutions over 5% can be achieved, colorMaker, Anaheim, California.
4. Merck Index, 13th Edition, Eds. P. Heckelman, A. Smith, M.J. Oneil, Merck Publishing Group, **2001**, p. 2617.
5. H. von Euler, H. Hellström, E. Klussmann. *Ark. Mineral. Geol.* **1931**, *10B*, 1-4.
6. P. Karrer, W. Straub. *Helv. Chim. Acta* **1938**, *21*, 1624-1636.
7. K. Shibata. *Biochem. Biophys. Acta* **1956**, *22*, 398-399.
8. H. Kläui. Hofmann-La Roche, Nutley, US 3206316, **1965**.
9. E. Lüddecke, A. Auweter, L. Schweikert. BASF, Ludwigshafen EP 930022, **1998**.
10. D. Horn, J. Rieger. *Angew. Chem. Int. Edit.* **2001**, *40*, 4331-4361.
11. P. Karrer, H. Salomon. *Helv. Chim. Acta* **1928**, *11*, 513-525.
12. R. Oberdieck. *Deutsche Lebensmittel Rundschau* **1991**, *87*, 246-252.
13. The World production of saffron in 2003 was around 200 t, corresponding to about 50 t crocin if occurring at 25% in saffron, Ref. 12. (Vanilla, Saffron Imports 949 Valencia St., San Francisco, CA. 94110, **2001**, retrieved from company's homepage 10.5.04, http://saffron.com/cons_guide.html).
14. M. Tsimidou, E. Tsatsaroni. *J. Food Science* **1993**, *58*, 1073-1075.
15. C. Stubenrauch. *Curr. Opin. Coll. Interface Sci.* **2001**, *6*, 160-170.
16. T.Q. Pham, F. Cornier, E. Farnworth, V.H. Tong, M.-R. Van Calsteren. *J. Agric. Food Chem.* **2000**, *48*, 1455-1461.
17. M. Erben-Russ, C. Michel, W. Bors, M. Saran. *J. Phys. Chem.* **1987**, *91*, 2362-2465.
18. I.B.C. Matheson, M.A.J. Rodgers. *Photochem. Photobiol.* **1982**, *36*, 1-4.
19. G. Speranza, P. Manitto, D. Monti. *J. Photochem. Photobiol. B: Biol.* **1990**, *8*, 51-56.
20. F.I. Adullaev. *Exp. Biol. Med.* **2002**, *227*, 20-25.

21. J.L. Gainer, University of Virginia, US4176179, **1997**.
22. K. Abe, H. Saito. *Phytotherapy Res.* **2000**, *14*, 149-152.
23. T. Konoshima, M. Takasaki, H. Tokuda, S. Morimoto, H. Tanaka, E. Kawata, L.J. Xuan, H. Saito, M. Sugiura, J. Molnar, Y. Shoyama. *Phytotherapy Res.* **1998**, *12*, 400-404.
24. B.J. Foss, S. Nalum Næss, H.R. Sliwka, V. Partali. *Angew. Chem. Int. Ed.* **2003**, *42*, 5237-5240.
25. B.J. Foss, H.R. Sliwka, V. Partali, S. Nalum Næss, A. Elgsæter, T.B. Melø, K. Razi Naqvi. *Chem. Phys. Lipids* **2004**, *xx*, xx-xx.
26. B.J. Foss, H.R. Sliwka, V. Partali, S. Nalum Næss, A. Elgsæter, T.B. Melø, K. Razi Naqvi, S. O'Malley, S.F. Lockwood. *Langmuir* **2004**, *xx*, xx-xx.
27. A.J. Cardounel, C. Dumitrescu, J.L. Zweier, S.F. Lockwood. *Biochem. Biophys. Res. Commun.* **2003**, *307*, 704-712.
28. B.J. Foss, H.R. Sliwka, V. Partali, A.J. Cardounel, S.F. Lockwood. *Bioorg. Med. Chem. Letters* **2004**, *14*, 2807-2812.
29. F. Zsila, M. Simonyi, S. F. Lockwood. *Bioorg. Med. Chem. Letters* **2003**, *13*, 4093-4100.
30. S.F. Lockwood, S. O'Malley, D.G. Watumull, L.A. Hix, H. Jackson, G. Nadolski, WO **2004/011423**. Hawaii Biotech Inc.
31. G.J. Gross, S.F. Lockwood. *Life Sciences* **2004**, *75*, 215-224.
32. L. A. Showalter, S. A. Weinman, M. Østerlie, S.F. Lockwood. *Comp. Biochem. Physiol. C* **2004**, *137*, 227-236.
33. L.M. Hix, S.F. Lockwood, J.S. Bertram. *Cancer Lett.* **2004**, *211*, 25-37.
34. H.L. Jackson, A.J. Cardounel, J. L. Zweier, S.F. Lockwood. *Bioorg. Med. Chem. Letters* **2004**, *14*, 3985-3991.
35. M. Mulqueen, P.D.T. Huibers. In *Handbook of Applied Surface and Colloid Chemistry* Vol. 2, Eds: K. Holmberg, D.O. Shah, MJ. Schwuger, Wiley, Chichester **2002**, chpt. 12.
36. B. von Szyszkowki. *Z. phys. Chem.* **1908**, *64*, 385-414.
37. L.D. Skrylev, E.A. Streltsova, T.L. Skryleva. *Russian J. Appl. Chem.* **2000**, *73*, 1364-1367.

38. B.J.Boyd, C.J. Drummond, I. Krodkiewska, F. Grieser. *Langmuir* **2000**, *16*, 7359-7367.
39. I Söderberg, C.J. Drummond, D.N. Furlong, S. Godkin, B. Matthews. *Colloids Surfactants A*, **1995**, *102*, 91-97.
40. D.K. Allen, B.Y. Tao. *J. Surfactants, Detergents* **2002**, *5*, 245-255.
41. T. Kawaguchi, H. Hamanaka, Y. Kito. *J. Phys. Chem.* **1991**, *95*, 3837-3846.
42. G. Garofalakis, B.S. Murray, S.B. Sarney. *J. Coll. Interface Sci.* **2000**, *229*, 391-398.
43. R. Kuhn, Y. Wang. *Chem. Ber.* **1939**, *72B*, 871-878.
44. J. Pencer and F. R Hallett. *Langmuir* **2003**, *19*, 7488-7497.
45. C.R. Cantor and P.R. Schimmel, *Biophysical chemistry. Part II: Techniques for the study of biological structure and function.* W.H. Freeman, San Francisco **1980**.
46. S.W. Provencher, CONTIN version 2, Users manual, EMBL-technical report DA07, Max-Planck Institut Biophysikalische Chemie, Göttingen **1984**.
47. U.R.M. Kjellin, J. Reimer, P. Hansson. *J. Colloid Interface Sci.* **2003**, *262*, 506-515.

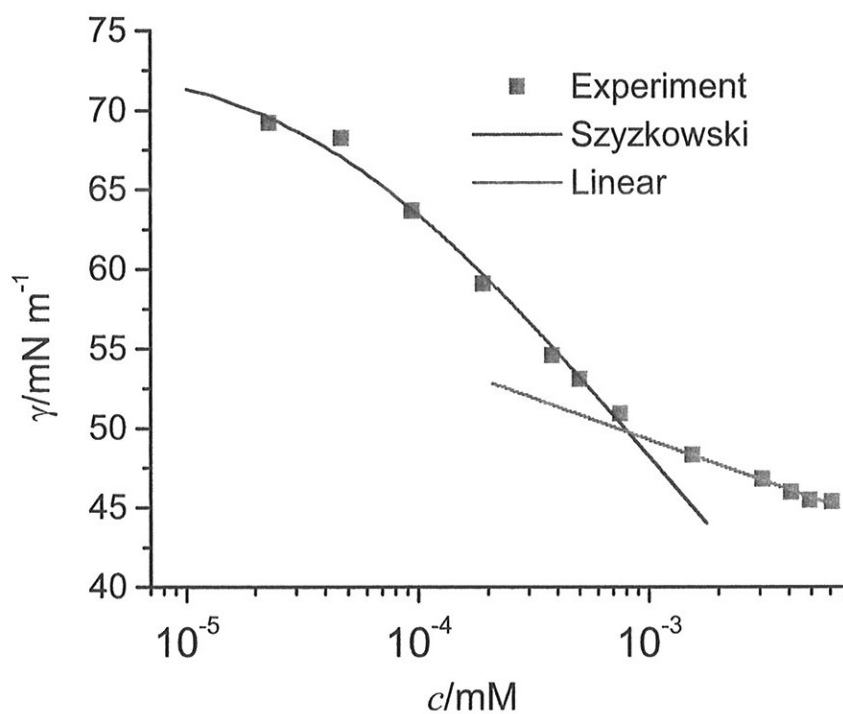


Fig. 1

Critical micelle concentration (c_M) of crocin by measuring surface tension. The solid curve is derived by fitting the data below 1 mM to the Szyszkowski equation with $\gamma^\circ = 73 \text{ mN m}^{-1}$, $a = 17.4 \text{ mN m}^{-1}$ and $b = 2.5 \times 10^{-4} \text{ L m}^{-1}$. The intersection of the lines determines $c_M = (0.9 \pm 0.1) \times 10^{-3}$ at $\gamma = 50 \text{ mN m}^{-1}$.

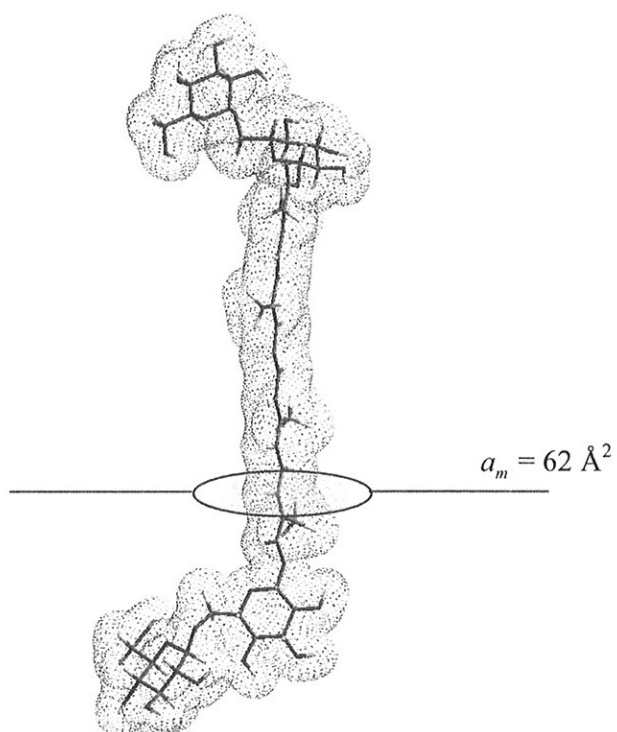


Fig. 2

Hypothetical orientation of crocin (**1**) at the water surface supposing part of the polyene chain participating in the hydrophilic group. [25lyso] The boundary or the interface is arbitrarily placed at C10.

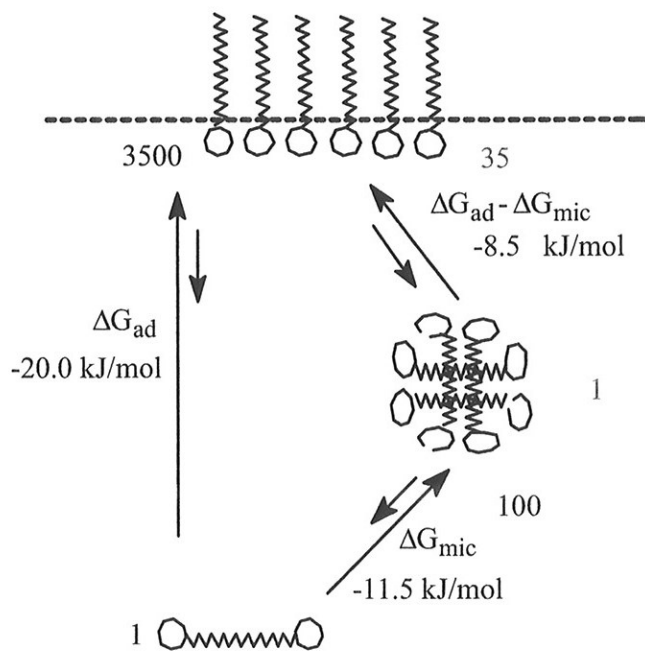


Fig. 3

Adsorption and micellation energy ΔG_{ad}° , ΔG_{mic}° , and equilibrium constants K of crocin (**1**) for surface monolayer and aggregate formation.

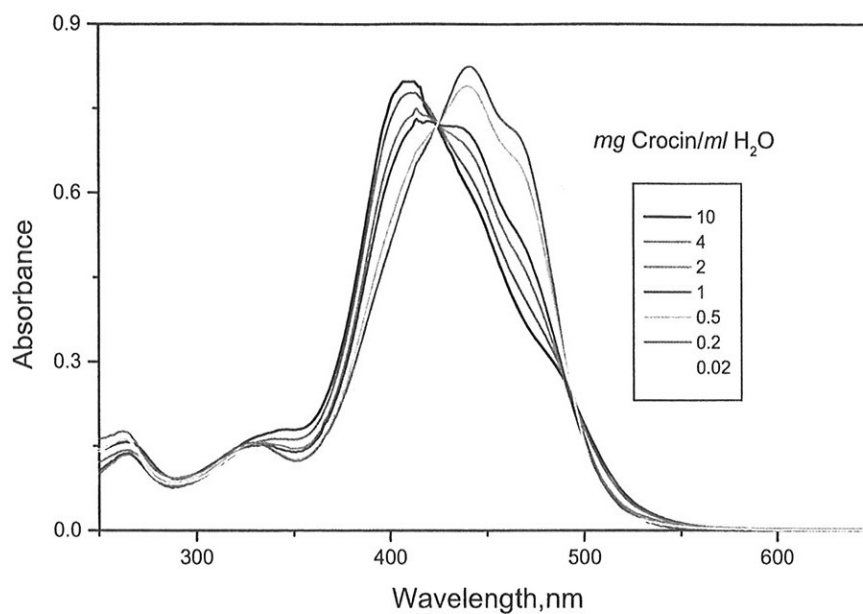


Fig. 4

UV-VIS spectra of crocin monomers (low concentration of crocin in water) and crocin aggregates (high concentration of crocin in water). The spectra of high concentrated crocin solutions in MeOH correspond to the water spectrum at low concentrations. The highly colored solutions were measured with path lengths between 0.08 to 0.2 mm.

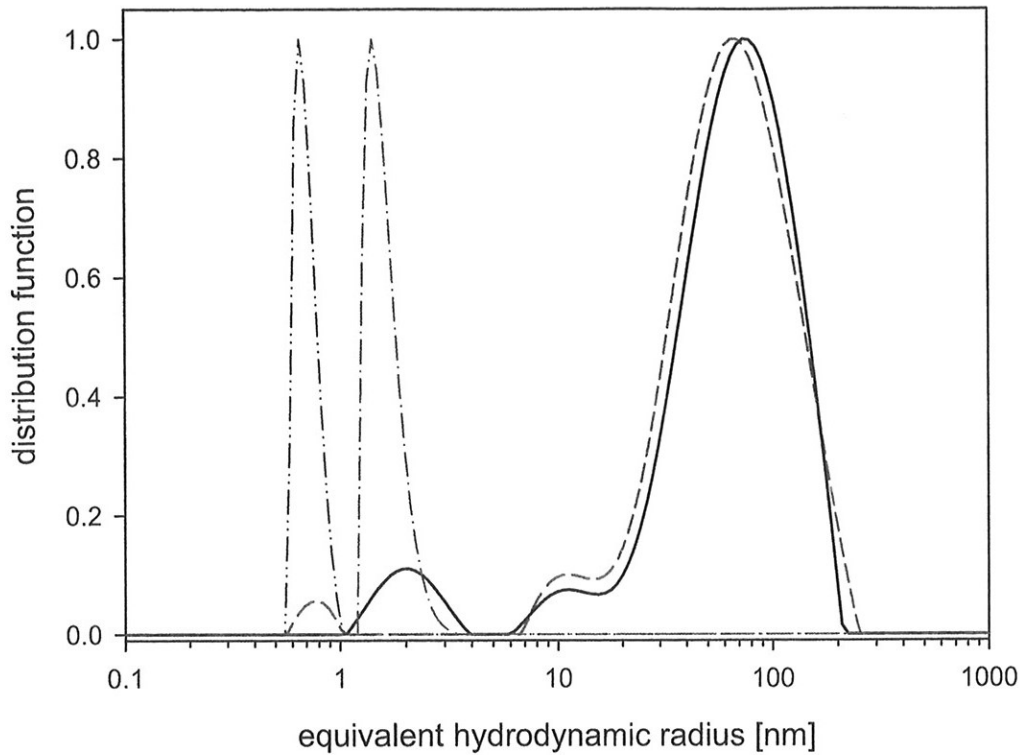


Fig. 5

Typical intensity-weighted distribution function for 0.6 mg/ml (short dashed line) and 2.0 mg/ml crocin (solid line) plotted versus the equivalent hydrodynamic radius. Typical number-weighted distribution function for 0.6 mg/ml (dash-dot-dot line) and 2.0 mg/ml crocin (dash-dot line) plotted versus the equivalent hydrodynamic radius. For 0.6 mg/ml crocin ($c < c_M$) mostly monomers of $r_H = 0.7$ nm occur, besides small amounts of aggregates in the range $r_H = 6-200$ nm. For 2.0 mg/ml crocin ($c > c_M$) small aggregates of $r_H = 2.1$ nm dominated, again accompanied with small amounts of larger aggregates in the range $r_H = 6-200$ nm.

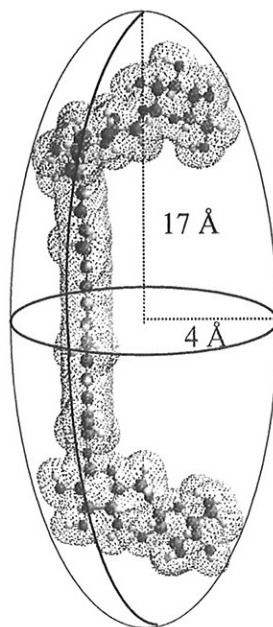
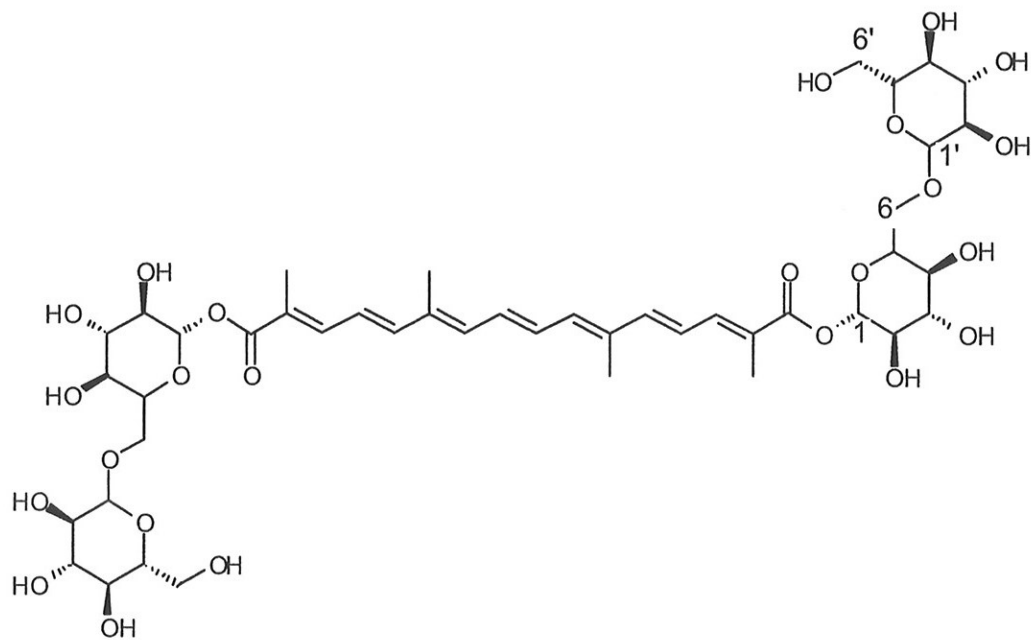


Fig. 6

A prolate ellipsoid with semi axes $a = 1.7$ nm and $b = 0.4$ nm is an appropriate model for crocetin monomers. Such an ellipsoid has $r_H = 0.8$ nm, in agreement with the measured value from DLS.



1

Bis(β -gentobiosyl)-8,8'-diapocarotenoate

Scheme 1

surfactant	γ_{cmc} mN/m	π_{cmc} mN/m	cmc M 10^{-3}	Γ 10^{-6} mol/m ²	a_m Å ²	ΔG_{mic}° kJ/mol	ΔG_{ad}° kJ/mol	$\Delta G_{mic}^{\circ} - \Delta G_{ad}^{\circ}$ kJ/mol	k_{mic}	k_{ad}	k_{ad-mic}	AMER $\Delta G_{ad}^{\circ} / \Delta G_{mic}^{\circ}$
crocin	50	23	0.9 ± 0.1	2.7 ± 0.1	62 ± 2	-11.5 ± 0.3	-20.0 ± 0.6	-8.5	100	3500	35	1.7
Cardax ^{TM a}	60	13	0.45 ± 0.05	0.7 ± 0.1	240 ± 30	-54.8 ± 0.8	-73.6 ± 3.2	-18.8	1800	23000	13	1.3
C30-lysophospholipid ^b	57	16	1.30 ± 0.2	4.5 ± 1	39 ± 9	-16.2 ± 0.4	-20.1 ± 1.4	-3.9	750	3500	5	1.2
sucrose-6-C12:0 ^c	37.4	35.6 ^d	0.455		56	-18.8 ^d	-30.8 ^d	-12.0 ^d	2200 ^d	300000 ^d	136 ^d	1.6 ^d
Maltose-6-C12:0 ^e	39.0	34.0 ^d	0.33	3.3	50	-19.6 ^d	-29.8	-10.2 ^d	3000 ^d	197000 ^d	65 ^d	1.5 ^d
maltose-β-C8:0 ^f	33.4	39.6 ^d	19.1		42	-9.7 ^d	-19.8	-10.0 ^d	55 ^d	3200 ^d	60 ^d	2.0 ^d

a) Ref. 25cardax, b) 24lysoCEJ, c) 37is, d) calculated from reported data, e) 47urmk, f) 36bjb

Table 1 Thermodynamical data for crocin (1) and related compounds.

Article 6

B. J. Foss, H.-R. Sliwka, V. Partali, A. J. Cardounel and S. F. Lockwood

Direct superoxide anion scavenging by a highly water dispersible carotenoid phospholipid evaluated by electron paramagnetic resonance (EPR) spectroscopy

Bioorg. Med. Chem. Lett. **2004**, *14*, 2807-2812.



Direct superoxide anion scavenging by a highly water-dispersible carotenoid phospholipid evaluated by electron paramagnetic resonance (EPR) spectroscopy

Bente Jeanette Foss,^a Hans-Richard Sliwka,^a Vassilia Partali,^a Arturo J. Cardounel,^b Jay L. Zweier^b and Samuel F. Lockwood^{c,*}

^a*Institutt for Kjemi, Norges Teknisk Naturvitenskapelige Universitet (NTNU), N-7491 Trondheim, Norway*

^b*Davis Heart & Lung Research Institute, 473 West 12th Avenue, Columbus, OH 43210-1252, USA*

^c*Hawaii Biotech, Inc., 99-193 Aiea Heights Drive, Suite 200, Aiea, HI 96701, USA*

Received 2 February 2004; revised 10 March 2004; accepted 19 March 2004

Abstract—Synthetic carotenoid analogs, with increased utility for biological applications, are sparingly reported in the literature. Synthetic modification, which may increase the water solubility and/or water dispersibility of lipophilic carotenoids, allows their use in aqueous environments as potent antioxidants against potentially deleterious reactive oxygen species (ROS) that can be generated in vivo. Superoxide anion, produced by activated human neutrophils, can be a source of additional harmful ROS and nonradical species such as singlet oxygen in vivo. In the current study, direct scavenging of superoxide anion by a well-characterized C30 carotenoid phospholipid mixture was evaluated in a standard in vitro isolated human neutrophil assay by electron paramagnetic resonance (EPR) spectroscopy, employing the spin-trap DEPMPO. The carotenoid phospholipid was tested in aqueous formulation (aqueous dispersibility >60 mg/mL), in which supramolecular assembly takes place, as well as in ethanolic formulation as a monomeric solution of the carotenoid phospholipids. The carotenoid phospholipid (a highly unsaturated zwitterionic surfactant) was compared with a previously characterized rigid, long-chain, highly unsaturated dianionic bolaamphiphile, which contains an additional three conjugated double bonds in its extended conjugated system. As previously reported, direct scavenging by the carotenoid phospholipid derivatives in monomeric ethanolic formulation was superior at each tested concentration to aqueous, aggregated formulations of the compounds. Additionally, the percent inhibition of superoxide signal was related to the apparent or effective length of the conjugated chromophore, consistent with previous reports of radical inhibition and singlet oxygen quenching by polyene carotenoids of differing length.

© 2004 Elsevier Ltd. All rights reserved.

1. Introduction

The conjugated double bond structure of the polyene chain of carotenoids is responsible for the characteristic color of the chromophore for particular carotenoids. Antioxidant capacity is related to effective or apparent polyene chain length, and to the number of conjugated double bonds.¹ As scavengers of oxygen radicals, carotenoids are particularly potent. The reaction kinetics depend not only on the individual carotenoid, but also

on the nature of the model used (solvent system), and the radical species involved.^{2,3} As nearly all of the 700 natural carotenoids are lipophilic,⁴ diverse strategies must be utilized to increase the water solubility of these compounds for introduction into aqueous test systems.^{5,6} Synthetic carotenoids with increased water solubility and/or water dispersibility have been sparingly reported in the literature.^{7,8} Supramolecular assembly in aqueous solution—which protects the individual molecules in the aggregated state from oxidation—limits scavenging of radical and nonradical species generated in or released into solution.^{7,9,10} Therefore, comparisons of the scavenging ability of these compounds must take into consideration the behavior of the individual molecules while in aqueous solution.

In the current study, electron paramagnetic resonance (EPR) spectroscopy was used to characterize the ability

Keywords: Carotenoid phospholipids; Zwitterionic surfactants; Astaxanthin derivatives; Carotenoid esters; Electron paramagnetic resonance; EPR; EPR spectroscopy; Spin traps; DEPMPO; Supramolecular assembly; Superoxide anion; Scavengers.

* Corresponding author. Tel.: +1-808-2209168; fax: +1-808-4877341; e-mail: slockwood@hibiotech.com

of a well-characterized carotenoid phospholipid mixture [1-(β -apo-8'-carotenoyl)-glycero-3-phosphocholine, 1-(β -apo-8'-carotenoyl)-glycero-2-phosphocholine, and 2-(β -apo-8'-carotenoyl)-glycero-3-phosphocholine in a 49:43:8 ratio (aqueous dispersibility >60 mg/mL; Fig. 1)]¹¹ to directly scavenge superoxide anion produced from maximally-activated isolated human neutrophils. The scavenging ability of this isomeric mixture of zwitterionic surfactant(s) was compared with that obtained both concurrently and previously with a rigid, long-chain, highly unsaturated bolaamphiphile (CardaxTM).⁷ The assay utilized here is a standard *in vitro* test system, in which the production of superoxide anion by stimulated human neutrophils is quantified by EPR in the presence of a spin trap (DEPMPO).⁷ The results corroborate earlier results obtained with synthetic carotenoids, in which the scavenging activity of the carotenoid derivative in aqueous solution is improved by the addition of less polar solvent, thereby disintegrating the aggregates into monomers. Percent inhibition (% inhibition) of superoxide anion signal detected with the DEPMPO spin trap revealed that the effective chromophore length—related to both the number of conjugated double bonds in the compound and λ_{max} —is one important determinant of the ultimate antioxidant potency of a particular carotenoid derivative.

2. Materials

The positional isomers of the carotenoid lysophosphatidylcholines [1-(β -apo-8'-carotenoyl)-glycero-3-phosphocholine, 1-(β -apo-8'-carotenoyl)-glycero-2-phosphocholine, and 2-(β -apo-8'-carotenoyl)-glycero-3-phosphocholine] synthesized for the current study are shown in Figure 1a–c. An isomeric mixture was tested, containing compounds 1a–1c in the ratio 49:43:8. The compounds were >95% pure by HPLC (as AUC). Clear red, evenly-colored aqueous suspensions were obtained

without heat, detergents, or additives after addition of test compound to deionized (DI) water, as described previously.¹¹ Aqueous formulations of the compound mixture were evaluated at four concentrations: 0.5, 1.0, 3.0, and 10.0 mM. As these compounds demonstrate supramolecular assembly in aqueous formulation,¹¹ the compounds were also tested in ethanolic formulation (41.2% final EtOH concentration in stock solution), in which only monomers exist (UV/vis spectroscopic evidence; Fig. 2). The ethanolic formulations tested were 0.1, 0.3, 0.5, 1.0, and 3.0 mM (Table 1).

CardaxTM in 33% ethanol (EtOH) at 0.1 mM (100 μ M), utilized as a reference standard, was tested as previously described.⁷ Briefly, the disodium salt disuccinate derivatives of astaxanthin [statistical mixture of stereoisomers 3*S*,3'*S*, *meso* (3*R*,3'*S*), and 3*R*,3'*R* in a 1:2:1 ratio; Fig. 3] were introduced into the aqueous test system as the monomeric ethanolic solution. CardaxTM was synthesized at >97% purity by HPLC (as AUC). The results of inhibition of superoxide anion signal, as detected by the paramagnetic spin-trap DEPMPO-OOH adduct, are given in Table 1.

Ethanol vehicle negative controls (0.3% final EtOH concentration in isolated neutrophil assay) were also evaluated. Mean percent inhibition of the ethanol-only vehicle was within the coefficient of variation of the scavenging assay (<5%, data not shown).⁷

3. Leukocyte isolation and preparation

Human polymorphonuclear leukocytes (PMNs) were isolated from freshly sampled venous blood of a single volunteer (S.F.L.) by Percoll density gradient centrifugation as described previously.^{7,12} Briefly, each 10 mL of whole blood was mixed with 0.8 mL of 0.1 M EDTA and 25 mL of saline. The diluted blood was then layered over

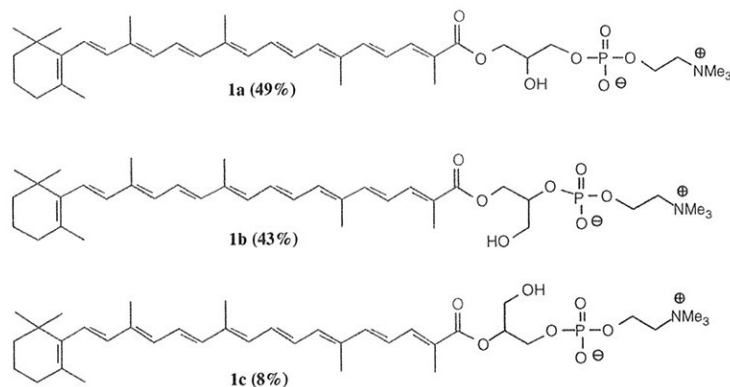


Figure 1. The positional isomers of the carotenoid lysophosphatidylcholines [1-(β -apo-8'-carotenoyl)-glycero-3-phosphocholine (**1a**); 1-(β -apo-8'-carotenoyl)-glycero-2-phosphocholine (**1b**); 2-(β -apo-8'-carotenoyl)-glycero-3-phosphocholine (**1c**)] synthesized for the current study. The compounds were tested as a mixture of the positional isomers in the ratio of compounds 1a–1c of 49:43:8. The compounds were >95% pure by HPLC (as AUC). The isomer mixture was tested in aqueous formulation, in which supramolecular assembly takes place, as well as in ethanolic formulation (41.2% final EtOH concentration in stock solution), which maintains the compounds in monomeric solution.

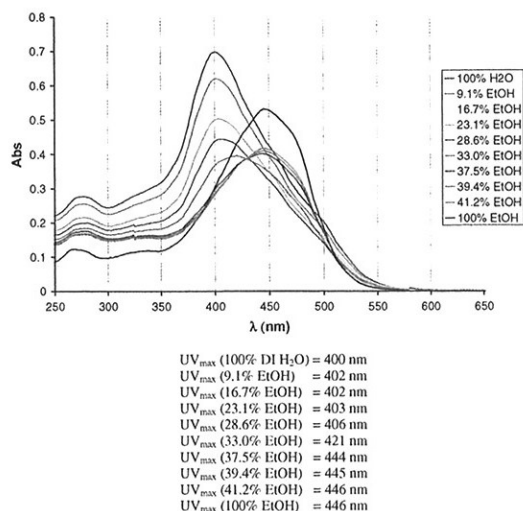


Figure 2. UV/vis absorption spectra of **1a-c** aggregates in water (440 nm) with increasing amounts of EtOH (Fig. 1). The λ_{max} increases to 446 nm at an EtOH concentration of 41.2%, at which point no further shift of the absorption maximum occurs (i.e., a molecular solution is reached). The λ_{max} in EtOH of 446 nm reflects the effective chromophore length of this compound mixture; for comparison, the λ_{max} of CardaxTM in EtOH is 481.5 nm.⁹ Blue-shifting of the absorption maximum in water versus the less polar solvent reflects supra-molecular assembly (aggregation).

9 mL of Percoll at a specific density of 1.080 g/mL. After centrifugation at 400g for 20 min at 20 °C, the plasma,

mononuclear cell, and Percoll layers were removed. Erythrocytes were subsequently lysed by addition of 18 mL of ice-cold water for 30 s, followed by 2 mL of 10× PIPES buffer (25 mM PIPES, 110 mM NaCl, and 5 mM KCl, titrated to pH 7.4 with NaOH). Cells were then pelleted at 4 °C, the supernatant was decanted, and the procedure was repeated. After the second hypotonic cell lysis, cells were washed twice with PAG buffer [PIPES buffer containing 0.003% human serum albumin (HSA) and 0.1% glucose]. Afterward, PMNs were counted by light microscopy on a hemocytometer. The isolation yielded PMNs with a purity of >95%. The final pellet was then suspended in PAG-CM buffer (PAG buffer with 1 mM CaCl₂ and 1 mM MgCl₂).

4. EPR measurements

All EPR measurements were performed using a Bruker ER 300 EPR spectrometer operating at X-band with a TM₁₁₀ cavity as previously described.^{7,13} The microwave frequency was measured with a Model 575 microwave counter (EIP Microwave, Inc., San Jose, CA). To measure superoxide anion (O₂⁻) generation from phorbol-ester (PMA)-stimulated PMNs, EPR spin-trapping studies were performed using the spin-trap DEPMPO (Oxis, Portland, OR) at 10 mM. PMNs (1 × 10⁶) were stimulated with PMA (1 ng/mL) and loaded into capillary tubes for EPR measurements. To determine the radical scavenging ability of CardaxTM in ethanolic formulation at 100 μM as a reference standard, as well as the aqueous and ethanolic formulations of the carotenoid phospholipid mixture, PMNs were

Table 1. Descriptive statistics for mean percent (%) inhibition of aqueous superoxide anion production for increasing concentrations of aqueous and ethanolic (concentration of EtOH in stock solution 41.2%) formulations of the C30 carotenoid phospholipid positional isomer mixture tested in the current study, as well as CardaxTM in 33% ethanol (EtOH) at 0.1 mM (100 μM)

Sample	Solvent	Concentration (mM)	N	Mean % inhibition	SD	SEM	Min	Max	Range
C30 carotenoid phospholipid mixture	Water	0.5	5	18.2	16.1	7.2	1	43	42
C30 carotenoid phospholipid mixture	Water	1.0	4	24.6	20.5	9.2	4	54	50
C30 carotenoid phospholipid mixture	Water	3.0	4	51.8	12.4	6.2	35	63	28
C30 carotenoid phospholipid mixture	Water	10.0	3	94.3	2.1	1.2	92	96	4
C30 carotenoid phospholipid mixture	EtOH	0.1	3	13.3	7.0	4.1	6	20	14
C30 carotenoid phospholipid mixture	EtOH	0.3	3	31.3	1.5	0.9	30	33	3
C30 carotenoid phospholipid mixture	EtOH	0.5	3	61.7	14.0	8.1	46	73	27
C30 carotenoid phospholipid mixture	EtOH	1.0	3	79.3	3.1	1.8	76	82	6
C30 carotenoid phospholipid mixture	EtOH	3.0	3	98.7	0.6	0.3	98	99	1
Cardax TM	EtOH	0.1	3	38.0	8.7	5.0	32	48	16

Sample sizes of 3 or greater were evaluated for each formulation. Dose-dependent increases in superoxide anion scavenging were observed for the C30 isomer mixture in both formulations; the aggregated aqueous formulation was less efficacious, and more highly variable, than the monomeric solution in EtOH. Mean % inhibition of 13.3% by the C30 positional isomer mixture at 0.1 mM (with 10 conjugated double bonds in the chromophore) was less than that observed with CardaxTM (38.0%; 13 conjugated double bonds in the extended conjugated system); the result was statistically significant (unpaired Student's *t*-test, *t* = 3.82, *p* = 0.019).

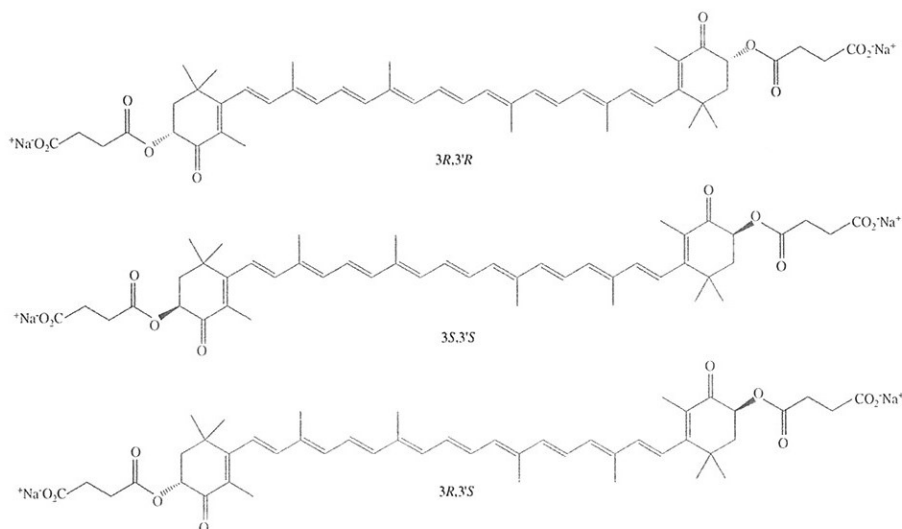


Figure 3. The three stereoisomers comprising the statistical mixture of stereoisomers of the disodium salt disuccinate diester of astaxanthin (Cardax™) synthesized for the current study (shown as the all-*E* geometric isomers). Cardax™ was >97% pure by HPLC (as AUC). The mixture of stereoisomers contains 3*S*,3'*S*, *meso* (3*R*,3'*S*), and 3*R*,3'*R* in a 1:2:1 ratio. Cardax™ was tested in ethanolic formulation (33% EtOH final concentration in stock solution) at 100 μM.

pre-incubated for 5 min with test compound, followed by PMA stimulation.

Instrument settings used in the spin-trapping experiments were as follows: modulation amplitude, 0.32 G; time constant, 0.16 s; scan time, 60 s; modulation frequency, 100 kHz; microwave power, 20 mW; and microwave frequency, 9.76 GHz. The samples were placed in a quartz EPR flat cell, and spectra were recorded. The component signals in the spectra were identified and quantified as reported previously.^{14,15}

5. Statistical analysis

Statistical analyses were performed with the NCSS statistical software package (NCSS 2001 and PASS 2002, Kaysville, UT). All statistical tests were performed at a type I error rate (α) = 0.05.

Figure 4 and Table 1 show the mean relative scavenging abilities, with accompanying EPR spectra, of each of the four aqueous formulations of the positional isomer mixture (concentrations 0.5–10.0 mM). The mean %

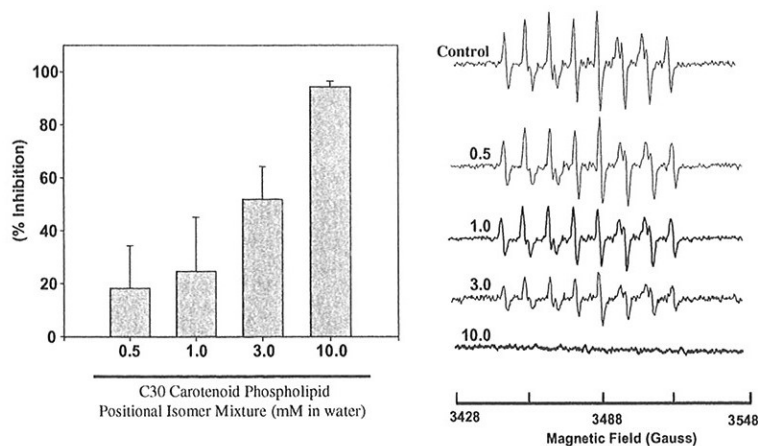


Figure 4. Mean percent inhibition of superoxide anion signal as detected by DEPMPO spin trap by the carotenoid phospholipid isomer mixture 1a–c (49:43:8 ratio; Fig. 1) in aqueous formulation. Each derivative in aqueous formulation was standardized to control EPR signal detected without addition of compound (set at 0% inhibition by convention). Dose-dependent, nonlinear increase in scavenging efficiency is seen. In each case, the aqueous formulation is less efficacious than the corresponding formulation in EtOH (Fig. 5).

inhibition increased in a nonlinear, dose-dependent fashion (from 18.2% to 94.3%); an approximate 20-fold increase in concentration was necessary to effect slightly greater than a 5-fold increase in scavenging efficiency. This phenomenon was reported for the first time for Cardax™ in water, a statistical mixture of stereoisomers that also demonstrates supramolecular assembly in pure aqueous formulation.⁷

Figure 5 and Table 1 show the mean relative scavenging abilities, with accompanying EPR spectra, of each of the five ethanolic formulations of the positional isomer mixture. The scavenging efficiency was nearly linear below 0.5 mM. The concentrations tested increased from 0.1 to 3.0 mM, a 30-fold increase in absolute concentration. The mean % inhibition of superoxide anion signal increased from 13.3% at the lowest concentration tested, to 98.7% (near complete inhibition) at 3.0 mM, the highest concentration evaluated in ethanolic formulation. At each identical concentration (0.5, 1.0, and 3.0 mM), the ethanolic formulation demonstrated increased scavenging ability over the aqueous formulation, a phenomenon described previously.⁷

A comparison of the direct superoxide anion scavenging efficiency between Cardax™ at 100 μM in ethanolic formulation (38.0%) and the positional isomer mixture of the carotenoid phospholipid at 100 μM in ethanolic formulation (13.3%) demonstrates significantly increased scavenging by the C40 carotenoid derivative (Student's unpaired *t*-test, *t* = 3.82, *p* = 0.019), with 13 conjugated double bonds in the extended conjugated system, versus the 10 conjugated double bonds in the carotenoid phospholipid chromophores. The effective chromophore of the astaxanthin derivative can be estimated from the λ_{\max} in ethanol of 481 nm;⁹ similarly, the

effective chromophore of the carotenoid phospholipids by the λ_{\max} in EtOH of 446 nm (Fig. 2).

Carotenoids are typically potent lipophilic antioxidants. They have been traditionally evaluated as antioxidants in model systems operating with organic solvents due to their hydrophobic nature.¹⁶ These compounds normally exert their antioxidant properties in cell membranes, lipoproteins, and the lipid compartments of other tissues *in vivo*.^{1,17} The present study evaluated the utility of a highly water-dispersible, highly unsaturated carotenoid phospholipid mixture—with aqueous dispersibility >60 mg/mL—to directly scavenge aqueous-phase superoxide anion produced by maximally-stimulated isolated human neutrophils. The ability of this zwitterionic carotenoid phospholipid surfactant mixture to scavenge superoxide anion in the aqueous phase *in vitro* was compared with the scavenging ability of the rigid, long-chain, highly unsaturated carotenoid bolaamphiphile Cardax™ (maximum dispersibility 8.64 mg/mL). The characterization of the scavenging ability of Cardax™ in the identical test system, repeated here, has been described previously.⁷

In the current study, dose-dependent increases in mean scavenging ability were identified for both the aqueous and ethanolic formulations of the carotenoid phospholipid mixture (Table 1; Figs. 4 and 5). Nonlinear increases in scavenging ability were seen for both formulations, a phenomenon related to the supramolecular assembly which occurs in aqueous formulation.^{7,9} At concentrations ≤ 0.5 mM in ethanol, the mean scavenging ability of the carotenoid phospholipid mixture was nearly linear, suggesting a stoichiometric relationship between the scavenging ability of the carotenoid phospholipids while in monomeric solution, and the

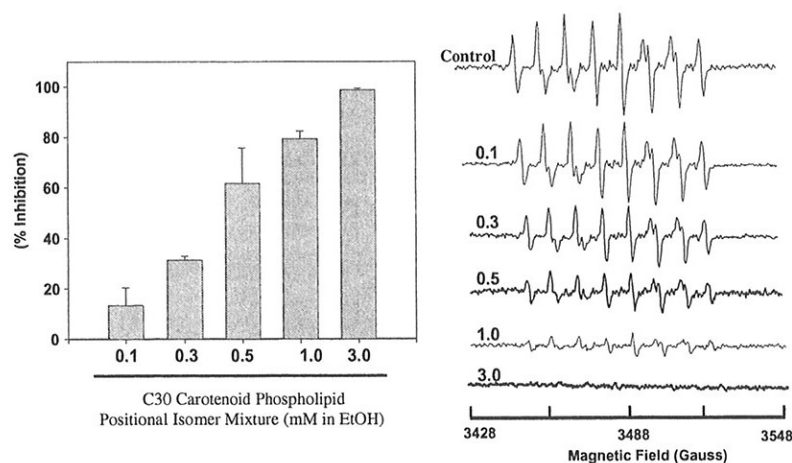


Figure 5. Mean percent inhibition of superoxide anion signal as detected by DEPMPO spin trap by the carotenoid phospholipid isomer mixture 1a–c (49:43:8 ratio; Fig. 1) in ethanolic formulation (final EtOH concentration in isolated neutrophil assay 0.4%). Each derivative in ethanolic formulation was standardized to control EPR signal detected without addition of compound (set at 0% inhibition by convention). Dose-dependent, nearly linear increases in scavenging efficiency are seen at concentrations ≤ 0.5 mM. At 3 mM, near-complete inhibition of superoxide anion signal was observed (98.7% inhibition). At each identical concentration tested, the ethanolic (i.e., monomeric) formulation is more efficacious than the corresponding formulation in deionized (DI) water (Fig. 4).

concentration of superoxide generated after maximal stimulation. The surfactant and aggregation properties of the positional isomers were expected to be virtually identical, as each contains the same polar head group and the same hydrophobic chain (Fig. 1a–c). The isomers in aqueous solution predominately form aggregates with an average hydrodynamic radius $r_H = 8$ nm; a few larger aggregates of sizes between $r_H = 40$ –600 nm have also been detected by dynamic light scattering (DLS).¹¹ As has been suggested for CardaxTM, aggregation in solution is dependent upon both the concentration of the target compound, and the ionic strength of the diluent (Foss et al., unpublished results). This may form one explanation for the loss of linearity at higher concentrations in ethanolic solution, after introduction into the buffered test assay.

Comparison of the mean scavenging efficiency of the positional isomer mixture in ethanol at 100 μ M (13.3%) with the mean scavenging efficiency of CardaxTM in EtOH at 100 μ M (38.0%) could reflect the contributions of the effective chromophores of each of these compounds to the overall antioxidant potential. As has been demonstrated previously for lycopene (λ_{max} in acetone 505 nm)¹⁸ and nonesterified, free astaxanthin (λ_{max} in acetone 480 nm)¹⁹ in model systems with regard to singlet oxygen quenching ability, it is the effective chromophore, and not the absolute number of conjugated double bonds, that determines quenching efficiency.¹⁶ In this case, the number of conjugated double bonds parallels the mean scavenging efficiency (13 vs 10), and is also indicative of the effective chromophore (λ_{max} of the positional isomers in EtOH = 446 nm, Fig. 2; and λ_{max} of CardaxTM in EtOH = 481.5 nm).⁹ The relative decrease in mean scavenging efficiency can be completely compensated for by the absolute differences in water dispersibility between the two compounds (>60 vs 8.64 mg/mL for the carotenoid phospholipids and CardaxTM, respectively).

In summary, the current study corroborates earlier investigations on the utility of novel carotenoid derivatives with increased water dispersibility for aqueous-phase scavenging of biologically relevant reactive oxygen species (ROS). Dose-dependent increases in scavenging of superoxide anion produced by maximally-stimulated human neutrophils were detected by EPR spectroscopy with spin trapping. In every case, monomeric solutions of the test compounds in ethanol were more efficacious than the aggregated aqueous formulations of the test compound at the same concentration. Dose-ranging studies revealed that the concentration of the carotenoid phospholipid mixture could be increased to near-complete suppression of the induced superoxide anion signal. On a molar basis, the carotenoid phospholipids

were slightly less potent direct radical scavengers than the previously evaluated astaxanthin derivative CardaxTM, an observation attributed to the difference in effective chromophore length between the two compound mixtures. This difference may be overcome by increasing the dose of the carotenoid phospholipid mixture in vivo (Lockwood, unpublished results). These compounds may have significant potential as aqueous-phase direct scavengers of ROS and other nonradical species such as singlet oxygen, which can be particularly destructive in biological systems.

References and notes

1. Britton, G. *FASEB J.* **1995**, *9*, 1551–1558.
2. Mortensen, A.; Skibsted, L. H.; Sampson, J.; Rice-Evans, C.; Everett, S. A. *FEBS Lett.* **1997**, *418*, 91–97.
3. Yanishlieva, N. V.; Marinova, E. M.; Raneva, V. G.; Partali, V.; Sliwka, H. R. *J. Am. Oil Chem. Soc.* **2001**, *78*, 641–644.
4. *Carotenoids Handbook*; Britton, G., Liaaen-Jensen, S., Pfander, H., Mercadante, A. Z., Egeland, E. S., Eds.; Birkhäuser: Basel, 2004.
5. Lockwood, S. F.; O'Malley, S.; Mosher, G. L. *J. Pharm. Sci.* **2003**, *92*, 922–926.
6. Horn, D.; Rieger, J. *Angew. Chem., Int. Ed. Engl.* **2001**, *40*, 4330–4361.
7. Cardounel, A. J.; Dumitrescu, C.; Zweier, J. L.; Lockwood, S. F. *Biochem. Biophys. Res. Commun.* **2003**, *307*, 704–712.
8. Blanchard-Desce, M.; Arrhenius, T. S.; Lehn, J. M. *Bull. Soc. Chim. Fr.* **1993**, *130*, 266–272.
9. Zsila, F.; Simonyi, M.; Lockwood, S. F. *Bioorg. Med. Chem. Lett.* **2003**, *13*, 4093–4100.
10. Bikádi, Z.; Zsila, F.; Deli, J.; Mady, G.; Simonyi, M. *Enantiomer* **2002**, *7*, 67–76.
11. Foss, B. J.; Naess, S. N.; Sliwka, H. R.; Partali, V. *Angew. Chem., Int. Ed. Engl.* **2003**, *42*, 5237–5240.
12. Fraticelli, A.; Serrano, C. V., Jr.; Bochner, B. S.; Capogrossi, M. C.; Zweier, J. L. *Biochim. Biophys. Acta* **1996**, *1310*, 251–259.
13. Wang, P.; Zweier, J. L. *J. Biol. Chem.* **1996**, *271*, 29223–29230.
14. Lee, C.; Miura, K.; Liu, X.; Zweier, J. L. *J. Biol. Chem.* **2000**, *275*, 38965–38972.
15. Roubaud, V.; Sankarapandi, S.; Kuppusamy, P.; Tordo, P.; Zweier, J. L. *Anal. Biochem.* **1997**, *247*, 404–411.
16. Miki, W. *Pure Appl. Chem.* **1991**, *63*, 141–146.
17. Iwamoto, T.; Hosoda, K.; Hirano, R.; Kurata, H.; Matsumoto, A.; Miki, W.; Kamiyama, M.; Itakura, H.; Yamamoto, S.; Kondo, K. *J. Atheroscler. Thromb.* **2000**, *7*, 216–222.
18. *Carotenoids: Spectroscopy*; Britton, G., Liaaen-Jensen, S., Pfander, H., Eds.; Birkhäuser: Basel, 1995; Vol. Ib, p 52.
19. *Carotenoids: Spectroscopy*; Britton, G., Liaaen-Jensen, S., Pfander, H., Eds.; Birkhäuser: Basel, 1995; Vol. Ib, p 48.

Article 7

T. B. Melø, K. R. Naqvi, B. J. Foss, S. F. Lockwood, V. Partali and H.-R. Sliwka

Carotenoids as electron donors and triplet energy acceptors in polar solvents: A flash photolysis investigation of crocin and water-soluble carotenoids using 1-nitronaphthalene as a sensitizer

in preparation

Carotenoids as Electron donors and triplet energy acceptors in polar solvents: A Flash Photolysis Investigation of Crocin and water-dispersible carotenoids using 1-nitronaphtalene as a sensitizer

Thor B. Melø^{a*}, K. Razi Naqvi^a, Bente Jeanette Foss^b, Samuel F. Lockwood^c, Vassilia Partali^b and Hans-Richard Sliwka^b.

^aInstitutt for Fysikk, ^bInstitutt for Kjemi, Norges Teknisk Naturvitenskapelige Universitet (NTNU), N-7491 Trondheim, Norway, ^cHawaii Biotech, Inc., 99-193 Aiea Heights Drive, Suite 200, Aiea, Hawaii 96701, USA.

* Correspondence author: thor.melo@phys.ntnu.no

Summary

The antioxidation properties of two newly synthesized micelle forming carotenoids, disodium astaxanthin-3,3'-disuccinate (CardaxTM) and carotenoid lysophosphocholine, and the naturally occurring, water-soluble crocin, have been investigated. 1-nitronaphtalene (NN) was used as a sensitizer in flash photolysis experiments, and the transfer rate of triplet NN energy to the carotenoid is close to being diffusion limited in all cases. The outcome of a collision encounter between NN and the carotenoids may either be energy- or electron transfer, and the ratio of the energy to electron transfer change with solvent polarity, ranging from 4 in acetonitrile to 0.3 water in all cases. In the case of crocin, the decay of triplet sensitizer seems also associated with a growth of product with a peak absorption at 362 nm, probably due to the sugar part of the crocin molecule.

Keywords: carotenoids, surfactants, aggregates, triplet transient state, carotenoid radical cation.

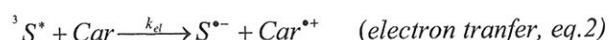
Introduction

Carotenoids are lipid soluble molecules, and one of the most important function of these molecules is their antioxidant activity. It means that carotenoids are electron donors to many biomolecules, which turns them into carotenoid cation radicals. For this vital event to happen in aqueous phase too, the carotenoids must be water soluble. Crocin (Scheme 1) is water soluble, and is composed of a carotenoid part linked to a sugar molecule. A few micelle forming carotenoids have been synthesized, which break up into monomers by adding minute amounts of organic liquids to the water solution.

In addition to being an electron donor, a carotenoid can also act as an acceptor of triplet energy. Hence the carotenoid quenches formation of singlet oxygen, which might happen by photoexcitation of a photosensitizing molecule. The triplet level of a carotenoid molecule is lower than that of the $^1\Delta$ level in O_2 , so singlet oxygen is not formed from a triplet carotenoid. 1-nitronaphthalene (NN) in the triplet state has the special property of, on a collisional encounter with a carotenoid, either to donate the triplet energy to a Car, or to accept an electron from Car. The ratio of the probabilities for energy- or electron transfer is called the bifurcation ratio, which depends upon the polarity of the solvent. By using NN as a sensitizer, both these antioxidation channels of a carotenoid may be investigated in the same experiment. These reactions are written as follows:



and



The outcome of a collision between the sensitizer (NN is hereafter called the sensitizer, abbreviated S) and a Car molecule may be one of the two possibilities listed above, either energy or electron transfer. The ratio of the probabilities for making an energy- or electron-transfer reaction is called the bifurcation ratio, which among other factors, will depend upon the solvent polarity. This special property of NN has been used earlier in similar investigations.

Three different carotenoids will be investigated using NN as a sensitizer in this paper. Firstly, crocin, which is water soluble and exist as monomers in water. Crocin is electrically neutral, while the second molecule to be investigated, disodium astaxanthin-3,3'-disuccinate (CardaxTM) (Scheme 1), is anionic. CardaxTM is synthesized from astaxanthine, by linking a small organic acid to both ends of the carotenoid. In pure water, Cardax form large aggregates, which dissolves into monomers by minute additions of acetonitrile, hereafter denoted MeCN. Thirdly, the zwitterionic carotenoid lysophosphocholine, called PhosCar (Scheme 1), will be investigated as the mixture of its three positional isomers. PhosCar is composed of a carotenoid, which exhibit a highly unsaturated fatty acid part, and a phosphate group, linked together by a glycerol residue. PhosCar forms small aggregates in water, however, in a water/MeCN mixture the aggregates will be broken up into monomers, when the MeCN/water ratio exceeds 0.2.

It has been shown that aggregates of PhosCar and CardaxTM are not acceptors of sensitizer triplet energy. In this paper it is the triplet- and electron-transfer efficiencies of these carotenoids as monomers that will be investigated, in solvents of different dielectric constant.

As one extreme, MeCN with a dielectric constant of 36 is used, as the other extreme water/MeCN =5:1, under which conditions the three carotenoids are monomeric, which has an estimated dielectric constant of 75.

Experiments

In Figure 1 is shown the transient absorption spectra of PhosCar and the sensitizer, NN, in pure MeCN. The triplet minus singlet (TmS) spectrum of NN alone has a peak at 625 nm and is also shown in the Figure. Its absorption band is present in the spectra from the mixture for the smallest delays. The peak at 505 nm is due to the Triplet-Triplet absorption in PhosCar. The triplet level of PhosCar is populated by energy transfer from ${}^3\text{NN}^*$, as described in equation 1 above. The peak at 820 nm is due to Car^{*+} , formed by electron transfer from Car to triplet NN, by which the nitronaphtalene anion is formed, described in eq.2. In the inset of Figure 1 is shown the absorbances at selected wavelengths; 505 nm, which is at the maximum of the ${}^3\text{Car}^*$, at 610 nm, where the ${}^3\text{S}^*$ absorption is dominating, and finally at 820 nm, which is at the peak of Car^{*+} , as a function of the delay between the pump- and the probe pulse. The absorbances of ${}^3\text{S}^*$ and Car^{*+} are multiplied by a factor so that all absorbances are equal for the initial delay. It is seen that ${}^3\text{S}^*$ decay fastest, according to the reactions shown above, and that both ${}^3\text{Car}^*$ and Car^{*+} are produced from ${}^3\text{S}^*$ in a bifurcation reaction. The lifetime of ${}^3\text{S}^*$ is short, only a few μs . In Table 1 is shown the ratio between the transient absorption at 505 and 820 nm for the initial delay, which is an indicator of the bifurcation ratio. In this case, it is clearly shifted towards energy transfer.

In order to determine the bifurcation ratio, the extinction coefficients of the T-T absorption as well as that of the carotenoid cation must be established. In doing so, the transient absorption spectrum, $\Delta A(\lambda, t)$, is a starting point;

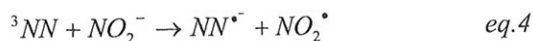
$$\Delta A(\lambda, t) = A(\lambda, t) - A(\lambda) = (\varepsilon_T \cdot c_T + \varepsilon_S \cdot (c - c_T)) \cdot l - \varepsilon_S \cdot c \cdot l = (\varepsilon_T - \varepsilon_S) \cdot c_T \cdot l, \quad \text{eq.3}$$

where $A(\lambda, t)$ and $A(\lambda)$ are the absorbances of the sample at time t after and before the flash, respectively. ε_T and ε_S are the extinction coefficients of the triplet and the ground state molecules. The pump flash causes a certain fraction (α) of the sensitizer molecules (S) to leave the ground state, and hence the concentration of triplets is; $c_T = \alpha \cdot c$. From this one sees that the T-T absorption spectrum is; $\Delta A(\lambda, t) + \alpha A(\lambda)$, where $\alpha A(\lambda)$ is called the ground state depletion. The α factor is found by addition a certain fraction of the ground state- to the transient absorption spectrum so that its ground state character is vanishing. When α is found, the extinction coefficients for the triplet state can be found by comparing the αA spectrum with that of $\Delta A + \alpha A$, since they originate from equal concentrations. Triplet state sensitizer molecules causes, by the reactions introduced above, new species to be formed in the solution. Their contribution to the transient absorption spectrum will have a similar expression as introduced above, containing a contribution due products and the corresponding ground state depletion. From this one sees that the bifurcation ratio is found by measuring the absorbances at the triplet and cation peak, divided by the corresponding extinction coefficients. The ratios of the extinction coefficients and the obtained bifurcation ratios are given below.

Table 1

Car/Solvent	$\epsilon_T/\epsilon_{Car}$	$\epsilon_{Car^{*+}}/\epsilon_{Car}$	Bifurcation ratio
Phos/MeCN	1.5	2.8	7.6 (3.33)
Phos/Aqua	1.2	2.2	0.6 (0.41)
Cardax/MeCN	1.9	2.4	2.7 (2.2)
Cardax/Aqua	1.2	1.5	(0.40)
Crocin in MeCN	1.7		
Crocin/Aqua	2.1	3.0	(0.61)

In Figure 2 is shown similar spectra as those in Figure 1, when S and PhosCar are in water/MeCN solution. In this case, the bifurcation ratio is shifted towards electron transfer, as to expected for a solvent of higher dielectric constant. Again, one sees that the decay of $^3S^*$ is matched by an increase in both $^3Car^*$ and Car^{*+} , however, since the lifetime of $^3Car^*$ is quite small, it is the growth of Car^{*+} that matches the decay of $^3S^*$. The lifetime of $^3S^*$ is slightly longer, about 15 μs , in the mixed solvent, in comparison to MeCN, where it is about 7 μs . According to eq. 2, NN anion radicals are formed in this reaction. In order to establish their identity, NO_2^- was added to NN in solution. It is then expected that NN^{*-} anions are formed from 3NN , according to the reaction;



The spectrum of the NN anion radicals, NN^{*-} , is shown in Figure 2. It has a peak at 380 nm, and the contribution of this spectrum to the transient absorption is larger in this case, as compared to pure MeCN, which is to be expected for a bifurcation ratio shifted in favour of electron transfer.

In Figure 3 is shown the transient absorption spectra for CardaxTM in MeCN. The Cardax triplet peak is broader and peaking at 550 nm, and the cation radical peak is shifted to 850 nm. As for Phoscar in MeCN, the bifurcation ratio is shifted towards energy transfer, and as usual, the lifetime of the Car triplet is quite small, while Car^{*+} is more longlived. In this case the $^3NN^*$ -and the $^3Car^*$ absorption bands are more overlapping in the 550-600 nm region than in the previous case. It can be subtracted from the measured transient absorption so that its contribution is vanishing, seen by the absence of its characteristic peak in the UV region. By doing so, one can plot the absorbances at 550 nm, only due to $^3Car^*$, and at 850 nm, only due to Car^{*+} . In the inset of the Figure is shown the time dependence of these absorbances, as well as that of $^3NN^*$. Again, the same picture emerges, that a collision of $^3NN^*$ and Car either leads to energy-or electron transfer, and in MeCN, energy transfer is favoured. The ratio between the peak heights are in Table 1. Extinction coefficients are determined according to the procedure described above, and the bifurcation ratio was found not very different from that of PhosCar.

The same procedure was used for CardaxTM in $H_2O/MeCN = 5:1$ solution, and the observed spectra are shown in Figure 4. Except for the differences to be expected from that of a longer Car, giving the $^3Car^*$ and the Car^{*+} peaks to be displaced towards longer wavelengths, the results are very similar to that of PhosCar.

In Figure 5 and 6 are given the same spectra for Crocin in MeCN and pure water, as those of PhosCar and Cardax. In order to simplify presentation, the spectra of $^3\text{NN}^*$ have been subtracted. The spectra are quite similar to the two previous compounds, and are essentially a sum of the TmS spectra of $^3\text{Car}^*$ and the Car cation minus its corresponding ground state depletion. Of the three carotenoids under investigation, the length of the carotenoid part of Crocin is shortest, as seen by the most blueshifted $^3\text{Car}^*$ and $\text{Car}^{\bullet+}$ peaks. In MeCN, the bifurcation ratio is strongly shifted towards energy transfer. In the case of Crocin, not seen in the other carotenoids, the decay of the carotenoid radical seems accompanied by the growth in a signal at 380 nm.

Discussion

In aromatic nitrocompounds intersystem crossing from $^1\text{S}^*$ is very large compared to the other competing processes, such as radiative- and nonradiative emission, due to the proximity of $n\pi^*$ and $\pi\pi^*$ states and charge transfer (CT) mediated internal conversion. These interactions not only shortens the fluorescence lifetime considerably, but also the triplet lifetime. However, in nitronaphthalenes the triplet lifetime is considerably longer, particularly in polar solvents where the triplet state is better described as a CT state than a $n\pi^*$ state. In line with this, in our experiments there is no detectable fluorescence from the pump flash. From the triplet state there can either be energy- or electron transfer, which according to Marcus-Hush theory is given by the expression:

$$k_{et} = \frac{2\pi}{\hbar} \cdot \frac{V_{DA}^2}{\sqrt{4\pi\lambda \cdot k_B T}} \cdot \exp\left(-\frac{(\lambda + \Delta G^0)^2}{4\lambda \cdot k_B T}\right)$$

where V_{DA} is the interaction energy between donor and acceptor and λ is the reorganization energy, which according to the Onsager model is:

$$\lambda = \frac{e^2}{4\pi\epsilon_0} \left[\frac{1}{2R_D} + \frac{1}{2R_A} - \frac{1}{R_{DA}} \right] \cdot \left[\frac{\epsilon(0) - 1}{2\epsilon(0) + 1} + \frac{\epsilon(\infty) - 1}{2\epsilon(\infty) + 1} \right]$$

where R is the molecular radii of the donor, acceptor and ions, respectively. ϵ is the dielectric constant of the solvent at static and very high frequencies, respectively. The static dielectric constant vary linearly with the mixing ratio of H_2O to MeCN, which have static dielectric constants of 80 and 38. Under these conditions, the electron transfer rate can be calculated as a function of the mixing rate and compared to actual measurements. When R_D is taken to be 3 Å, $R_A = 4$ Å and $R_{DA} = 5$ Å, the relative changes in k_{et} can be calculated and compared to measurements, shown in Figure 7.

The measurements indicates that the measured rates changes with water content in a biphasic way, first there is a rather steep increase followed by a rather linear change, as to be expected from changes in the overall dielectric constant of the solvent. The initial step increase in electron transfer rate may originate from a change in the reorganization energy, due to a change in the molecular radii.

The rate constant of energy transfer from the sensitizer (S) to the Car seem to be quite similar for the Car under investigation. The concentration of Car is approximately 10^{-5} M^{-1} in all

cases, and when Δt , the lifetime of the sensitizer triplet, is taken to be 10^{-5} s (see the Figures), one gets the rate constant of energy transfer to be:

$$k_{et} = \frac{\Delta[{}^3S^*] / \Delta t}{[{}^3S^*] \cdot [Car]} = \frac{e^{-1}}{[Car] \cdot \Delta t} = 0.37 \cdot 10^{10} M^{-1} s^{-1},$$

which is close to being diffusion limited. The expected rate constant for a diffusion limited reaction is;

$$k_D = 4\pi D \cdot R = 4\pi \cdot \frac{kT}{6\pi r \eta} \cdot R = 0.66 \cdot 10^{10} M^{-1} s^{-1},$$

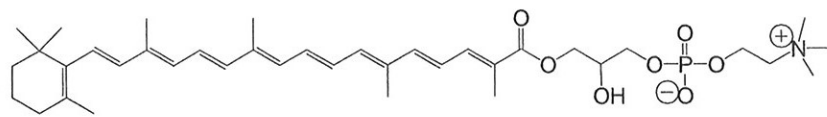
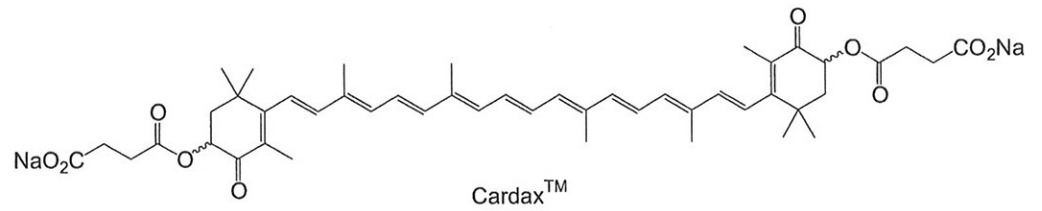
where R is the closest distance between the reaction molecules and D the diffusion coefficient, which is determined by the viscosity of the solvent and the radius of the diffusing particle. In the expression above, η is taken to be the viscosity of water at 25 °C ($1.0 \cdot 10^{-3} \text{ Nsm}^{-2}$) and R, as an estimate, is taken to be 20 Å. The ratio of the viscosity of MeCN to H₂O is 0.6, so the energy transfer rate is expected to be reduced by this factor in MeCN compared to H₂O. However, in all case the lifetime of the ${}^3S^*$ is about 7 μs in MeCN and 15 μs in H₂O, so another factor, the dielectric constant, is more crucial to energy transfer. The longest lifetime of ${}^3S^*$ is seen for Phoscar in H₂O, as to be expected since PhosCar is the largest molecule of the three Car under investigation.

References

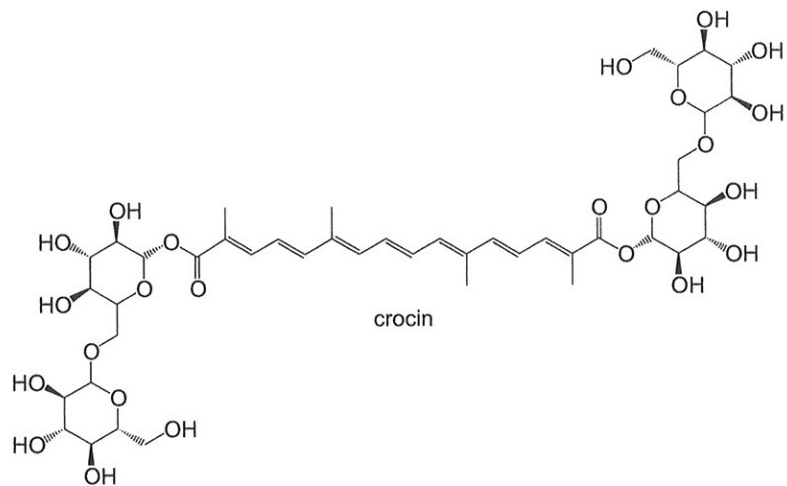
T.Fournier, S. M. Tavender and A. W. Parker. Competitive Energy and Electron-Transfer Reactions of the Triplet State of 1-Nitronaphtalene: A Laser Flash Photolysis and Time-Resolved Resonance Raman Study. *J. Phys. Chem. A* **1997**, *101*, 5320-5326.

J. H. Tinkler, S.M. Tavender, A. W. Parker, D. J. McGarvey, L. Mulroy and T.G. Truscott. Investigation of Carotenoid Radical Cations and Triplet States by Laser Flash Photolysis and Time-Resolved Resonance Raman Spectroscopy: Observation of Competitive Energy and Electron Transfer. *J. Am. Chem. Soc.* **1996**, *118*, 1756-1761.

.....



carotenoid lysophosphocholine (PhosCar)



Scheme 1

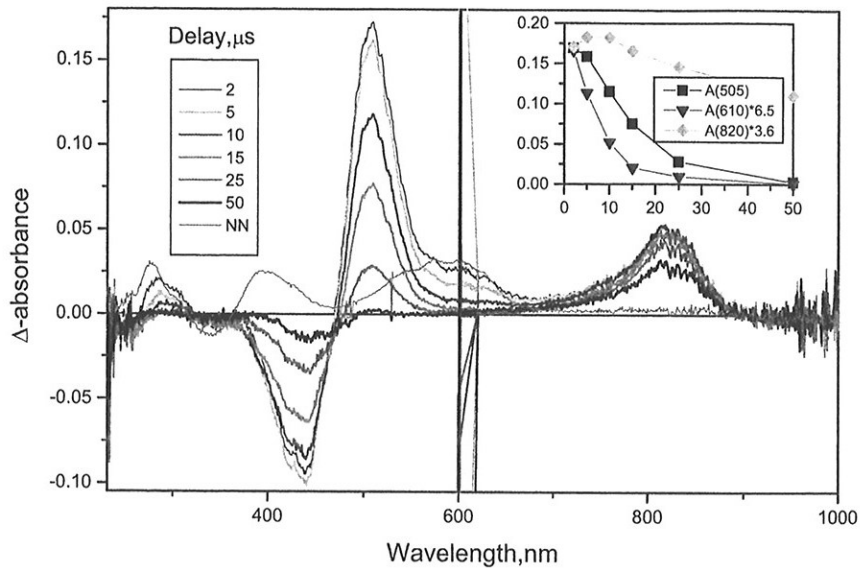


Fig. 1. PhosCar in MeCN.

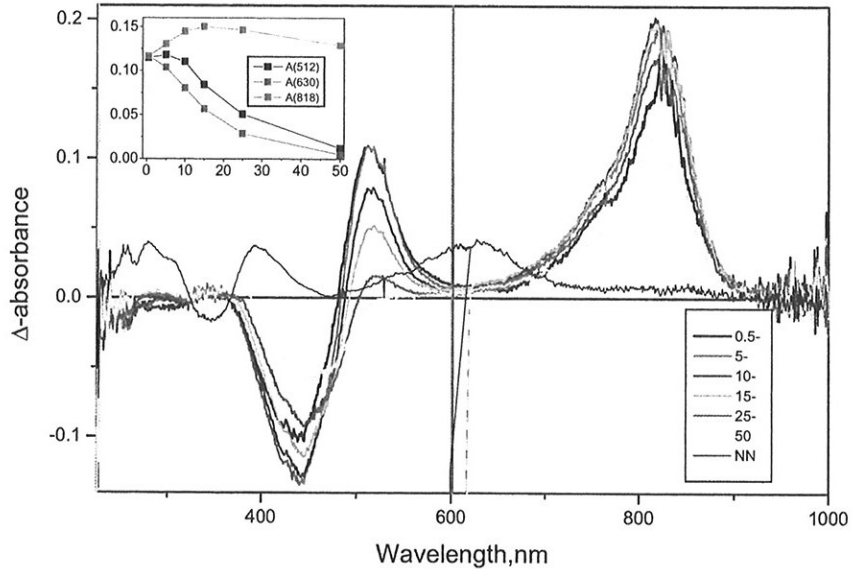


Fig. 2. PhosCar in water/MeCN.

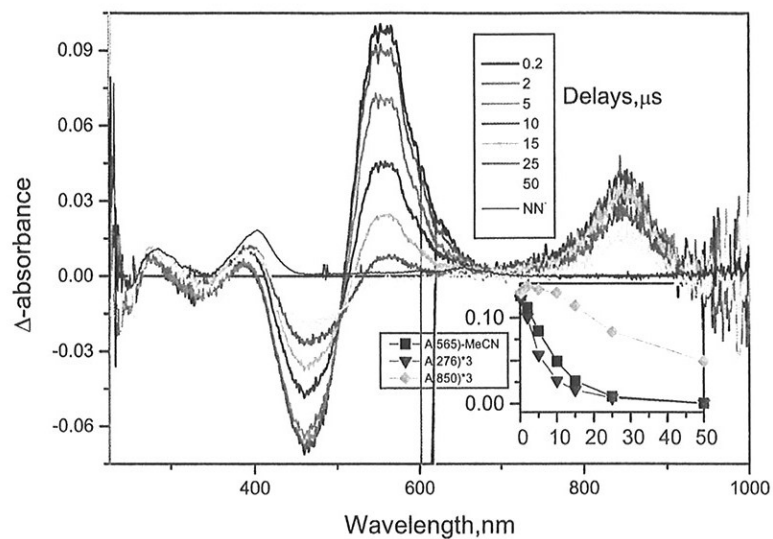


Fig. 3. CardaxTM in MeCN.

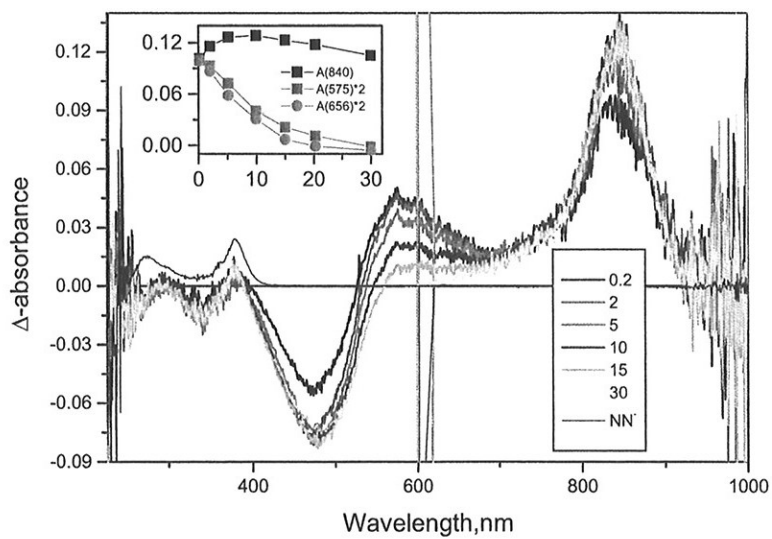


Fig. 4. CardaxTM in water/MeCN.

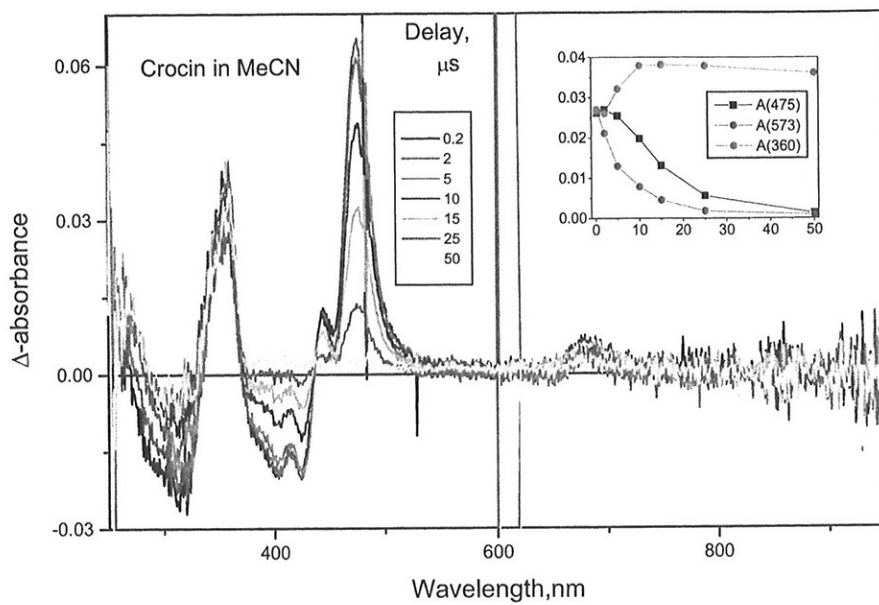


Fig. 5. Crocin in MeCN.

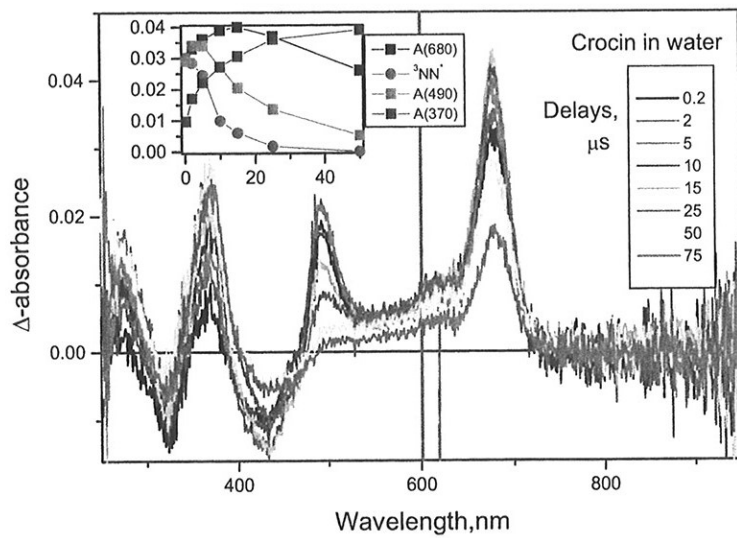


Fig. 6. Crocin in water.

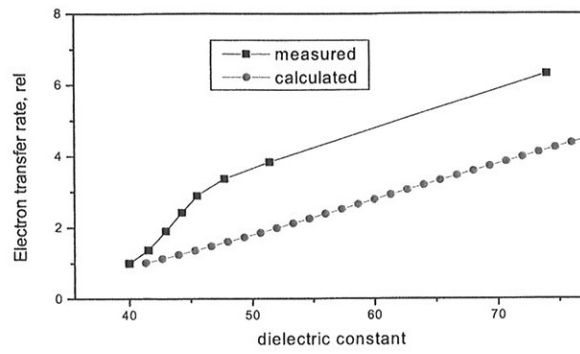


Figure 7.

Article 8

B. J. Foss, A. Ion, V. Partali, H.-R. Sliwka and F. G. Banica

O¹-[6-(Methylselanyl)hexonoyl] glycerol as an anchor for self-assembly of biological compounds at the gold surface

Collect. Czech. Chem. Commun. **2004**, *69*, 1971-1996.

***O*¹-[6-(METHYLSELANYL)HEXANOYL]GLYCEROL AS AN ANCHOR FOR SELF-ASSEMBLY OF BIOLOGICAL COMPOUNDS AT THE GOLD SURFACE**

Bente Jeanette FOSS^{a1}, Ana ION^b, Vassilia PARTALI^{a2}, Hans-Richard SLIWKA^{a3} and Florinel Gabriel BANICA^{a4,*}

^a Department of Chemistry, Norwegian University of Science and Technology (NTNU), 7491 Trondheim, Norway; e-mail: ¹ bente.jeanette.foss@chem.ntnu.no,

² vassilia.partali@chem.ntnu.no, ³ hrs@nvg.ntnu.no, ⁴ f.banica@chem.ntnu.no

^b Department of Analytical Chemistry and Instrumental Analysis, University Politehnica of Bucharest, Romania; e-mail: ana_ion@chim.upb.ro

Received September 8, 2003

Accepted May 7, 2004

Presented at the 36th Heyrovský Discussion on Electrochemistry of Biological Systems and Their Models, Třešť, June 15–19, 2003.

Adsorption of *O*¹-[6-(methylselanyl)hexanoyl]glycerol (SeOG) on the gold surface was investigated by cyclic voltammetry, phase-sensitive AC voltammetry, electrochemical impedance spectroscopy and piezoelectric microgravimetry. SeOG adsorption results in a stable and compact surface layer with the coverage degree close to unity for an adsorption time of 30 to 80 min and 4.6 mM SeOG acetonitrile solution. Such a layer displays minute defects (pinholes) with the radius of ca. 1–3 μm, separated by 6–50 μm intervals (depending on the adsorption time). The adsorbed compound undergoes anodic desorption in the gold oxide region and also undergoes a cathodic process leading to the removal of the surface layer. Both these processes are similar to those demonstrated by short-chain alkanethiols and have been interpreted as a indication for the conversion of the seleno to selenol function as a result of a dissociative adsorption process. Apparently, the main component of the surface layer is *O*¹-(6-selanylhexanoyl)glycerol that results by the cleavage of the C6–Se bond in SeOG. The two free hydroxy groups in SeOG allow to use it as a bridge for binding other compounds to the gold surface. This possibility was illustrated by building up surface layers of a carotenoid derivative (*O*¹-(8'-apo-β-apo-caroten-8'-oyl)-*O*²-[6-(methylselanyl)hexanoyl]glycerol, **II**) or carotenoid- and phosphocholine-derivatized SeOG (*O*¹-(8'-apo-β-caroten-8'-oyl)-*O*²-[6-(methylselanyl)hexanoyl]-*O*³-[[2-(trimethylammonio)ethoxy]phosphoryl]glycerol, **III**). The compound **III** generates a less densely packed layer due to the constraints induced by the phosphocholine substituent. Each of these compounds undergoes anodic reactions that are typical of carotenoids in the adsorbed state. However, the polar and hydrophilic phosphocholine residue in **III** shifts the anodic peak to a less positive potential. SeOG allows therefore to tune the molecular environment of a surface attached compound by means of a suitable co-substituent.

Keywords: Carotenoids; Glycerol; Selenides; Self-assembled monolayers; Electrochemistry.

Self-assembly of organic compounds at solid surfaces is a convenient method for preparing surfaces with well defined characteristics¹⁻⁴. A straightforward method for preparing self-assembled monolayer (SAM) consists of chemisorption of thiols or disulfides to metals like gold or silver. Disulfide adsorption results in S-S bond cleavage and the ensuing SAM is identical to that generated by the relevant thiol, with the sulfur head strongly attached to the metal surface. The high degree of organization is the result of two combined effects. First, the metal lattice may provide a suitable template. Second, intramolecular interactions within the surface layer stimulate the formation of an orderly network.

The SAM research represents a very active field with promising applications in various areas such as sensor technology⁵⁻⁷, electroanalytical chemistry^{8,9} and microfabrication¹⁰. In addition to physical methods of surface investigation, electrochemistry provides techniques for exploring properties of SAMs on metal surface, as demonstrates the comprehensive review by Finklea¹¹.

Although the investigation of organosulfur self-assembled monolayers has been the subject of many publications, selenium derivatives attracted a limited attention. The interest in organoselenium SAMs was initially stimulated by attempts to overcome problems with sulfur as a functional headgroup¹². Subsequently, the selenium headgroup became attractive from the viewpoint of the conductance of molecular wires, because it enables higher electronic coupling efficiency compared with sulfur¹³⁻¹⁵. This is in accord with the theoretically derived rule stating that the conductance close to the quantum unit can be obtained with a given molecular structure by increasing the atomic number of the anchoring group¹⁶.

Detailed studies on SAM formation at metal surface by alkaneselenols^{12,17,18}, aromatic selenols¹⁹⁻²¹, aromatic diselenides²²⁻²⁴ and monoselenides²⁵⁻²⁷ are available. Due to the relatively weak interaction between gold and selenium, alkaneselenols form incommensurate structures at the gold surface¹², in contrast to alkanethiols which give rise to commensurate surface structures.

Scanning tunneling microscopy (STM) proved that benzeneselenol forms ordered structure upon chemisorption at a gold surface¹⁹. In contrast, benzenethiolate cannot form organized structures under similar conditions. This behavior was interpreted as a proof for a stronger Au-Se interaction¹⁹, in accord with further investigations by surface-enhanced Raman spectrometry²⁰ (SERS).

Diselenides undergo Se–Se bond cleavage during adsorption and the resulting SAM is similar to that generated by analogous selenols in accord with the behavior of disulfides^{22–24}.

In the case of monoselenide adsorption on the gold surface, the state of the adsorbate seems to depend strongly on the structure of the precursor and the SAM preparation procedure. Thus, selenophene undergoes non-dissociative chemisorption under atmospheric vapor deposition, whereas the dissociative mechanism takes place upon ultrahigh vacuum deposition²⁶. As a rule, the interaction between chalcogenophene analogues and the gold surface is stronger when the atomic number of chalcogen is higher²⁶.

On the other hand, the aromatic benzyl phenyl selenide is adsorbed in intact form, as proved by SERS investigations²⁷. No relevant data in this respect are yet available for dialkyl selenides, but an STM examination demonstrated that dibutyl selenide forms ordered structures at the gold surface²⁵.

For comparison, it is interesting to note that organic sulfides preserve the structure when adsorbing on the gold surface^{28–36}. Some exceptions are still possible³⁰. Thus, an X-ray photoelectron spectrometry (XPS) investigation demonstrates that dioctadecyl sulfide is physically adsorbed from a 1 mM CH₂Cl₂ solution, with no C–S bond cleavage^{30a}. However, the C–S bond cleavage seems to occur when a monosulfide SAM was formed during long time immersion at high temperature, or using CHCl₃ as a solvent^{30a}.

We report here the results of an investigation by electrochemical methods and piezoelectric microgravimetry of the adsorption of *O*¹-[6-(methylselenanyl)hexanoyl]glycerol (SeOG; Table I, formula I) on the polycrystalline gold surface. SeOG is a suitable anchor for binding other molecules to the surface via the free hydroxy groups in the glycerol residue. As an example, the binding of a carotenoid (*O*¹-(8'-apo-β-apo-caroten-8'-oyl)-*O*²-[6-(methylselenanyl)hexanoyl]glycerol; Table I, formula II) and both a carotenoid and a phosphocholine fragment (*O*¹-(8'-apo-β-caroten-8'-oyl)-*O*²-[6-(methylselenanyl)hexanoyl]-*O*³-{[2-(trimethylammonio)ethoxy]phosphoryl}glycerol; Table I, formula III) is presented. Carotenoids are of outstanding biological importance, playing a key role in photosynthesis³⁷. On the other hand, synthetic supramolecular systems including carotenoids are actively investigated for the purpose of mimicking photosynthetic solar energy conversion³⁸. Another stimulus to the study of carotenoids assemblies emerges from the field of molecular electronics, particularly after an evidence of good conductivity of an individual carotenoid molecules has been published³⁹. In this context, immobilization of carotenoids to metal surfaces is

an important issue. The thione⁴⁰⁻⁴³, seleno^{42,44}, or thiol function^{39,45} has been used to attach carotenoids to the gold surface.

Investigation of SeOG adsorption is an important step before proceeding to the study of the surface behavior of some complex assemblies including SeOG as a bridge. In addition, this investigation allows to acquire more insight into adsorption of organic selenides on the gold surface.

TABLE I
Chemical compounds used as electrode surface modifiers

	I	II	III
-R ¹		-H	
-R ²	-H		
-R ³	-H		

EXPERIMENTAL

SeOG has been synthesized and purified according to the published procedures^{46,47}. Compound II was synthesized and purified according to the published procedures⁴⁸, and III was synthesized by an original method⁴⁹. The three compounds have been prepared by specific synthesis, avoiding isomerisation, and have been characterized by common spectroscopic methods (mass spectrometry, nuclear magnetic resonance spectrometry, absorption spectrometry in the visible range). The given structures in Table I are consistent with the spectral data.

Electrolyte solutions were prepared with fresh ultra-pure water (Millipore, resistivity 18 MΩ cm). All the reagents were of analytical grade, except the organic solvents that were of HPLC grade.

A polycrystalline gold disk electrode was prepared from a gold wire (Aldrich 99.99%, 1 mm diameter) sealed by epoxy resin in a glass tube (electrode No. 1). Alternatively, a Metrohm gold disk electrode of 2 mm diameter (electrode No. 2) was used in some experiments. The electrode surface was conditioned by mechanical polishing followed by prolonged cyclic voltammetry scanning in 0.01 M HClO₄ in the potential region from 0.00 to 1.45 V. An Ag|AgCl (1 M KCl) reference electrode was connected with the test solution using an 1 M KNO₃ electrolyte bridge; the auxiliary electrode consisted of a platinum plate. Other details are available in⁴³.

The SeOG adsorption was achieved by immersing the gold substrate in a 4.6 mM SeOG solution in acetonitrile in the dark, at room temperature (20 ± 1 °C), under nitrogen atmosphere. The same procedure was followed with compounds **II** and **III**, except for the composition of the adsorbate solution (4 mM solution of **II** in acetonitrile and 3.9 mM solution of **III** in methanol). After a suitable time period, the electrode was rinsed with the pure solvent and pure water. The modified electrode was then transferred to an aqueous solution containing an appropriate electrolyte, for performing electrochemical investigations.

Staircase cyclic voltammetry (CV), phase-sensitive alternating current voltammetry (ACV) and electrochemical impedance spectroscopy (EIS) experiments have been performed at room temperature (20 ± 1 °C) with Autolab PGSTAT 30 (Eco Chemie). Whenever the electrical charge had to be assessed, CV was run in the "integration" mode, i.e. the output was recorded as the average current over each potential step. Dissolved oxygen was removed from the test solution by bubbling with pure nitrogen. During experiments, nitrogen stream was directed above the solution. The EIS measurements have been performed in 0.1 M KNO_3 containing 5 mM $[\text{Fe}(\text{CN})_6]^{3-}$ and $[\text{Fe}(\text{CN})_6]^{4-}$ at the equilibrium potential (determined by potentiometry under open circuit conditions) and with a superimposed sine wave voltage of 10 mV.

Fitting and simulation of the electrochemical data was done with Autolab GPES 4.8 and FRA 4.8 software. Additional data reduction operations have been carried out with Origin® 6.1 software (OriginLab Corporation).

An electrochemical quartz crystal microbalance (EQCM) model 5510 (Institute of Physical Chemistry, Warsaw, Poland)⁵⁰ was connected to the auxiliary analog input of the PGSTAT 30 instrument to record simultaneously the electrolytic current and the EQCM frequency. A 10 MHz piezoelectric crystal with Ti-backed gold electrodes (5.0 mm diameter) has been mounted in vertical position. The Ti underlayer was selected to prevent problems at extreme anodic potentials⁵¹. The piezoelectrode had an electrochemically active area of 23.6 mm² and a roughness factor of 1.54 (determined according to^{52a}). The calibration of the EQCM was performed with the anodic stripping peak of silver⁵⁰. Prior to SeOG adsorption, the piezoelectrode surface was conditioned by three CV scans under the same conditions as with the polycrystalline gold electrodes.

RESULTS AND DISCUSSION

Anodic Behavior of Adsorbed SeOG Layer

An evidence of SeOG adsorption is provided by the anodic behavior of the modified electrode (Fig. 1a). The first scan (curve 1 in Fig. 1a) displays the anodic peak A, which is lower in the second scan (curve 2). The 3rd and 4th scans are identical and differ very few from the second one. It is clear that a steady state was already attained during the 3rd scan. The above finding demonstrates that SeOG adsorbs irreversibly during the electrode contact with the SeOG solution in acetonitrile. The peak A, which is similar to that induced by a short-chain alkanethiol SAM¹¹, can be assigned to the oxidative desorption of the organic surface layer. The anodic desorption occurs

almost completely during the first scan, as proved by a comparison of curves 2 and 4 in Fig. 1a. Simultaneously gold oxidation takes place. Gold oxide reduction occurs in the region of the cathodic peak B. Peak B current after desorption (Fig. 1a, curves 2–4) is higher than that recorded with the clean gold electrode (curve 5). This trend was detected with all gold electrodes used in this work and point to an increase in the real surface by cor-

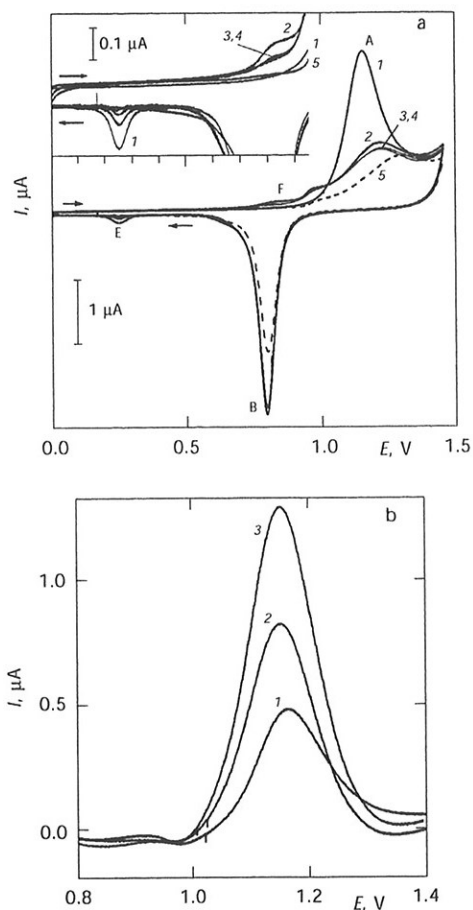


FIG. 1
 a Electrochemical behavior of the SeOG-modified gold electrode (No. 1) in the anodic potential region, 0.01 M HClO₄. Adsorption time 60 min, scan speed 20 mV s⁻¹. 1 1st scan; 2–4 subsequent scans; 5 plain gold electrode. Peak A: anodic desorption and gold oxidation; peak B: gold oxide reduction. Inset: enlarged view of the CV curves in the potential region from 0.0 to 0.9 V. b Background corrected voltammograms showing the anodic desorption current in the region of peak A. Adsorption time (in min): 1 1; 2 6; 3 60. For other conditions see Fig. 1a

rosion during the formation of the adsorbed layer. Such a process was investigated in details in connection to adsorption of alkanethiols^{52b}. As in that case, the corrosion degree increases with the adsorption time. Thus, the peak B current remained almost unchanged after desorption when the adsorption time was 1 min but increased with this parameter. Moreover, lit.^{52b} demonstrates that polar solvents like acetonitrile (which has been used in this work) favor the corrosion. A direct proof for an increase in the real surface during adsorption was provided by the alternating current (AC) capacity recorded (i) at pure gold, before performing the adsorption, and (ii) after performing the anodic desorption as in Fig. 1a. The capacity current was always higher after desorption than before adsorption. On the other hand, Fig. 1a demonstrates that the peak B appears to be unchanged with the advance of the scan sequence. A similar behavior was also noticed with a gold electrode modified with 4'-thioxo- β,β -caroten-4-one⁴³. The molecular structure of the adsorbate and its hydrophilic character allows water molecule to approach the metal surface in order to provide the oxygen required in the anodic reaction. Consequently, maximum coverage by oxygen is already attained during the first scan. This contrasts the behavior of alkanethiol SAMs. Due to both compact structure and hydrophobic character, an alkanethiol layer may prevent efficiently the formation of the gold oxide layer.

Figure 1b displays several background subtracted voltammograms for the anodic desorption process. In each case, the background was the gold oxidation current measured on the steady state curve. For six different modification times, ranging from 1 to 60 min, the corrected curve has a symmetrical shape with a peak potential of 1.15 ± 0.01 V and half-width of 0.132 ± 0.006 V. The invariability of the peak parameters proves that the mechanism of the oxidative desorption does not change with the increase in the surface coverage degree. This behavior may be assumed as an evidence of the absence of strong intramolecular interaction in the surface layer.

Selenium Transformations in the Anodic Potential Region

Figure 1a displays the cathodic peak E at 0.25 V on the first reverse scan. This peak should be due to a reaction product of the processes that occurs on the previous anodic scan. The anodic counterpart of E forms at 0.75 V on the next scan (peak F); it is distorted due to the interference of gold oxide formation. An enlarged view of the E/F couple is shown in the inset to Fig. 1a. The inset demonstrates that this couple vanishes after a few scans.

Peaks E and F may be related to electrochemical reactions involving selenium, which was initially present in the adsorbed organic layer. In order to assess their nature, cyclic voltammograms have been recorded for a selenious acid solution in the same background electrolyte (Fig. 2). The first anodic scan (from 0.4 to 1.45 V, curve 1 in Fig. 2) displays only the anodic reaction of gold with minute differences from the curve recorded in the background electrolyte alone (curve 3). However, the reverse scan displays the cathodic peak E' at the same potential as the peak E in Fig 1a. On the subsequent anodic scan (curve 2), the product of peak E' reaction is oxidized in the region of the peak F' which lies at the same potential as the peak F in Fig. 1a. It is important to note that the peak E' appeared even if the previous anodic scan was limited to 0.95 V so as to prevent any anodic reaction.

In agreement with lit.^{53a}, the peak E' is ascribed to the reduction of selenite ion adsorptively accumulated at the electrode surface during the previous anodic scan. Se(0) results and is further reoxidized to SeO_3^{2-} in the region of the peak F'. Peak E' does not form if the first scan starting at 0.4 V goes in the cathodic direction. In this case, SeO_3^{2-} reduction involves bulk solution ions and results in a broad peak with the half peak potential at 0.125 V. The tail of this peak is responsible for the asymmetric shape of the peak E'.

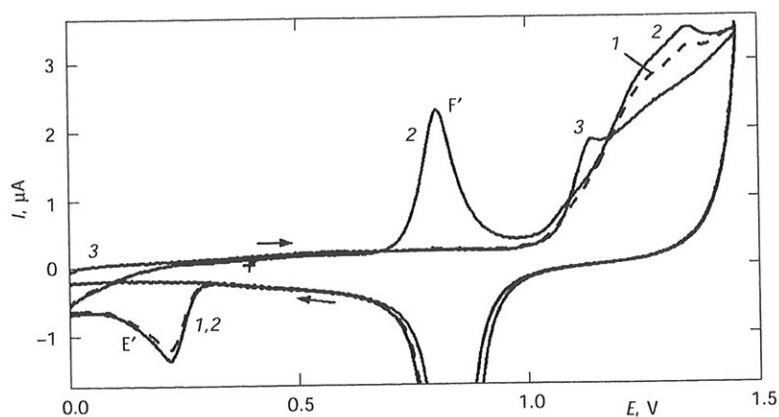


FIG. 2
Two cyclic voltammograms in the presence of $50 \mu\text{M H}_2\text{SeO}_3$ in 0.01 M HClO_4 (curves 1 and 2) and in 0.01 M HClO_4 alone (curve 3). Start at 0.40 V in the anodic direction. Scan speed 20 mV s^{-1} ; electrode No. 2

An alternative interpretation^{53b} assumes that the peak E' is due to the reduction of the selenate ion which form by the anodic reaction of selenite. This point of view is at variance with our data that demonstrate the independence of the peak E' on any preliminary anodic process.

SeO₃²⁻ adsorption in the anodic region is a reversible process. In order to prove this assertion, Se(0) was deposited and then the electrode was subjected to a series of successive CV scans in the background electrolyte alone, from 0 to 0.95 V and back. Under these conditions, peak F' is well developed on the first anodic scan, but E' is disproportionately smaller. Both peaks vanished after a few scans. It is clear that adsorbed SeO₃²⁻ which forms under peak F' diffuses away when the electrode is polarized at less anodic potentials.

By analogy with the behavior of inorganic selenium, peaks E and F in Fig. 1a can be interpreted as follows. The first anodic scan (curve 1 in Fig. 1a) results in the break of the Se-C bond in the adsorbate and Se(-2) is oxidized to adsorbed SeO₃²⁻ by the uptake of 6 electrons per molecule. SeO₃²⁻ is partially desorbed during the following cathodic scan and the remaining adsorbed form is reduced to Se(0) in the region of peak E. Se(0) is then oxidized to SeO₃²⁻ by the peak F reaction. As long as Se is present in the SeO₃²⁻ form, it may diffuse away leading to the gradual disappearance of both peaks E and F.

EQCM Investigation of the Anodic Processes

The anodic desorption process was monitored by EQCM during a multiscan CV run between 0.375 and 1.450 V (Fig. 3). The cathodic limit was selected so as to prevent SeO₃²⁻ (which form under the first anodic scan) from being reoxidized to Se(0). Consequently SeO₃²⁻ may diffuse freely away and does not affect the mass change on the next scans.

Curve 1 in Fig. 3a shows the shift in the resonance frequency during the first scan and displays a positive maximum in the region of peak A. The maximum is the convolution of two processes: desorption of the adlayer and gold surface oxidation. The first process results in a positive frequency shift and the second induces an opposite effect. Curve 2 in Fig. 3a was recorded during the 4th scan and is typical of a plain gold electrode. It is almost indistinguishable of the 2nd and 3rd scans since the desorption goes close to completion under the first anodic scan. The frequency shift on curve 2 results only from gold oxidation and gold oxide reduction. By subtracting curve 2 from curve 1 in Fig. 3a, curve 3 results, which represents the remaining effect of the desorption process only. It is clear from this

curve that the negative mass variation is an effect of an irreversible desorption process that occurs under the direct scan. The horizontal position of the reverse branch of curve 3 demonstrates that no readsorption occurs during the reverse potential sweep. The absence of the readsorption may be due to the oxidative transformation of the Se head into SeO_3^{2-} which at least partially remains in the adsorbed state and may diffuse away during an anodic scan, in accordance with the conclusion of the previous section.

The mass change corresponding to the desorption process was 39.6 ng for a modification time of 17 min (Fig. 3) and of 50.6 ng for a modification time of 30 min. The electrical charge corresponding to the desorption process was of 164 and 188 μC , respectively. Accordingly, 23 and 25.8 g, respectively, correspond to the transfer of 1 mol of electrons.

If we accept that SeO_3^{2-} forms, 6 electrons per molecule are expected to be transferred. A mass-charge correlation leads to 11 electrons per molecule if SeOG was adsorbed in unaltered form and desorbs in the anodic region. If

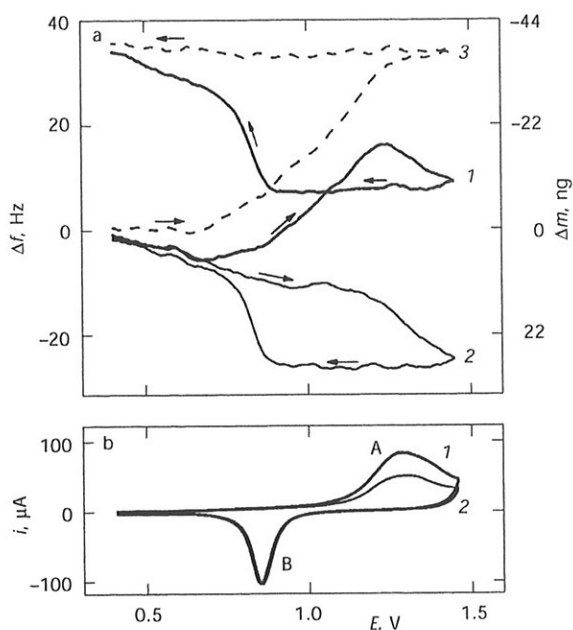


FIG. 3

The EQCM (a) and CV data (b) for the anodic desorption at a SeOG-modified gold piezoelectrode, 0.1 M HClO_4 . Adsorption time 17 min, scan speed 50 mV s^{-1} . 1 1st scan; 2 4th scan; 3 the result of subtracting curve 2 from curve 1 in a

we infer that SeOG splits under adsorption and the product (*O*¹-(6-selanylhexanoyl)glycerol, SeHG) desorbs, this ratio is 10.4. Both figures are non-realistically high. These ones have been calculated under the hypotheses that selenium also leaves the surface during the anodic process of peak A. On the contrary, if it is assumed that SeO_3^{2-} remains in the adsorbed state and only the hydrocarbon fragment is removed, a ratio of about 6 electrons per molecule results, in accordance with the oxidation of Se(-2) to Se(+4). However, the irreversible adsorption of SeO_3^{2-} is a limiting case, which is at variance with the results in the previous section.

It is likely that, in addition to removal of organic adlayer, the shift in frequency is partially determined by other factors, like insertion of water into irregularities of the gold surface. At the same time, SeO_3^{2-} contribution to the mass shift cannot be assessed because it desorbs partially and diffuses away gradually during the first potential scan. On the other hand, the redistribution of electric charges at the interface after removing the organic layer may contribute substantially to the overall current, leading to an overestimation of the charge for the anodic desorption. Data in Fig. 1b also lead to anomalous charge values (1.04 mC per cm² of geometric area, for curve 3). In this case, the high rugosity of the mechanically polished electrode may contribute to the high charge value, in addition to the non-Faradaic process.

It is clear that the complexity of the anodic reaction and the intercourse of Faradaic and non-Faradaic processes prevent a reliable interpretation of the EQCM data. Despite these limitations, data in Fig. 3 demonstrate that the SeOG-generated SAM is relatively stable in the anodic region up to the onset of gold oxide formation.

Kinetics of SeOG Adsorption

The capacity current recorded by ACV (Fig. 4, curve 1) enabled assessing the changes in the surface state as a function of SeOG adsorption time. The capacity current decreases with the increase in the modification time and becomes almost independent of the electrode potential. This behavior is similar to that demonstrated by alkanethiol SAMs¹¹. In terms of the Helmholtz model, this behavior proves that adsorption leads to an increase in thickness of the Helmholtz layer and a decrease in the dielectric constant as a result of water substitution by the organic absorbate. No indication of multi-layer formation was noticeable.

The electric charge passed during the anodic desorption allows, in principle, to calculate the amount of adsorbed compound, provided the stoichio-

metry of the electrochemical reaction is exactly known. As far as such information is not yet available, the charge itself may be used as a variable in the adsorption kinetic equation instead of the surface concentration of the adsorbate. This procedure was adopted in this work with some additional precautions. Thus, in order to make sure that the desorption is completed, three successive CV scans as in Fig. 1a have been performed in each case. The total charge (Q_t) for the anodic process occurring from 1.00 to 1.45 V was calculated for each of the three scans. It was assumed that it represents the sum of three components corresponding to adsorbate anodic desorption (Q_d), gold oxide formation (Q_{Au}) and oxygen evolution (Q_{ox}):

$$Q_{t,i} = Q_{d,i} + Q_{Au,i} + Q_{ox,i} \quad (1)$$

The subscript i stands for the scan number ($i = 1-3$). As a rule, the desorption is complete after the second scan and the total charge for the third scan ($Q_{t,3}$) results from the contribution of the last two terms in Eq. (1). Therefore, the overall charge for the anodic desorption ($Q_d = Q_{d,1} + Q_{d,2}$) was calculated as follows:

$$Q_d = Q_{t,1} + Q_{t,2} - 2Q_{t,3} \quad (2)$$

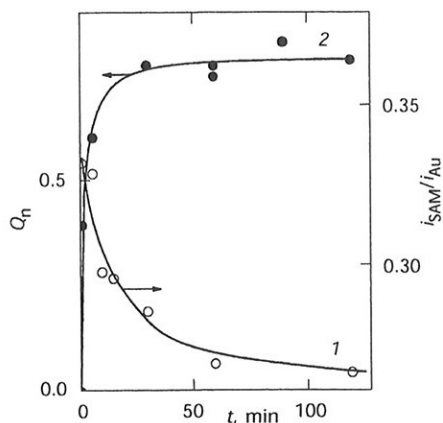


FIG. 4

Effect of the adsorption time on the AC capacity current at 0.00 V (1) and on the normalized desorption charge for the anodic desorption under the conditions of Fig. 1a (2). Electrode No. 1. Curve 1 conditions: 0.01 M HClO₄, frequency 200 Hz, amplitude 5 mV, phase angle -90°. To account for the variability in the surface area, the AC for the covered electrode (i_{SAM}) was normalized to the AC measured after performing the anodic desorption (i_{Au})

where $Q_{t,1}$ and $Q_{t,2}$ denote the total charge for the first and second scan, respectively.

In order to remove the effect of random variations in the electrode surface area, Q_d was normalized to the electric charge for peak B (Fig. 1a). This charge (Q_B) was assumed to be proportional to the real electrode area and was calculated as the average of three successive scans. Therefore, the normalized desorption charge (Q_n) was calculated as follows:

$$Q_n = Q_d / Q_B . \quad (3)$$

With the aim of investigating the kinetics of the adsorption, Q_n was measured after performing the modification for various time intervals, t (Fig. 4, curve 2) and the Q_n-t curve was checked by various kinetic models. The best fit resulted when using the diffusion-controlled Langmuir kinetic model^{54,55}, formulated as follows:

$$Q_n = Q_{n,1} [1 - \exp(-K_{DL}ct^{1/2})] , \quad (4)$$

where $Q_{n,1}$ is the limiting value of the normalized charge and c stands for the solution concentration of the adsorbing species. The constant K_{DL} depends on the adsorbate diffusion coefficient (D) and surface concentration at equilibrium⁵⁴ (Γ_e):

$$K_{DL} = \frac{2}{\Gamma_e} \left(\frac{D}{\pi} \right)^{1/2} . \quad (5)$$

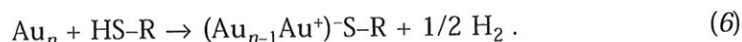
The effect of the adsorption time on Q_n is shown in Fig. 4, curve 2, which demonstrates that Q_n attains a limiting value for adsorption time over 30 min. The limiting specific charge is of 13.6 mC cm^{-2} , in a reasonable agreement with data in Fig. 1b, curve 3. The difference is a consequence of the variability in the electrode real surface. Under the conditions of Fig. 4, curve 2, the fitting by Eq. (4) results in $K_{DL} = 18 \text{ l mol}^{-1} \text{ s}^{-1/2}$ and $Q_{n,1} = 0.784$. The validity of the diffusion-controlled Langmuir model demonstrates that the adsorption itself is a fast process and the mass transfer of the adsorbate determines the overall rate. This conclusion remains valid despite the approximated character of Eq. (2) and is in a fair agreement with curve 1 in Fig. 4.

It is interesting at this point to mention the kinetic features of dialkyl sulfide adsorption on the gold surface³³. The adsorption rate for such com-

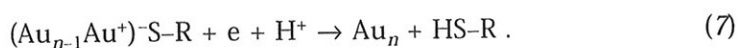
pounds is very low and no diffusion control of the rate-determining step was detected. This behavior strongly contrasts with that of SeOG.

Cathodic Behavior of the SeOG Adsorbed Layer

Cathodic reactions at an organosulfur-SAM-covered electrode allows to distinguish between the thiol or thioether form of the adsorbate. As pointed out before, thioether undergoes physical adsorption with no significant modification in the oxidation state of the gold site. In contrast, thiol adsorption is an oxidative process that was represented as follows¹¹:



Consequently, a reduction reaction occurs when the SAM covered electrode is polarized to a sufficiently cathodic potential¹¹:



This reaction is accompanied by desorption. In contrast to thiols, thioethers do not develop a cathodic response³⁴. Moreover, thioether layers are destroyed by contact with the aqueous alkaline solution that is used as electrolyte in cathodic desorption experiments²⁸. By analogy, a cathodic response of the SeOG-modified electrode may be interpreted as an evidence of the occurrence of the adsorbate in the selenol form.

Figure 5a displays successive CV scans that have been recorded in the potential region from 0 to -1.5 V with a SeOG-modified electrode (the vertex point is out of scale). On the first cathodic scan, three successive peaks, labeled C1, C2 and C3 appeared. Peak C1 vanished after the first scan, whereas C2 and C3 diminished gradually and disappeared after the fourth scan.

The state of the electrode surface after the scans in Fig. 5a was assessed by recording the AC under the conditions of Fig. 4, curve 1 and by probing the anodic behavior under the conditions of Fig. 1a.

The AC increased by a factor of about 3 after performing the CV scans in Fig. 5a and reached a value that was close to that measured for the plain gold electrode. On the other hand, an anodic CV scan following the cathodic polarization does not display any evidence of surface coverage (Fig. 5b, curve 6). It is clear therefore that the peaks C1-C3 in Fig. 5a arise from a cathodic desorption process similar to that induced by a thiol SAM (reaction (7)). This behavior suggests that the C-Se bonds split by adsorption

and the actual adsorbate is a product or a mixture of SeOG molecule cleavage products (i.e. methaneselenol and SeHG).

The fine structure of the cathodic response may be interpreted on the basis of the results of the cathodic desorption of alkanethiol SAMs^{56,57}. Accordingly, the fine structure appears due to the desorption of thiolates from domains with different size and organization degrees. Thus, the wave C1 may be assigned to the desorption of small ordered domains or disorganized domains. A comparison of the capacitive current values in Fig. 5a, measured on direct scans in the region between 0 and -0.4 V, shows a marked difference between the first and the second scan, followed by minor changes on the following scans. This implies that most of the adlayer was removed in the C1-wave region, during the first scan. An oxidative readsorption is hardly visible on the reverse branch of CV curve 1 in Fig. 5a (at about -0.7 V) and is missing on the next scans. Consequently, it may be inferred that the surface compound is rapidly lost in the bulk solution, in accord with the fair solubility of SeOG in water. For this reason, waves C2 and C3 cannot be assigned to capacitive processes due to the rearrangement of the desorption products inside the double layer region. These waves may rather be ascribed to the removal of organized domains that require a higher activation energy for desorption. Data in Fig. 5a suggest that ordered

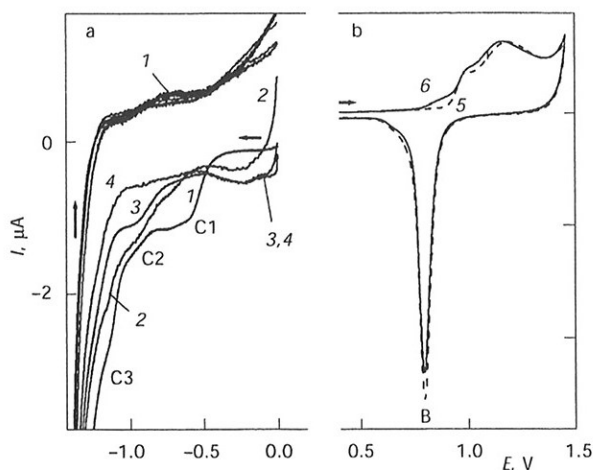


FIG. 5

a Cyclic voltammetry at a SeOG-modified electrode (No. 2) in the cathodic region. 1 1st scan; 2 2nd scan; 3 4th scan; 4 5th scan. Electrolyte 0.5 M KOH; scan speed 100 mV s^{-1} , modification time 30 min. b CV scans in the anodic region under the conditions of Fig. 1a. 5 Plain gold electrode; 6 the modified electrode, after the experiment in Fig. 5a

domains might form only a minor part of the adlayer, in accord with the heterogeneous crystal structure of the gold substrate.

An alternative interpretation of the fine structure in Fig. 5a may rely on the hypothesis of a mixed adlayer including both methaneselenol and SeHG. However, this interpretation is at variance with the data in Fig. 1b, which demonstrate no fine structure for the anodic desorption signal. The high solubility and mobility of methaneselenol, as well as the competition by SeHG may prevent it from accumulating at the gold surface.

The cathodic reaction of the SeOG-modified electrode was also investigated by EQCM. The voltammogram recorded at the gold piezoelectrode (Fig. 6, curve 1) shows the same features as those obtained with the electrode 2 (Fig. 5a), i.e. at least three distinct cathodic peaks. For comparison, the potentials of C1–C3 (Fig. 5a) have been indicated by vertical dotted lines in Fig. 6. It is known that electrochemical experiments in alkaline solutions are sensitive to impurities, e.g. oxygen. In order to prove the absence of such problems, the voltammogram 2 in Fig. 6 was recorded at the clean gold electrode. It is clear that no spurious electrochemical reactions occur in the region of peaks C1–C3. Owing to the difference in substrate crystallinity, the height of cathodic peaks in Fig. 6 differs from that in Fig. 5a. The dominant peak in Fig. 6 is C2, previously assigned to the desorption of organized domains. Such domains must be more extended at the surface of an evaporated gold substrate like that used in the EQCM ex-

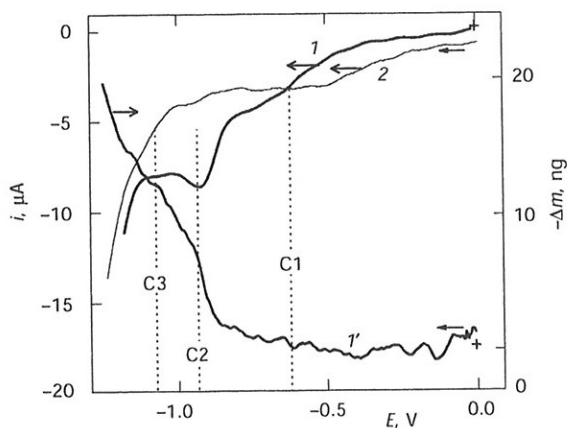


FIG. 6
EQCM data for the cathodic reactions at a SeOG-modified gold piezoelectrode, 0.5 M KOH. Scan speed 50 mV s^{-1} , modification time 17 min. 1 Current-potential curve; 1' EQCM response; 2 voltammogram recorded at the clean gold surface

periment. In accord with the cathodic peak current, a major shift in the resonance frequency corresponds to the peak C2 (Fig. 6, curve 2), whereas a minute frequency change accompanies the slight signal C1. The strong increase in Δf at extreme cathodic potentials is probably due to the formation of hydrogen bubbles⁵⁸, which prevent the detection of frequency changes associated with C3.

EQCM data confirm that the Faradaic cathodic currents at the SeOG-modified electrode are accompanied by the removal of the adlayer, as it happens in the case of alkanethiol SAMs^{56,57,59} when the degree of organization for the SeOG-generated surface layer strongly depends on the crystal structure of the gold substrate. On the other hand, the cathodic behavior of the SeOG-generated layer is similar to that of a benzeneselenol SAM generated by adsorption of diphenyl diselenide²⁴. In order to find the correlation between the mass change and the electric charge, peak C2 in Fig. 6 was selected. The electric charge calculated after performing polynomial baseline correction was correlated with the mass change measured by EQCM. The result (266 g/F) demonstrates that the desorbed species is SeHG (molar weight 268) and one electron is consumed per each molecule, in accord with the stoichiometry of alkanethiol desorption (Eq. (7)).

Coverage Degree and Surface Layer Morphology

The state of the adsorbed SeOG layer was assessed by assuming that it follows the microdisk array model^{11,60,61}. According to this model, the modified surface exhibits non-covered metal islets (pinholes) where the direct contact with the solution phase is possible. Consequently, if a modified metal surface acts as a working electrode in the presence of an electroactive compound, the latter may react at pinhole sites only. It was assumed for simplicity that the pinholes are disk-shaped, have a uniform size (radius r_a) and are separated by constant intervals ($2r_d$).

An analysis of the EIS data for a reversible redox system at an electrode covered by an inert SAM makes it possible to calculate the coverage degree (θ) as well as the parameters^{60,61} r_a and r_d . This approach is valid for $1 - \theta < 0.1$, where the following equation holds:

$$1 - \theta = r_a^2 / r_d^2 . \quad (8)$$

Although the geometry of the pinhole array should be more complex, this model offers an insight into the average pinhole parameters and pro-

vides a basis for the interpretation of experimental conditions effects on the coverage degree and the morphology of the adsorbed layer.

Data from EIS for the $[\text{Fe}(\text{CN})_6]^{3-}/[\text{Fe}(\text{CN})_6]^{4-}$ couple have been collected for several modification times (Table II). Data passed the Kroning-Kramer test⁶² and fit well the Randles circuit including a constant phase element (CPE) instead of a pure capacitor. Here, the impedance of the CPE was defined as follow^{63a}:

$$Z_Q = (j\omega Y_0)^{-n}, \quad (9)$$

where $j = (-1)^{1/2}$, ω is the angular frequency, and Y_0 and n are the parameters of the CPE ($0 < n < 1$). Data in Table II demonstrate that the charge transfer resistance (R_{ct}) increases with the modification time, pointing to a similar variation of the coverage degree. Double-layer capacitance (C)^{63b} values are significantly higher for pure gold than for the modified electrode, demonstrating that the hydrophobic polymethylene moiety in SeOG determines the charge distribution at the modified interface. This interpretation is also supported by variation of the n coefficient, which approaches the value for an ideal capacitor ($n = 1$) with increasing modification time. At the same time, the Warburg impedance slope (σ), Eq. 12 is, as expected, almost insensitive to the surface modification. This proves that the mass transport is localized in the solution phase only and the partition of the redox probe between the solution phase and the adsorbed layer (as emphasized in⁶⁴) has no effect in this system. Small fluctuations in the solution resistance (R_s) are due to the uncontrolled changes in the position of the electrolyte bridge tip.

TABLE II

Parameters of the Randles circuit for the SeOG-modified gold electrode with the estimated percent errors in parentheses. The same experimental conditions as in Fig. 7

Modifica- tion time, min	R_s $\Omega \text{ cm}^2$	R_{ct} $\Omega \text{ cm}^2$	CPE			σ $\Omega^{-1} \text{ s}^{1/2} \text{ cm}^{-2}$	C $\mu\text{F cm}^{-2}$
			$Y_0, \Omega^{-1/n} \text{ s}$	n	$Y_0^n, \Omega^{-1} \text{ s}^n \text{ cm}^{-2}$		
0	5.14(0.41)	2.16(1.93)	$5.54 \cdot 10^{-7}$ (9.8)	0.864(1.72)	$1.25 \cdot 10^{-4}$ (23)	29.1(0.26)	36.8(26.64)
30	2.79(0.85)	42.8(0.46)	$3.92 \cdot 10^{-8}$ (1.23)	0.889(0.36)	$3.32 \cdot 10^{-5}$ (5.57)	29.3(1.15)	14.6(6.04)
80	5.61(0.41)	780.3(0.26)	$3.82 \cdot 10^{-7}$ (1.06)	0.959(0.13)	$2.23 \cdot 10^{-5}$ (2.1)	29.1(2.37)	18.6(2.17)

The Warburg impedance slope, σ , was calculated using the fitting parameter Y_0 for the Warburg impedance as $1/(\sqrt{2} \cdot Y_0)$. C was calculated as $Y_0^n (\omega_m'')^{n-1}$ (ref.^{63b}), where ω_m'' correspond to the maximum Z'' value in the $Z'-Z''$ semicircle.

Pinhole parameters have been determined by the method of Finklea et al.⁶⁰, which consists of the analysis of the Faradaic impedance (Z_F) dependence on the frequency of the superimposed AC voltage, according to the following relations:

$$Z'_F = \frac{R_{ct}}{1-\theta} + \frac{\sigma}{\omega^{1/2}} + \frac{\sigma}{1-\theta} \left[\frac{(\omega^2 + q^2)^{1/2} + q}{\omega^2 + q^2} \right]^{1/2} \quad (10)$$

and

$$Z''_F = \frac{\sigma}{\omega^{1/2}} + \frac{\sigma}{1-\theta} \left[\frac{(\omega^2 + q^2)^{1/2} - q}{\omega^2 + q^2} \right]^{1/2}, \quad (11)$$

where Z'_F and Z''_F represent the in-phase and the out-of-phase components of Z_F , respectively. The amounts σ (Warburg impedance slope), R_{ct} (charge transfer resistance) and q were defined as follows:

$$\sigma = \left(\frac{2}{D} \right)^{1/2} \frac{RT/F}{FAc} \quad (12)$$

$$R_{ct} = \frac{RT/F}{FAck^0} \quad (13)$$

$$q = \frac{D}{0.36r_a^2}, \quad (14)$$

where D and c represent the diffusion coefficient and the concentration of the redox probe components, respectively, whereas k^0 is the standard rate constant for the charge transfer reaction.

The Faradaic impedance was calculated by subtracting from the overall value the contribution of the non-Faradaic components as determined in the high frequency region. Typical patterns for Z'_F and Z''_F dependence on $\omega^{-1/2}$ are presented in Fig. 7. Further, instead of performing a graphical analysis of each linear portions in the Z'_F vs $\omega^{-1/2}$ plot⁶⁰, data have been subjected to a non-linear curve fitting procedure, according to either Eq. (10) or Eq. (11). R_{ct} , σ , θ and q have been the fitting parameters and $\omega^{-1/2}$ the independent variable. Finally, D was calculated from Eq. (12) and introduced into Eq. (14) to find r_a ; r_d was determined from Eq. (8). Curves calculated by Eqs (10) and (11) using numerical values of the fitting parameters were plotted in Fig. 7; they matched very well the experimental values.

Pinhole parameters are summarized in Table III, where θ values satisfy the condition $1 - \theta < 0.1$, in accord with the constraints of this model. At the same time, the values resulting from the fitting by either Eq. (10) or Eq. (11) are in a fair agreement, proving the validity of the model for this system.

An inspection of the results in Table III demonstrates that both r_a and r_d increase with increasing modification time, although θ undergoes very slight change. This effect may be interpreted as a result of pinhole coalescence leading to the formation of larger islets located at a larger distance

TABLE III
Coverage degree and pinhole parameters for the SeOG-modified gold electrode

Modification time, min	Fitting variable	Coverage degree	r_a , μm	r_d , μm
30	Z'_F	0.969	1.02	5.85
	Z''_F	0.978	1.10	7.41
80	Z'_F	0.994	3.07	49.16
	Z''_F	0.996	2.88	38.46

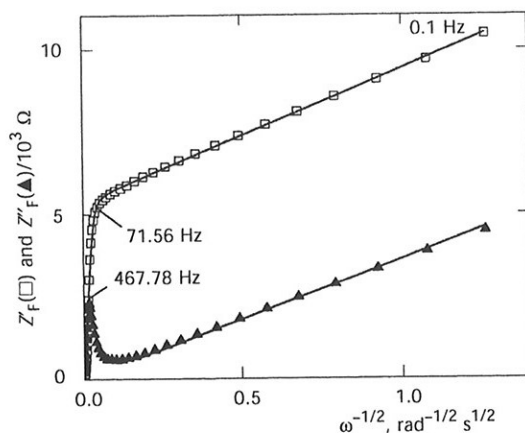


FIG. 7

Faradaic impedances (in-phase Z'_f (\square) and out-of-phase Z''_f (\blacktriangle) components) recorded for the gold electrode (No. 2) modified with SeOG. Adsorption time 30 min. Electrolyte: 0.1 M KNO_3 , 5 mM $\text{K}_3[\text{Fe}(\text{CN})_6]$, 5 mM $\text{K}_4[\text{Fe}(\text{CN})_6]$. Frequency: from 20 kHz to 0.1 Hz (40 values equally distributed on a logarithmic scale). Lines represent the fitting curves according to Eqs (10) and (11)

from each other. This demonstrates that the adsorbate molecules experience some mobility, which manifests itself at longer modification times. The coalescence of pinholes was also noticed previously for the dodecane-1-selenol¹⁸ and benzeneselenol¹⁹ surface layers.

The good agreement with the microdisk array model implies that the SeOG-generated SAM fulfils the restrictions of this model¹¹, namely relatively uniform pinhole dimensions and spacing.

SeOG as an Anchor for Immobilization of Carotenoids at the Gold Surface

We present in this section two examples of SeOG applications in attaching carotenoid derivatives (**II** and **III**) to the electrode surface. For convenience of the synthesis, 6-(methyloxy)hexanoyl grouping in **II** and **III** was attached as the R² substituent in glycerol, in contrast to SeOG where it appears in position 1. Experiments with O²-[6-(methyloxy)hexanoyl]glyc-

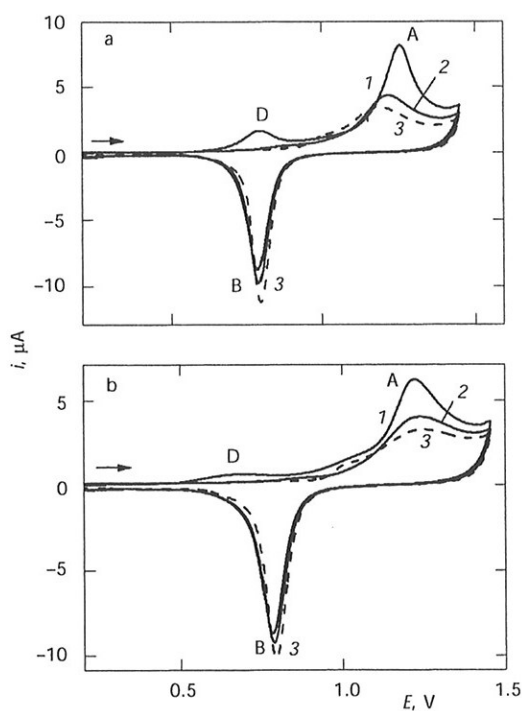


FIG. 8

Anodic reactions at the gold electrode No. 2 modified by compounds **II** (a) and **III** (b). The same conditions as in Fig. 1a. Adsorption time 30 min. 1 1st scan; 2 2nd scan; 3 steady state curve

erol in the adsorbed state at the gold surface showed that this behaves similarly to SeOG. Modification of the gold electrode by compounds **II** and **III** was performed by solution phase adsorption, as described in Experimental. The surface was thereafter checked by CV scans in the anodic potential region as in Fig. 1a. As follows from Fig. 8, the presence of each compound at the electrode surface is demonstrated by the anodic desorption peak A, which is similar to that recorded with the SeOG-modified electrode (Fig. 1). This proves that **II** and **III** have been attached to the gold surface through the Se function. Both of them desorb during the first anodic scan (curves 1 in Fig. 8), as the second scan (curves 2) displays only the anodic wave for gold oxide formation. In both cases, the second scan (curves 2) is close to the steady state curve (3) proving that most of the surface layer was desorbed during the first anodic scan, as it happens with SeOG itself (Fig. 1a). The fact that peak B shows only a minute increases from the first scan to the steady state curve points to the same conclusion.

In addition, both **II** and **III** induce the anodic peak D, which is missing in the case of SeOG (Fig. 1a, curve 1). An anodic peak like D was previously detected with 4'-thioxo- β,β -caroten-4-one chemisorbed on the gold surface via sulfur⁴⁰⁻⁴³. Consequently, peak D was assigned to the anodic oxidation of the polyene fragment R³ (Table I, **II** and **III**), which is a carotenoid residue. In accord with the current view, the first step in such a reaction should be the formation of a cation-radical⁶⁵. In the absence of a nucleophile, this may be further oxidized to a dication. However, in our experiments, the electroactive surface layer is in contact with water that may react immediately with the primary product. Such a process is favored in the case of **III** whose molecule contains the hydrophilic phosphocholine residue. Under these circumstances, the inactivation of the primary product proceeds faster. As a consequence, the peak D for **III** develops at a less positive potential as compared with **II**. At the same time, both peaks A and D are more intensive for **II** (Fig. 8a) than for **III** (Fig. 8b), proving that the phosphocholine substituent constrains the compound **III** adlayer to adopt a less densely packed morphology.

The above results demonstrate that SeOG may act as a convenient bridge for attaching highly-unsaturated compounds like carotenoids to the gold surface. In addition, binding of a second moiety to glycerol allows preparing mixed surface layers. Further details will be reported in a forthcoming paper.

CONCLUSIONS

SeOG interaction with the gold surface leads to the formation of a rather stable and compact adsorbed layer, which shows much of the characteristics of a short-chain alkanethiol SAM. Thus, the adsorbate binds irreversibly to the metal surface and the metal-adsorbate bond has a strongly polar character, as demonstrated by the charge transfer process that accompanies the cathodic desorption. Also, the anodic oxidative reaction reminds of the behavior of adsorbed alkanethiols.

It was demonstrated that SeOG adsorption is accompanied by the cleavage of the C-Se bonds and that the adsorbed layer consists mostly of SeHG. This behavior contrasts with that of dialkyl thioethers, which adsorb in the intact form. The reason for this difference may be the difference in the chemical bond strength for C-S and C-Se (714.1 and 590.4 kJ mol⁻¹ at 298 K, respectively), in diatomic molecules⁶⁶.

SeOG may act as a convenient bridge for attaching organic compounds to the gold surface through the ester function as evidenced in this paper for carotenoid and phosphocholine derivatives. Further applications of SeOG as an anchor for amine derivatives (including amino acids, peptides and proteins) may be envisaged. In such case, cyanogen bromide or cyanuric chloride would be suitable coupling agents⁶⁷.

SYMBOLS

A	area of the electrode surface
c	concentration
C	capacitance
D	diffusion coefficient
f	frequency
F	Faraday constant
k^0	standard rate constant for the charge transfer reaction
K_{DL}	constant in the diffusion-controlled Langmuir model (Eq. (5))
n	the exponent of the CPE ($0 < n < 1$)
$Q_{t,i}$	total charge for the peak A on the i -th scan
$Q_{d,i}$	charge for the anodic desorption on the i -th scan
$Q_{Au,i}$	charge for gold oxide formation on the i -th scan
$Q_{ox,i}$	charge for oxygen evolution plus contributions by the double layer modifications on i -th scan
Q_B	charge for the peak B
Q_d	total charge for anodic desorption
Q_n	normalized desorption charge (Eq. (3))
$Q_{n,l}$	the limiting value of the normalized charge
r_a	average radius of disk-shaped pinholes
r_d	average half-distance between pinholes

R	gas constant
R_{ct}	charge transfer resistance
R_s	ohmic resistance of the solution
t	time
T	temperature
Y_o	the ideal capacitance
Z_f	Faradaic impedance
Z_f'	the in-phase component of Z_f
Z_f''	the out-of-phase component of Z_f
Z_Q	impedance of the constant phase element
Δf	frequency shift
Γ_e	surface concentration at equilibrium
θ	coverage degree
ω	angular frequency
σ	slope of the Warburg impedance

A. Ion gratefully acknowledges financial support of the Norwegian Research Council.

REFERENCES

1. Ulman A.: *MRS Bull.* **1995**, 20, 46.
2. Ulman A.: *Chem. Rev.* **1996**, 96, 1533.
3. Xu J., Li H. L.: *J. Colloid Interface Sci.* **1995**, 176, 138.
4. Schreiber F.: *Prog. Surf. Sci.* **2000**, 65, 151.
5. Wink T., van Zuilen S. J., Bult A., van Bennekom W. P.: *Analyst* **1997**, 122, 43R.
6. Flink S., van Veggel F. C. J. M., Reinhoudt D. N.: *Adv. Mater.* **2000**, 12, 1315.
7. Gooding J. J., Mearns F., Yang W. R., Liu J.: *Electroanalysis (N. Y.)* **2003**, 15, 81.
8. Mandler D., Turyan I.: *Electroanalysis (N. Y.)* **1996**, 8, 207.
9. Mirsky V. M.: *Trends Anal. Chem.* **2002**, 21, 439.
10. Kumar A., Abbott N. L., Kim E., Biebuyck H. A., Whitesides G. M.: *Acc. Chem. Res.* **1995**, 28, 219.
11. Finklea H. O. in: *Electroanalytical Chemistry* (A. J. Bard and I. Rubinstein, Eds), Vol. 19, p. 109. M. Dekker, New York 1996.
12. Samant M. G., Brown C. A., Gordon J. G.: *Langmuir* **1992**, 8, 1615.
13. Patrone L., Palacin S., Bourgojn J. P.: *Appl. Surf. Sci.* **2003**, 212, 446.
14. Patrone L., Palacin S., Bourgojn J. P., Lagoute J., Zambelli T., Gauthier S.: *Chem. Phys.* **2002**, 281, 325.
15. Yaliraki S. N., Kemp M., Ratner M. A.: *J. Am. Chem. Soc.* **1999**, 121, 3428.
16. Di Ventra M., Lang D. N.: *Phys. Rev. B: Condens. Mater.* **2002**, 65, 5402.
17. Nakano K., Sato T., Tazaki M., Takagi M.: *Langmuir* **2000**, 16, 2225.
18. Protsailo L. V., Fawcett W. R., Russell D., Meyer R. L.: *Langmuir* **2002**, 18, 9342.
19. Dishner M. H., Hemminger J. C., Feher F. J.: *Langmuir* **1997**, 13, 4788.
20. Huang F. K., Horton R. C., Myles D. C., Garrell R. L.: *Langmuir* **1998**, 14, 4802.
21. Han S. W., Lee S. J., Kim K.: *Langmuir* **2001**, 17, 6981.
22. Bandyopadhyay K., Vijayamohanan K.: *Langmuir* **1998**, 14, 625.

23. Bandyopadhyay K., Vijayamohan K., Venkataraman M., Pradeep T.: *Langmuir* **1999**, *15*, 5314.
24. Aslam M., Bandyopadhyay K., Vijayamohan K., Lakshminarayanan V.: *J. Colloid Interface Sci.* **2001**, *234*, 410.
25. Nakamura T., Kimura R., Matsui F., Kondoh H., Ohta T., Sakai H., Abe M., Matsumoto M.: *Langmuir* **2000**, *16*, 4213.
26. Kondoh H., Nakai I., Nambu A., Ohta T., Nakamura T., Kimura R., Matsumoto M.: *Chem. Phys. Lett.* **2001**, *350*, 466.
27. Han S. W., Kim K.: *J. Colloid Interface Sci.* **2001**, *240*, 492.
28. Troughton E. B., Bain C. D., Whitesides G. M., Nuzzo R. G., Allara D. L., Porter M. D.: *Langmuir* **1988**, *4*, 365.
29. Hagenhoff B., Benninghoven A., Spinke J., Liley M., Knoll W.: *Langmuir* **1993**, *9*, 1622.
30. a) Takiguchi H., Sato K., Ishida T., Abe K., Yase K., Tamada K.: *Langmuir* **2000**, *16*, 1703; b) Noh J., Kato S. H., Kawai M., Hara M.: *J. Phys. Chem. B* **2002**, *106*, 13268.
31. Beulen M. W. J., Huisman B.-H., van der Heijden P. A., van Veggel F. C. J. M., Simons M. G., Biemond E. M. E. F., de Lange P. J., Reinhoudt D. N.: *Langmuir* **1996**, *12*, 6170.
32. Lee H. Y., He Z. L., Hussey C. L., Mattern D. L.: *Chem. Mater.* **1998**, *10*, 4148.
33. Jung C., Dannenberger O., Xu Y., Buck M., Grunze M.: *Langmuir* **1998**, *14*, 1103.
34. Zhong C. J., Brush R. C., Anderegg J., Porter M. D.: *Langmuir* **1999**, *15*, 518.
35. Dishner M. H., Hemminger J. C., Feher F. J.: *Langmuir* **1996**, *12*, 6176.
36. Trevor J. L., Lykke K. R., Pellin M. J., Hanley L.: *Langmuir* **1998**, *14*, 1664.
37. Blankenship R. E.: *Molecular Mechanisms of Photosynthesis*. Blackwell, Oxford 2002.
38. Gust D., Moore T. A., Moore A. L.: *Acc. Chem. Res.* **2001**, *34*, 40.
39. Leatherman G., Durantini E. N., Gust D., Moore T. A., Moore A. L., Stone S., Zhou Z., Rez P., Liu Y. Z., Lindsay S. M.: *J. Phys. Chem. B* **1999**, *103*, 4006.
40. Ion A., Banica F. G., Partali V., Sliwka H. R.: *J. Heyrovsky Memorial Symposium on Advances in Polarography and Related Methods, Prague, August 30–September 1, 2000*, Book of Abstracts, p. 63.
41. Ion A., Banica F. G., Partali V., Sliwka H. R.: *International Symposium on New Directions in Electroanalysis, University of Salford, April 22–25, 2001*, Book of Abstracts, Lecture No. 7.
42. Ion A., Banica F. G., Foss B. J., Partali V., Sliwka H. R.: *13th International Carotenoid Symposium, Honolulu, January 6–11, 2002*, Book of Abstracts, p. 19.
43. Ion A., Partali V., Sliwka H. R., Banica F. G.: *Electrochem. Commun.* **2002**, *4*, 674.
44. Ion A., Banica F. G., Foss B. J., Partali V., Sliwka H. R.: *13th International Carotenoid Symposium, Honolulu, January 6–11, 2002*, Book of Abstracts, p. 114.
45. Liu D. Z., Szulcowski G. J., Kispert L. D., Primak A., Moore T. A., Moore A. L., Gust D.: *J. Phys. Chem. B* **2002**, *106*, 2933.
46. Kodali D. R.: *J. Lipid Res.* **1987**, *28*, 464.
47. Oghi T., Kondo T., Goto T.: *Tetrahedron Lett.* **1977**, *46*, 4051.
48. Naalsund T., Malterud K. E., Partali V., Sliwka H. R.: *Chem. Phys. Lipids* **2001**, *112*, 59.
49. Foss B. J., Partali V., Sliwka H. R.: Unpublished results.
50. Koh W., Kutner W., Jones M. T., Kadish K. M.: *Electroanalysis (N. Y.)* **1993**, *5*, 209.
51. Hoogvliet J. C., van Bennekom W. P.: *Electrochim. Acta* **2001**, *47*, 599.
52. a) Tian M., Pell W. G., Conway B. E.: *Electrochim. Acta* **2003**, *48*, 2675; b) Edinger K., Grunze M., Woll C.: *Ber. Bunsen-Ges. Phys. Chem.* **1997**, *101*, 1811.
53. a) Andrews R. W., Johnson D. C.: *Anal. Chem.* **1975**, *47*, 294; b) Alanyalioglu M., Demir U., Shannon C.: *J. Electroanal. Chem.* **2004**, *561*, 21.

54. Rahn J. R., Hallock R. B.: *Langmuir* **1995**, *11*, 650.
55. Dannenberger O., Buck M., Grunze M.: *J. Phys. Chem. B* **1999**, *103*, 2202.
56. Wong S. S., Porter M. D.: *J. Electroanal. Chem.* **2000**, *485*, 135.
57. Kawaguchi T., Yasuda H., Shimazu K., Porter M. D.: *Langmuir* **2000**, *16*, 9830.
58. Buttry D. A., Ward M. D.: *Chem. Rev.* **1992**, *92*, 1355.
59. Schneider T. W., Buttry D. A.: *J. Am. Chem. Soc.* **1983**, *115*, 12391.
60. Finklea H. O., Snider D. A., Fedyk J.: *Langmuir* **1993**, *9*, 3660.
61. Amatore C., Saveant J. M., Tessier D.: *J. Electroanal. Chem.* **1983**, *147*, 39.
62. Bonanos N., Steele B. C. H., Butler E. P., Johnson W. B., Worell W. L., MacDonald D. D., McKubre M. C. H. in: *Impedance Spectroscopy* (J. R. Macdonald, Ed.), p. 191. J. Wiley, New York 1987.
63. a) *Autolab Electrochemical Systems*, Application Note Appl0/3 (www.ecochemie.nl); b) Hsu H. C., Mansfeld F.: *Corrosion* **2001**, *57*, 747.
64. Markovich I., Mandler D.: *J. Electroanal. Chem.* **2000**, *484*, 194.
65. Liu D. Z., Gao Y. L., Kispert L. D.: *J. Electroanal. Chem.* **2000**, *488*, 140.
66. Lide D. R. (Ed): *CRC Handbook of Chemistry and Physics*. CRC Press, Boca Raton 2002.
67. Barker S. A. in: *Biosensors, Fundamentals and Applications* (A. P. F. Turner, I. Karube and G. S. Wilson, Eds), p. 85. Oxford University Press, Oxford 1987.

Article 9

B. J. Foss, H.-R. Sliwka, V. Partali, C. Köpsel,
B. Mayer, H.-D. Martin, F. Zsila, Z. Bikádi, M. Simonyi

**Optically active oligomer units in aggregates of a highly unsaturated, optically
inactive carotenoid phospholipid**

Chemistry - European Journal 2004, submitted

Optically active oligomer units in aggregates of a highly unsaturated, optically inactive carotenoid phospholipid

Bente Jeanette Foss, Hans-Richard Sliwka*, Vassilia Partali, Christian Köpsel, Bernhard Mayer, Hans-Dieter Martin*, Ferenc Zsila, Zsolt Bikadi, Miklos Simonyi*

B. J. Foss, H.-R. Sliwka, V. Partali, Norges Teknisk Naturvitenskapelige Universitet (NTNU) Institutt for Kjemi, N-7491 Trondheim (Norway) email: hrs@nvg.ntnu.no

B. Mayer, C. Köpsel, H.-D. Martin, Institut für Organische Chemie und Makromolekulare Chemie, Heinrich-Heine-Universität, D-40225 Düsseldorf, email: martin@uni-duesseldorf.de

F. Zsila, Z. Bikadi, M. Simonyi, Department of Bioorganic Chemistry, Chemical Research Center, H-1525 Budapest, email: msimonyi@chemres.hu

Keywords: carotenoids, phospholipids, helical structure, molecular modeling, primary aggregation unit

Abstract

Enantiomers of glycerophospholipids show low or no optical activity. Accordingly, optical activity was not observed with the (*R*)-enantiomer of a highly unsaturated carotenoyl lysophospholipid in molecular solution. In spite of this, strong Cotton effects are detected in water. The amphiphilic carotenoid-phospholipid monomers associate to aggregates, whose optical activity is created by oligomeric entities. These small helical assemblies cannot exist independently. Yet, the calculated octamer represents the simplest repeating primary unit sufficiently expressing the absorption properties and supramolecular optical activity.

Introduction

The chiroptical properties of glycerolipids are rarely investigated, while the two other groups of vital biomolecules, carbohydrates and proteins with their well-established exclusive building blocks of D-sugars and L-amino acids, receive a lot of attention. Despite the fact that the biosynthesis of lipids also results in only one specific enantiomer, a chiral, functional discrimination of enantiomeric lipids has hardly been found. Membranes consist of pure phospholipid enantiomers, but with respect to penetration and other physical properties, phosphocholines behave as achiral molecules.^[1-3] It was only recently that a decisive enantiomeric interaction between odorants and lipids was detected in the olfactoric system.^[4] Another reason for neglecting chiroptical investigations of glycerolipids is their invisibility. (Phospho)lipids show notoriously low or no specific rotations, likewise, electronic optical activity (EOA) is weak or absent due to the lack of chromophores.^[5] The few natural chromophoric lipids contain ajenoic acids C12:5, C14:5 in triglycerides^[6] and parinaric acid C18:4 in phosphatidylcholines.^[7] The CD, or fluorescence detected CD (FDCD), of these lipids has not yet been measured, nor have chiral lipids been prepared from synthetic conjugated tetraenic fatty acids.^[8] In any case, the acyl chains in these unsaturated lipids are only partly accessible by EOA-spectroscopy. In various attempts to introduce chromophores, phospholipids with stilbene, biphenyl, terphenyl and azobenzene fatty acids have been synthesized.^[9-11] Likewise, a glycerophosphatidylcholine enantiomer with styrylthiophene acyl groups was synthesized, devoid of optical activity.^[12] Undoubtedly, the mentioned lipids contain rather xenobiotic acyl groups and are, therefore, different from lipids of naturally occurring fatty acids.

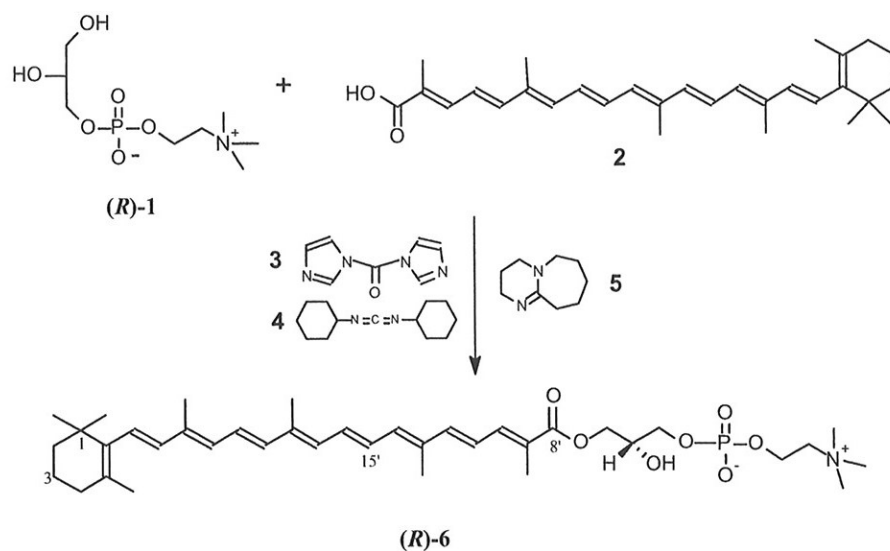
For historical reasons OA is restricted to wavelengths from 200-800 nm. Although the accessible chiroptical spectral range has successively been enlarged to both lower and higher wavelengths, enantiomers resist being defined as "optically inactive" when no signal in the classical wavelength scale is detected. Thus, the highly unsaturated carotenoylphospholipid (**R**)-6 (in MeOH), not exhibiting EOA in the usual accessible range of the dichrograph, (Figs. 1a, 1c), is considered optically inactive. However, (**R**)-6 shows optical activity in water, Fig. 1a. The chiroptical properties of (**R**)-6 result from self-assembling of optically inactive monomers to supramolecular structures.^[13,14] By calculating the absorption and CD spectra of a manifold of oligomeric structures we found that a helical oligomer composed of approximately eight monomers may serve as a basic unit explaining satisfactorily the spectroscopic properties of (**R**)-6 aggregates.

We report here on the synthesis of lysophospholipid (**R**)-6, on its chiroptical properties and the calculation of a basic aggregation unit.

Results and discussion

Lysocarotenoylphosphatidyl choline ((**R**)-6) was synthesized in low yield by reacting the natural (+)-(2*R*)-glycero-3-phosphocholine (3-*sn*-GPC) ((**R**)-1) with the rigid and fully chromophoric carotenoid acid (C30-acid)^[15,16] **2** in the presence of imidazol **3**, DCC (**4**) and DBU (**5**),^[17] Scheme 1. Dissolved in methanol, carotenoid derivative (**R**)-6 did not show EOA, Figs. 1a, 1c.^[18] A chiral perturbation of the polyene chain is not expected to occur in (**R**)-6 and, in addition, Cotton effects (CE) in the absorption

region of the polyene chain above 400 nm are difficult to detect.^[19,20] In some colorless glycerides weak CE were observed around 220 nm ($n-\pi^*$ transitions of the ester group),^[21-24] sometimes with opposite signs for the same enantiomer.^[25] The measurement of the weak specific rotation of lysophospholipids requires high compound concentrations (3-5%).^[26] Such deep orange colored solutions of **(R)-6** are not transparent and, therefore, hardly detectable in the polarimeter.^[27] Optically *inactive* enantiomers^[28,29] have been, incorrectly, called “cryptochiral”, because “chirality” frequently, but inadmissibly, is considered to be equivalent with EOA.^[30-34] The more appropriate and descriptive term “cryptoactive” for glyceride enantiomers without detectable EOA has been largely ignored.^[5] Nevertheless, we will rank the carotenoylglycerophospholipid **(R)-6** to the class of cryptoactive compounds or to compounds with *accidental optical inactivity*.^[35]



Scheme 1

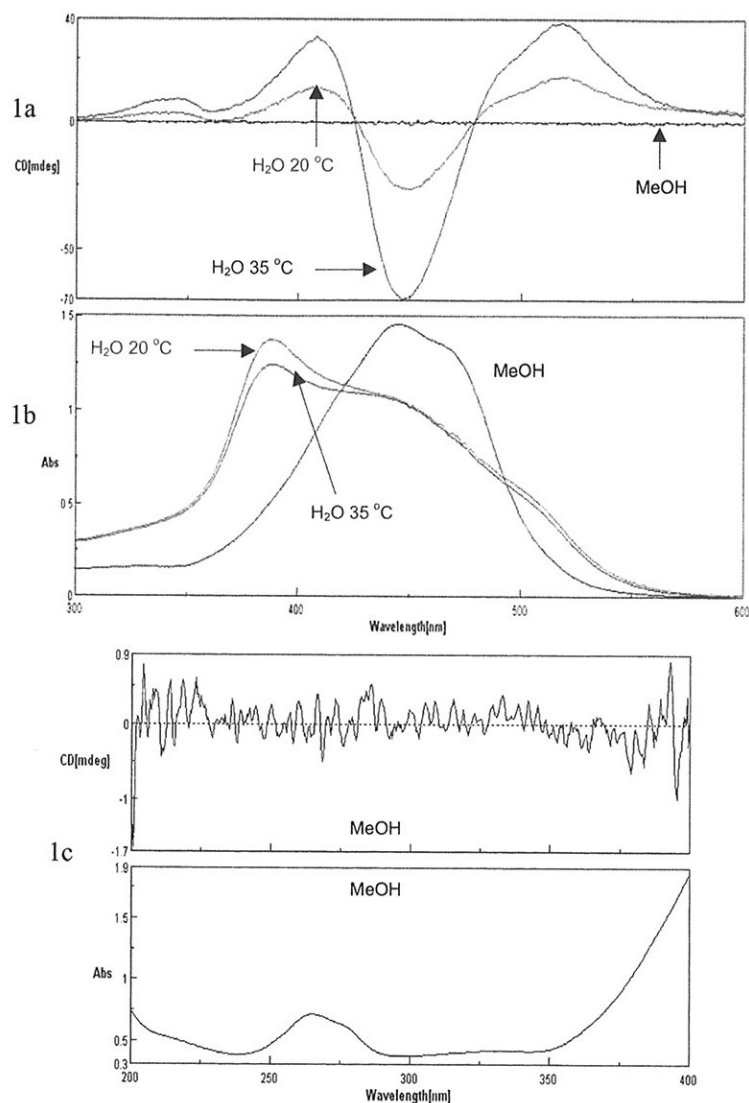


Fig. 1. CD-spectra 1a, absorptions spectra 1b (300 - 600 nm) and CD- and absorption spectra 1c (200 - 400 nm) of (*R*)-6, path length = 1 cm, $c = 2 \times 10^{-5}$ M > critical micelle concentration $c_M = 1.5 \times 10^{-3}$ M.

In water, the amphiphilic carotenoylphospholipid (*R*)-6 forms clear, orange colored dispersions, mostly of aggregates with an average size of 6 nm.^[13,14] The strong absorption band of the monomeric solution observed at 445 nm in methanol ($\pi-\pi^*$ transitions of the polyene chain, **Fig. 1b**) splits in water into two exciton bands, a prominent signal at 380 nm in the H-aggregate and a slightly visible shoulder at 510 nm in the J-aggregate region.^[36,37] The association of monomers into aggregates accelerated at higher temperature, the intensity of the CE increased when standing at 35 °C, **Fig. 1a**. While the flat line in the CD-spectrum convincingly proves the lack of CE in the molecular solution of (*R*)-6 (in methanol) the CD spectrum of (*R*)-6 in

water showed strong CE (Fig. 1a), a positive signal at 410 nm, a strong negative band in the absorption region of the polyene chain (445 nm) and again a positive band at 520 nm. Since simply water was added to optically inactive (*R*)-6 the obtained CE can only be generated from induced optical activity, originating from a chiral association of (*R*)-6 monomers. In principle, the observed optical activity of the aggregates could arise from a handed orientation of all monomers in a possibly existing unilamellar vesicle.^[13,14] However, it is also possible that few monomers first associate to small primary units, which then constitute the supramolecular structure. In order to determine the origin of EOA in the aggregates we tried to simulate the absorption and CD spectra. At first sight, the experimental CD spectrum seems to be a mixture of blue-shifted negative and red-shifted positive exciton couplets. The most simple model explaining such type of spectral behavior may be a tetramer with both right and left handed overlay angles. Molecular mechanics calculations were performed using the Sybyl 6.6 program^[38] to find a minimum energy conformation. The calculated tetramer (Fig. 2) appeared to be in accordance with the spectral data.

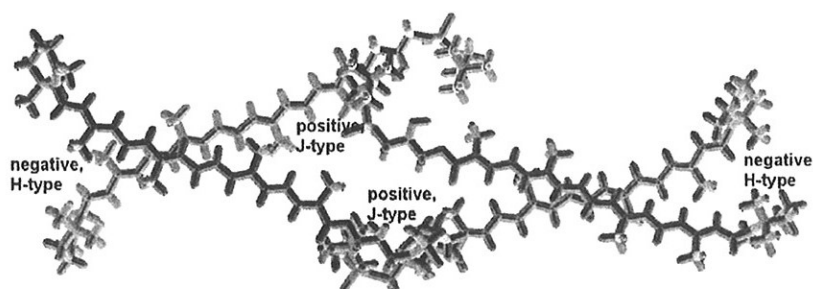


Fig. 2 The simplest basic unit with both negative H-type and positive J-type arrangements

However, the tetramer arrangement did not fully recognize the exciton interactions according to the excitation model of Buss et al.^[39] In order to account for these interactions two tetrameric substructures were combined and optimized using Molecular Dynamics (MD) and Force-Field-CVFF^[40-42] calculations in the DISCOVER-program.^[43] The UV-Vis and CD spectra of the aggregates could then be simulated with the carotenoid acid 2 in the AM1-model applying a configuration interaction (CI) with three occupied and two unoccupied MOs and considering singly as well as doubly excited configurations. The lowest excitation was calculated for 519 nm with a transition moment of 2.74 D. These values were then used within the excitation model employing the dipole-dipole approximation. The computation resulted finally in a structure (Fig. 3), which satisfactorily explains the recorded spectra (cf. Fig. 4).

We conclude therefore that oligomers with the approximate size of 8 form the primary units leading to the observed chiroptical absorption.^[44] The configuration of these oligomers is determined by the stereogenic center in the hydrophilic part of monomeric (*R*)-6. The CD-spectra express supramolecular chirality of the aggregates

resulting from a helical P-orientation of the polyene chain in the calculated oligomer, **Fig. 3**.

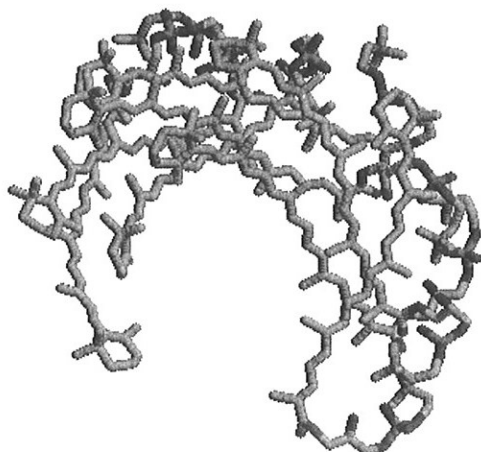


Fig. 3 Optically active P-oligomer unit, built from eight optically inactive (*R*)-6 monomers

Basic units in aggregates have rarely been reported,^[45,46] e.g. the monomers of the mentioned styrylthiophene phospholipid create a tetramer unit.^[12] The formation of aggregation units is in accordance with the observation of quantized aggregation numbers AN,^[47] where the total AN can only be a multitude of monomers in the primary aggregation unit.

Aggregates of chiral carotenoids often show characteristic exciton couplets in the CD-spectra caused by chromophore overlapping in specific, ordered arrangements.^[48-51] Such ordered arrangements are not encountered in the oligomer discussed here. The inadequate agreement of the maxima, minima and zero point crossings of the CD spectrum with that of the absorption spectrum reflects the rather irregular structure of the calculated oligomer. Further, it follows from **Fig. 3** that no defined H- or J-arrangements exist in the depicted octamer. The interchromophoric geometry of the molecules in the octamer causes a shift of the absorption maxima to shorter as well as to longer wavelengths.

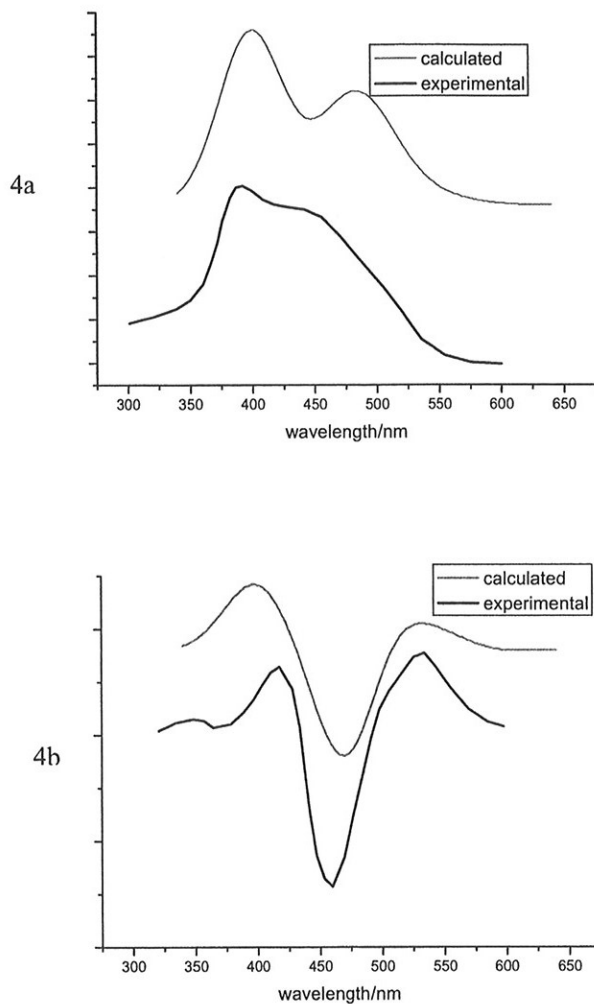


Fig. 4 Absorption (4a) and CD (4b) spectra: the calculated spectra are calibrated by +40 nm for better adjustment.

A basic unit, such as the selected octamer, cannot exist as an independent entity in water, since the polar and non-polar groups are oriented in an unfavorable position. In addition, dynamic light scattering measurements did not detect oligomeric particles corresponding in size to the association of eight monomers.^[13,14] Therefore, we define the oligomer unit as the lowest spatial extent of monomer association inheriting all the spectroscopic and chiroptical properties of the aggregates. Such basic units in aggregates could possibly be compared with elementary (Bravais) units in crystals. Aggregate formation is sensitive to subtle experimental conditions. Besides the absorption at 380 nm, **Fig. 1b**, aggregate dispersions absorbing at 390 or 400 nm were sometimes observed suggesting the possible presence of other oligomer structures in these higher absorbing aggregates.^[14]

The few known CE of glycerophospholipid aggregates arise from the ester carbonyl group located in the hydrophilic part of molecules at the exterior of the aggregates.^[22,23] In contrast, the CE of (*R*)-**6** are formed by the hydrophobic polyene chromophore and correspond to molecular interactions inside the aggregates (micelles) or inside the membrane (lamellar vesicles). Aggregates of (*R*)-**6** should possess an enantiomorphous membrane with the potential to differentiate enantiomeric reactants. In a preliminary experiment the membrane opening protein melittin did not disrupt the membrane of (*R*)-**6**, demonstrated by the absence of energy and electron transfer in flash photolysis experiments.

Conclusion

Reviewing our experimental results and molecular calculations we conclude that the highly unsaturated, optically inactive glycerophospholipid (*R*)-**6** forms in water enantiomeric primary units of moderate size: an octameric oligomer may represent the simplest repeating unit, satisfactorily expressing absorption properties and supramolecular EOA.

It appears reasonable to hypothesize that other (crypto)optically active glycerolipid monomers also may associate to small, enantiomeric units within supramolecular assemblies.

Acknowledgement

We thank H. Ernst (BASF AG, Ludwigshafen) and S. Servi (Politecnico di Milano) for a generous gift of C30-Ester and (*R*)-glycerophosphocholine, respectively, and T.B. Melø and K.R. Naqvi (Department of Physics, NTNU) for the flash-photolysis experiments.

Experimental

The product was isolated by means of flash chromatography (Silica 60A 40-63 mm, SDS). The column was prepared with CHCl_3 , the product solved in CHCl_3 and eluted with $\text{CHCl}_3/\text{CH}_3\text{OH}$ (80/20), gradually increasing water and methanol to $\text{CHCl}_3/\text{CH}_3\text{OH}/\text{H}_2\text{O}$ (40:50:10). Smaller amounts were purified on analytic DC plates (Silika 60 F254, Merck) with $\text{CHCl}_3/\text{CH}_3\text{OH}/\text{H}_2\text{O}$ (40:50:10) as eluent. The product yield was determined from the VIS spectrum.^[52]

(R)-1-(β -Apo-8'-carotenoyl)-3-glycerophosphocholin [(R)-6] The intermediate carotenoylimidazol was synthesized reacting β -apo-8'-carotenoic acid **2**^[16] (77 mg, 0,18 mmol) with 1,1'-carbonyldiimidazol (**3**) (292 mg, 1,8 mmol) and 1,3-dicyclohexylcarbodiimid (**4**) (371 mg, 1,8 mmol) solved in CHCl_3 (10 ml). The reaction mixture was stirred under nitrogen (20 °C, 4 hours). *sn*-1-Glycerophosphocholine ((**R**)-**1**) (100 mg, 0,39 mmol), $[\alpha_D^{18}] = -2.5^\circ$, $c = 0,05$ g/ml H_2O , $p = 0,88$, $[\alpha_D^{19}] = -2.84^\circ$, $c = 0.088$ g/ml H_2O ^[53] and 1,8-diazabicyclo[5.4.0]undec-7-en (**5**) (119 mg, 0,78 mmol), solved in DMSO, were added to the solution and the reaction mixture was stirred under nitrogen (40 °C, 24 h). The solution was washed with saturated NaCl (aq) to remove most of DMSO and then dried over Na_2SO_4 . After evaporation of solvent under reduced pressure chromatographic work-up gave (**R**)-**6** (5 mg, 4%). UV-Vis in MeOH and H_2O : **Fig. 1b, c**. CD in MeOH and H_2O : **Fig. 1a, c**. The ^1H and ^{13}C -spectra did not indicate isomerisation by acyl migration.^[54]

Attempt for membrane disruption: Phospholipid (**R**)-**6** in water was irradiated with rose bengal as sensitizer. The transient absorption spectra of carotenoid triplets (^3car) or of carotenoid cation radicals (car^+) could not be observed. Melittin (Bachem) was added and, after few minutes, the solution was irradiated. Again, no energy or electron transfer occurred. The photophysics of (**R**)-**6** and other water dispersible carotenoid will be published elsewhere.

Description of the calculation methods

Calculation of the tetrameric structure: Molecular mechanics (MM) calculations have been performed by the Sybyl 6.6 program.^[38] on a Silicon Graphics Octane workstation under Irix 6.5 operating system. The MM calculations were based on MMFF94 force field^[55] applying energy minimization by the conjugate gradient technique with 0.001 kcal/mol·Å gradient. Tetramers were built up from energy-minimized monomers using the dock command of Sybyl.^[38]

Calculation of the octameric structure: Molecular dynamic (MD) calculations were performed by the Discover 2.9.7 program^[43] on SGI ORIGIN 2000 mainframe under Irix 5.1 operating system. The applied force field was CVFF.^[40-42] In order to determine the conformational space the starting geometry was first equilibrated at 300K for 500 ps followed by slowly cooling to 100K. The final geometry was obtained by the steepest descent technique for 1000 steps and finally by the conjugate gradient with 0.001 kcal/mol·Å gradient. AM1 (MOPAC 93, Fujitsu Limited, PentiumIII, 700 MHz, Windows NT4.0) method with a CI of the 3 highest occupied and the 2 lowest unoccupied MOs was used to calculate the excitation energies and transition moments. The individual transition moments were superimposed on the individual molecules within in the aggregates. Applying the principle of dipole-dipole

interactions,^[56] an energy matrix was constructed and diagonalized as usual. In this way the eigenvalues and, thus, the excitation energies of the aggregates and the corresponding oscillatory and rotatory strengths were obtained.

References

1. W. Guyer, K. Koch. *Chem. Phys. Lipids* **1983**, *33*, 313-322.
2. E.M. Arnett, J.M. Gold. *J. Am. Chem. Soc.* **1982**, *104*, 636-639.
3. D. Andelman. *J. Am. Chem. Soc.* **1989**, *111*, 6536-6544.
4. N. Nandi. *J. Phys. Chem. A* **2003**, *107*, 4588-4591.
5. W. Schlenk. *J. Am. Oil Chem. Soc.* **1965**, *42*, 945-57.
6. J.Cason, R. Davis, M.H. Sheehan. *J. Org. Chem.* **1971**, *36*, 2621-2625.
7. B. Schmitz, H. Egge. *Chem. Phys. Lipids* **1984**, *43*, 139-151.
8. D.V. Kuklev, W.L. Smith. *Chem. Phys. Lipids* **2004**, *130*, 145-158.
9. X. Song, C. Geiger, I. Furman, D.G. Whitten. *J. Am. Chem. Soc.* **1994**, *116*, 4103-4104.
10. X. Song, J. Perlstein, D.G. Whitten. *J. Am. Chem. Soc.* **1997**, *119*, 9144-9159.
11. H.C. Geiger, J. Perlstein, R.J. Lachicotte, K. Wyrozebski, D.G. Whitten. *Langmuir* **1999**, *15*, 5606-5616.
12. X. Song, J. Perlstein, D.G. Whitten. *J. Phys. Chem. A* **1998**, *102*, 5540-5450.
13. B.J. Foss, S. Nalum Næss, H.R. Sliwka, V. Partali. *Angew. Chem. Int. Ed.* **2003**, *42*, 5237-5240; *Angew. Chem.* **2003**, *115*, 5395-5398.
14. B.J. Foss, H.R. Sliwka, V. Partali, S. Nalum Næss, A. Elgsæter, T.B. Melø, K. R. Naqvi. *Chem. Phys. Lipids* **2004**, *xx*, xx-xx.
15. V. Partali, L. Kvittingen, H.-R. Sliwka, T. Anthonsen. *Angew. Chem. Int. Edit.* **1996**, *35*, 329-330.
16. E. Larsen, J. Abendroth, V. Partali, B. Schulz, H.-R. Sliwka, E.G.K. Quartey. *Chem. Eur. J.* **1998**, *4*, 113-117.
17. M. Tomoi, K. Inomata, H. Kakiuchi. *Synt. Commun.* **1989**, *19*, 907-915.
18. Phosphatidylcholine does not form aggregates in MeOH, I.W. Kellaway, L. Saunders. *Biochim. Biophys. Acta* **1970**, *210*, 185-186.

19. K. Noack, A.J. Thomson. *Helv. Chim. Acta* **1979**, *62*, 1902-1921.
20. H.-R. Sliwka. *Helv. Chim. Acta* **1999**, *82*, 161-169.
21. S. Gronowitz, B. Herslöf, R. Ohlson, B. Töregård. *Chem. Phys. Lipid* **1975**, *14*, 174-188.
22. P. Walde, E. Blöchiger. *Langmuir* **1997**, *13*, 1668-1671.
23. P. Walde, E. Blöchiger, K. Morigaki. *Langmuir* **1999**, *15*, 2346-2350.
24. L.M. Colombo, C. Nastruzzi, P.L. Luisi, R.M. Thomas. *Chirality* **1991**, *3*, 495-4502.
25. P. Michelsen, S. Gronowitz, B. Åkesson, B. Herslöf. *Chem. Phys. Lipids* **1983**, *32*, 137-143.
26. N.B. Smith, A. Kuksis. *Can. J. Biochem.* **1978**, *56*, 1149-1153.
27. ORD measurements of carotenoids are performed in 0.1% solutions with path-lengths of 1 mm: L. Bartlett, W. Klyne, W.P. Mose, P.M. Scopes, G. Galasko, A.K. Mallams, B.C.L. Weedon, J. Szabolcs, G. Tóth. *J. Chem. Soc. C* **1969**, 2527-2544.
28. H. Nakashima, M. Fujiki, J.R. Koe, M. Motonaga. *J. Am. Chem. Soc.* **2001**, *123*, 1963-1969.
29. A.F.M. Kilbinger, A.P.H.J. Schenning, F. Goldoni, W.J. Feast, E.W. Meijer. *J. Am. Chem. Soc.* **2000**, *122*, 1820-1821.
30. A. de Meijere, A.F. Khlebnikov, R.K. Kostikov, S.I. Kozhuskhov, P.R. Schreiner, A. Wittkopp, D.S. Yufit. *Angew. Chem. Int. Ed.* **1999**, *38*, 3474-3477.
31. C.W. Thomas, Y. Tor. *Chirality* **1998**, *10*, 53-59 (1998).
32. H.W.I. Peerlings, M.P. Struijk, E.W. Meijer. *Chirality* **1998**, *10*, 46-52.
33. G. Wulff, U. Zweering. *Chem. Eur. J.* **1999**, *5*, 1898-1904.
34. "Cryptochiral" was erroneously introduced for enantiomers without detectable EOA (K. Mislow, P. Bickart. *Isr. J. Chem.* **1977**, *15*, 1-6). The relation "optical activity = chirality" was later corrected: chirality is independent of chemical and physical evidence (A.B. Buda, T. Auf der Heyde, K. Mislow. *Angew. Chem. Int. Edit.* **1992**, *31*, 989-1007). The phenomenon of optical activity cannot be limited to transmission measurements of the ground state in the generally accessible EOA-range. Optical activity appears also at longer or shorter wavelengths in emission -, dispersion and transition spectra. De Meijere noticed in a footnote on "cryptochirality" that racemates and *meso* compounds could be termed cryptochiral, Ref. 30, but even methane would be cryptochiral: P.W. Atkins, J.A.N.F. Gomes. *Chem. Phys. Lett.* **1976**, *39*, 519-520. The term "cryptoactive" was proposed in 1965

by Schlenk, knowing that optical activity can be hidden behind the shortfall of instruments or measuring techniques, Ref. 5.

35. J.K. O'Lane. *Chem. Rev.* **1980**, *80*, 41-61.
36. E. Lüddecke, A. Auweter, L. Schweikert. BASF, Ludwigshafen, EP 930022 **1998**.
37. D. Horn, J. Rieger. *Angew. Chem.* **2001**, *113*, 4460-4492; *Angew. Chem. Int. Edit.* **2001**, *40*, 4331-4361.
38. Sybyl 6.6 program, Tripos Inc., St. Luis, MO, USA.
39. H.J. Nolte, V. Buss. *Tetrahedron* **1975**, *31*, 719-723.
40. P. Dauber-Osguthorpe, V.A. Roberts, D.J. Osguthorpe, J. Wolff, M. Genest, A.T. Hagler. *Proteins: Structure, Function, Genetics* **1988**, *4*, 31-47.
41. A.T. Hagler, S. Lifson. *J. Am. Chem. Soc.* **1974**, *96*, 5327-5335.
42. R.J. Maple, U. Dinur, A.T. Hagler. *Proc. Natl. Sci. USA* **1988**, *85*, 5350-5354.
43. DISCOVER 2.9.7, Biosym Technologies, Inc./Molecular Simulations (MSI), Inc., San Diego, USA.
44. The adsorption maxima of higher carotenoid associations converge to a constant value. Whereas the absorption of small oligomers is significantly different, λ_{\max} of oligomers consisting of 8, 10 or 12 monomers are only separated by few nanometers. Our conclusion that the primary unit approximates an octamer means that the presence of a heptamer or hexamer is excluded, but possibly decamers or dodecamers may be present. (B. Mayer, H.-D. Martin, unpublished results).
45. H. Chen, K.Y. Law, J. Perlstein, D.G. White. *J. Am. Chem. Soc.* **1995**, *117*, 7257-7258.
46. A. Chowdhury, S. Wachsmann-Hogiu, P.R. Bangal, I. Raheem, L.A. Peteanu. *J. Phys. Chem. B* **2001**, *105*, 12196-11201.
47. J.A. Butcher, G.W. Lamb. *J. Am. Chem. Soc.* **1984**, *106*, 1217-1220.
48. M. Simonyi, Z. Bikadi, F. Zsila, J. Deli. *Chirality* **2003**, *15*, 680-698.
49. N. Berova, D. Gargiulo, F. Derguini, K. Nakanishi, N. Harada. *J. Am. Chem. Soc.* **1993**, *115*, 4769-4775.
50. M.S. Spector, A. Singh, P.B. Messersmith, J.M. Schnur. *Nano Letters* **2001**, *1*, 375-378.
51. H. Auweter, J. Benade, H. Bettermann, S. Beutner, C. Köpsel, E. Lüddecke, H. D. Martin, B. Mayer. *Proceed. Pigments in Food Technology* (Eds. M.I.M. Mosquera,

M.J. Galan, D.H. Mendez), Dep. Legal (SE-646-99), Sevilla **1999**, pp. 197-201, ISBN 84-699-0185-0.

52. B.D. Davies, Carotenoids, in *Chemistry and biochemistry of plant pigments*, Ed. T.W. Goodwin, Academic Press, London **1976**, pp. 38, 149.

53. A.F. Rosenthal. *Methods Enzymol.* **1975**, 35, 429, 443.

54. B.J. Foss, J. Kranc. *Magn. Reson. Chem.* **2004**, 42, 373-380.

55. T. Halgren. *J. Am. Chem. Soc.* **1990**, 112, 4710-4723.

56. M. Speis, J. Messinger, N. Heuser, V. Buß, in G. Gauglitz (Ed.) "Software-Entwicklung in der Chemie 3", Springer, Berlin-Heidelberg **1989**, 387-395.